NASA

MEMORANDUM

1958 NASA/USAF SPACE PROBES

(ABLE-1)

FINAL REPORT

VOLUME 3.   VEHICLES, TRAJECTORIES, AND FLIGHT HISTORIES

By Space Technology Laboratories, Inc.
Los Angeles 45, Calif.

NATIONAL AERONAUTICS AND SPACE ADMINISTRATION
WASHINGTON

June 1959

1958 NASA/USAF SPACE PROBES

(ABLE-1)

FINAL REPORT

VOLUME 3. VEHICLES, TRAJECTORIES, AND FLIGHT HISTORIES

18 February 1959

CONTENTS

CONTENTS (Continued)

CONTENTS (Continued)

ILLUSTRATIONS

ILLUSTRATIONS (Continued)

ILLUSTRATIONS (Continued)

TABLES

3.0   THE LAUNCHING VEHICLE

3.1   Vehicle Description

3.1.1   Configuration

The Thor Able-1 is a four-stage vehicle consisting of three propulsion stages and a terminal stage composed of eight vernier rockets, an orbit injection rocket and the payload. Interstage structural attachments between successive stages are provided with means for in-flight separation. A nose fairing, jettisoned during second-stage operation, covers the third and fourth stages. Figure 3-1 illustrates the over-all configuration.

a.   Stage 1.

The first stage is a standard SM-75 Thor missile produced by Douglas Aircraft Company and modified for this use. The AC Sparkplug guidance system was removed and the flight control system was modified to accommodate the bending dynamics of the four-stage configuration. Structural modifications to the basic Thor airframe were minor, and consisted largely of the addition of a conical frustum semi-monocoque first-stage transition section to accommodate the second stage.

b.   Stage 2.

The second stage is the AJ 10-101 vehicle stage produced by the Aerojet General Corporation, and is an extensively modified AJ 10-40 propulsion system. A compartment containing major components of the second-stage control system, destruct system, electrical system, instrumentation, and telemetry is added to the forward tank cylindrical skirt. A conical frustum semi-monocoque second-stage transition section is added to the aft tank cylindrical skirt, and is connected to the first-stage transition section by four explosive bolts which provide the means for second-stage separation. The second-stage transition section is the same structure used in the Able 5500-nautical mile re-entry test vehicle. A stainless steel sheet and Refrasil cord heat shield is attached to the forward end of the second-stage transition section and protects both second- and first-stage transition section structures from excessive aerodynamic heating.

2

Fourth Stage ———————

Stage 4 Separation Plane ———————

Third Stage ———————

Stage 3 Separation Plane (Sta. 124.82)——►

Stage 2 Control Compartment ———————

Stage 2 Forward Skirt ———————

UDMH Fuel Tank ———————

Helium Tank ———————

WIFNA Oxidizer Tank ———————

Stage 2 Aft Skirt ———————

Stage 2 Transition Section ———————

Stage 2 Separation Plane ———————

Stage 1 Transition Section ———————

Stage 1 Guidance Bay ———————

Stage 1 RP-1 Fuel Tank ———————

Stage 1 Lox Tank ———————

———— Sta. 29.41

Nose Fairing

———— Sta. 119.13

Second Stage

———— Sta. 332.90

(Reference: General
Arrangement, STL
Dwg. L-10269 C)

———— Sta. 1085.9

Figure 3-1. Able-1 Over-all Configuration

c. Stage 3.

The third stage consists of the Allegheny Ballistics Laboratory X-248-A3 solid propellant rocket. The Stage 3-4 interconnect structure and separation mechanism is attached to the rocket case forward closure boss by a single explosive bolt. The third-stage rocket nozzle flange is attached by two explosive bolts to a beam extending across the front end of the second-stage control compartment, and the aft end of the rocket motor case is supported by four compression struts which drop away when the separation bolts are fired at staging.

d. Stage 4.

The fourth stage consists of the payload package, eight small Atlantic Research 1XS-50 vernier rockets, and a Thiokol TX-8 orbit injection rocket. The stage is attached to the front end of the third-stage motor case by an explosive bolt on the longitudinal axis and is supported by an annular interconnect structure. A compression spring forces separation of third and fourth stages when the separation bolt is fired. The eight vernier rockets are mounted on a casting which is attached to the aft end of the payload package by a two-piece circumferential band. The two explosive bolts which hold the band in place during flight are fired to jettison the vernier rocket assembly when desired. Four small compression springs insure jettisoning the vernier rocket cluster. The third and fourth stage assembly is shown in Figure 3-2, and Figures 3-3 and 3-4 show details of the interconnecting structure and separation mechanism.

e. Nose Fairing.

A two-piece fairing protects the third and fourth stages from aerodynamic forces and aerodynamic heating during first-stage operation. The fairing is jettisoned 10 seconds after second-stage ignition. The two halves are joined by two explosive bolts and two pyrotechnic actuators. When these devices are fired, the two halves are projected radially outward from the vehicle.

3.1.2 Operation

Sections 3.5, 3.6, and 3.7 describe the operational characteristics of the control, electrical, and telemetry subsystems used with the second stage of the

4
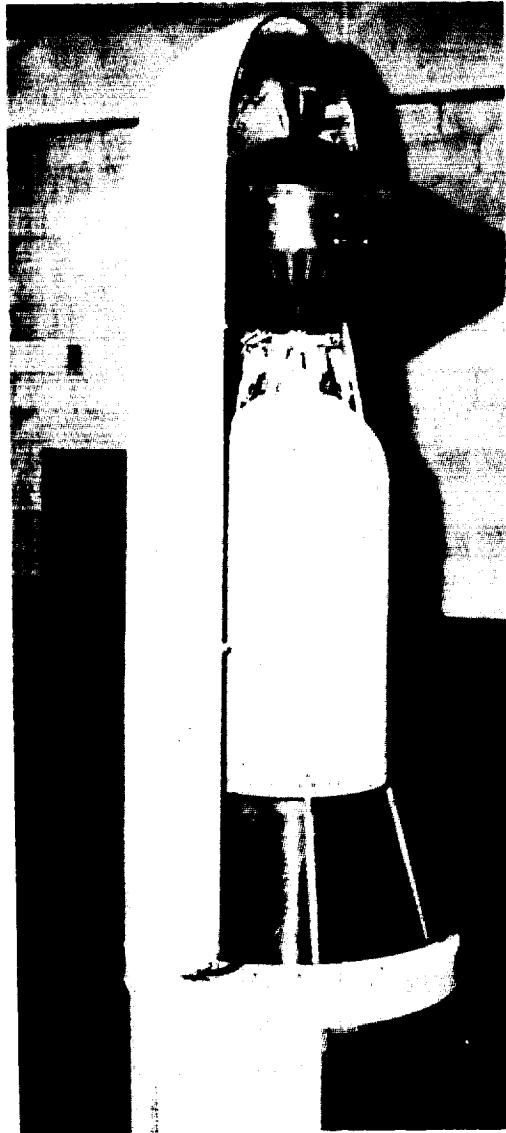
Figure 3-2. Third and Fourth Stages Assembled on Control and
Instrumentation Compartment.
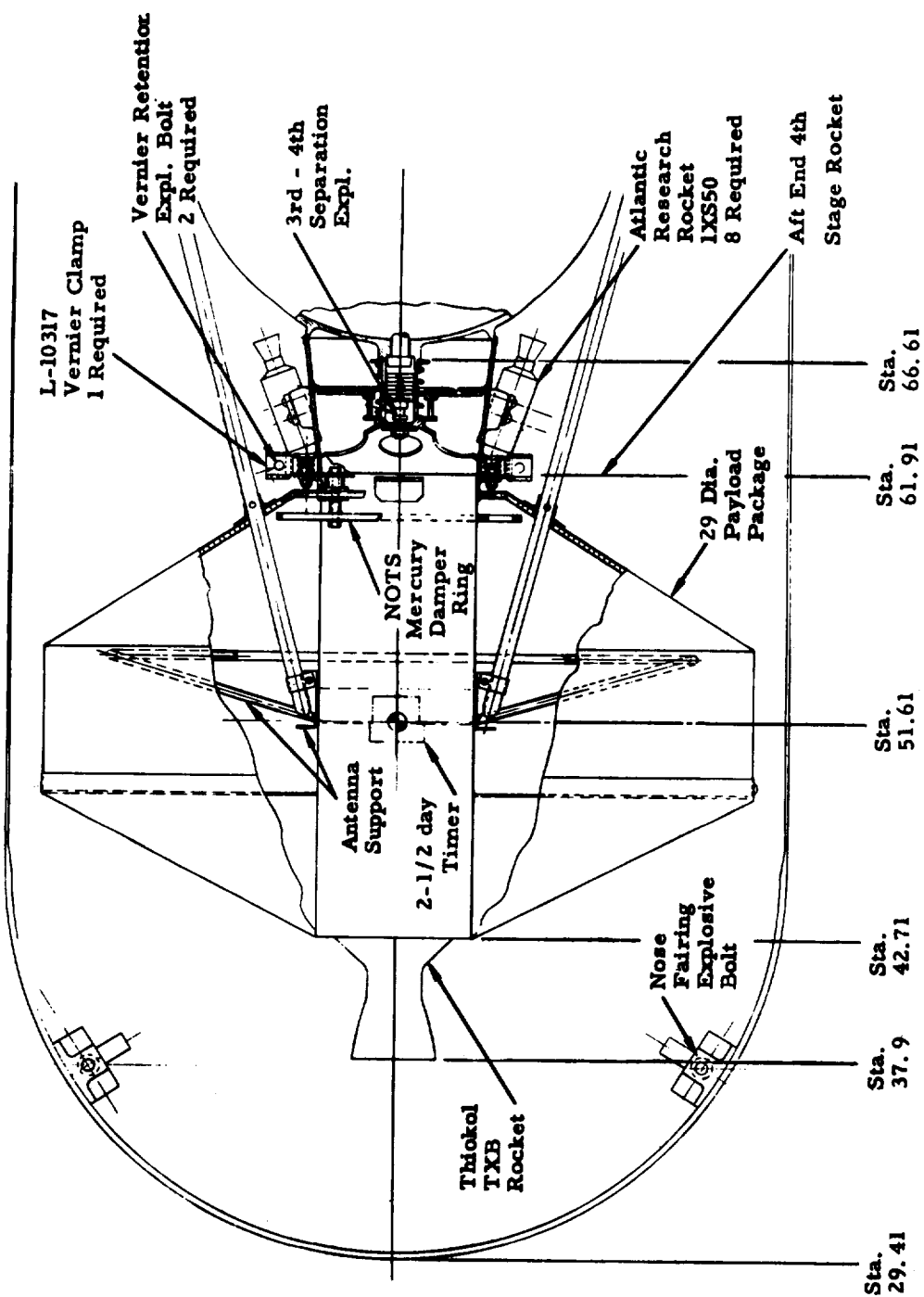
Figure 3-3. Detailed View of Fourth Stage and Interconnect Structure.

6

SECTIONED
FRONT END OF
3RD STAGE
MOTOR CASE

3RD & 4TH STAGE
SEPARATION
BOLT

ADAPTER
SEPARATION
SPRING

3RD STAGE
ADAPTER

VERNIER
CLAMP
BAND

VERNIER
ROCKETS

VERNIER
RING

INJECTION
ROCKET
ADAPTER

VERNIER
CLAMP RING
SEPARATION
BOLTS

VERNIER
SEPARATION
SPRINGS

4TH STAGE
INJECTION
ROCKET
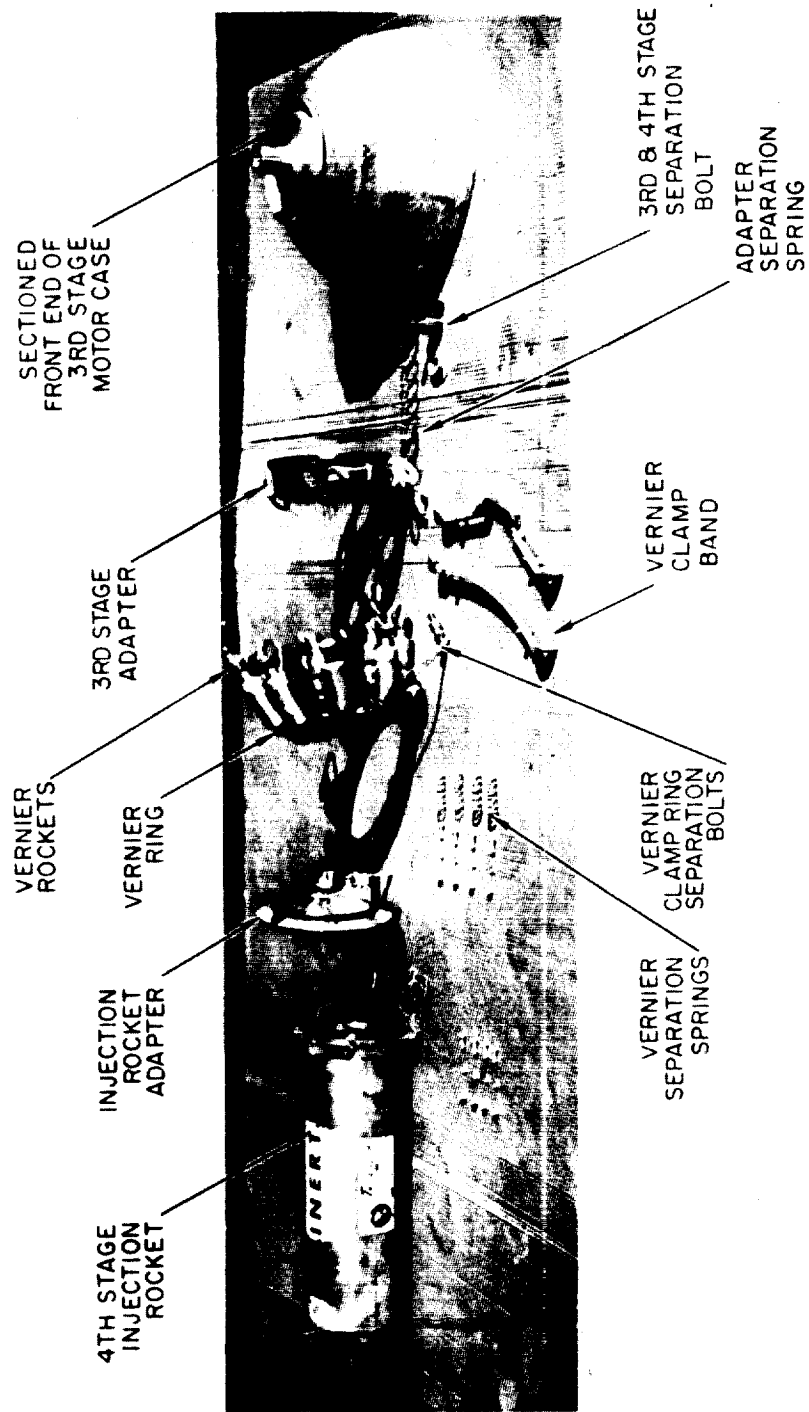
Figure 3-4.   Exploded View of Third to Fourth Stage Interconnect and
Separation Structure.

Able-1 launching vehicle. The in-flight event sequence governing vehicle operation is described in Section 3.6.2.

Control of the Able-1 launching vehicle was provided as follows:

a. First Stage

Angular control - - pitch, roll programs, first-stage control system

Cutoff - - propellant depletion (chamber pressure switch)

b. Second Stage

Angular control - - pitch program, second stage control system

Cutoff - - August, October shots, cutoff determined by second stage integrating accelerometer. November shot cutoff by radio command at predetermined value of radial range rate.

c. Third Stage

Angular control - - spin stabilization

Cutoff - - propellant depletion

d. Fourth Stage Vernier Rockets

Angular control - - spin stabilization

0 - 8 vernier rockets fired by radio command after third stage burnout. Number of rockets fired determined by vernier firing task described in Section 3.11

e. Fourth Stage Injection Rocket

Fired by radio command at a time determined by computations at the Able Operations Center.

3.1.3 Trajectory Considerations

a. Trajectory Constraints

The powered and free-flight trajectory was selected to maximize the probability of lunar capture for the expected vehicle dispersions considering several constraints.

(1) The injection rocket attitude and the third-stage attitude are the same in inertial coordinates.

(2) At the time of nominal injection rocket firing the vehicle should be well above the horizon of Hawaii (preliminary trajectory analysis indicated that the command transmitter for injection rocket firing should be located at Hawaii).

(3) The payload capability of the vehicle could not be excessively degraded.

(4) The relative velocity of the vehicle with respect to the moon had to be sufficiently low for the approximately 2800 ft/sec increment imparted by the injection rocket to result in capture.

b. Specific Trajectory

The basic considerations that were involved in the selection of nominal trajectories are discussed in the appendix.* These studies revealed that a free-flight trajectory with an initial flight path angle with respect to the local vertical of approximately 70° and an energy corresponding to a velocity of approximately 35,400 ft/sec at an attitude of 200 miles satisfied the above constraints and resulted in approximately maximum probability of success. As an example of a typical trajectory, the parameters for the nominal trajectory for 8 November are as follows.

Lift-off occurs at 0230 EST with an initial azimuth of 75.4°. Third stage burnout occurs 306 seconds later when the vehicle is 515 nautical miles downrange, at an altitude of 224 nautical miles and has an inertial velocity of 35,216 ft/sec. Details of the powered flight are summarized in Figure 3-5.

Following third-stage burnout, a nominal vernier correction adds a velocity increment of 74 ft/sec. At lift-off, the earth and moon are separated by 196,000 nautical miles (228,000 miles, 1189 million feet) from center to center. At the nominal retrorocket firing time of 3785 minutes, the center to center distance is 193,000 nautical miles (222,500 miles, 1174 million feet). After 3785 minutes, the vehicle is approximately 6250 nautical miles (7190 miles, 38 million feet) from the center of the moon. The velocity of the vehicle with respect to the moon at that time is approximately 4672 ft/sec. The retrorocket adds a velocity increment of 2750 ft/sec in a direction

_____
*See Lunar "Trajectories" in the Appendix, page 159.
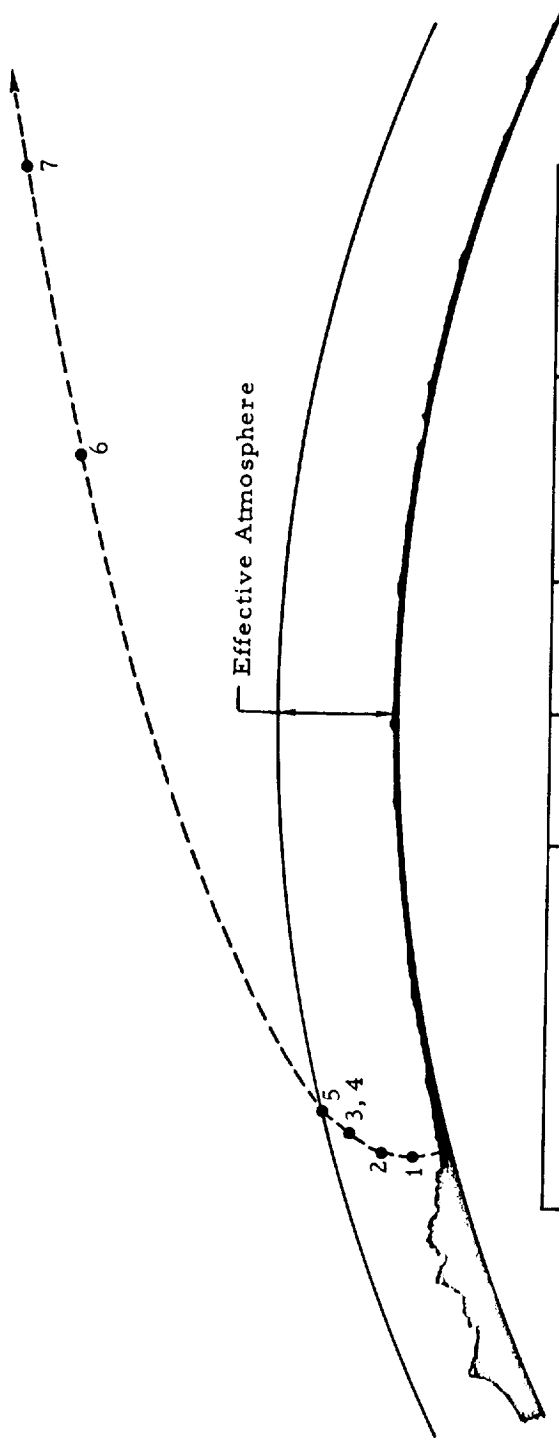
	Time (sec)	Altitude (naut mi)	Downrange Distance (naut mi)	Inertial Velocity (ft/sec)
1. Start (Vertical)	0	0	0	1342
2. Begin Gravity Turn	10	0.1	0	1349
3. End Gravity Turn	140	36.2	48.7	10520
4. Begin Const. Altitude	140	36.2	48.7	10520
5. First-Stage Cutoff	159.5	51.5	82.7	15927
6. Second-Stage Cutoff	269.3	168.7	371.5	23515
7. Third-Stage Cutoff	306.3	224.0	515.0	35216

Effective Atmosphere

Figure 3-5. Powered Flight Profile.

essentially opposing the original velocity but at a slight angle of approximately 10°. The velocity after the injection rocket is fired is 2201 ft/sec with respect to the moon. In the resulting orbit around the moon, the vehicle's closest approach to the moon is 1213 nautical miles (1398 miles, 7.38 million feet). The greatest distance from the moon is 12,420 nautical miles (14,300 miles, 75.6 million feet).

Figure 3-6 shows a profile of the nominal free-flight trajectory to the vicinity of the moon. Figure 3-7 shows the effect of the retrorocket upon the payload velocity with respect to the moon, and Figure 3-8 shows a typical lunar orbit.

c. Allowable Dispersions

For the specific trajectories selected, a typical set of maximum dispersions which, after vernier firing, would still result in lunar capture are:

Velocity error	$\pm$ 100 ft/sec
Flight path angular error	$\pm$ 2.5°
Azimuth error	$\pm$ 5°

These allowable errors were coupled with a dispersion analysis of the powered flight of the vehicle in order to calculate probability of success (including reliability factors).

To illustrate the motivation for the development of the command/ doppler vernier systems and Stage 2 cutoff system, the calculated probabilities for these cases are tabulated below.

System	Peak Probability	Comments
Accelerometer Stage 2 cutoff only	0.35	Originally conceived system
Accelerometer cutoff and command/doppler system	0.57	Permits retrorocket firing on command
Accelerometer cutoff command/ doppler and vernier	0.73	This system carried in August and October
Doppler cutoff of Stage 2, command/doppler and vernier	0.87	This system carried in November

10,000 miles = 1/2 inch
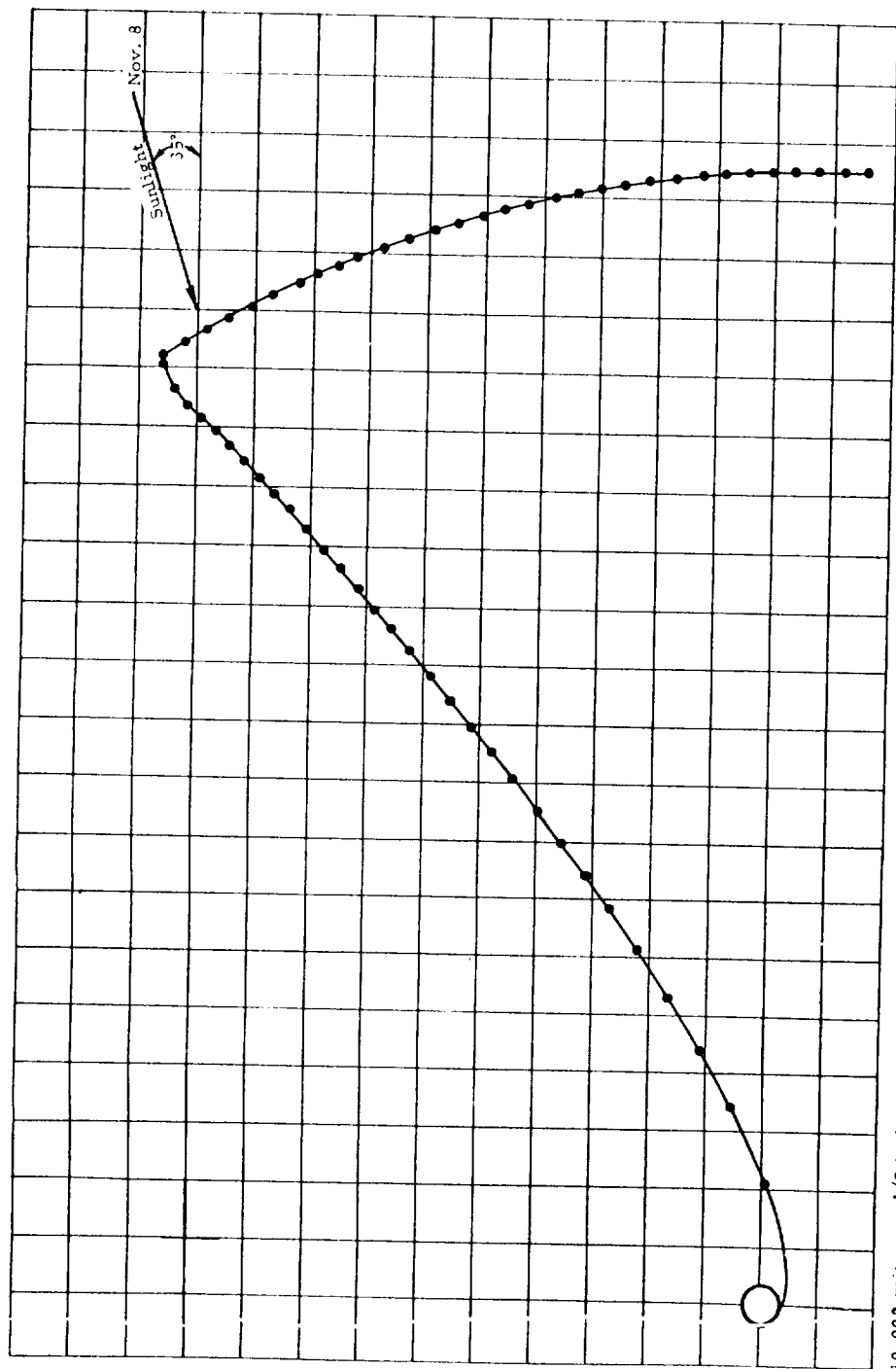
Figure 3-6.   Pre-Flight Trajectory Profile for November 8, 1959 (Nominal).
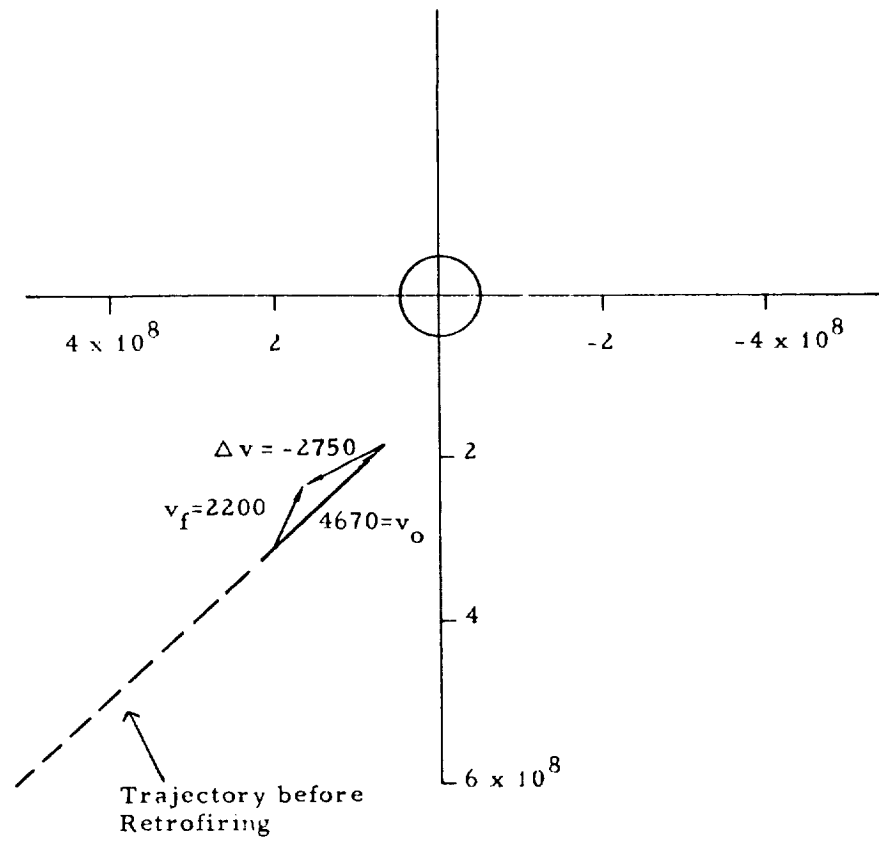
Figure 3-18. Effect of the Retrorocket Upon the Payload
Velocity with Respect to the Moon.
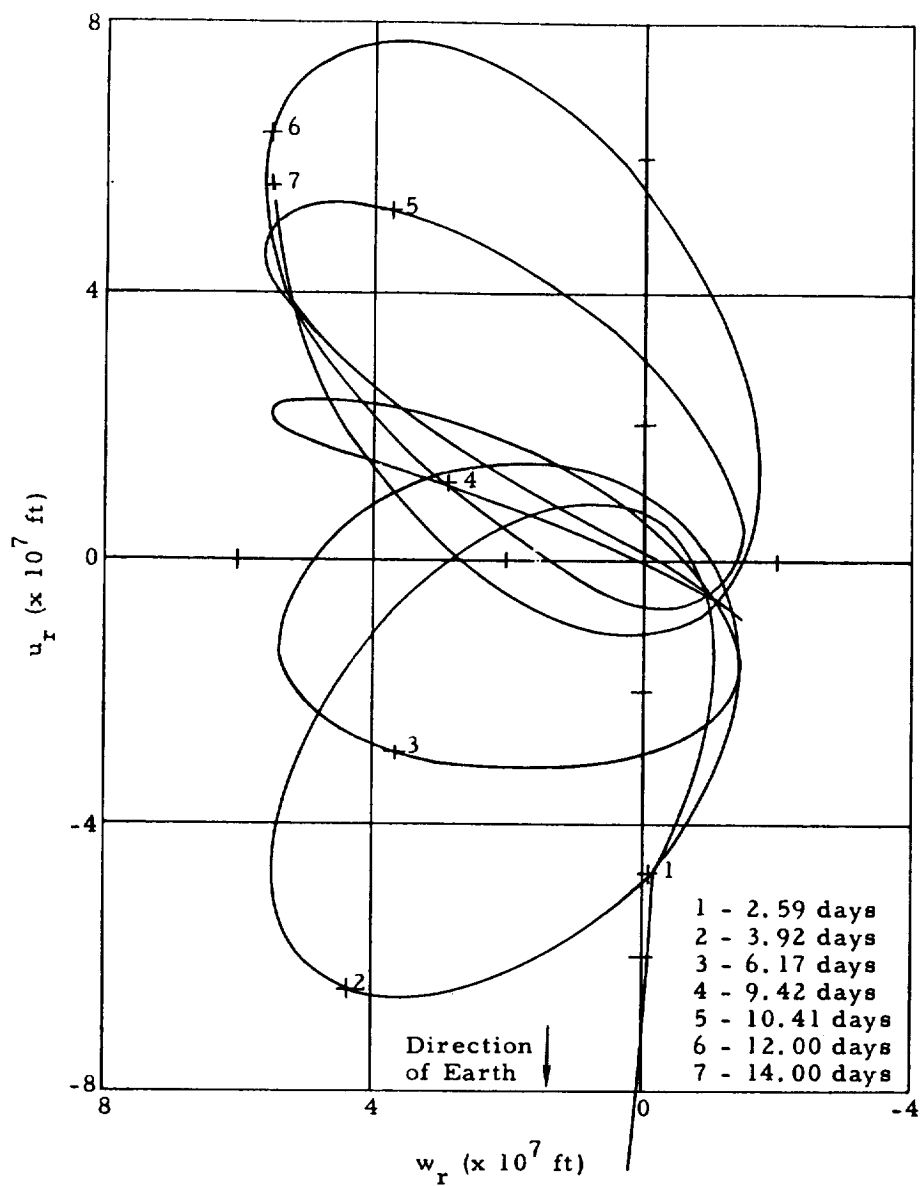
Figure 3-8. Nominal Lunar Orbit in Moon-Centered, Rotating Coordinates (u_r, w_r plane) (August 18th Launch Date).

3.1.4   Launch Interval

Early in the Able-1 development program the decision was made to provide no trajectory compensation for launch holds. Early trajectory studies revealed that a launch interval of the order of 15 minutes was possible without compensation. A study of holds in prior Thor countdowns revealed that unless a launch interval of the order of an hour or more could be provided, the extra complexity of changing programmer and cutoff settings from the blockhouse during the terminal count was not warranted. Performance studies revealed that an excessive performance penalty would result from compensation for a one-hour interval, motivating the decision for no compensation.

Compensation for launching on different days was accomplished through the use of a different Thor roll program for each day of launch. It was therefore necessary to define fairly precisely the time interval over which the vehicle could be launched and the number of days of possible launches per month. This was done by means of a study which first determined, from the allowable and actual dispersions, the probability of orbiting versus time of launch for each of the likely launch days. (It had first been determined that only four days each month resulted in adequately high peak probabilities.) Figures 3-9 and 3-10 show the probability of lunar capture as a function of time on launch dates 7 August 1958 and 7 November 1958. (Note higher probability in November due to doppler shutoff.)

Using these curves and making certain assumptions regarding countdown operations, missile performance, and missile reliability, it is possible to calculate a "probability of success" and choose optimum times for attempting a launch.

The principal assumptions are:

a.   The probability of getting to T minus 35 minutes on a day following a "scrub" is 0.85.

b.   The probability of getting from T minus 35 to T minus 0 within the allotted time is 0.60.

c.   The reliability of the missile (i.e. the probability of operation in flight with no significant malfunction) is 0.80.
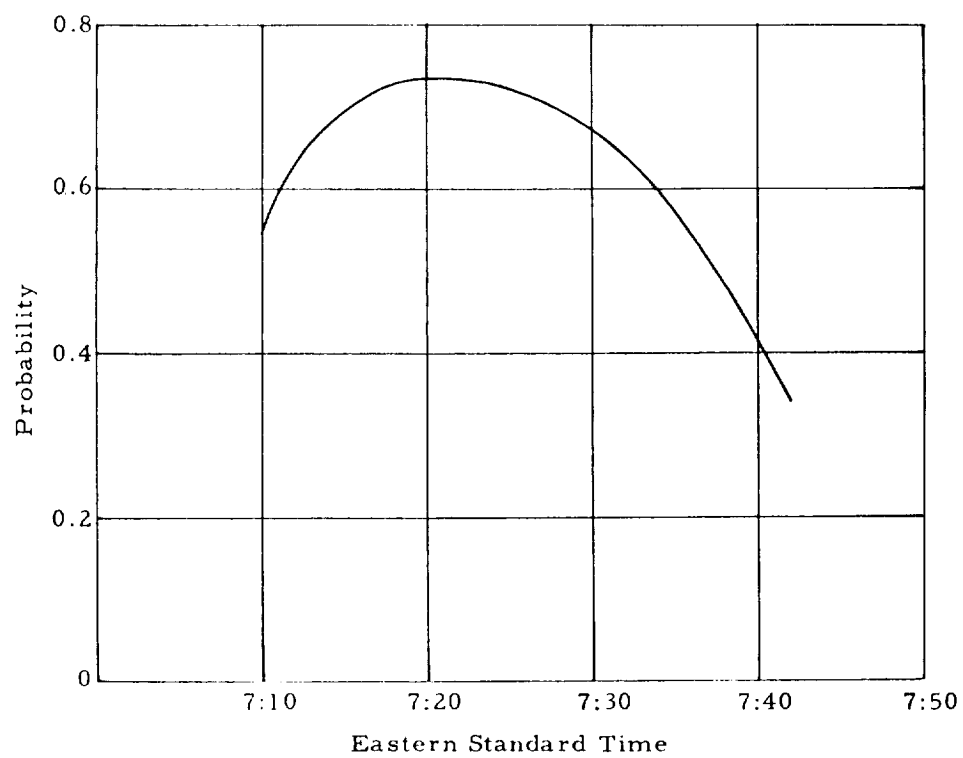
Figure 3-9.   Probability of Lunar Capture Versus
Lift-off Time on 17 August 1958.
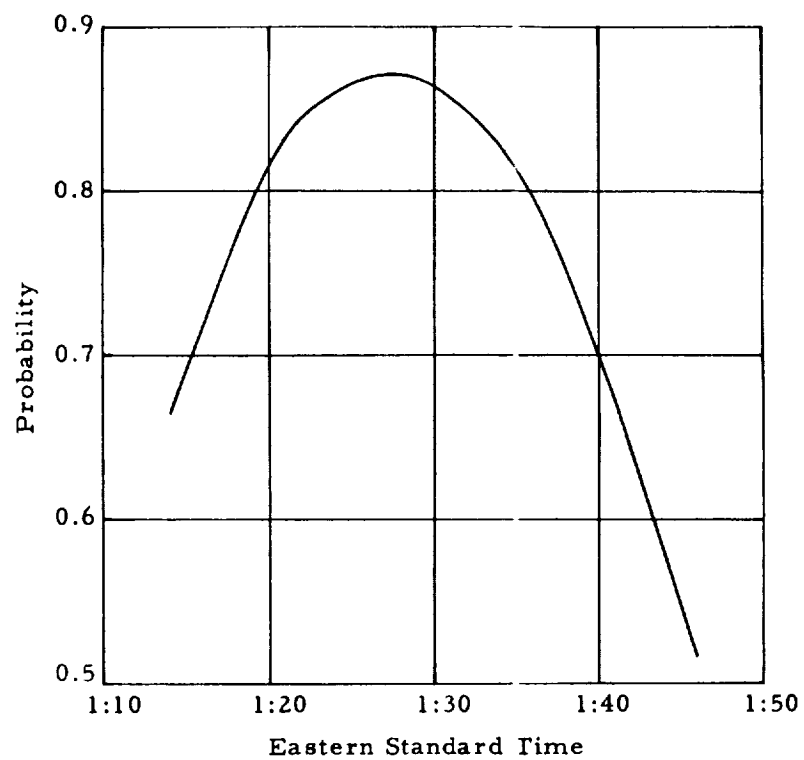
Figure 3-10. Probability of Lunar Capture Versus
Lift-off Time on 7 November 1958.

The curve of Figure 3-11 shows the composite "probability of success" versus time. As long as the countdown is continuing on schedule, the solid curve prevails. If, on a given day, the test is scrubbed, refer to the lower, or dashed, curve.

A calcualtion of optimum launch cutoff times (i.e., after this time it is better to wait until the following day) gave these results for the August launch.

	Nominal Launch Time, T minus 0	Cutoff Time
17 August	0714 EST	0734 EST
18 August	0818 EST	0842 EST
19 August	0919 EST	0945 EST
20 August	1017 EST	---

The actual allowed launch interval for each day was thus in excess of 20 minutes.

3.2 Structure

3.2.1 Structural Description

a. Stage 1.

No major changes were made in the basic Thor airframe. The three nose cone latches were removed from the guidance bay, and the first-stage transition section was bolted on at those points. This structure, designed by STL and built by Aerojet-General, is a semi-monocoque conical frustum employing aluminum frames and stringers and mag-thorium skin. The design provides a two-inch high circumferential gap between the transition section and the top of the Thor to permit the efflux of second-stage engine exhaust during thrust build-up. During first-stage operation the gap is covered with an aluminum alloy blast band held in place by two explosive bolts. These bolts are fired to jetti-son the band just before second-stage engine ignition. Ignition of either bolt will insure jettisoning of the band.

A thin nonstructural stainless steel heat shield covers the first-stage transition section and is separated from the mag-thorium skin by spiral windings of 3/16th-inch diameter Refrasil Cord, spread 1-1/2 inches apart.

18
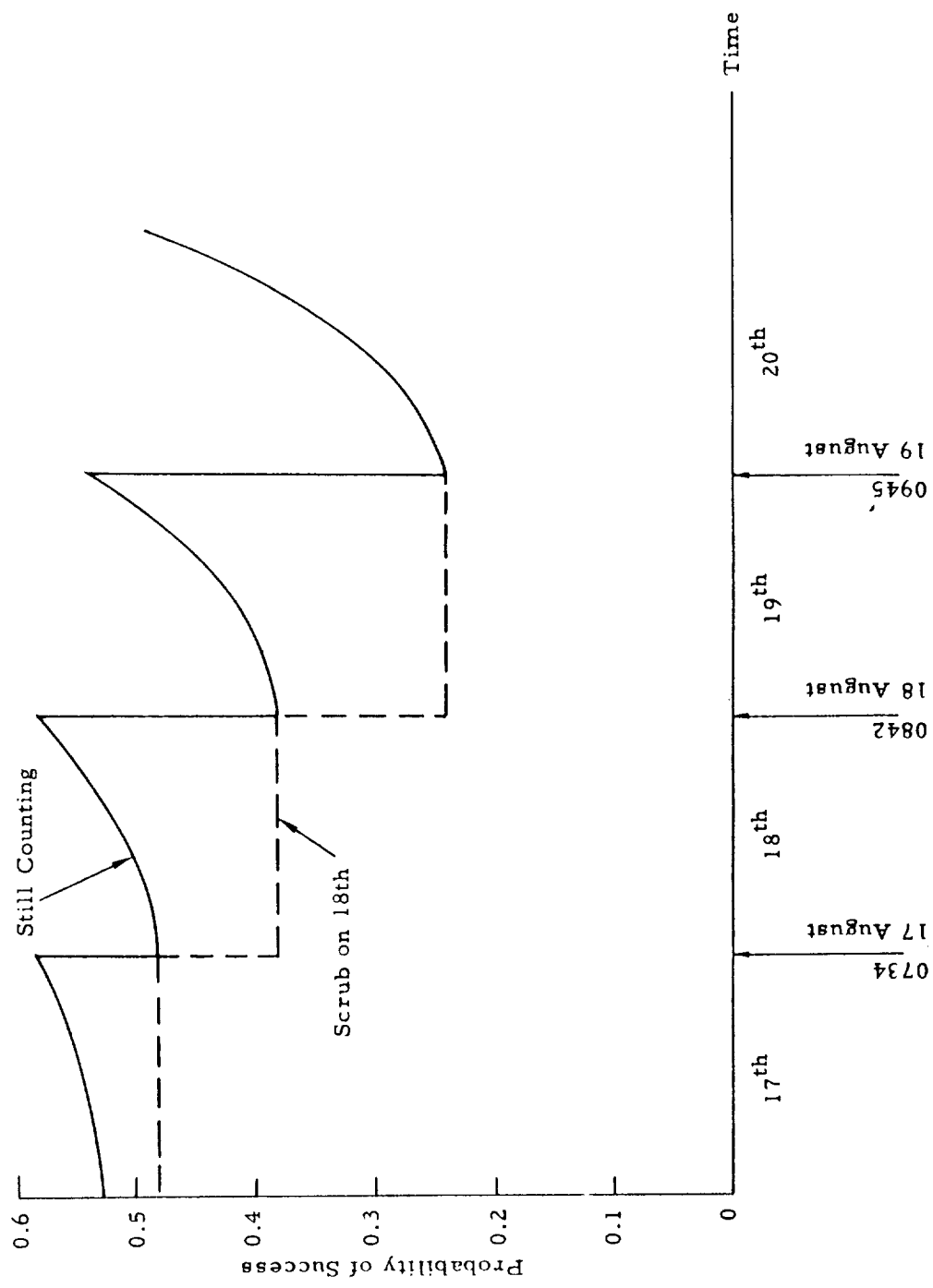
Figure 3-11. Probability of Success versus Time (August).

b. Stage 2.

No structural changes were required in the basic AJ 10-40 tankage. The second-stage tankage is a welded type 410 stainless steel structure, and consists of a fuel tank, oxidizer tank, and a helium tank which also acts as a bulkhead between the two tanks. Short stainless steel tank extensions are welded to the fuel tank (forward) and to the oxidizer tank (aft). Two semimonocoque mag-thorium cylinders are attached to the forward and aft tank extenstions and are referred to as the forward and aft skirts.

The control compartment is attached to the forward tank skirt and is a cylindrical semimonocoque structure employing aluminum frames and stringers and mag-thorium skin. This structure has two large access doors that are load carrying when in place. There is a central web that divides the control compartment longitudinally and serves as an equipment mounting surface. An aluminum channel spans each end of the control compartment and is attached to the web and frames. The jettisonable nose fairing is supported on a ring at the forward end of the control compartment. The third-stage rocket nozzle is attached to the forward channel by two explosive bolts preloaded in tension and two shear pins. Four socket fittings attached to the compartment periphery at its forward end accept the four compression struts which support the third stage. The spin rockets (eight on the first two flights, twelve on the third flight) are mounted on brackets inside the control compartment at the forward end, and on the third flight, two small separation retrorockets were also mounted to the control compartment structure. A portion of the control compartment and the third-stage support structure are shown in Figure 3-12.

The mag-thorium monocoque cylindrical skirt attached to the aft tank extension includes two load-carrying circular access doors, and joins the tankage to the conical frustum second-stage transition section. The second-stage transition section attaches to the first-stage transition section at the separation plane by four explosive bolts. The second-stage transition section is a semimonocoque structure employing aluminum frames and stringers and mag-thorium skin, and is the same design employed on the original Able vehicles.

A stainless steel heat shield similar to that on the first-stage transition section covers the second-stage transition section.
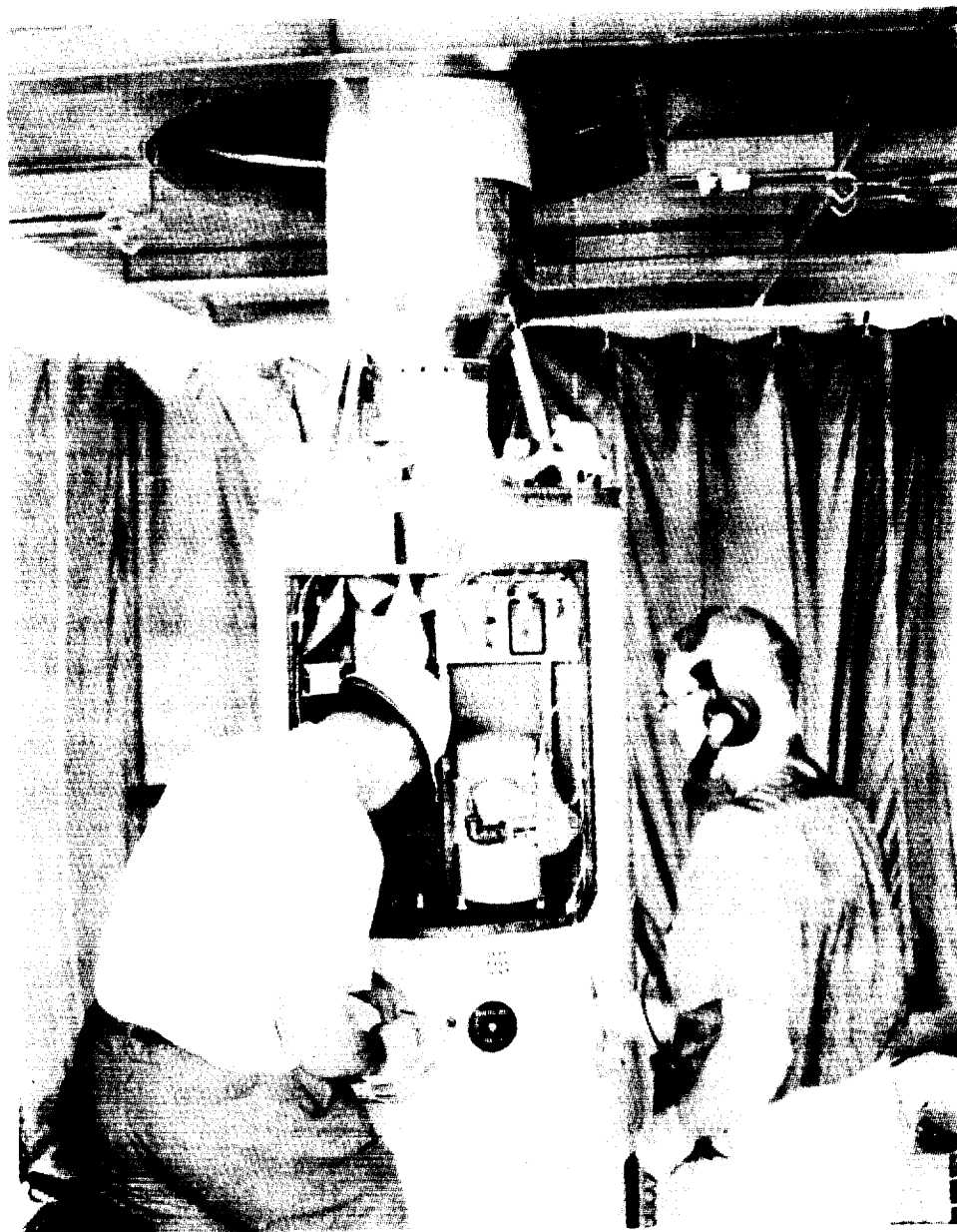
Figure 3-12. Control Compartment and Third Stage Support Structure.

The control compartment, second-stage transition section, and heat shield were all designed by STL and fabricated by Aerojet-General.

c. **Stage 3.**

The third stage consists of the ABL X-248-A3 rocket motor and interconnecting structure. The second-stage to third-stage interconnecting structure consists of a group of four ball-end aluminum tube struts preloaded in compression on installation, and the third-stage rocket nozzle itself. The upper ends of the compression struts are inserted into socket fittings mounted on a circumferential band that is bonded to the aft end of the rocket case. Figure 3-13 shows the strut installation. The strut preload is large enough to resist all flight bending moments without permitting any strut to go out of action, and it is reacted internally by a tension load in the nozzle itself. The compression struts are individually calibrated to insure that the proper preload is obtained when the struts are installed. The tension load is provided by the two explosive bolts which clamp the nozzle exit plane flange to the transverse beam in the second-stage control compartment. Two shear pins mounted in this beam transmit shear forces across the separation plane from the rocket nozzle.

The Stage 3 - 4 interconnect structure consists of a single explosive bolt and two annular compression members made from magnesium castings, as shown in Figures 3-3 and 3-4. The aft compression member, the third-stage adaptor, bears on the outer flange of the third-stage rocket motor boss. The forward compression member also supports the vernier rockets, and is clamped to the fourth-stage adaptor fitting by a circumferential band held together by two explosive bolts which permit its eventual jettisoning. Ignition of either bolt will insure jettisoning the assembly. The fourth-stage injection rocket adaptor fitting is made from a magnesium casting and is bolted to the aft end of the injection rocket. The Stage 3 - 4 separation bolt connects the third-stage case rocket boss to the fourth-stage adaptor fitting, and its tension preloads the compression members sufficiently to resist all in-flight bending moments. The boss on the head end of the rocket case was modified to provide a satisfactory means of structural attachment for the payload. A ring and four strut support fittings were attached to the case, just forward of the nozzle, by
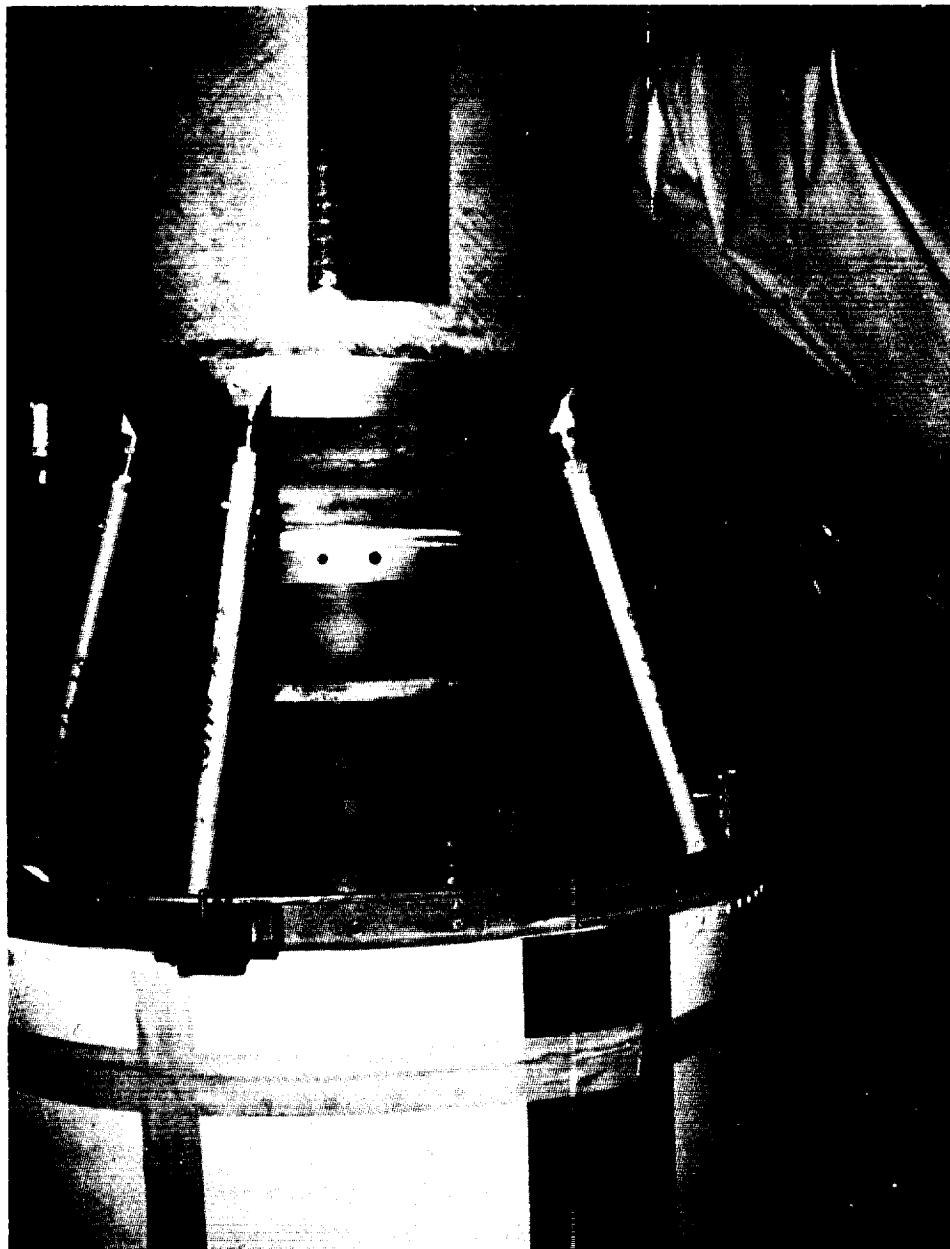
Figure 3-13.   Third Stage Support Strut Installation.

means of adhesives. Firing tests were made with this modification to assure the structural integrity of the case had not been impaired.

All interconnecting and separation structure was designed and fabricated by STL.

d. Payload Structure.

The payload shell, which is composed of a short cylindrical portion and two conical frustums, is made from honeycomb fiberglass consisting of a Hexcel core of nylon resin-impregnated glass cloth bonded to epoxy-impregnated glass cloth faces. Equipment is mounted on the inner periphery of the cylindrical portion which is locally reinforced where required. The cylindrical portion is supported off the injection rocket case by the two conical frustum ends and by a central aluminum spider ring. A ring to provide a satisfactory mounting surface was added at the bend end of the case. The payload structure, shown in Figure 3-3, was designed by STL and fabricated by Summit Industries.

e. Nose Fairing.

The two-piece clamshell nose fairing was designed by STL and fabricated by Aerojet-General. It is made of thin layers of fiberglass cloth impregnated with phenolic resin. The two halves are held together by two explosive bolts and two pyrotechnic actuators which when fired eject the two halves radially outward from the missile. The fairing was designed to sustain the aerodynamic loads and heating occuring during first-stage operation, and is jettisoned 10 seconds after second-stage initiation.

3.2.2 Structural Design Criteria

The following structural design criteria were employed in the design of the Able-1 airframe:

a. Strength and Rigidity

The structure was designed to sustain design limit loads within the design environment without experiencing excessive yielding or deflections which would cause malfunction or failure of structure and components. Design limit

loads are those loads which may be expected during normal handling and operation of the vehicle. The occurrence of certain flight loads is predicted on a statistical basis.

The structure was designed to sustain design ultimate loads within the design environment without experiencing structural failure. Design ultimate loads are the product of design limit loads and an appropriate factor of safety. The factor of safety used for external loads was 1.25. For loads due to internal pressures, larger factors of safety were used in the range from 1.33 to 1.50.

b. Structure Allowables

Material properties were obtained from recognized sources, including ANC-5, NACA-TN's, and material fabricators' reference data. The effects of temperature on allowables were accounted for. Instability allowables were obtained by conservative, rational analyses and, where possible, from published test data. The structural allowables for critically loaded composite structures were verified by structural confirmation tests.

c. Environment and Loads

Basic external loads and environment were determined by conservative, rational analyses and, where analysis was not possible, by engineering judgment based on experience with other missiles. Results of wind tunnel tests were used in predicting aerodynamic forces.

d. Internal Load Distributions and Margins of Safety

Internal load distributions and critical loading conditions for each structural member were determined by analysis. The effects of extreme temperatures, transient heating, structural deflections, and dynamic loading were either included in the analyses, or conservative assumptions were made. Positive margins of safety were required, and were shown analytically and/or demonstrated by test.

3.2.3 Structural Design Conditions

A number of loading conditions were considered in the structural design, including the following:

a. Transportation and Handling

Care was exercised to prevent transportation and handling from causing loads large enough to affect the structural design.

b. Prelaunch

An analysis was made to determine the maximum steady-state ground wind the structure could withstand for the vehicle in the prelaunch condition, considering both steady-state loads and dynamic loads due to vortex shedding. That velocity was found to be 44 knots.

c. Flight

The airframe was largely designed by powered flight loads and temperatures. A first-stage trajectory causing maximum external loads and aerodynamic heating was employed in design. It was established that first-stage, second-stage, and a portion of third-stage structure were critically loaded either near the time of maximum dynamic pressure and angle of attack or at first-stage burnout. Other third-stage structural components and the fourth-stage structure were critically loaded at third-stage burnout. The design conditions used for these three times of flight are summarized below.

(1) Maximum Dynamic Pressure and Angle of Attack

Flight time, $t \cong 60$ sec

Dynamic pressure, $q = 850$ psf

Angle of attack, $\alpha = 7$ deg

Engine deflection, $\delta = 7$ deg

Axial acceleration, $n = 2.2$ g

The angle of attack used to determine loads at the time of maximum dynamic pressure is the maximum angle achieved as a result of flying trimmed through the Sissenwine 99 per cent horizontal wind profile, and occurs in the near vicinity of maximum dynamic pressure. The use of the combination of maximum dynamic pressure and maximum angle of attack helps account for uncertainties in the actual trajectory. The corresponding engine gimbal angle

shown above is not the trim angle, but represents a 100 per cent increase to account for effects not included in the load analysis such as gusts, missile elastic effects, and engine overtravel.

(2) Stage 1 Burnout

Flight time, $t \simeq 156$ sec

Dynamic pressure, $q = 0$

Engine deflection, $\delta = 3$ deg

Axial acceleration, $n = 12.2$ g (assumed 1 per cent PU error)

This condition is accompanied by critical aerodynamic heating of all major structural components. The exact engine deflection at burnout cannot be predicted; but based on previous Thor flights, the 3 degree value used above represents a conservative value.

(3) Stage 3 Burnout

Flight time, $t \simeq 312$ sec

Axial acceleration, $n = 24.4$ g

3.2.4 Dynamic Considerations

A number of important dynamic considerations were taken into consideration, including the following:

a. Bending Modes and Frequencies

For the autopilot design, it was necessary to compute the bending modes and frequencies of the vehicle for various times of flight. Frequencies for the entire vehicle were significantly lower than those for the Thor missile; for example, the lowest in-flight bending frequency was 3.27 cps as compared to 6.95 cps for the Thor alone. As a result, various changes were made in the first-stage autopilot.

b. Axial Modes and Frequencies

Axial modes and frequencies were calculated to help establish the proper staging time delay between first-stage MECO and second-stage separation so that no impact would occur between stages.

c.   Torsional Modes and Frequencies

Torsional frequency calculations were made for the third and fourth stage combination to determine whether the lowest torsional frequency was sufficiently removed from the spin rate to prevent its being excited. It was found to be 26 cps which indicated that spin-up would not cause oscillations.

d.   Spin Stabilization of Third Stage

At second-stage burnout, eight spin rockets are fired to impart a rotation of about 2.5 revolutions per second to the vehicle. This spin rate reduces to a negligible amount the effects of both Stage 3 thrust misalignment and residual turning rate on the third-stage velocity vector. Spin also obviates the requirement for active attitude control systems during third- and fourth-stage burning.

A spinning body that has any energy dissipation (damping) will eventually rotate about its largest moment of inertial axis. The payload vehicle (Stage 4) is designed such that its largest moment of inertia is about the roll axis and the initial spin-up is about this axis. However, the pitch-yaw movement of inertia of the third- fourth-stage combination is greater than its roll moment of inertia. To obtain the desired ratio of inertias as soon as possible after spin-up, separation of the third stage occurs immediately after it has burned out.

e.   Angular Precession of Payload

Successful operation of the television camera required that any precessional angular velocity of the payload existing after injection rocket firing be reduced to zero within 30 minutes.

Extraneous torques from various sources will generate a precessional motion, or wobble, in the spinning vehicle. These disturbances can result from misalignment of the spin-up rockets, separation angular impulses, micrometeorite impingements, third stage and injection rocket thrust misalignments, and center-of-gravity offsets. A large spin momentum will keep the wobble angle relatively small, but will not damp out the motion. Therefore, a damping system is required to reduce the precessional motion.

Dynamic tests (see Section 3.2.8) indicated that more damping capability than afforded by structural damping would be required, so a damper device, developed initially by the Naval Ordnance Test Station at Inyokern, was designed and mounted on the payload about its spin axis. This device consists of an annular tube partially filled with mercury, and removes energy through viscous shear resulting from relative motions in the mercury induced by any precessional motions of the spinning body.

3.2.5 Weight and Balance

The nominal values for the weights, horizontal centers of gravity, and moments of inertia are given in Table 3-1. The weights and centers of gravity are based on modified test data. The moments of inertia are computed (no test data were available). Table 3-1A presents the estimated weight, balance and moment of inertia data for Missiles 130 and 129 at second stage cutoff. The data are presented for second stage alone and for second, third and fourth stages for locations of the residual propellants.

3.2.6 Aerodynamic Heating

Aerodynamic heating calculations were performed for various portions of the Able-1 vehicle. The critical locations from a structural and heating point of view were the second stage control compartment, the second stage engine skirt, the interconnecting fairing between first and second stages, and the guidance compartment of first stage. It was found that the 0.090-inch magnesium alloy skin of the interstage would severely overheat unless protected. Consequently, a 0.010-inch stainless steel shroud was wrapped around the interstage and separated from the magnesium skin by refrasil windings. The temperatures predicted at the other locations were within allowable limits.

A fiberglas heat shield was designed for the telemetering antenna on the second stage control compartment to protect the antenna against aerodynamic heating. Likewise, an analysis was made of the heating which the payload structure would experience after the nose fairing was jettisoned. It was found necessary to delay the jettisoning until 10 seconds after blowing

Table 3-1. Weights, Centers of Gravity, and Moments of
Inertia Values for Able-1.

Condition	Time sec	Weight lb	Horiz. C.G. sta., in.	I_{Pitch} slug ft^2	I_{Roll} slug ft^2
Stages 2 + 3 + 4 + nose-fairing + Stage 1 - 2 transition section	159.5	4988.8	214.7	5630.1	83.3
Stages 2 + 3 + 4 + nose-fairing	159.5	4898.1	212.3	5261.1	75.2
Stages 2 + 3 + 4 + nose-fairing	169.5	4603.0	212.1	4736.1	57.6
Stages 2 + 3 + 4	169.5	4490.1	215.6	4720.0	52.0
Stages 2 + 3 + 4 at Stage 2 cutoff	265.9	1790.0	179.3	3130.0	51.4
Stages 3 + 4	267.9	594.1	83.5	41.3	5.7
Stages 3 + 4 at Stage 3 burnout	305.4	127.8	70.6	18.3	1.8
Stage 4 including verniers	469.5	82.1	53.3	1.1	1.4
Stage 4	775.0	76.4	52.3	1.1	1.4
Stage 4 at injection rocket burnout		52.3	52.2	0.9	1.3

Table 3-1A. Weights, Balance, and Moments of Inertia Values for
Missiles 129 and 130 of Able-1 at Stage 2 Cutoff.

Missile	Item	W	Horiz. C. G.	I_{Pitch}	I_{Roll}
Able-1 No. 2 (Missile No. 130)	Stage 2 jettison, fuel and oxid. at bottom of tanks	1231	228.6	1172	46
	Stage 2 jettison fuel at top, oxid. at bottom	1231	226.0	1253	46
	Stage 2 jettison oxid. at top, fuel at bottom	1231	217.9	1007	46
	Stages 2 + 3 + 4 at St. 2 MECO fuel and oxid. at bottom of tanks	1828	181.2	3197	53
	Stages 2 + 3 + 4 at St. 2 MECO fuel at top, oxid. at bottom	1828	179.5	3059	53
	Stages 2 + 3 + 4 at St. 2 MECO oxid. at top, fuel at bottom	1828	174.1	2615	53
Able-1 No. 3 (Missile No. 129)	Stage 2 jettison, fuel and oxid. at bottom of tanks	1186	227.9	1129	44
	Stage 2 jettison, fuel at top, oxid. at bottom	1186	226.1	1208	44
	Stage 2 jettison, oxid. at top, fuel at bottom	1186	217.0	970	44
	Stages 2 + 3 + 4 at St. 2 MECO fuel and oxid. at bottom of tanks	1787	179.3	3125	51
	Stages 2 + 3 + 4 at St. 2 MECO fuel at top, oxid. at bottom	1787	178.1	2990	51
	Stages 2 + 3 + 4 at St. 2 MECO oxid. at top, fuel at bottom	1787	172.0	2556	51
Nominal Condition	Stage 2 jettison, fuel and oxid. at bottom of tanks	1196	226.9	1138	45
	Stage 2 jettison fuel at top, oxid. at bottom	1196	225.6	1218	45
	Stage 2 jettison, oxid. at top, fuel at bottom	1196	217.6	978	45
	Stages 2 + 3 + 4 at St. 2 MECO fuel and oxid. at bottom of tanks	1790	179.3	3130	51
	Stages 2 + 3 + 4 at St. 2 MECO fuel at top, oxid. at bottom	1790	178.4	2995	51
	Stages 2 + 3 + 4 at St. 2 MECO oxid. at top, fuel at bottom	1790	173.1	2560	51

the first stage-second stage separation bolts in order to keep the payload covering temperature within allowable limits.

3.2.7 Structural Tests

Structural confirmation tests were performed on the following structural components:

a. Interstage structure assembly between Thor and AJ 10-101, including the following components:

Skirt assembly (aft)	AGC Dwg. No. 0-050075
Stage 2 transition	AGC Dwg. No. 1-053801
Stage 1 transition	AGC Dwg. No. 1-053721
Bracket Assembly	AGC Dwg. No. 1-054293

The assembly was tested for both limit and ultimate critical loading conditions (see Section 3.2.3). Results indicated that the structure would sustain limit loads without excessive deformation, and ultimate loads without rupture. The assembly was then loaded axially until failure occurred at loads slightly larger than the equivalent combination of critical ultimate axial load and critical bending moments.

b. Nose Fairing Assembly--AGC Drawing No. 1-055027. The structure successfully withstood a test which simulated the airloads at maximum dynamic pressure.

c. Stage 2 to Stage 3 Attachment. Although no structural test of the over-all assembly was performed, the compression rods and their end fittings were tested at loads greater than the required preloads (limit load) without excessive deformation or failure. Torque equal to approximately 1.25 times the applied torque was applied to the strut adjustment screws so that the load in the struts was approximately equal to the ultimate load for the strut. There was no failure of the engine case, the struts or the nozzle hold down attachment.

d. The final payload package successfully withstood all environmental vibration and centrifuge acceleration tests.

e. Douglas Aircraft analysis and test results on Thor guidance bay and tank structure indicated ample margins for Able-1 loads.

f. The second-stage tankage was extensively pressure-tested by Aerojet during development. Able-1 flight loads were not to be critical for this structure.

g. The second-stage control compartment stress analysis indicated margins of safety large enough to make testing not mandatory for Able-1.

h. The third-stage ABL 248 case stress analysis indicated margins of safety large enough to make testing not mandatory for Able-1.

It was not considered necessary to perform structural confirmation tests on any other portion of the Able-1 airframe.

3.2.8 Functional and Dynamic Tests

Dynamic tests were made as follows:

a. Nose Fairing Jettison Tests

Tests were performed at the Aerojet Azusa facility to demonstrate the ability of the nose fairing pyrotechnic actuators to cause satisfactory separation of the two halves of the nose fairing. All explosive bolts and actuators functioned properly, and proper jettisoning was observed. The actuators for the jettisonable nose fairing were designed to project the two halves of fairing laterally outward from the vehicle with a velocity of 10 ft/sec, sufficient to prevent collision with the second-stage.

b. Damping of Payload Precession

Structural damping of a model payload was measured by suspending it as a torsional pendulum in an altitude chamber. It was found that the measured damping was too small to meet the requirements. The NOTS mercury damper was attached to the payload, and subsequent tests showed that the damper reduced a 5° precession angle to zero in less than 30 seconds.

c. Dynamic Balancing of Payload

The dynamic balance of the Able-1 flight payload was checked by spinning it on a test fixture. It was found that dynamic balancing was not necessary if the components were symmetrically mounted and the payload was statically balanced.

d. Test of Separation Capability

A test of the separation capability of the first-stage, second-stage interconnect structure was made at Aerojet. The transition section was attached to the second-stage and the sequence of separation was initiated. The blast doors were jettisoned and the separation bolts were fired. Internal temperatures and pressures were measured in the second-stage engine compartment. All items functioned properly without damaging temperature or pressure rise.

3. 3   Propulsion

3. 3. 1   First Stage

Procurement of Thor Vehicles Numbers 127, 129, and 130 for use in Able-1 tests was accomplished through BMD as GFE. Deliveries were made directly from Douglas Aircraft Company to AFMTC by Air Transport.

The Thor is powered by the North American XLR79-NA-5 engine developing a sea-level thrust of approximately 150, 000 pounds and regeneratively cooled by RP-1. Thrust vector control is provided by gimbaling of the main engine. Two vernier engines each rated at 1000 pounds thrust are provided for roll control and final adjustment of burnout velocity.

Nominal engine performance (including main engine and verniers) for Missile 129 as well as variation of thrust, specific impulse and flow rate during the flight to altitude are given in Table 1, see Appendix D (confidential).*

3. 3. 2   Second Stage

The second stage, Aerojet Model AJ 10-101 rocket propulsion system, consists of a gimbaled, regeneratively cooled-thrust chamber, propellant tanks, helium pressurization system, interconnected plumbing, gimbal actuator, roll-control system, separation system for detachment from first and third stage, necessary airframe structures, and a destruct system.

The thrust chamber is rated at 7800 .b nominal thrust in vacuum but when roll control is used the slight reduction in tank pressure causes a reduction in thrust and flow rate as shown in Table 3-2. Nominal specific impulse is 271 seconds in vacuum. The propellants utilized are inhibited white fuming nitric acid (WIFNA) as the oxidizer and unsymmetrical dimethylhydrazine (UDMH) as the fuel, with a nominal mixture ratio of oxidizer of fuel of 2. 8:1 by weight. The propellants are pressure fed to the thrust chamber by high pressure helium augmented by a solid propellant heat generator.

Thrust vector control is accomplished by gimbaling the engine in response to pitch and yaw signals from the guidance system. Roll control is achieved by expelling regulated pressurized helium gas through two nozzles for clockwise and two nozzles for counterclockwise motion.

*This Confidential Appendix is printed under a separate cover.

Table 3-2. Stage 2 Thrust Table

$$I_{sp} = 271 \text{ sec}$$

Time sec	6-sec roll control	
	F lb	Wt lb/sec
0	7780	28.7
5	7780	28.7
10	7780	28.7
15	7750	28.6
20	7720	28.5
25	7700	28.4
30	7670	28.3
35	7670	28.3
40	7670	28.3
45		
50	↑	↑
55		
60		
65		
70		
75		
80		
85	↓	↓
90		
95	7670	28.3
t* = 97 sec		
100	7620	28.1
102	7480	27.6
104	7370	27.2
106	7260	26.8
108	7150	26.4
110	7020	25.9
112	6910	25.5

t* = begin of thrust decay due to depletion of helium for 6 seconds of roll control. Additional impulse from engine after shutoff command 1600 lb-sec.

Procurement of the AJ 10-101 stages was accomplished through BMD as GFE. The second-stage transition section and control compartment were supplied through Aerojet by subcontractors. The nose fairing was fabricated by Aerojet. The brackets, etc., for the control-compartment equipment, the third-stage supports, the third to forth structure and the payload structure were obtained from subcontractors or were fabricated in STL shops.

3.3.3 Third Stage

The vehicle employed as the third stage of the Able-1 missile was a solid propellant motor which was developed by the Allegheny Ballistics Laboratory under contract with BuOrd. This unit, designated X-248A2, was developed as an advanced high-performance third stage for the Vanguard missile, but had not been flight tested. It was therefore necessary for BMD/STL to evaluate the performance of this motor at altitude, prior to its use on Project Able-1.

Data obtained from wind-tunnel tests at a simulated altitude of 100,000 feet indicated that the rocket would achieve the required velocity increment for the specified payload weight. However, the tests revealed the necessity of a complete redesign of the ignition system. This igniter redesign was a joint effort between the Space Technology Laboratories and the Allegheny Ballistics Laboratory, and the unit designation was changed to X-248A3 to identify the new igniter. Evaluation testing of the new ignition system was conducted at the Allegheny Ballistics Laboratory's facilities with STL representatives witnessing all tests and participating in their evaluation. Table 3-3 summarizes the tests that were conducted with this motor and Table 3-4 is a similar summary of the igniter development tests.

The physical characteristics and nominal performance of the X-248A3 motor are listed in Table 2, see Appendix D, confidential). The propellant utilized by this unit is a double-base composition designated as BUU. The motor case is of fiberglass constructed and is a product of the Young Development Laboratories. The nozzle expansion section is steel and conical in configuration. The resulting mass fraction is 0.890 based on the propellant weight and 0.907 ba based on the weight consumed during firing of the motor. The base on the head of the rocket case was modified to provide a satisfactory means of structural attachment for the payload. A ring and 4 stru support fittings were attached to

Table 3-3. Summary of ABL X-248 Motor Test Firings.

I. Total number of tests[a]   36

    a. Static tests [a]   35
    b. Flight tests   1

II. Type of igniter used:

    a. Original igniter   20

        (1) Tested at ABL   18
        (2) Tested at AEDC   2 (vacuum)

    b. NRL igniter   12

        (1) Tested at ABL   9
        (2) Tested at AEDC   3 (vacuum)

    c. STL igniter   4

        (1) Tested at ABL[a]   3 (1 vacuum)
        (2) Flown from AFMTC   1

III. Number of vacuum ignition tests   6

    a. NRL igniter   5

        (1) Tested at ABL   2
        (2) Tested at AEDC   3

    b. STL igniter   1

        (1) Tested at ABL[a]   1

IV. Test Temperature range, °F   40 to 100

    a. Tests at ambient   22
    b. Tests at 100°F   6
    c. Tests at 40°F   8

(a) There were also two X-241 motors fired at ABL, one of which was in vacuum and one at atmospheric pressure.

Table 3-4. Igniter Development Tests for X-248A3 Motor
(STL Configuration Igniter).

I.   Total number of tests [a]   9

    a.   Tests at atmospheric pressure   4

    b.   Tests in vacuum (0.4 to 0.8 mm Hg)   5

II.   Type squib used [b]   S11A2

    a.   Number of squibs   2 (in parallel)

III. Type of pyrotechnic used:

    a. B/KNO_3 (USF-2L)   3 parts

    b. Zr/Ni (Bermite)   1 part

IV.   The S11A2 squib is also being used in the NRL type igniter for this
same motor. The exact number of tests on this program is unknown,
but it is understood that ignition has been totally successful.

(a)   Other tests were conducted during the development program, but
varied more significantly from the final igniter configuration.

(b)   This squib was selected primarily on the basis of its successful
performance (26 consecutive flights) or the X-17 RTV Program.

the case just forward of the nozzle, by means of adhesives. Firing tests were made with this modification to assure the structural integrity of the case had not been impaired.

Four of these units were procured for the Able-1 program, three of which were flown. The fourth served as backup. Procurement of these motors was through BuOrd from ABL. Excellent cooperation was provided by the Navy on this program, permitting the use of its facilities at ABL and expediting the delivery of the motors.

Upon receipt of these units at AFMTC they were stored in air conditioned magazines at $75^{\circ}F$ until installation on the missile. The temperature was also maintained at about $75^{\circ}F$, after installation, through the use of air conditioning equipment installed on the gantry. Therefore, at the time of ignition the temperature of the motor in flight was such that nominal performance would be realized.

3.3.4   Vernier and Spin Motor

The vernier and spin rockets utilized on the Able-1 Project were solid propellant units and were developed by the Atlantic Research Corporation for the Navy's Vanguard Program. Since these rockets were already qualified, confirmation of their altitude performance was the only remaining requirement prior to their use on the Able-1 vehicle. The confirmation was achieved through wind tunnel tests at AEDC at a simulated altitude of 100,000 feet.

Table 3, see Appendix D (confidential), presents the physical characteristics and nominal performance of the IXS-50. This unit utilizes a composite type ammonium perchlorate propellant designated Arcite 362. The motor case is 4130 steel.

Each Able-1 missile utilized eight of these units as payload verniers and eight as spin motors (Vehicle No. 3 used twelve of the IXS-50 rockets as spin motors and two as retrorockets for preignition separation of second and third stages). A sufficient quantity of IXS-50 units was procured to allow for spares.

3.3.5 Fourth Stage

The fourth stage or injection rocket for the Able-1 vehicle was a solid propellant motor developed by the Thiokol Chemical Corporation. The Thiokol TX8 motor was modified to include a new charge design and ignition system. The modified version of this unit was designated TX8-6. Development testing of this modified unit was conducted at Thiokol's Huntsville facility, and wind tunnel tests at a simulated altitude of 100,000 feet were subsequently performed at AEDC. This measured altitude performance confirmed the unit's capability of imparting the necessary velocity increment to the payload for establishing an orbit around the moon. A ring to provide a satisfactory mounting surface was added at the head end cf the injection rocket case.

Table 4, see Appendix D (confidential), summarizes the physical characteristics and nominal performance of the TX8-6. The propellant was a composite type ammonium perchlorate propellant designated as L-701. The motor case was 7075-T6 aluminum.

A total of six of these units was procured for AFMTC, three of which were flown on this program. The remaining three served as backup.

3.4 Ordnance

Explosive bolts or explosive actuators on the missile are used in the following ways:

a. To separate Stage 1 and 2 - 4 bolts

b. To remove a band covering blast vent ports at first-stage transition section - 2 bolts

c. Jettison the nose fairing - 2 bolts and 2 actuators (thrust devices)

d. To separate Stage 2 and 3 - 2 bolts

e. To separate Stage 3 and the payload - 1 bolt

f. To jettison the cluster of vernier rockets from the payload - 2 bolts

In addition, a missile destruct system is employed to destroy the second stage simultaneously with the command destruction of the first stage. The destruct system, armed by a lanyard at lift-off, ignites 14 feet of RDX primacord when an electrical signal is transmitted from the first stage.

All explosive components were identical in their electrical and explosive characteristics, i.e., they employed the same primer and detonator. They differed, however, in size, shape, and strength according to their function on the missile. All items used the RXL 517B electrical primer (Atlas Powder Co.). There have been no observed failures, in STL tests, of the primer to initiate the detonator.

The RXL 517B primer was chosen for this application because of its continual production in reasonable quantities and because a large back-log of test data exists to substantiate its high reliability. Firing tests of several thousand items, at various temperatures, under vibration, in water, and in a vacuum, verified a predicted reliability of 99.9 per cent at 0.315 amp. A summation of results from the testing of approximately 3500 items yields, for 0.170 amp, a probability of 0.001, for 0.249 amp a probability of 0.50, and for 0.315 amp a probability of 0.999. To increase the probability of functioning and to provide an adequate design margin, the explosive components are initiated on the missile with a current varying from 1.3 amps to 2.5 amps, depending on the particular circuit.

The primers, when received from Atlas, are subjected to quality controls tests according to MIL STD 105A, and to functioning and environmental tests. There have been no observed failures in the functional and environmental tests and the MIL STD 105A qualification tests indicate that, at a firing current of 1.0 amp or more, the functioning probability could be higher than 0.997 at 90 per cent confidence. The observed functioning time (interval from application of energy to detonation) is 7.0 millisec at 0.5 amp, 1.5 millisec at 1.5 amp, and 230 microsec at 8 amp.

Samples of the explosive bolts, assembled for use, are subjected to the following tests:

    a. High temperature stability.

    b. Temperature and humidity.

    c. Altitude functioning.

    d. Mechanical environment tests; vibration, shock, drop tests, and torque.

    e. Salt spray, sand, dust, and water immersion.

42

f. Structural characteristics tests; hardness, tensile failure, and bending failure.

3.5 Control System

3.5.1 First Stage

The first-stage attitude control system was a standard Thor control system with modifications as required to accommodate the dynamics of the four-stage vehicle. These modifications consisted of relocating the rate gyros at station 494 and redesigning the pitch and yaw frequency compensation networks.

First-stage steering was attained by the pitch and roll programmers. No yaw steering was used, and the pitch program was the same for all launch times. Depending on a specific launch time and date, an appropriate roll program was used to attain the required azimuth.

3.5.2 Second Stage

a. Autopilot

The second-stage attitude control system was the same as the Project Able-0 system, and no design modifications were necessary. The major electrical components of the control system--the gyros, amplifiers, demodulators, and associated hardware--were basic Thor components.

A functional block diagram for the pitch and yaw control system is shown in Figure 3-14. The pitch and yaw systems are identical. Control is obtained by gimbaling the main engine about the required missile axes by means of hydraulic actuators.
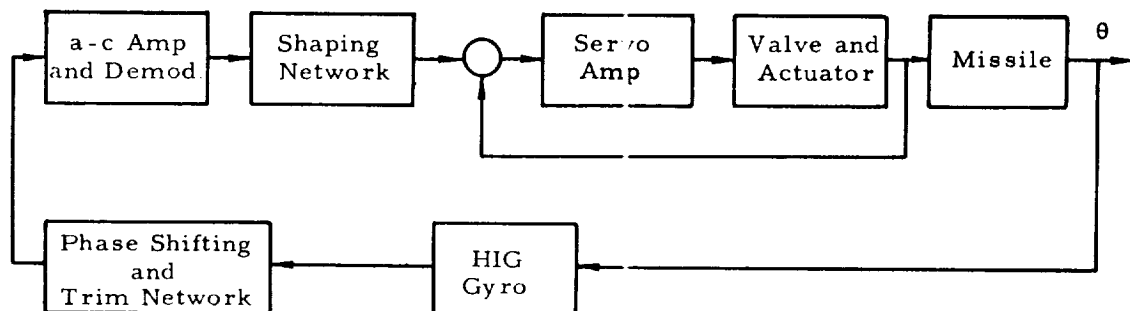
Figure 3-14. Pitch or Yaw Control System.

As indicated in the figure, no rate gyros were used in the system. An increase in system reliability was obtained by eliminating the need for rate gyros. Their function was performed by a lead shaping network. Analyses of the effects of missile bending were performed to ascertain the required shaping networks. A stability analysis of the effect of propellant sloshing was also conducted, and it was found that no anti-slosh compensation would be required.

An on-off type of roll control system was used, a schematic of which is shown in Figure 3-15. Roll torques are exerted on the missile by four jets of fixed thrust vector orientation. The jets, located on the periphery of the missile, are controlled by solenoid-operated valves. Two jets, each of 7.5 pounds of thrust, are effective for each direction of rotation. The propellant tank helium pressurization system supplies the gas for the jets.
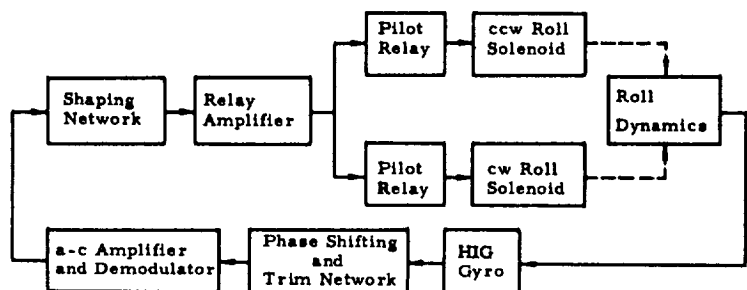
Figure 3-15. Roll Control System.

The action of the system is such that no corrective torques are applied for roll angles below ±3 degrees. For errors of greater magnitude, full corrective torque is exerted. The result is a continuous, controlled oscillation of approximately ±3 degrees amplitude.

b. Main Engine Gimbaling System

The main engine was gimbaled by a hydraulic actuation system to provide corrective torques about the missile pitch and yaw axes. A functional schematic of the system is shown in Figure 3-16. Hydraulic oil, maintained at

1100 psi by the pump and accumulator, is applied to the actuators. The engine deflection from null is sensed by potentiometer pick-offs and subtracted from the input signal to complete the positioning loop.

Since oil and actuator rod compliance result in small engine oscillations which can couple with missile flexibility to produce instability, it is necessary to provide damping to this oscillation. This was obtained by drilling a hole of 0.015-inch diameter in the actuator piston.

——— Electrical Connections

- - - - - Hydraulic and Mechanical Connec ions
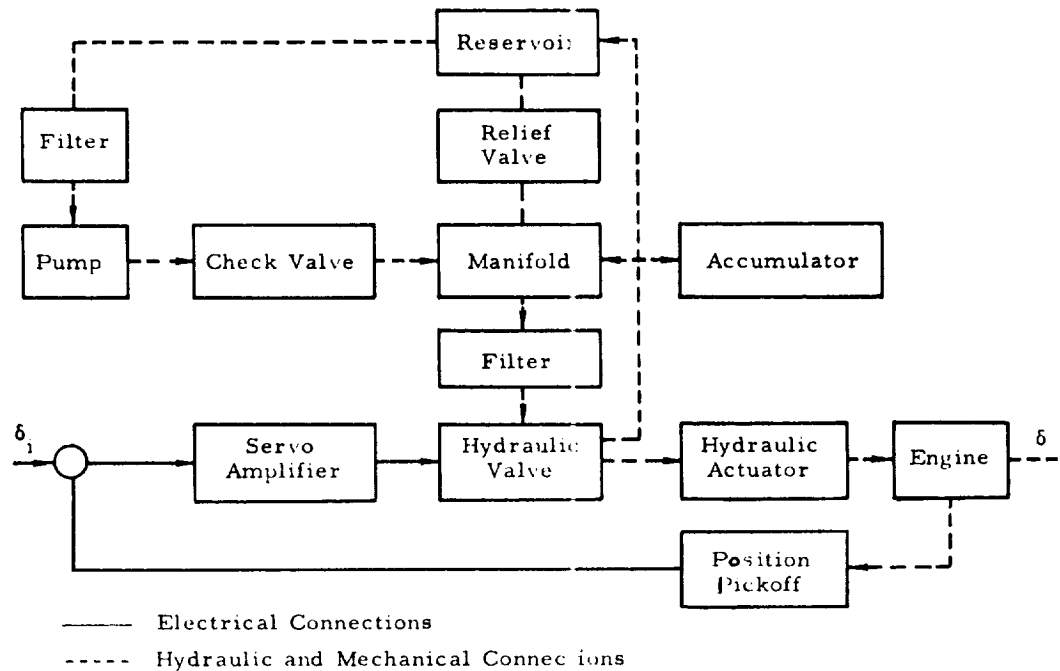
Figure 3-16. Motor Gimbaling System.

Extensive frequency and transient response tests were conducted on the actuation system prior to and during the Able flight test program. These tests indicated satisfactory performance of the servo.

c. Integrating Accelerometer

The integrating accelerometer was utilized to provide a second-stage pitch program signal to the autopilot during a predetermined velocity interval and to provide a second-stage engine cutoff signal at a preset velocity. The latter task was altered to that of an arming function for the final missile firing.

The Able-1 integrating accelerometer is of the pendulous-gyro type, designed to operate switches at preset velocities. The accelerometer is constructed around a floated single-degree-of-freedom gyro whose gimbal is unbalanced. A block diagram is shown in Figure 3-17. The unbalanced gimbal, when centered, is aligned so that it is sensitive to accelerations only along the missile axis. Accelerations along this axis will produce a torque in the gyro which is proportional to the unbalance of the gyro gimbal and will tend to rotate the gimbal about its output axis. The rotation produces a pick-off error voltage, which is phase-detected, amplified, and fed to a servo motor. The servo motor is connected through a gear train to turn the gyro assembly about its input axis in a direction which produces a gyroscopic precession torque opposed to the torque caused by acceleration. The accelerometer is thus a closed-loop servo system which nulls the difference between the unbalance torque and the gyro-scopic precision torque. The gyroscopic torque is directly proportional to the precession velocity about the gyro input axis (which is the output shaft of the accelerometer) and the gyro angular mementum. Thus, the scale factor of the instrument depends directly on the frequency of the wheel motor supply, and the position of the accelerometer output shaft is proportional to the integral of acceleration along the missile axis.

Since the gyro input axis is aligned with the missile roll axis, movement of the missile in roll is also detected. However, this effect is small and cancels out during normal operation because of the missile roll control system. When the missile is spun up after engine cutoff, the missile rotation is the major input; thus, the accelerometer becomes a roll rate detector.

The output shaft is connected through gear trains to a monitoring potentiometer, and cam-actuated switches which are adjusted for a preset rota-tion. Auxiliary circuits control the gyro temperature and enable the system to be caged to a preset zero or starting point.

The accelerometer uncages at lift-off of the first stage and integrates the total axial "thrust" acceleration of the first and second stages. When the preset velocity to start programming the second stage is reached, a switch in the unit is closed, sending a signal to the autopilot. The switch remains closed until a second preset velocity is reached, at which time it opens and removes the program signal. When a third preset velocity is reached, a
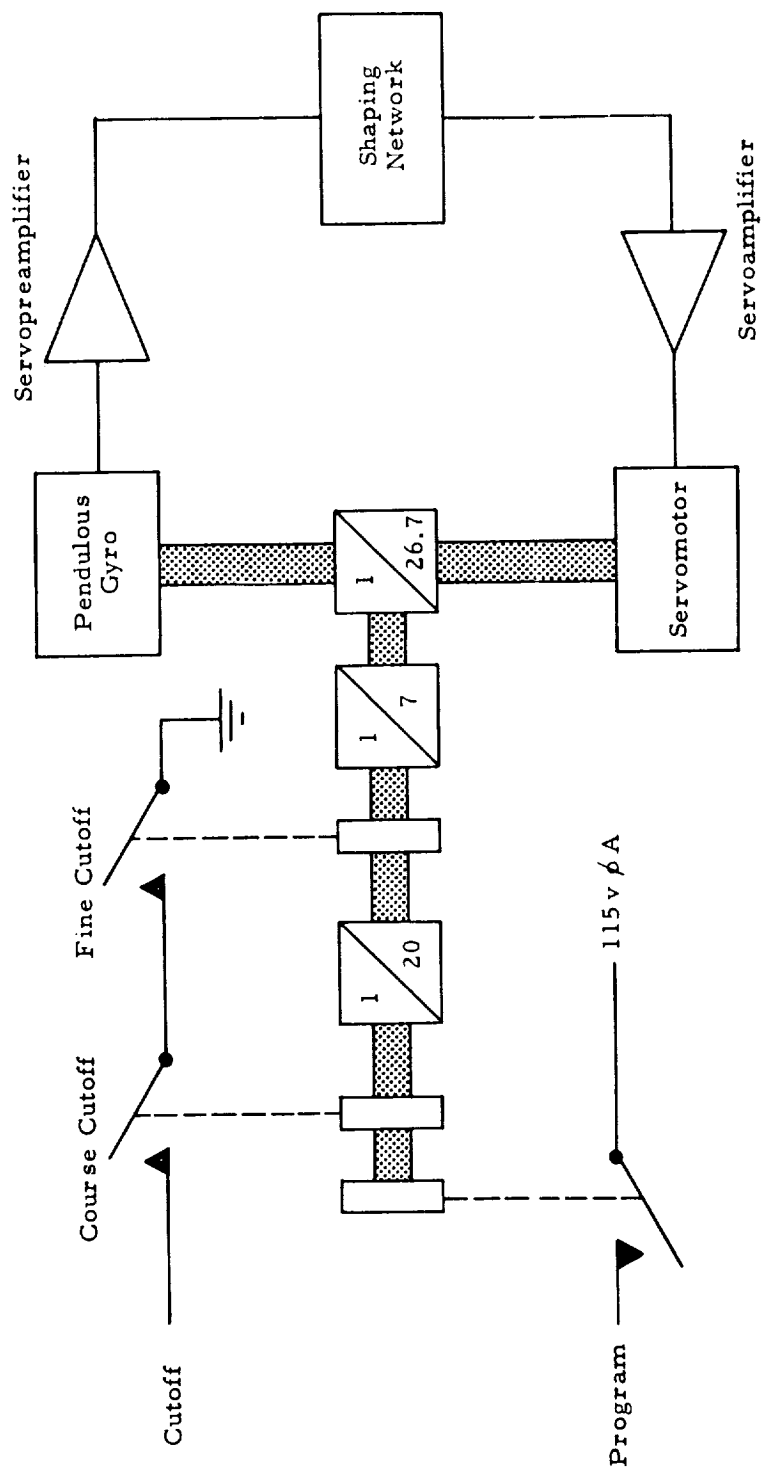
Figure 3-17. Block Diagram Type B-1 Integrating Accelerometer.

second set of switches closed to supply the control system with a signal to initiate second-stage engine shutdown. The second set of switches are connected in series and operates from different output shafts so that both a "fine" and "course" velocity adjustment may be obtained.

The accuracy of measurement of the cutoff velocity, up to 15 g's, is of the order of 0.1 percent, and the velocity increment can be preset to values between 5000 and 28,000 ft/sec. The accuracy of "program" velocity interval measurements are in the order of ±1 per cent due to the present cam-switch arrangement and may be adjusted over a range of 200 to 12,000 ft/sec.

Controls required for checkout and operation of the accelerometer are "cage," "uncage," and "preheat." The preheat control provides for warming up the unit prior to missile power being turned on. At the same time, this function disables the servo loop internal to the accelerometer. The control may thus be used to "hold" the accelerometer at any point in its rundown. In the "cage" mode, the unit automatically returns itself to zero. When uncaged, the unit integrates the total acceleration along its sensitive axis.

The accelerometer was manufactured by Reeves Instrument Corporation of Garden City, New York, and is designated their Model 3707-1. The basic unit was designed for the Vanguard program with extensive modifications being made to meet STL requirements. These included the addition of a new servo motor, the caging control, the preheat control, the monitoring potentiometer, and cutoff cams and modifications of the servo loop shaping network. Additional modifications were made after being received by STL, including the addition of a program cam and minor wiring changes. The accelerometers used on the Able-1 program were identical to the one used on the third Able-0 flight with the exception of the addition of the program cam. A complete sequence of tests were conducted after modification and calibration at STL. No design defects or major component failures were detected during the program. However, minor quality control problems were uncovered in the units furnished by Reeves. These included poor solder joints, a broken wire, improper use of glyptal, improper switch mounting and circuit grounds, all of which were uncovered during laboratory testing.

Hangar checkout of accelerometers with the missiles proceeded without incident. Field adjustments at AFMTC were made to change the cutoff velocity and to remove the accelerometer cutoff signal on the third flight. Field laboratory calibration indicated a sticking gyro in one unit. The gyro unit was subsequently returned to Los Angeles and from there to Reeves for replacement and recalibration.

d. Subsystem Testing

The HIG gyroscopes supplied by Minneapolis-Honeywell for the autopilot were acceptance-tested by STL. In addition to the usual electrical and workmanship tests, a stiction test was performed in which each gyro was torqued from stop-to-stop at a rate of about 60^3 per hour. Stiction is a condition in which foreign particles suspended in the damping fluid migrate to any of several critical locations. Some of these particles occasionally wedge in one or more of the gaps, prohibiting proper gimbal response to small torques about the output axis, with subsequent degradation of system performance. Gimbal position was monitored via the signal generator and displayed on a strip recorder. In such a test, stiction is evidenced by abrupt discontinuity in the ensuing gimbal position trace. The test was repeated in each of three orientations. In all, 63 gyroscopes were tested. Of the 32 units rejected, 27 were rejected on the basis of the stiction test. Those units satisfactorily meeting all requirements were delivered to RCA for mating with the autopilot amplifier assembly supplied by the Radio Corporation of America, West Los Angeles, California.

At RCA each autopilot (electronics assembly and three HIG gyroscopes) was completely checked out, given a production environmental test, rechecked and delivered to STL. The production environmental test consisted of one exposure along each axis to sinusoidal vibration of 2 g's rms, 5-1000 cps at a sweep rate of 1 octave/minute (about 7 minutes in each direction).

Upon arrival at STL, each subchassis was given a functional test, the various chasses were reassembled, and the entire autopilot was calibrated. At the conclusion of calibration, each autopilot was mated with a hydraulic system, engine and power inverter, and compatibility tests were run. Upon demonstrating compatibility, all control loop gains were determined.

The system was then dynamically tested by introducing a step input (electrically) at the input to the a-c amplifier in each channel of the autopilot.

Early in the program, a representative autopilot successfully passed environmental tests consisting of 6 g's peak-to-peak, 5-2000-cps sinusoidal vibration in three axes, 6 g's rms complex wave vibration in three axes, 2 hours of storage at + 135°F, and 8 hours of storage at - 35°F, with operation while stabilized at the temperature extremes. At the end of the complex wave tests, a mechanical failure of the roll relay shock mound chassis occurred. This failure was attributed to fatigue resulting from overtesting during the early complex wave testing. Other than this failure, all autopilot operation appeared satisfactory under the enviromental conditions specified for Project Able.

3.6 Second-Stage Electrical System

3.6.1 Description

The Able-1 second-stage electrical system consisted of the following major components:

a. 400 cps inverter - Bendix Aviation Corp. , Eatontown, N. J.

b. Primary power battery - Yardney Battery Co. , New York, N. Y.

c. Relay junction box - Space Technology Laboratories

d. Electrical cable system - Pacific Automation Products, Burbank

e. Destruct system filter - Space Technology Laboratories

A brief description of each component follows.

The 400-cps a-c power is generated by a Bendix rotary inverter rated at 500 VA output. The output was Y connected at 115V ±0.5V line to neutral.

The battery consists of 21 Yardney HR-15 silver zinc secondary cells. The unit is capable of delivering the required 65 amperes at 28V ±1.0V for about 12 minutes.

The Able-1 relay junction box performs the following functions:

a. It completes electrical connections between the second-stage umbilical connector and all missile functions controlled or monitored from the GSE system.

b. It provides external-internal control of electrical power.

c. It contains the pilot relays for the roll control system.

d. It provides power distribution of the 28-V d-c and 115-V 400-cps power systems.

e. It constitutes a central sequencing and timing control for the staging, propulsion and control system events. These events are as follows:

(1) Attitude gyro caging and uncaging

(2) Ignition of adapter section blast door explosive bolts

(3) Stage 2 propulsion system start signal

(4) Ignition of Stage 1 - 2 separation bolts

(5) Ignition of propulsion system tank pressurization squib

(6) Ignition of nose fairing jettison explosives

(7) Cutoff of Stage 2 propulsion system

(8) Ignition of spin rockets

(9) Ignition of Stage 3 separation bolts

(10) Fire of Stage 3 igniter.

The destruct-system filter is an r-f filter to prevent premature detonation of the second-stage destruct system due to spurious r-f radiation, both external and/or internal to the missile.

3.6.2 Sequencing and Timing

Table 3-5 shows the complete in-flight sequence of events and indicates the device which initiates the action.

3.6.3 Subsystem Testing

The hangar testing of the second stage electrical system consisted of the "covers-off" and 'covers-on" tests. During these tests, the sequencing system was completely exercised and during "covers-on" test, the various igniter circuits were tested by actually detonating igniter squibs.

The missile power system was checked during "covers-on" tests by using an actual flight type battery and closely monitoring both the d-c power from the battery and the voltage and frequency of the inverter.

The following tests of the electrical system were conducted during the "on-stand" period.

a. Compatibility test of missile and launch facility equipment: This test was performed to insure that the missile was completely compatible with the launch facility equipment and to calibrate certain ground monitor instruments whose characteristics were tailored to each particular missile,

Table 3-5. In-Flight Electrical Sequencing and Timing.

Time (seconds)	Stage in which Event Occurs	Action	Equipment Initiating Action
X + 0	1	First motion	
X + 0.1	1	Lift-off switch activates	Microswitch
		Programmer starts	Relay - CEA
		Gyros uncaged	Relay - CEA
	2	Electrical umbilical ejects Accelerometer uncaged	Lift-off signal operates spring release with lanyard backup from umbilical mast
		Arm destruct initiator - Stage 2	Lanyard from umbilical mast
X + 2	1	Roll program initiated	
		Roll rate varies from day to day. Proper rates recorded in DTO.	
X + 9	1	Roll program complete	Douglas programmer relays - CEA
X + 10	1	Pitch program initiated	
X + 140	1	Pitch program complete	
		Programmer output 0 deg/sec	
X + 148 approx.	1	Main engine cutoff (MECO) circuitry armed	
X + 40 approx.	2	Second stage engine Start circuit armed	Acceleration switch set for approx. 6.5 g's + 5 sec
*X + 152.25	1	MECO armed	Propellant float switch set to operate when either tank has 4-1/2 sec of fuel remaining
		Vernier tanks repressurized	
X + 156.75	1	First stage MECO	90 per cent chamber pressure switch initiates shutdown but does not send signal to center engine
	2	Start staging sequence	Relay closure in first stage generated by 90 per cent first stage chamber pressure switch
		Blow blast band	Relay activated by the start staging sequence signal
		Start 2-sec time delay	

*This time and all times following are based on the reference trajectory.

Table 3-5. In-Flight Electrical Sequencing and Timing (continued).

Time (seconds)	Stage in which Event Occurs	Action	Equipment Initiating Action
X + 158.75	2	Uncage gyros Engine fire signal Start 5-min timer	Relay in relay junction box (RJB)
X + 159.+	2	Blow separation bolts	Chamber pressure switch set to operate at 60 per cent of second stage engine thrust (TPS with TVS_2 backup)
		Start 10-sec timer	
X + 159.3	2	Second stage separation complete	
X + 169 approx.	2	Pyrotechnic in helium tanks is set off	10-sec timer
		Blow explosive bolts in N. C. shroud	
X + 257	2	Start pitch program - total 13.6 deg down	Switch on accelerometer coarse shaft
X + 267	2	Stop pitch program	Switch on accelerometer coarse shaft
X + 270	2	Cut off main engine	Accelerometer fine shaft (armed by coarse shaft) (TPS backup)
		Ignite spin rockets	
		Start 2-sec timer	
X + 272	3	Ignite Stage 3 motor	2-sec timer
		Blow Stages 2 and 3 explosive bolts	
		Cage Stage 2 gyros	
X + 310	3	Rocket motor burns out	Depletion of propellant
X + 460	3	Separation bolt blows to separate Stages 3 and 4	4-min timer started at X + 158.75
	3 and 4	Separation occurs	Separation spring
	4	Arm Stage 4 ignition	Switch actuated by physical separation
X + 224,000 ±1800 sec	4	Rocket motor fires	Timer initiated prior to launch

54

b. Integrated Thor-Able electrical system test: This test was conducted to demonstrate that the three electrical interfaces between Able and Thor were compatible and that there were no radiation interference problems. These electrical interfaces were:

(1) the lift-off signal to eject the Able umbilical

(2) the destruct system

(3) the main engine cutoff signal to start the Able sequence.

c. At T minus 2 days a group of electrical subsystem tests were performed to verfiy that the autopilot and accelerometer system were operating properly.

d. A final check of the sequencing, timing, and igniter systems was performed at T minus 1 day.

e. An integrated Thor-Able T minus 1 day electrical system test was performed to recheck, prior to entering the countdown, the destruct and main engine cutoff systems.

f. The internal-external power system, the autopilot and accelerometer and the destruct and main-engine-cutoff signals were given a final check at T minus 490 minutes during the countdown.

3.7 Second-Stage Telemetry

3.7.1 Description

The equipment of the second-stage telemetry system is listed in Table 3-6. The specifications of this 3-channel FM/PM and PAM system are indicated in Table 3-7.

Table 3-6. Telemetry Equipment List.

Part	Model No.	Manufacturer
Transmitter	TXV-17	Bendix Pacific
Voltage Controlled Oscillator	TSO 200B	United Electrodynamics
Electronic Commutator	60000298	Space Technology Laboratories
Pressure Transducer	1805	
	1806	Transonics
Power Converter	TPD-100A	United Electrodynamics
Batteries	HR-1	STL design - Yardney

Table 3-7.. Telemetry System Specifications.

Power Output:	2.0 watts
Frequency:	238.5 mc
Weight:	22.6 lb
No. of Channels:	3
No. of Measurements:	25
Operating Life (batteries):	40 min

The antenna system consisted of four 11.34-inch folded unipoles, equally spaced around the circumference of the missile and fed in turnstile fashion so as to provide essentially isotropic coverage. The radiated field was right-circularly-polarized from the aft end of the missile. The input impedance of each antenna is 150-ohms resistive. This impedance transforms through the cabling system to 37.5 ohms.

3.7.2 Measurements

Three channels were employed to transmit 25 measurements from prelaunch to second- and third-stage separation. The first channel, IRIG Band 1 (400 cps), was the alternator output and provided a means of measuring alternator frequency stability. The second channel, IRIG Band 13 (14.5 kc), was a voltage-controlled oscillator whose input was pulse amplitude modulated by an electronic commutator. The third channel, IRIG Band 14 (22 kc), was an events channel, a voltage-controlled oscillator modulated by the events listed in Tables 3-8 and 3-9.

3.8 Ground Support Equipment

The hangar checkouts in Florida are conducted using much of the same test equipment used later in the launch area. The Electrical Checkout Trailer (Figures 3-18 and 3-19) is used in the hangar for the "covers-off" and "covers-on" tests. The trailer is equipped to simulate actual launch-complex conditions. Other pieces of equipment used for hangar checkout are later taken to the launch area for similar checkouts there. In this way, tests can be run under a close approximation of actual conditions.

Table 3-8.   Measurement List for Able-1
Missile No. 1.

Channel 13   14.5 kc

Commutated   5 rps

1. Pitch gimbal   ±3 deg
2. Yaw gimbal   ±3 deg
3. 28 volts   0-35 vdc
4. Motor chamber pressure   0-300 psia
5. Roll demodulator   ±6 deg
6. Pitch demodulator   ±6 deg
7. Yaw demodulator   ±6 deg
8. Accelerometer fine shaft
9. Helium regulator output   0-350 psia
10. Zero
11. 2.5
12. Zero
13. Zero
14. 5.0 volts master pulse

Channel 14   22 kc

Blip Strip

Lift-off
Arm Stage 2
Pc Stage 1
Fire Stage 2
Fire separation bolts
TPS switch opens
Stage 2 separation
Fire HGA squibs
Roll CCW
Roll CW
Stage 2 Pc
TPS switch
Stage 3 separation

Channel 1   400 cps

Alternator Frequency

Table 3-9.   Measurement List for Able-1
Missiles No. 2 and No. 3.

Channel 13   14.5 kc

Commutated

1.	Pitch gimbal	±3 deg
2.	Yaw gimbal	±3 deg
3.	28 volts supply	0-35 vdc
4.	Motor chamber pressure	0-300 psia
5.	Roll demodulator	±6 deg
6.	Pitch demodulator	±6 deg
7.	Yaw demodulator	±6 deg
8.	Accelerometer fine shaft	
9.	Helium Regulator	0-350 psia
10.	Pitch control field	
11.	Accelerometer servo loop error	
12.	Zero	
13.	2.5 volts	
14.	5.0 volts (master pulse)	

Channel 14   22 kc

Blip Strip

Lift-off
Arm Stage 2
Pc Stage 1
Fire Stage 2
Fire separation bolts
TPS switch opens
Stage 2 separation
Fire HGA squibs
Roll CCW
Roll CW
Stage 2 Pc
TPS switch
Stage 3 separation

Channel 1   400 cps

Alternator Frequency

58
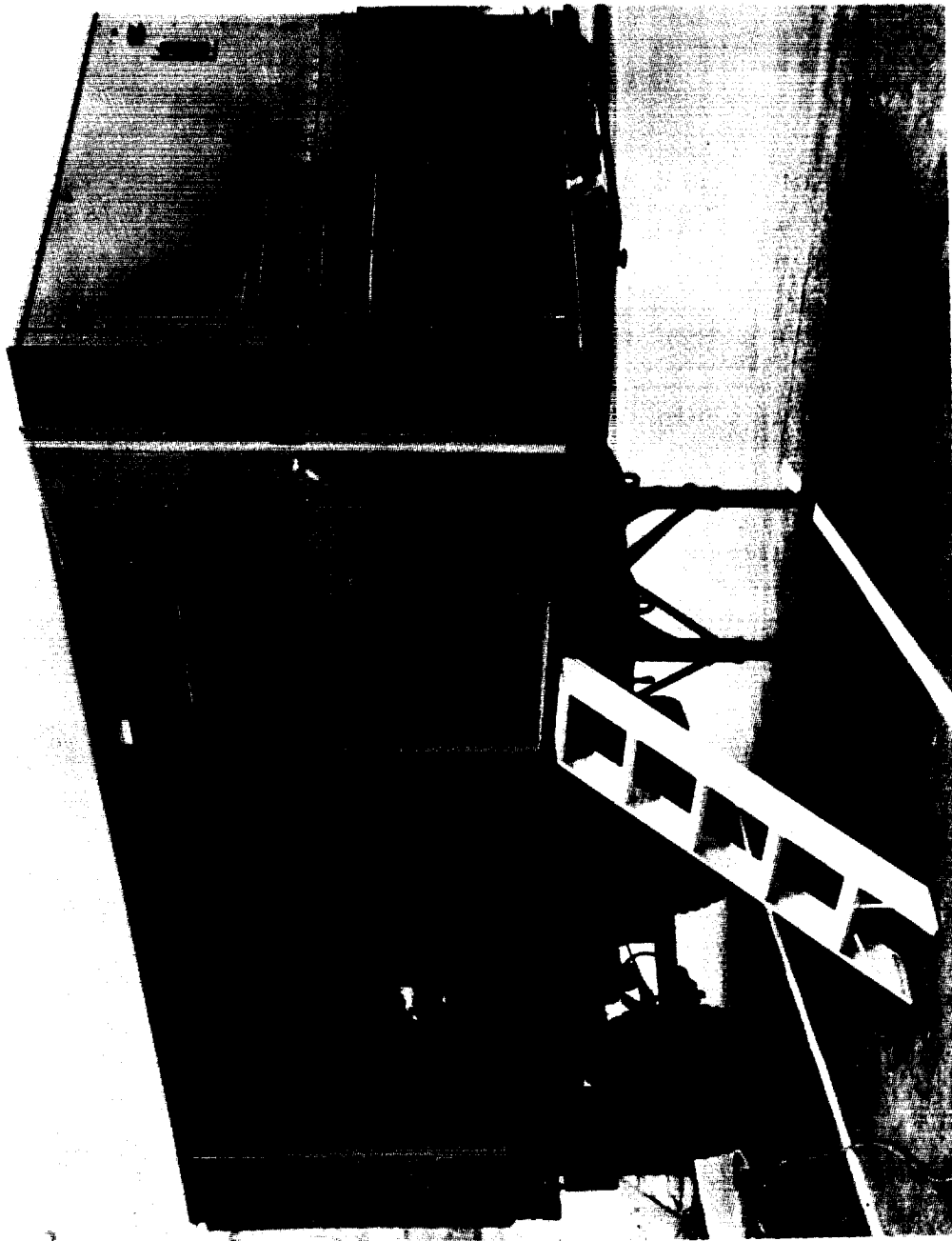
Figure 3-18. Electrical Checkout Trailer (Exterior).
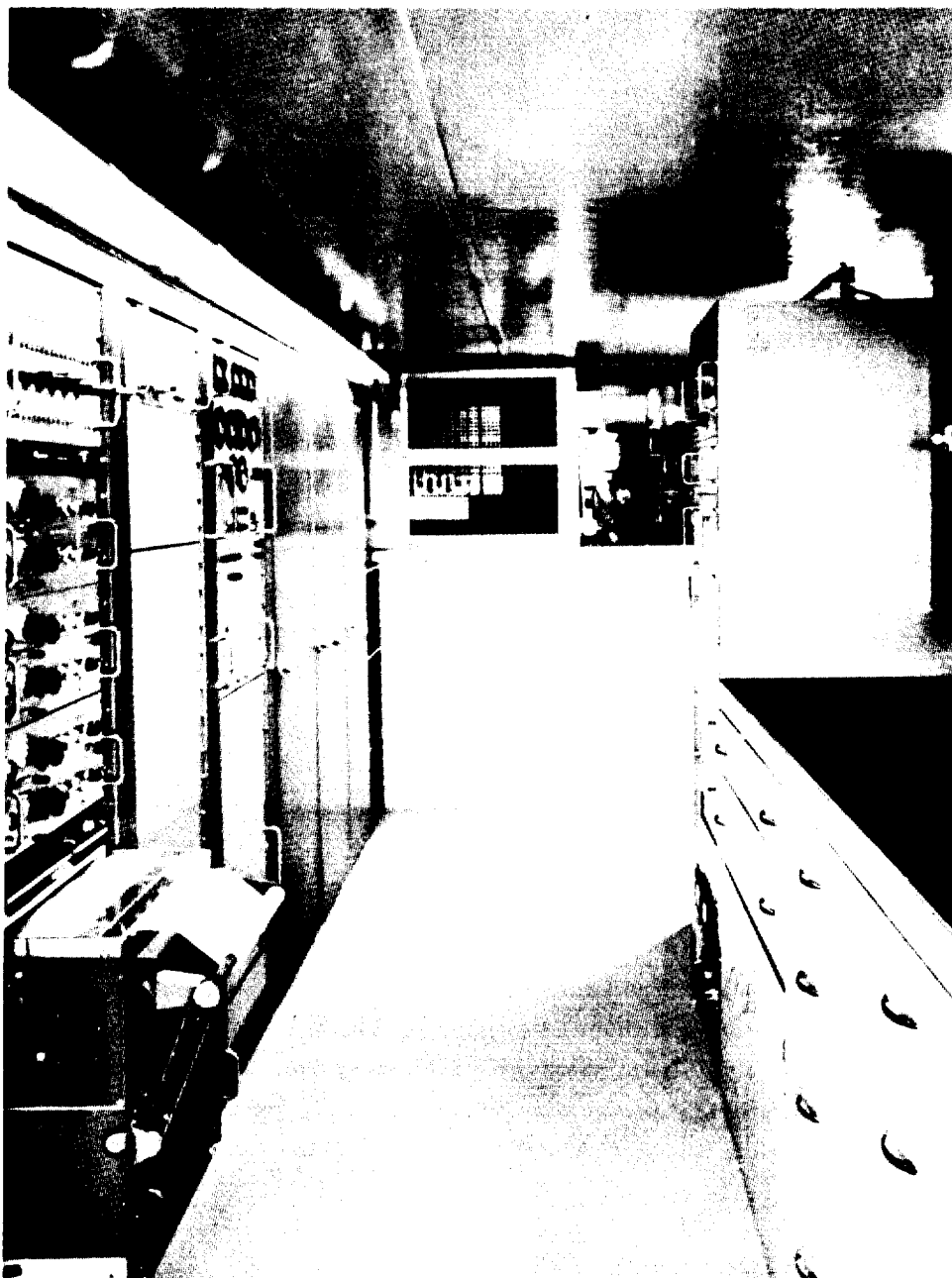
Figure 3-19. Electrical Checkout Trailer (Interior).

For prelaunch checkouts the electrical checkout trailer is moved to the launch area when the missile goes on stand. The trailer is connected to the terminal room and to two test cables that run up the service tower to the checkout levels. The trailer also has the capability of being connected directly to the missile through the umbilical cable for direct checks. There is a 28V power supply in the terminal room beneath the stand which is connected to a relay rack for control of all functions that are remotely controlled from the blockhouse. Two cables run to the blockhouse from the terminal room and terminate in the blockhouse console.

The blockhouse console is divided into two parts. One part for control and monitoring of electrical functions and the other for control and monitoring of engine and propulsion functions. A helium pressurization panel is located on the launch deck beside the base of the umbilical tower for pressurization of the missile helium tank prior to flight and for checkout. This console can be remotely controlled (through the relay racks) from the propulsion panel in the blockhouse console. The regulators have to be set directly at the pressurization panel on the stand. A test junction box is used to terminate the cables coming from the trailer at the checkout level and from there the cables are routed to their various check points.

For launch, the checkout trailer is moved back to the hangar area where it is used to monitor and compute various flight times to support the vernier firing task.

All functions on the missile are controlled from the blockhouse console (through the relay racks in the terminal room) to the missile through the umbilical cable. After the helium regulators are set, pressurization is controlled from the blockhouse propulsion panel. Certain propulsion functions are monitored from an instrumentation van which is parked permanently outside the blockhouse. This van can be controlled remotely from the blockhouse so that it may be used during launch without endangering an unprotected operator.

3.9   Preflight Tasks

3.9.1   Preparation on Launch Stand

Preparations and checkout on the launch stand comprise repetition of the systems tests controlled from the blockhouse console, compatibility of the

missile with the launch equipment and with the booster stage, and final subsystem calibrations. The following additional tests, which cannot be made in the hangar, are performed: signal strength measurements of the telemetry and of the payload package, r-f interference tests including the booster stage and payload, and command-destruct tests utilizing the first-stage command-destruct equipment. Formal electrical system compatibility and acceptance tests for both the Able stage and the booster stage are run soon after the missiles are mated. This test, together with a short propulsion leak test, suffices to qualify the Able stage for final calibration and sequence runs at T minus 2 and T minus 1 days.

3.9.2 Countdown (see Table 3-10)

The trajectory for the Able-1 mission required a high degree of precision in launch time (see section 3.1). A period of approximately 20 minutes on each of four successive days constituted the permissible launch time for a given month. Experience with the basic Thor program and with the Thor-Able program showed that the use of a standard countdown would not result in this required timing accuracy. In consultation with DAC Operations Group in Florida, it was decided to incorporate several scheduled holds into the countdown. This resulted in a division of the countdown into the four major groups of tasks described below.[*]

a. Second-Stage Propellant Loading

The first task was the hoisting of loaded oxidizer and fuel propellant tanks and the filling of the second-stage tanks. This task was accomplished by a trained propellant servicing crew supplied by AGC. For safety purposes, those participating in the task had to wear protective clothing. Wearing this clothing during the hot Florida midday resulted in discomfort and physical fatigue; consequently, for the second and third launches these tasks were scheduled for the early morning hours.

---

[*]DAC, "WS 315A Thor-Able-1 Countdown Manual," 1 August 1958, and subsequent revisions. See Table 3-13 for milestone countdown.

Table 3-10. Flight Milestone Countdown Project Thor/Able-1.

T minus 765	Countdown Initiation (Task 1)
	Second Stage Propellants on Station
T minus 760	Second Stage Propellant Servicing Begins (Task 2)
T minus 490	Second Stage Propellant Servicing Complete
	Note: 120 Min Built-in Hold Begins at this Point
T minus 490	Range Countdown Initiation
T minus 485	Thor Engine Checks Begin (Task 3)
T minus 440	Electrical Checks Begin (Task 4)
T minus 320	Electrical Systems Test Complete
	First Stage Fueling Begins (Task 5)
	Thor Ordnance Task Begins (Task 6)
	Able Ordnance Task Begins (Task 7)
T minus 280	First Stage Fueling Complete
T minus 200	Thor Ordnance Task Complete
T minus 180	Able Ordnance Task Complete
	Able Secure Task Begins (Task 9)
T minus 135	Able Secure Task Complete
	Note: 120 Min Built-In Hold Begins at this Point
T minus 135	First Stage Loxing Begins (Task 11)
	Second Stage Helium Pressurization Check Begins (Task 8)
	Tower Removal Task Begins (Task 12)
T minus 120	Regulator Setting Begins (Task 13)
T minus 105	Second Stage Helium Pressurization Check Complete
T minus 75	Regulator Settings Complete
	Tower Removal Complete
T minus 75	DAC Final Preparations Begin (Task 14)
T minus 35	1st Stage Loxing Complete
	Final Preparations Complete (except for Stand-by crew)
	Note: 60 Min Built-in Hold Begins at this Point
T minus 35	Terminal Count Begins (Task 15)
	Vernier Firing Task Begins (Task 16)
T minus 0	Start
T plus 4 sec	Mainstage
T plus 10 min	Vernier Firing Task Complete
	Pad Clearance

b. **Electrical Systems Check, Ordnance Task, First-Stage Engine Checks and Fueling**

The second group of tasks included the first stage engine sequence checks, the electrical systems checks which included programmer runs, command destruct tests, all systems tests for both stages, the electrical checkout of payload package, a first-stage fuel test and the hooking-up and continuity check of all ordnance items on both stages. This set of tasks was scheduled between times T minus 490 minutes and T minus 135 minutes. A 2-hour built-in hold was scheduled at T minus 135 minutes.

c. **Tower Removal, Regulator Setting and Loxing**

The time from T minus 135 minutes to T minus 35 minutes was scheduled to include loxing the first stage, removal of the service tower, and regulator setting for both the first-and second-stage engine consoles. The loxing task was separated from the second group of tasks to minimize the time of low temperature conditions and, should it prove necessary, to increase the probability of recycle on the following day.

These tasks were followed by a scheduled 60-minute hold at T minus 35 minutes. Communications checks with the world-wide communication network and the operational intercommunication sets to be used in the terminal count firing task were checked out during this hold period.

d. **Terminal Count**

The terminal count commenced at T minus 35 minutes scheduled to reach T minus 0 at vernier engine start. It normally takes approximately 4 seconds for main engine thrust to build up to the point where lift-off occurs. The vernier firing task consisted mainly in gathering of data from the telemetry stations, skin tracking radar, and the Azusa computer, processing it in the 704 computer and using the information so derived to determine the number of payload vernier rockets to be fired at approximately T plus 10 minutes.

3.10 Vernier Firing Task

To increase the probability of lunar capture by decreasing the velocity dispersion existing in third stage burnout, a total velocity

increment of ± 74 ft/sec was available from 8 small (50 lb-sec impulse) solid propellant vernier rockets mounted on a ring behind the payload. One to eight of these vernier rockets were to be fired on radio command from the ground to obtain the desired velocity increment. Determining the number of verniers to be fired was the vernier-firing task.

Since these verniers could change only the magnitude of the velocity vector, it was necessary to determine the exchange between potential energy and kinetic energy and, thus, to translate all dispersions into velocity dispersions. The primary task, then, was to find a procedure which used only data available in real time at AFMTC to estimate the various burnout parameters. The desired accuracy of such a procedure was ± 9 ft/sec equivalent velocity, which corresponded to the velocity increment obtainable from about one-half of a vernier rocket. It was necessary that the procedure for estimating third-stage burnout parameters be simple so that all computation could be carried out and the verniers could be fired within 15 minutes after lift-off.

To determine the effects of various disturbances on burnout parameters, perturbed trajectories were run and a number of empirical formulas were derived relating burnout attitude, velocity, and velocity angles to measured quantities. These empirical formulas took such quantities as burning time, altitude and velocity angle at first-stage burnout, radar elevation from Millstone Hill, Massachusetts, and doppler range rate during the early part of free flight, and from them deduced the burnout parameters. It was found, for instance, that errors in flight-path elevation angle at first-stage burnout were closely correlated to errors in third-stage burnout altitude. The highest reliability in the determination of third-stage burnout parameters was obtained by using data from near the end of powered flight. Thus, emphasis was placed on Millstone data at second-stage burnout, and doppler data in free flight shortly after third-stage burnout.

Since the raw data to be used in the empirical formulas were to come from many sources, an extensive communications net was set up, which included the telemetry stations, the Azusa computer, the FPS-16 (XN-1) radar site, and the doppler trailers. In addition, a 24-hour telephone line was set up between the vernier-control room at Cape Canaveral and Millstone Hill Radar. Data sources are indicated in Table 3-11.

Table 3-11. Data Sources for the Vernier-Firing Task.

Source of Data	Data Provided
Able Telemetry Trailer	Lift-off Time First Stage Burnout Time Second Stage Burnout Time
Base Telemetry	First Stage Burnout Second Stage Burnout
FPS-16 (XN-1 Radar	First Stage Burnout Time First Stage Burnout Altitude
Azusa 704	First Stage Burnout Time First Stage Burnout Velocity First Stage Burnout Altitude First Stage Burnout Velocity Angle
Millstone Radar	Second Stage Burnout Radar Coordinates (Range, Azimuth, and Elevation)
Able-1 Ground Station	Range Rate in Free Flight

From these various sources, data were taken in and posted in the vernier-control room. In order to reduce the computation time required to an absolute minimum, the empirical formulas were reduced to large graphs showing the number of rockets to be fired directly as a function of the raw data. Then an algebraic sum of the results of various combinations of formulas were taken, and the appropriate firing command transmitted to the command doppler receiver in the payload.

4.0 TRACKING AND COMMUNICATIONS

4.1 Introduction

Space probe vehicles require continuous ground surveillance from launch time until missile battery exhaustion, impact, or missile flight beyond detection range. The surveillance system must yield precise tracking information in order to plot the trajectory of the space probe vehicle accurately as well as providing for the reception of telemetered information from the space vehicle.

Surveillance stations must also provide intra-missile control over retro-rockets, for example, actuate or discontinue experiments which interfere with doppler measurements involving high battery drain.

4.1.1 Ground Stations

Ground tracking stations were established by STL at AFMTC, Florida, Hawaii, and Singapore, with the Jodrell Bank radio telescope installation of the University of Manchester in England also cooperating in tracking operations. This telescope, together with an instrumentation trailer supplied by STL, provided a very powerful ground receiving facility. Another cooperating organization, the Millstone Hill, N.H., radar station of MIT also provided a tracking facility.

Calculations based on trajectory data received by teletype from the ground stations were performed at a central computing point at the STL Operations Center in Los Angeles to determine new estimates of the actual trajectory. The revised trajectory estimates were in turn used to calculate new steering data to assist the ground stations in tracking operations.

4.1.2 Cooperating Agencies

The efforts of the primary ground system were assisted by many cooperating agencies. Arrangements were made with the NRL Control Center, Washington, D. C., for the relaying of tracking data from Minitrack stations to the Operations Center in Los Angeles via the STL communications center at Cape Canaveral. The Operations Center was also in contact with the NRL Control Center by telephone so that their interpretation of the Minitrack tracking data would be readily available to the Operations Center. The presence of NRL

68

technical personnel at the Operations Center during the October and November launches also greatly facilitated interpretation of the Minitrack data.

Although the Operations Center furnished the Smithsonian Astrophysical Observatory with nominal tracking data for its key optical tracking stations as well as estimates of the actual trajectory of the October shoot in an attempt to obtain optical records of re-entry, several factors contributed to the unavailability of data from these sources.

Nominal tracking data was also made available to a number of groups throughout the country who wished to attempt either tracking or the recording of telemetry data.

4.2   Description of Ground Station Subsystems

Each ground station had a number of subsystems such as receivers, transmitters, data recording equipment, etc. , which are here functionally described.

4.2.1   Phase-lock Receivers

All signals from the probe were received at 108.06 or 108.09 mc at each of the ground stations. Since these weak signals were to be detected in spite of noise, phase-lock receivers were used exclusively. Figure 4-1 is a diagram of such a receiver.

From the diagram, it can be seen that this receiver is basically a double-superheterodyne receiver in which the signal at the last IF frequency of 455 kc is compared, in a phase-detector, with a crystal-controlled 455-kc oscillator. A d-c voltage representing the phase error varies the frequency of a voltage-controlled oscillator at 100 mc (which heterodynes the incoming signal from 108.06 mc to 8 mc) so that the relative phase shift is held very nearly constant. This type of receiver achieves coherent signal detection.

By proper choice of filter constants in the d-c phase-error feedback path, the output bandwidth of a phase-lock receiver is made extremely small. In the case of the receivers shown in Figure 4 1 , the output bandwidth is only 20 cycles per second (for weak signals) and the preamplifier noise figure is approximately 2 5 db. These receivers are, therefore, able to lock onto
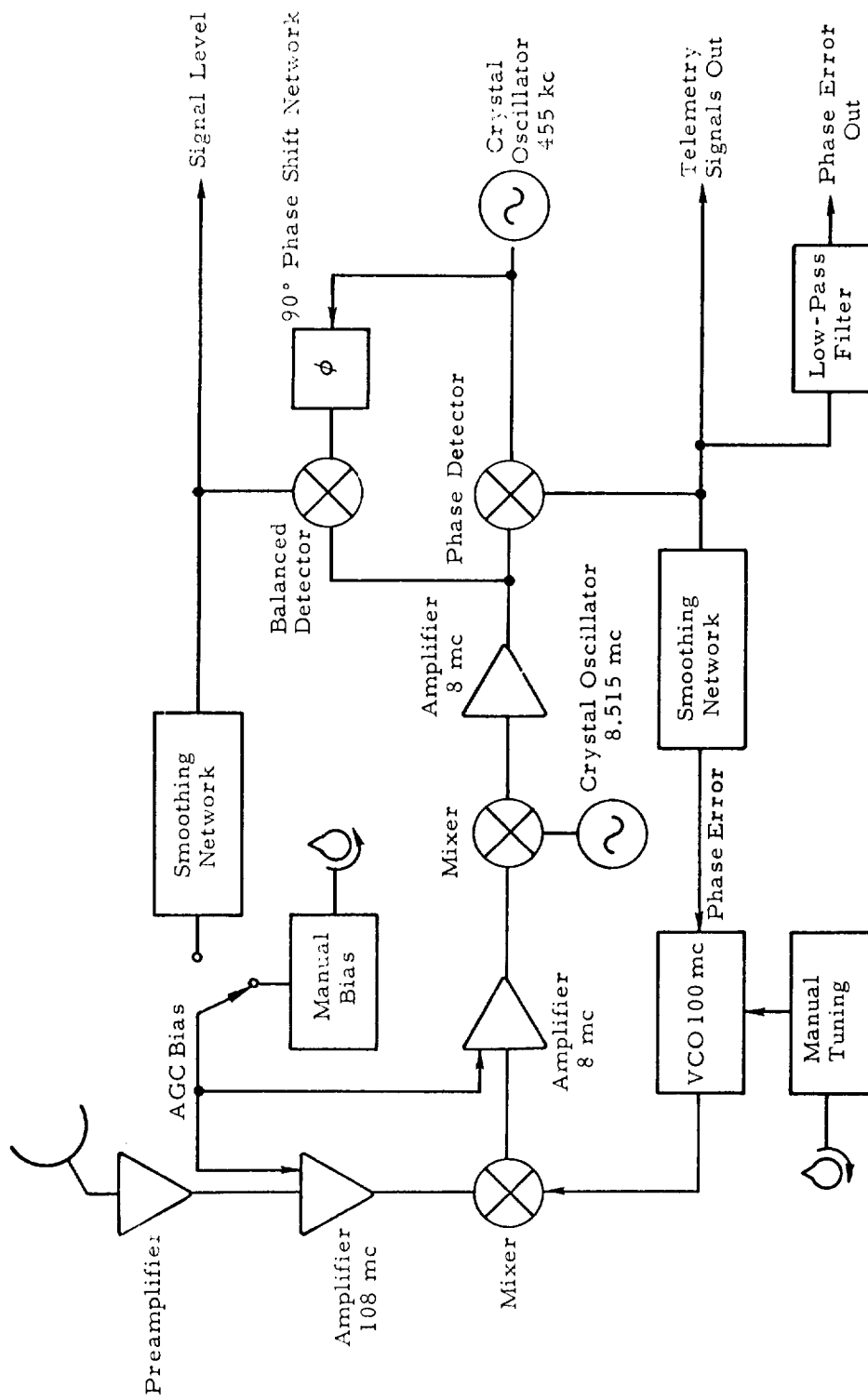
Figure 4-1. Phase-lock Receiver.

signals of -155 dbm or better. The phase detector demodulates the telemetry information so that the telemetry subcarriers are available for recording onto magnetic tape or for data reduction by discriminators directly from the phase detector output.

4.2.2 Command/Doppler Subsystem

The Able-1 lunar probe utilized a command/doppler system to fire vernier and retrorockets to improve the probability of lunar capture.

To achieve this, a high-power transmitter was provided at 114.8 mc. The probe had a special command/doppler phase-lock receiver which scanned a narrow frequency band around 114.8 mc continuously. Whenever a signal was received, the probe receiver locked onto it and retransmitted back to the earth a signal whose frequency was exactly 16/17 of 114.8 mc, or about 108.06 mc.

Doppler measurement involves a comparision of the transmitted and received frequencies by very accurate means, so that the exact doppler shift can be determined. Figure 4-2 shows the block diagram of the apparatus that was used for this measurement. An elaborate chain of mixers and frequency multiplying circuits were used which eventually produced an output signal whose frequency was eight times the doppler shift at 106.06 mc.

The output of the doppler data extraction unit of Figure 4-2 (16 times the doppler frequency) was tabulated by a digital counter which displayed the total number of signals of 16 f_d occurring in a one second interval. This count was printed once each two seconds by a digital printer along with a printout of range time which was correlated with lift off time.

Command tones were transmitted to the payload by the use of transmitter referred to above. These command tones were phase-modulated sine waves from 2000 cps to 3500 cps. Each command consisted of simultaneous transmission of 2 out of 4 possible tones; a total of 6 commands were available in such a system. Since transmission of undesired commands might seriously jeopardize the success of a mission, elaborate interlock and safety circuits were provided at the ground station to avoid accidental transmission of false commands.
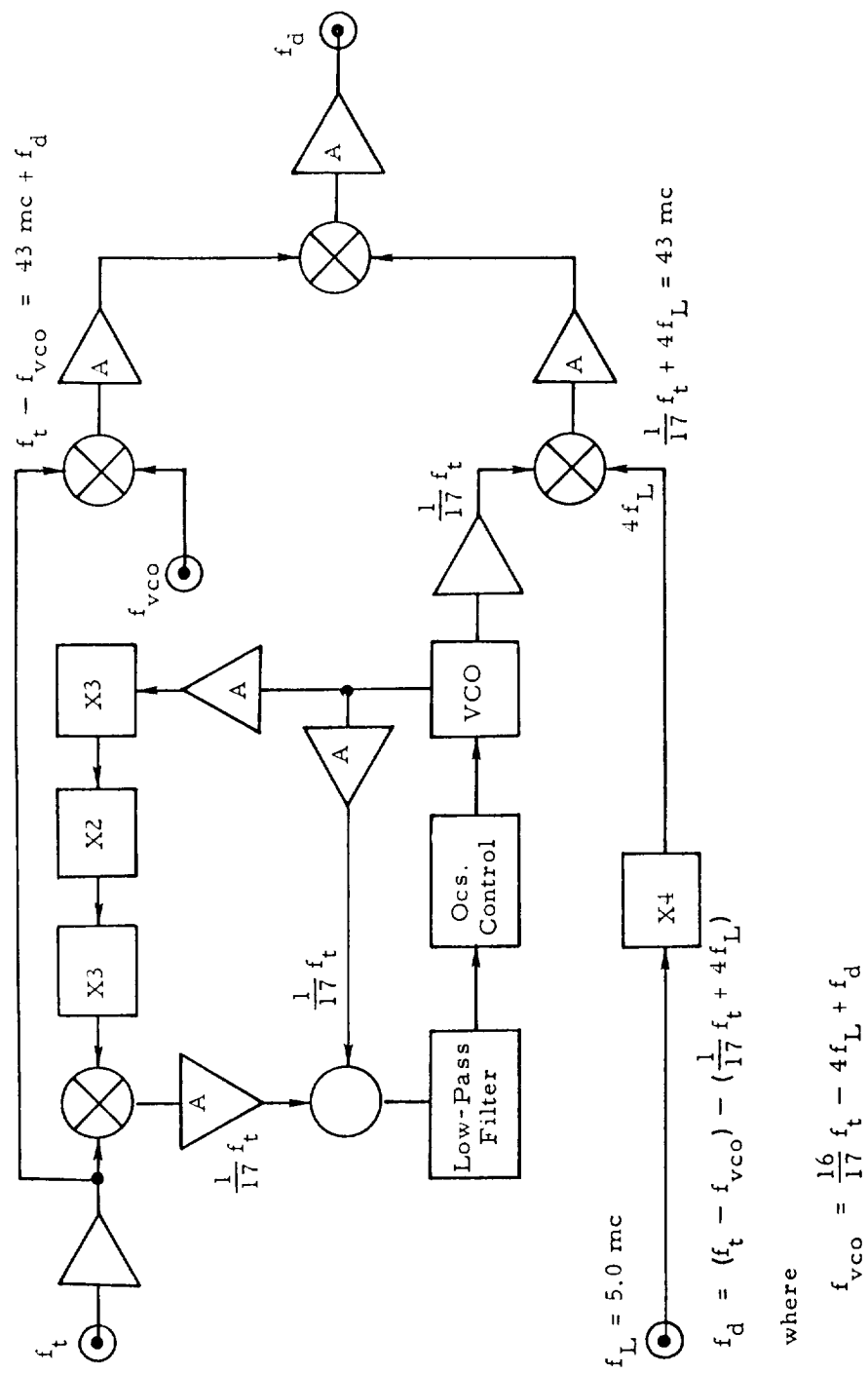
Figure 4-2. Doppler Data Extraction.

$f_L = 5.0 \text{ mc}$

$f_d = (f_t - f_{vco}) - (\frac{1}{17} f_t + 4 f_L)$

where

$f_{vco} = \frac{16}{17} f_t - 4 f_L + f_d$

This command transmitter was used finally as a ranging unit. For this application, a 2-cps tone was phase-modulated onto the transmitter carrier frequency. The 16/17 circuit in the probe followed these frequency exclusions accurately. A range reading with an accuracy of a few hundred miles was therefore obtained by measuring the phase difference between the transmitted 2-cps tone and a similar tone which is demodulated by the phase-lock receiver on the ground. This range measurement is redundant at 50,000 miles but for the Able-1 program such redundancy was of no significance.

4.2.3 Tracking Techniques

Several tracking techniques were used to determine the position of the vehicle. These included the following:

a   An AFMTC facility at Azusa determined the trajectory of the first stage.

b.   The Millstone station skin-tracked the second stage using 400-mc long-range radar. This skin-tracking gave accurate data from about five minutes after lift-off until well after the second stage had separated from the third stage.

c.   Minitrack stations operated by NRL tracked the payload with two-axis interferometers. Table 4-1 shows the location of the minitrack stations and their visibility period.

Table 4-1 . Minitrack Stations

Station	Visibility Period (minutes after lift-off)
Antigua	5 - 18
Antigua	415 - 465
Grand Turk	8 - 18
Antofagasta	455 - 495
Santiago	455 - 495
Ancon	485 - 525
Clossom Point	485 - 525
Coto Paxi	495 - 535
San Antonio	500 - 555
Fort Stewart	505 - 545
San Diego	655 - 695
Woomera	1100 - 1135
Johannesburg	1535 - 1575

d. The command/doppler system at AFMTC measured radial range rate for the first sixteen minutes after launch.

e. The Manchester station measured azimuth and elevation by tracking the telemeter transmitter at 108.06 mc from eleven minutes after lift-off for the full duration of the time for which the probe was above its horizon. Angular accuracy of better than one-half degree was obtained.

f. The Millstone radar station switched to passive tracking with a phase-lock receiver about one-half hour after launch and gave azimuth and elevation data henceforth for all of the time the probe was above its horizon.

g. The Hawaii station gave azimuth and elevation data from the 60-foot parabolic TLM-18 antenna for all of the time the probe was above its horizon.

h. The Hawaii station was equipped with a two-axis interferometer with a base line of 282 feet for each axis. It was hoped that this interferometer would give an angular accuracy of about 0.01 degree, however, the calibration of this subsystem proved difficult because of spurious reflections, with the result that no useful interferometer data was actually obtained.

i. The Hawaii station was equipped with a command/doppler transmitter and doppler data extraction circuitry to permit the accurate measurement of two-way doppler.

j. The antenna system at the Singapore station had too broad a beam width to provide significant tracking information.

k. There was an attempt to track and photograph the probe with a large astronomical telescope at Palomar Observatory. For a description of this system see Appendix B.

4.2.4 Interferometer

Two methods for using the interferometer at Hawaii were tried. These methods are illustrated in Figures 4-3 and 4-4. The first of these shows a correlation technique in which the sum of two interferometer antennas is compared to the difference vector by a coherent phase-detector. This method has the advantage of not requiring a central antenna, although the signal-to-noise ratio of the detector output for weak signals is not nearly as good as it
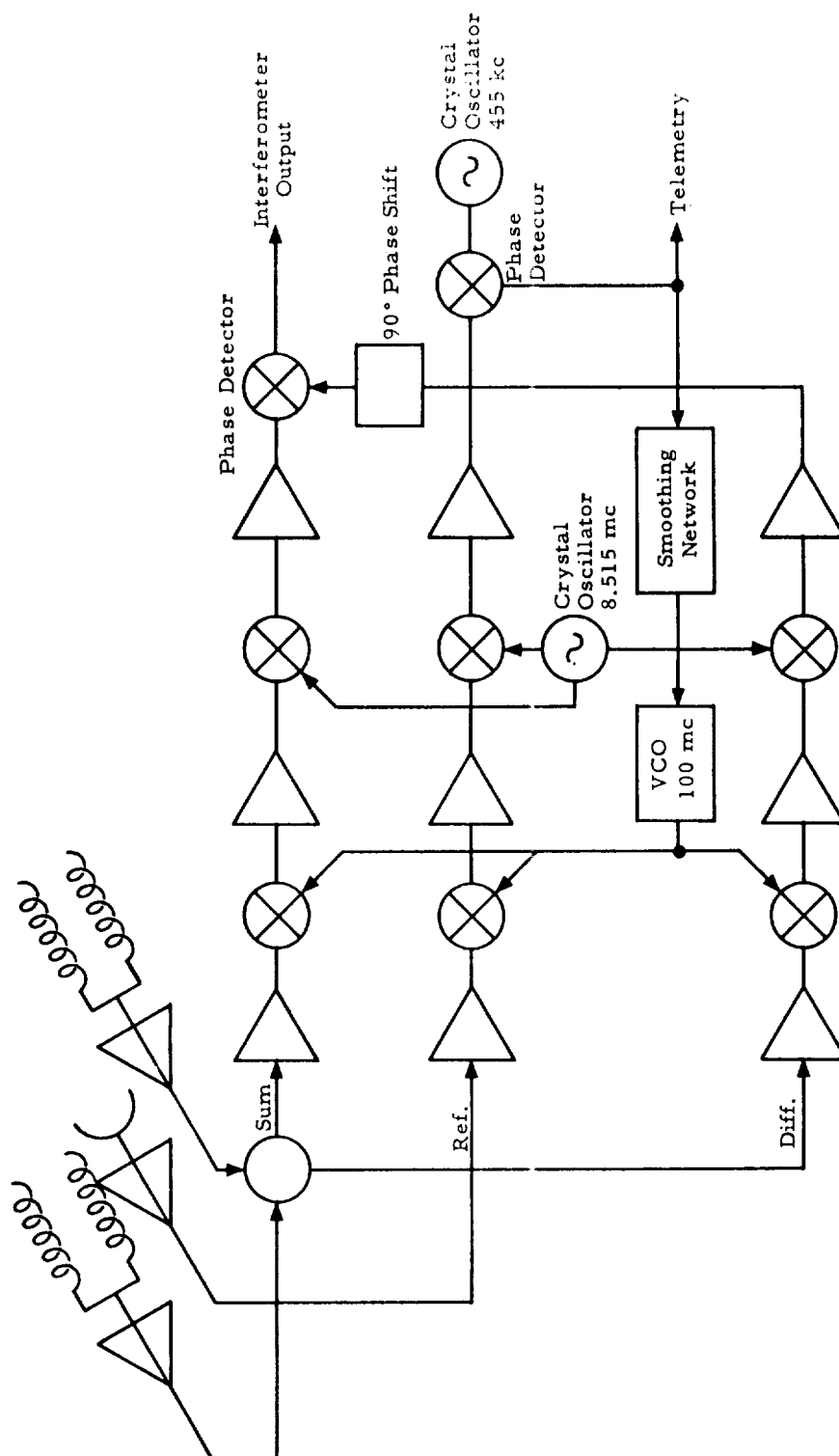
74

Figure 4.3. Interferometer Block Diagram. (Cross-correlation of "sum" and "difference" signals, for best results with unequal antenna signals).
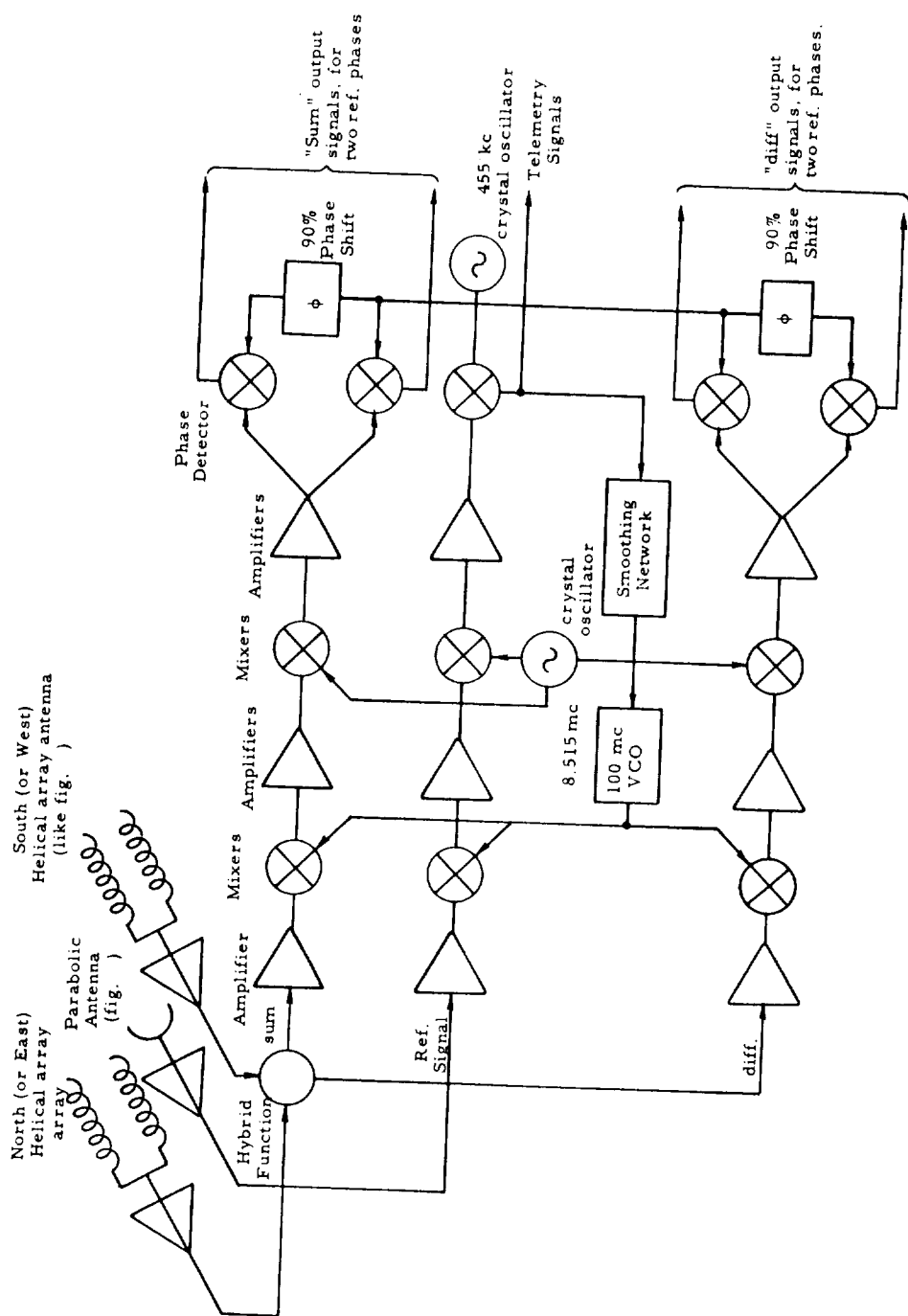

Figure 4.4. Interferometer Block Diagram. (Coherent detection of "sum" and "difference" signals, for best signal-to-noise ratio at output).

is for the system of Figure 4 4 . This degradation in performance is caused by the correlation of two noise signals (the sum and the difference signals).

Figure 4-4 shows a different type of interferometer circuitry in which the difference vector from the two interferometer antennas is compared to a reference signal obtained from the large parabolic antenna located at the center of the interferometer array. Because the geography of this center antenna is such that it is not in the center of the array except for signals arriving from directly overhead, the difference vector is compared to the parabolic antenna signal in two separate phase detectors with a 90° shift in the reference phase between the two detectors. In principle, such a scheme should give good results if the difference vector vanishes at interferometer nulls. However, it is believed that reflections from ground, buildings, and structures within the interferometer array caused an unbalance in the signal to the antennas. This unbalance destroyed the utility of this technique.

4.2.5 Data Reduction and Storage

The following types of information were recorded and reduced for teletype transmission to the operations center in Los Angeles:

a. Telemetered information such as temperature, ionization, magnetic field, etc.

b. Direct observations of the carrier such as signal strength, polarization, signal strength fluctuations.

c. Tracking information.

All possible information was recorded at each station on a 7-track Ampex tape recorder, model FR-107. This included telemetered information as received by the phase-lock receiver, voice commentary on the operations approximate carrier frequency, and local parameters such as signal strength, and phase error by means of audio voltage-controlled oscillators. Each station also made a galvanometer recording of the output of discriminators which detected the telemetered subcarriers from the payload. Time, signal strength, and (for the Hawaii station) interferometer output, were also recorded on Sanborn recording. Appendix C is the Able-1 data acquisition format revised on the basis of Flight 1 and applied with appropriate modifications to Flight 2 in November.

The following data handling equipment was available at each ground station:

a. Ampex 7-track tape recorder, Model FR-107. At its normal running speed of 7-1/2 in./sec, a useful bandwidth of at least 10 kc was obtained for each recording track.

b. Sanborn Model 150 8-channel galvanometer recorder. Signals from d-c to about 50 cps could be recorded at paper speeds from 0.2 to 100 mm/sec. 1mm/sec recordings were used normally.

c. Hallamore subcarrier discriminators. These discriminators employed an audio-phase-locked loop principle to demodulate each of the standard RDB subcarriers (numbers 1 through 6). A d-c output signal was obtained from each discriminator which is an analog of the frequency of that subcarrier. Noise bandwidths from 5 to 100 cps were obtained under varying conditions.

d. Hallamore voltage-controlled oscillators. Voltage-controlled oscillators for RDB channels from 1 to 10 were provided, to allow slowly-changing d-c voltages (such as signal strength, gain control bias, interferometer output) to be recorded on magnetic tape as slowly-changing audio-frequency signals.

e. Hewlett-Packard Counter, Model 523B. This counter had a 1 mc oscillator which was used as a secondary frequency standard for each ground station. The counter was used to calibrate voltage-controlled oscillators and discriminators.

Data reduction was crudely accomplished vy visional inspection of Sanborn recordings. Hourly reports were sent by teletype to Los Angeles summarizing the observations made during the previous hour from Sanborn recordings, from azimuth and elevation measurements, and from any other sources. The data reduction process resulted only in quick-look information. Careful analysis of both Sanborn recordings and of the magnetic tape recordings in Los Angeles was also required to fully exploit the available information.

4.2.6 Ground Station Communications and Data Transmission

The communication network of the Able-1 program was designed to fulfill two primary functions: (1) to provide orientation information rapidly to

each of the ground tracking installations to enable them to locate and detect the beacon output of the fourth stage of the Able-1 vehicle, and (2) to process data rapidly as required for firing the fourth stage vernier rockets.

The location of stations and the general relationship of elements of the communication system are shown in Figures 4-5 and 4-6 . The Operations Center at STL functioned as the control point for the tracking network.

The basic communications system between ground stations and the Operations Center in Los Angeles was a teletype network. During operations, a 24-hour leased wire teletype service at 60 wpm was provided for Hawaii, Manchester, Singapore, and AFMTC TWX facilities were used to communicate with Millstone as needed each day.

Backup telephone facilities were used during critical periods. Two conference nets were used: one linked Hawaii, Manchester, and the Operations Center, the second conference net linked Millstone, AFMTC, and the Operations Center. These telephone facilities were used during launch and for several hours thereafter until the operation became routine.

During periods between operations, teletype service was maintained for 8 hours per day to Hawaii, for 12 hours per day to Manchester and Singapore, and 24 hours per day to AFMTC. TWX service to Millstone was always available.

These communications links were used for administrative traffic such as logistics, technical discussions, etc., between operations. During operations these communications networks were used to inform the ground stations of exact time of launch, of steering information, and for transmission of instructions. The stations also sent home-tracking and telemetry information.

The Operations Center in Los Angeles had a teletype printer for each circuit (with Hawaii and Manchester sharing one teletype machine). The Operations Center was located adjacent to the IBM 704 computer facility in order that flow of information between the trajectory computing facility and the ground stations be as smooth as possible. This Operations Center was also used as headquarters for the Project Director
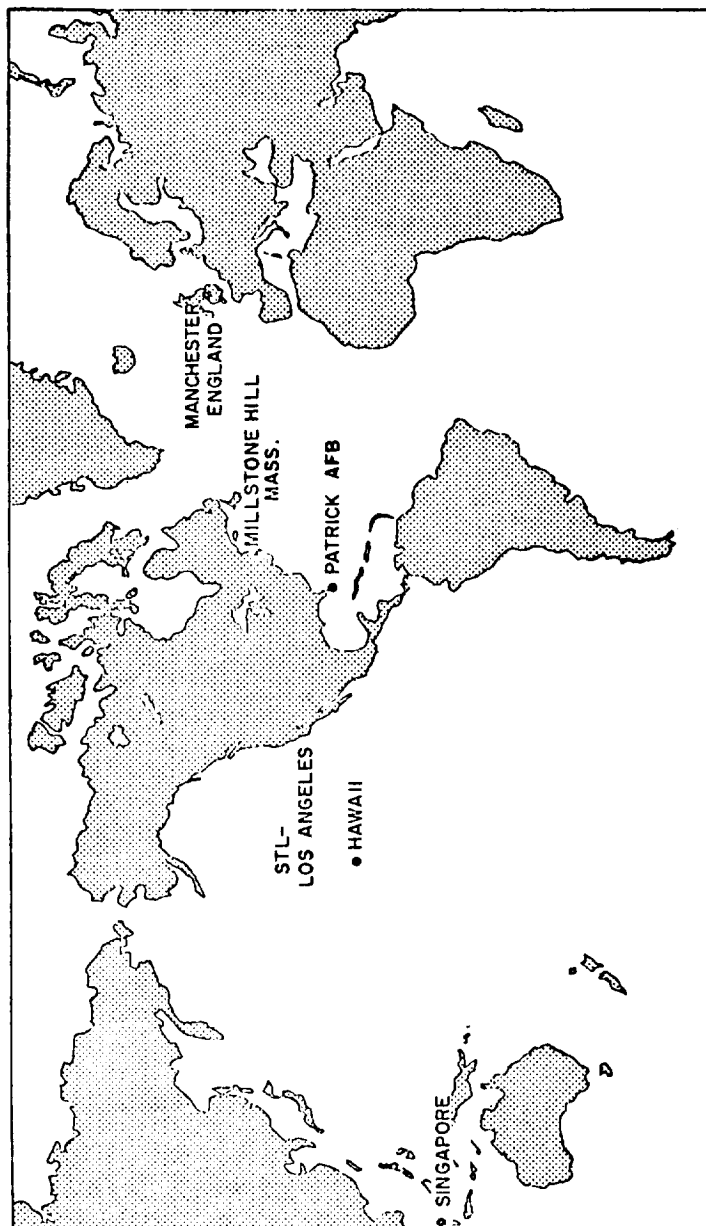
Figure 4-5. Ground Communication Net.

80
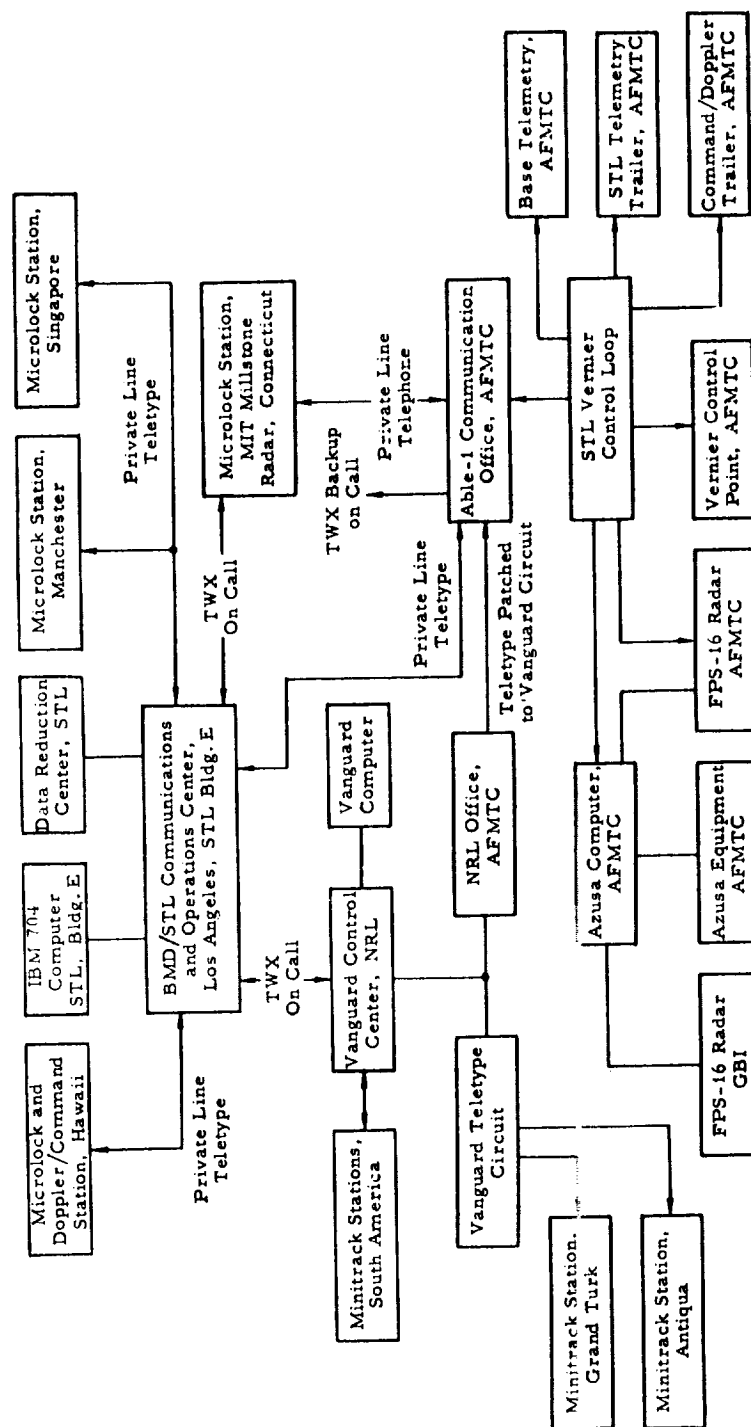
Figure 4-6. Ground Station Network.

4.2.7   Special Tracking and Photographing Task with an Astronomical Telescope

    a.   Introduction

        A few hours after launch, the third and fourth stages of the Able-1 missile were far enough from the earth and had small enough angular motion in the sky to stay easily in the field of view of a large astronomical telescope. Sunlight reflected from the third stage (and possibly also the fourth stage for the first one-third day of flight) was expected to provide a bright enough source to be within the range of a telescope of good quality with an aperature of 40 inches or more. Consequently, arrangements were made with the Mount Wilson and Palomar Observatories to attempt to photograph the third stage and, if possible, also the fourth stage with the 48-inch telescope.

    b.   Importance of Obtaining a Photograph

        A photograph of a lunar probe would be of great value for at least three reasons:

        (1) It would demonstrate the value and capabilities of optical surveillance. The current space probes depend entirely upon radio means for tracking and surveillance. Whereas radial-velocity and range data can be obtained to high precision with radio techniques, angular positions obtained by even the largest radio installations are extremely poor compared to those obtained with ease by only moderate optical instruments. Even a 6-inch optical telescope is capable of determining angular positions accurately to a second of arc. To obtain similar accuracy at a radio frequency of 100 mc would require a telescope (or interferometer) with an aperture of about 200 miles. Radio methods may be sufficient to navigate a missile to the vicinity of the moon, but advantages of precise angular data for more ambitious projects is obvious.

        (2) Several moderately-spaced optical observations would enable the fixing of a precise trajectory of the vehicle. This would be especially desirable if the vehicle had ultimately escaped the range of detection of the radio receivers or if the radio equipment on the missile had failed to operate properly.

(3)   A photograph of a missile on its way to the moon, or even far from the earth would have obvious prestige value. A detailed description of the preparations undertaken for lunar probe photography is located in Appendix A.

4.3   Station Installations

Each ground station is described briefly below. A more complete tabulation of the facilities at each station is provided in Table 4-2 and Appendix B.

4.3.1   Communications Office, AFMTC

The Able-1 vehicle was launched at AFMTC, Florida, where the launch data was gathered by the communications office. The launch and flight data necessary to support the Manchester station was sent from AFMTC communications office to the Operations Center in Los Angeles. The Operations Center had less than one-half hour to compute the trajectory and transmit pertinent information to Manchester. Because of the need for rapid processing of the first 10 minutes of flight data, telephones and intercom, or messengers were provided at AFMTC to speed delivery of the material from the source to the communications office. Information regarding launch time, time of power flight, and tracking radar angles was also required. The communications office was in operation by 8 July 1958 for participation in prelaunch tests and support of the Able-1 program.

4.3.2   Able-1 Ground Station, AFMTC

The Able ground station installation at AFMTC was intended as a launch control station, and as a station for reception of telemetry signals after launch. This station was also responsible for checking of the payload and of the second stage doppler/command transceiver during countdown.

The station is located on an isolated plot of ground about 2 miles from the Able-1 launching pad. A photograph of the station is shown in Figure 4-7 .

The station consisted of two trailers with electronic equipment and provided its own diesel-driven generator power. The station had the following communications facilities with the base:

TABLE 4-2

| Item	AFMTC	Hawaii	Manchester	Singapore	Millstone	STL	Total
Receivers							
Microlock - 108.06/108.09 mc	1	2	1	1	1	1	7
Microlock - 378 mc	0	0	0	0	0	0	-
Microlock - 972 mc	0	0	0	0	0	0	0
Test - 972 mc	0	-	-	-	-	-	0
Communications - 153 mc	0	0	0	0	0	0	-
Faraday rotation at 108 mc	-	-	-	-	-	-	-
Transmitters							
Command/Doppler - 115 mc - 250 w	1	0	-	-	-	-	1
Command/Doppler - 115 mc - 5 kw	0	1	-	-	-	-	1
Command/Doppler - 402 mc - 10 kw	0	0	0	0	-	-	0
Communications - 147 mc - 10w	0	-	-	-	-	-	0
Communications - 147 mc - 1200w	0	0	0	0	0	0	0
Antennas							
Helical Array - 108/114 mc - 20 db gain	0	4	0	1	0	0	5
Helix - 108/114 mc - 14 db gain	2	1	0	0	0	0	3
Parabola - 60 ft - 108/114/147/153/ 378/402/972 mc	-	-	-	-	-	-	-
Parabola - 85 ft - 108/147/378 mc	-	-	-	-	-	-	-
Parabola - 250 ft - 108/153/378/402 mc	-	-	-	-	-	-	-
Helical Array - 378 mc - 20 db gain	-	-	-	-	-	-	-
Helix - 378 mc - 14 db gain	-	-	-	-	-	-	-
Dipole - 147/153 mc - 0 gain	-	-	-	-	-	-	-
Faraday rotation experiment - 108 mc	-	-	-	-	-	-	-
Doppler Data Extraction							
108/115 mc - 16 fd output	1	1	-	-	-	-	2
378/402 mc - 1 fd output	-	-	-	-	-	-	-
108/378/972 mc propagation	-	-	-	-	-	-	-
Command Unit							
115 mc	1	1	-	-	-	-	2
402 mc	-	-	-	-	-	-	-
Ranging Unit							
378/402 mc carrier; 20 kc, 100 cps subcarriers; AGS-type data processing	-	-	-	-	-	-	-
108/115 mc carrier; 2 cps subcarrier	1	1	-	-	-	-	2
Data Recording and Reduction							
Ampex FR-107 tape recorder	1	2	1	1	(1)	1	6(+1)
Sanborn 8-channel recorder	1	1 + 6/8	1	1	-	1	5-6/8
Discriminators - Hallamore	6	6	6	x2	-	6	30
Discriminators - new Taber design	-	-	-	-	-	-	-
Sampling switch - for multidata recording on one Sanborn track	-	-	-	-	-	-	-
Subcarrier oscillators, Hallamore	5	20	5	5	-	-	35
Test Equipment							
Signal Generator, HP Model 608D	1	1	1	1	1	-	5
Noise Generator, Kay Electric Co., Model	1	1	1	1	-	-	4
Signal Generator, HP Model 612	-	1	1	1	-	-	2
Signal Generator, Meas..Corp., Model 80R	-	1	1	-	-	-	1
VTVM, HP Model 400H	2	2	2	2	-	-	8
VTVM, HP Model 410B	1	2	1	1	-	-	5
VTVM, Kintel Model 202B	1	1	1	1	-	-	4
Frequency Meter, Gertch Model FM3R	1	1	1	1	-	-	4
Frequency Meter, HP Model 500B	1	1	1	1	-	-	4
Oscillator, HP Model 200CD	1	2	1	1	-	-	5
Wide band oscillator, HP Model	-	-	-	-	-	-	-
Electronic Counter, HP Model 523B	1	1	1	1	-	-	4-
Oscilloscope, HP Model 130BR	1	1	1	1	-	-	4
Oscilloscope, Teletronix 545 or equiv.	-	1	-	-	-	-	1
Panadaptor, Panoramic Radio Model	1	1	-	-	-	-	2
Megacycle Meter, Booton Model	1	2	1	1	-	-	5
Precision Clock, American Time Prod., Model	1	1	1	1	-	-	4
WWV Receiver	1	2	1	1	-	-	5
Function Generator, HP Model	1	1	-	-	-	-	2
RF Impedance Bridge, HP Type	-	1	-	-	-	-	1
Crystal-controlled oscillator, 378 mc	-	-	-	-	-	-	-
Crystal-controlled oscillator	-	-	-	-	-	-	-
Facilities							
Trailer, equipment	2	3	1	1	-	-	7
Diesel-Electric Generator, 60 kw	5	3	0	2	-	-	10
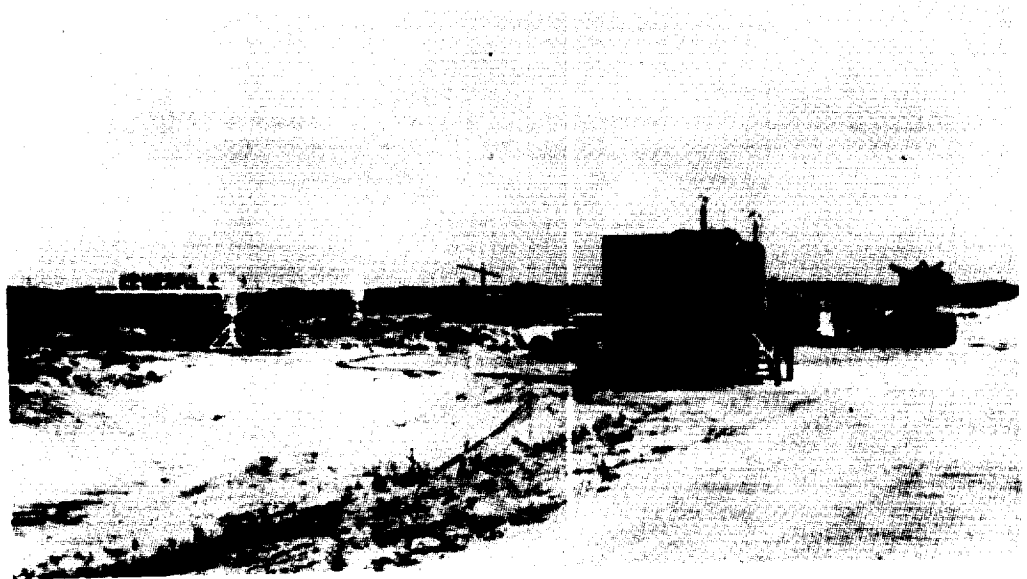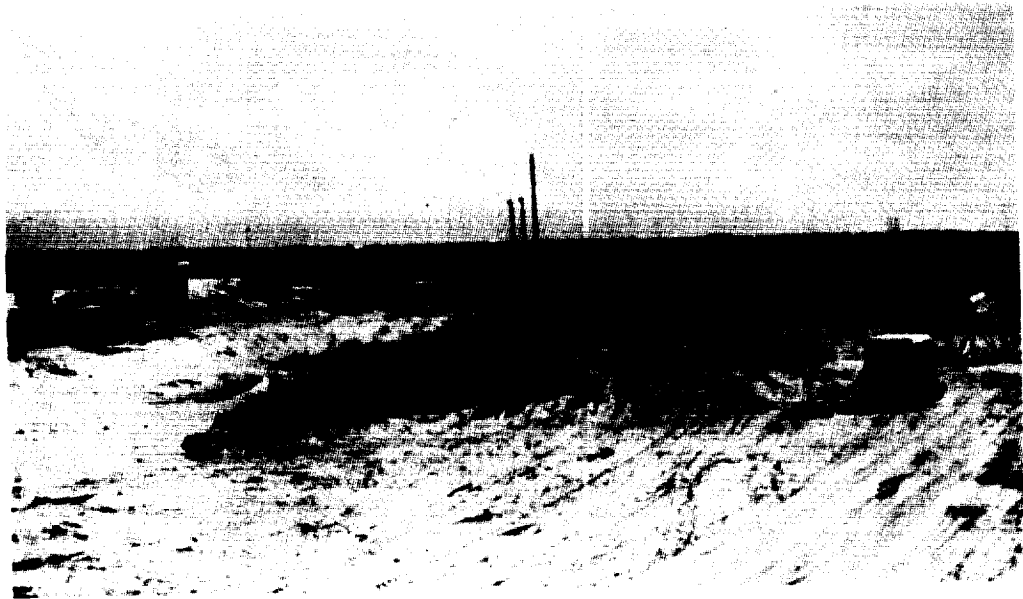
Figure 4-7. AFMTC Station

a. Black telephone

b. Vernier loop telephone

c. Base timing

d. Thor countdown speaker.

The AFMTC ground station had the following functions:

a. Checkout of second stage doppler/command transceiver and command circuits.

b. Checkout of payload doppler/command transceiver and vernier firing circuits.

c. Checkout of payload telemetry.

d. Measure the velocity of the missile to 0.1 feet per second.

e. Shutdown the second stage when its proper terminal velocity has been achieved.

f. Fire the proper number of vernier rockets based on exact velocity measurements after third stage burnout

g. Determine that vernier rockets have fired properly.

h. Receive telemetry information until contact with the payload is lost as the payload drops below the horizon.

To achieve these functions the AFMTC station had the normal phase-lock receiver at 108.06 mc, data recording installation including tape recorder, Sanborn recorder, discriminators, voltage-controlled oscillators, etc. The receiver utilized a manually-steered helical antenna of 19-db gain and a pre-amplifier at the antenna which has a noise figure of about 2.5 db.

The station had a 250-watt transmitter at 114.813 mc which was used for the doppler/command functions. This transmitter fed a manually-steered helical antenna with 14-db gain. It also had doppler data extraction equipment capable of measuring the round trip doppler shift very precisely and which recorded the doppler shift each second (for the second stage control function) and each two seconds for the vernier rocket firing functions. Recording was

accomplished in both cases by a digital printer driven by an H. P. counter. An audio command-tone generator was also prov.ded with a capability of modulating the transmitter. This command-tone generator had six push buttons (with proper interlock and timing circuits), so that the station could transmit any desired command to the payload.

4.3.3 Hawaii

The Hawaii station was located at the southernmost point in the Hawaiian Island chain at South Point on the island of Hawaii. Figure 4-8 is a photograph of the Hawaiian installation. The station was located about two miles from the tip of the island in gently sloping pastureland. There was an unobstructed view of the ocean and the horizon from about 060° true south and around to about 300° true. Volcanic mountains shielded the station from the nearest sizable towns of Kailua and Hilo, each of which is about 70 miles from the site. Therefore, there was very little man made radio interference at the station.

a. Antenna System

The primary antenna at the Hawaii station was a 60-foot parabolic antenna mounted at the top of a 70-foot tower of steel and concrete. This antenna (a modified TLM-18 antenna manufactured by Radiation, Inc.) could be rotated through 360° in azimuth and through 95° in elevation. At its receiving frequency of 108.06 mc the antenna had a beamwidth of about 8°.

The parabolic antenna was at the center of a group of four helical array antennas manufactured by the Rantec Corporation. These array antennas were arranged in a square pattern with one diagonal north-south and the other diagonal east-west forming an interferometer array. The distance across the diagonal was 262 feet. One of these antennas was also used as a transmitting antenna for the 114-mc transmitter. Each of the helical array antennas consisted of four helices. The array has a gain of about 19 db over an isotropic antenna. Figure 4-9 shows one of these antennas.

A transmitter site was originally obtained about 1300 feet NW of the parabolic antenna. A manually-steered single helix antenna of 14-db gain was located at the site and originally intended for use with the 114-mc transmitter. However, the transmitter was shifted to the south interferometer
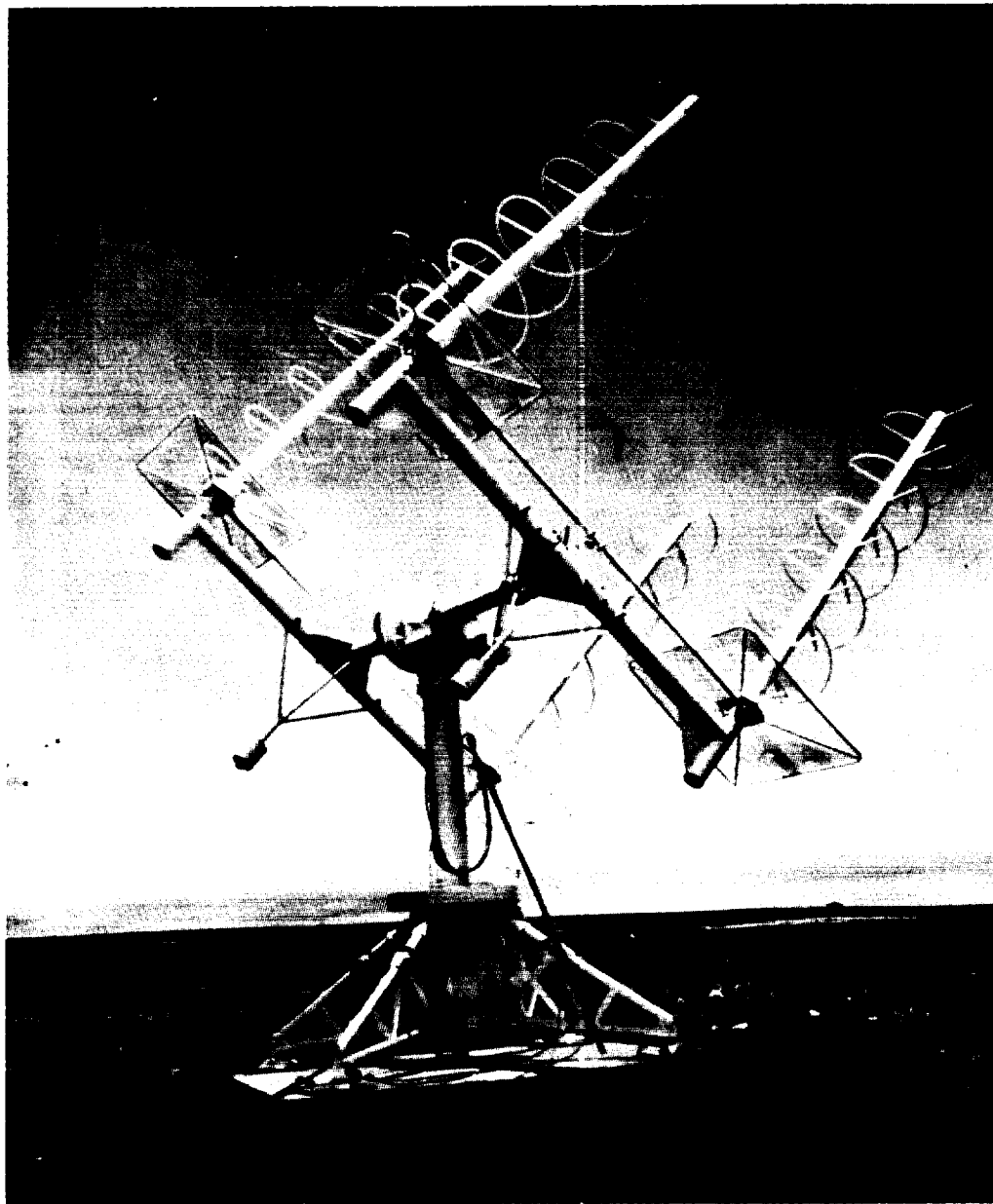
Figure 4-8. The Hawaii Ground Station

Figure 4-9. An Array of Helical Antennas at the
Hawaii Ground Station.

antenna during the October shoot so that the transmitting antenna was not used. A calibration antenna tower about 100 feet high was also located at the transmitter site. This tower has a dipole antenna (vertically polarized) at its top which was used to calibrate all of the receiving antennas.

Calibration was also attempted with helicopters towing an STL built self-contained transistorized transmitter.

b. Support Equipment

The Hawaii station had a complete dual receiving installation consisting of a pair of phase-lock receivers which could receive 108.06- or 108.09-mc signals, two Ampex tape recorders, two Sanborn galvanometer recorders, and a double set of voltage-controlled oscillators. This dual installation allowed simultaneous recordings of telemetry from two frequencies.

A 5-kw Gates transmitter was located on a separate trailer van at the south helical array antenna. This transmitter was provided to permit the firing of the retrorocket which was to have placed the payload in orbit around the moon, and in conjunction with the phase-lock receiver, to measure the doppler-shift and hence the exact velocity of the payload.

A doppler data extraction equipment was provided which compared transmitted and received frequencies and produced a signal equal to sixteen times the doppler frequency. This signal was counted with an H. P. counter and recorded on a digital printer.

The Naval Ordnance Test Station (NOTS) provided quick-look equipment for reconstructing a television picture of the moon. This equipment was designed to interpret the TV picture which was to have been transmitted at 108.09 mc for the August and October firings and to provide a photographic replica of the moon's surface.

A ready-room was constructed which provided office space for the station manager, and lounging area for relaxation of the staff crew, as well as rest room and sleeping facilities during shots and work space for the reduction of data.

The electronic equipment (except for the 5-kw transmitters) was housed in two converted M-119 trailers parked at the base of the parabolic antenna.

Power for the station was obtained from three 60-kw diesel-driven generators which were located on the ground to the rear of the parabolic antenna structure. A 2000-gallon fuel storage tank provided for about ten days of operation without refueling. Two commercial telephone lines were brought into the station from the Hilo exchange.

c.   Communication Equipment

The communication equipment at Hawaii was a teletypewriter-perforator set with service maintained eight hours per day and increased to 24 hour service during operations.

4.3.4   Manchester

The Manchester station was located near Manchester, England, at The Jodrell Bank radio telescope installation of Manchester University. This radio telescope, a photograph of which is shown in Figure 4-10, had a 250-foot parabolic antenna as its primary facility. The antenna could be pointed in any direction from a control room located several hundred feet from the antenna. Space Technology Laboratories installed an instrumentation trailer near this control room which contained the basic receivers and data processing equipment. A small temporary hut for use as an office was also constructed near the trailer, and the rear of the trailer was extended by another temporary structure which housed the teletype machine and provided additional space.

Operation at Manchester was a cooperative venture in which the British supplied personnel to operate their antenna steering system and STL supplied personnel to operate the receivers and instrumentation portion of the system.

a.   Antenna System

The 250-foot parabolic antenna is a very deep dish with the focal length equal to half of the radius of the dish. Antenna feeds are supported at the focal point by a mast which projects outward from the center of the parabola. The dish is 250 feet in diameter and the feed mast is approximately 62 feet long.
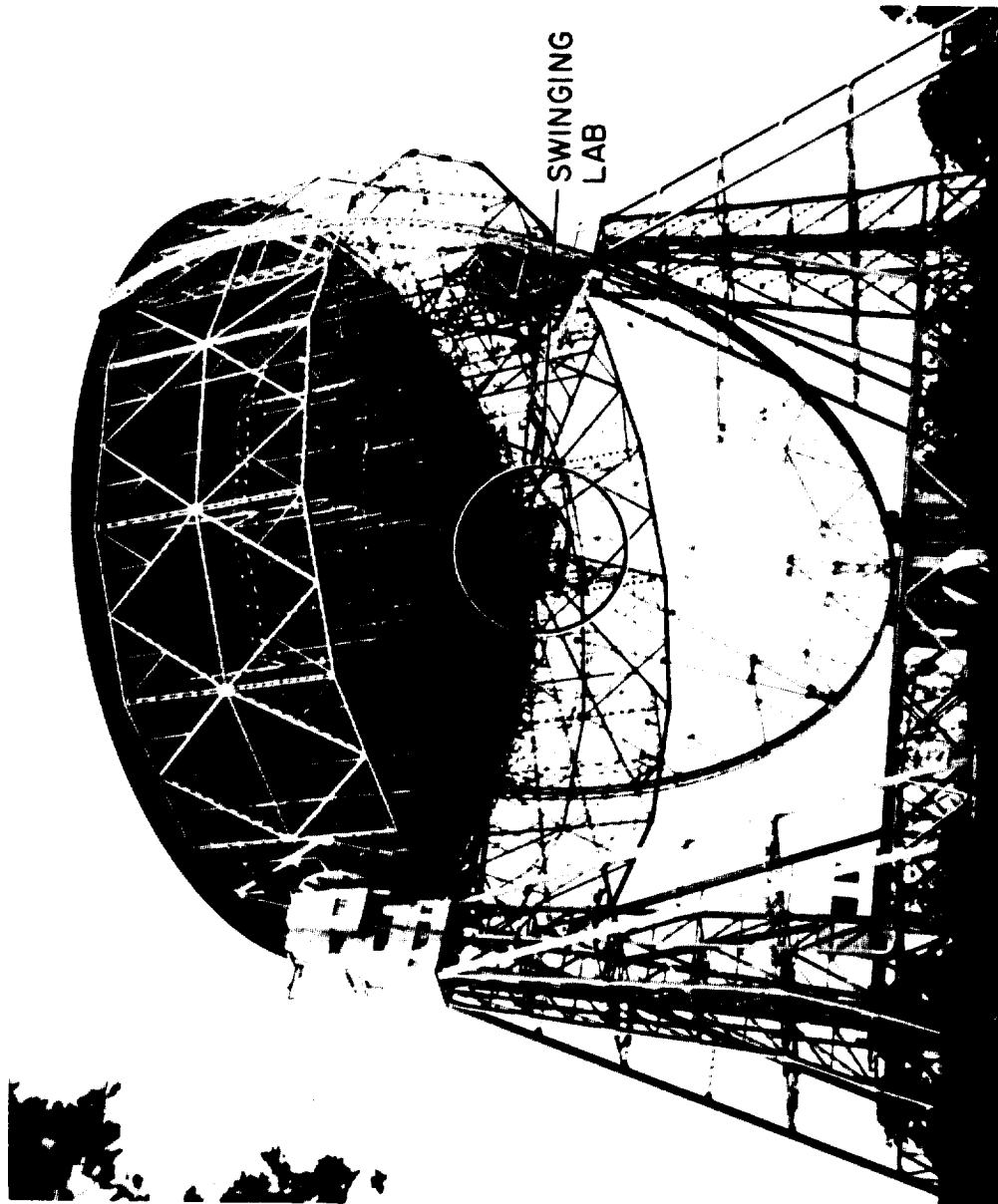
SWINGING LAB

Figure 4-10. The 250-Foot Parabolic Antenna at Manchester Station.

This mast may be used to support preamplifiers and other equipment. A swinging laboratory was installed behind the surface of the parabolic dish and near its center and so pivoted that it remained upright even though the antenna was tilted from vertical to horizontal. The swinging laboratory (shown in Figure 4-11) was about 8 feet wide and 10 feet long. Access to the laboratory could be obtained by taking an elevator from the base of the tower supporting structure up to the top of the tower supports; a catwalk (which could be used only when the antenna is pointed straight up) then permitted one to walk out through the superstructure underneath the parabolic antenna to the swinging laboratory. This same catwalk also provided access through an aperture in the center of the surface of the parabola to the reflecting surface and (by a ladder) to the top of the mast which supported the antenna feed.

All signal and power cables ran from the antenna feed through the swinging laboratory out to the elevation pivots at the supporting towers and down the supporting towers back to the pivot for the azimuth motion, then down a 20-foot vertical hollow shaft to a horizontal tunnel which carried the cables to the antenna control building. Cables from the trailers were over 1000 ft long.

The 250-foot antenna had a beam width of 2° at the frequency of 108 mc used for the Able-1 program. The antenna feed (constructed by the British) performed very well. The first side lobes are better than 20 db below the main antenna beam.

b. Tracking Method

The antenna system tracked the space probe by carefully plotting signal strength as the elevation angle (or as azimuth angle) changed in discrete steps. Plots obtained in this way were symmetrical and allowed determination of the actual elevation (or azimuth angle) to better than $1/4^{\circ}$ accuracy. Since the antenna control system was located in the control building, a remote indication of signal strength was provided from the Microlock receiver in the STL trailer for the use of the British telescope operators.

c. Space Technology Laboratories Instrumentation

The STL trailer included a single phase-lock receiver which could be tuned to 108.06 mc or to 108.09 mc at the operator's choice. This shift in
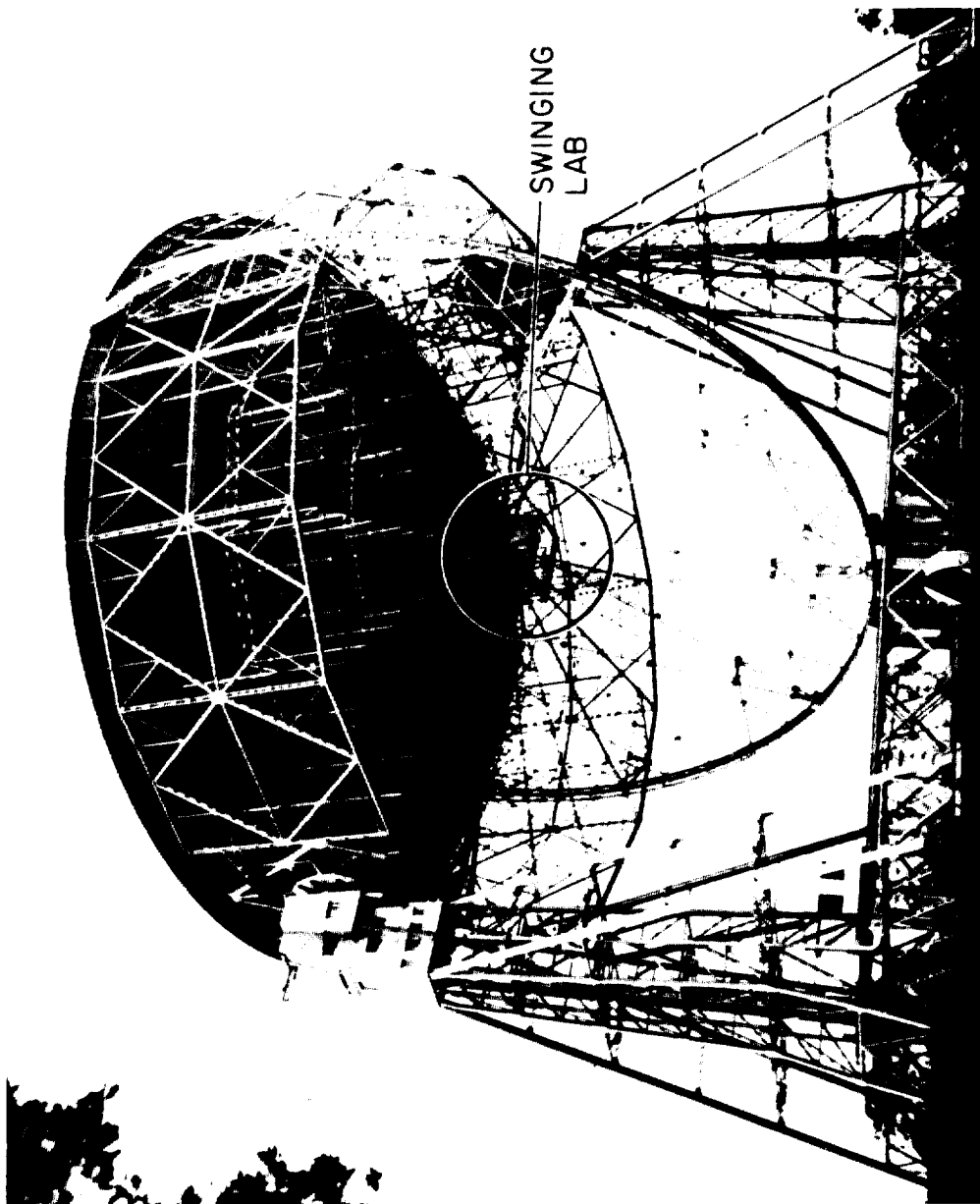
SWINGING
LAB

Figure 4-11. The Swinging Laboratory at Manchester.

tuning was achieved by changing the oscillator crystal of the 8.5-mc oscillator within the receiver.

An Ampex FR-107 tape recorder was used to record both the phase modulation and the amplitude modulation signals from the Microlock receiver. Timing signals, voice commentary and a group of voltage-controlled oscillators for the recording of gain control bias, signal strength, etc., were also recorded.

The phase-lock receiver output (which contained the telemetered information from the payload) was recorded on magnetic tape and also on a Sanborn recorder after being demodulated by a bank of Hallamore subcarrier discriminators.

The Manchester station did not have the doppler/command transmitter or doppler readout equipment.

4.3.5 Singapore

The Singapore station was located about 5 miles north of this city on the receiving antenna farm of Cable and Wireless, Ltd. One helical array antenna, the instrumentation trailer, and the diesel-driven generators were located in a vacant field near a row of bungalows which were used normally for housing of Cable and Wireless personnel. One of these bungalows was made available to STL for use as an office and ready room.

The Singapore site offered material test advantages including a longitude between that of Manchester and Hawaii, freedom from radio interference at 108 mc, and the proximity of a large city whic 1 facilitated problems of housing, supplies, and logistics. An alternate site nea) Manila had also been considered but was rejected because of high radio noise.

a. Antenna System

The Singapore station had a single helical array antenna which was physically identical to each of the array antennas of the interferometer at the Hawaii station. This antenna had about 19 db cf gain over an isotropic radiator and a bandwidth of about 30°. A one-speed electric motor allowed the antenna to be pointed in any direction. The antenna position was indicated by one-speed syncrodials with simple switching used to control the reversible electric motors on the antenna drive.

b.   Instrumentation

The instrumentation for Singapore was very similar to that provided at Manchester. This included a phase-lock receiver, Ampex tape recorder, Sanborn chart recorder, and two discriminators to demodulate the telemetered information from the lunar probe for display on the Sanborn recorder.

The signals from WWV were obtained only sporadically. The best timing signals available were those from the Chinese station in Peking.

Two 60-kw diesel-driven generators were provided for primary power.

Communications from Singapore to the Operations Center at Space Technology Laboratories were accomplished by radio teletype. Transmission was from Singapore to London, England, via Cable and Wireless. Signals were wired into the Manchester station and relayed on to Los Angeles via a Manchester radio link to the east coast of the United States with Bell System wire lines across the continent. Twelve hour service was provided except during tracking operations when twenty-four hour service was provided.

4.3.6   Millstone

MIT constructed a large tracking radar facility at Millstone Hill, New Hampshire. The antenna was operated under the direction of the Lincoln Laboratories. It was an 84-foot parabolic reflector manufactured by D.S. Kennedy and Company and had a gain of approximately 26.8 db at 108 mc/sec. This station was capable of detecting the Able-1 second-stage as soon as it rose above the local horizon from AFMTC using a high power radar set. The radar was used to track the second stage (by skin tracking) through second stage burnout and for several minutes after the third stage was separated.

When the second stage dropped below the local horizon, the Millstone antenna was converted to passive reception of the 108.06-mc telemetry from the payload. The payload was then tracked by the phase-lock receiver, with telemetry information recorded on an Ampex tape recorder. No quick-look data reduction was provided at Millstone. The Millstone station was a

cooperative venture between MIT and STL. M T provided all of the operating personnel and all of the equipment except for a phase-lock receiver and its associated preamplifier and calibrating signal generators.

Communications between Millstone and the STL Operations Center were accomplished by teletype. During tracking operations teletype service was continuous. Long distance telephone service was also used between Millstone and AFMTC. Millstone tracking data on the second stage was used as one source of data to determine the burnout conditions at the end of the third stage, thus determining the proper number of vernier rockets which must be fired to adjust the velocity of the payload.

4.3.7 Malabar Station, Melbourne, Florida

At the Malabar Station near Melbourne, Florida, RCA and Radiation Incorporated, jointly operated a 60 foot diameter reflector manufactured by D. S. Kennedy and Company. This dish is quite similar to the one at South Point, Hawaii, and was used for telemetry.

4.3.8 Army Ballistic Missile Agency

The Army Ballistic Missile Agency at Cape Caneveral and Huntsville, Alabama used a six-turn helix and a 60-foot diameter Kennedy reflector respectively as tracking antennas on 108.09 mc.

4.4 Functioning of Ground Stations During Flights

4.4.1 AFMTC Station

During each launch the AFMTC station participated heavily in countdown activities to ensure proper functioning of the airborne counterparts to the doppler/command telemetry ground equipment

At launch and thereafter for about 17 minutes, the AFMTC station produced accurate doppler information, using the doppler/command system to measure the range rate of the payload. This and other data were used to determine the number of vernier rockets to be fired; the indicated number (all verniers in both October and November flight) was then fired by command.

After the first 17 minutes of flight (October and November shots) telemetry data was received whenever the payload was above the local horizon.

During the second day of the October shoot, the command transmitter was operated and attempts were made to separate the vernier rocket ring and, subsequently, to fire the retrorocket. Although there were indications from the payload transmitter that the payload locked onto the ground transmitter carrier, neither of the commands was executed. This failure is now attributed to the low temperature of the payload at the time of command. The batteries provided for squib firing cannot deliver sufficient power at low temperature.

4.4.2 Millstone Station

Millstone station successfully acquired the second stage on their 400-mc radar during the October and November shoots, and skin-tracked the second stage for some minutes after separation of the second and third stages. At the termination of the skin-tracking portion of the operation, when the second stage dropped below their local horizon, the antenna feed was shifted to 108 mc, and tracking and telemetry data were obtained for the duration of the flight in October.

During the November flight only the skin-tracking phase was completed, since the third stage did not ignite.

4.4.3 Manchester Station

The Manchester station acquired the payload on both the October and November flights and tracked it as long as it was above the local horizon. For the October flight this tracking period lasted for many hours on each of two days; for the November flight, the payload was very low on the horizon and was tracked only sporadically and for a few minutes as it passed to the south of the station.

During the October flight the flight path deviated from the predicted path by a few degrees; this deviation caused the initial acquisition (made about 11 minutes after launch) to be made on a minor lobe of the antenna. After about 40 minutes of tracking (with a signal that appeared to be very weak) the error was corrected and further tracking was done with the main lobe. Accuracy of tracking data from Manchester was excellent, and the telemetry data was very good due to the large aperture of the antenna at that station.

4.4.4   Hawaii Station

The Hawaii station participated only in the October flight, since the other two flights did not traverse that part of the world. During the October flight the payload was tracked from the time it rose above the horizon until it sank below the horizon at the end of the tracking day. On the second day the payload was tracked as it approached the earth and was finally lost as it plunged toward the earth in the southeastern Pacific region.

Tracking and telemetry data were obtained throughout. Tracking data was better than expected from the 60-foot dish; the interferometer tracking data proved to be useless because of the existence of a large number of multi-paths caused by structures on the antenna site.

The doppler/command system was used a number of times on both tracking days in attempts to fire the retrorocket and to release the vernier rocket ring. Indications were frequently received that the payload had detected and momentarily acquired the ground transmitter carrier; however, the cold batteries in the payload were evidently not sufficiently powerful to fire the squibs and execute the commands.

4.4.5   Singapore Station

The Singapore station participated only in the October flight, since the other two flights did not traverse that part of the world. During the October flight the payload was tracked from the time it rose above the horizon until it sank below the horizon at the end of the tracking day. The Singapore station tracked the payload as it went through its apogee of about 70,000 miles; there was only one day of tracking as the payload re-entered the earth's atmosphere in the southeastern Pacific Ocean on its second lap around the world.

During the one day of tracking, the Singapore station obtained telemetry information, but since the antenna system at that station is not highly directional, useful tracking information was not obtained.

4.5   Data Handling: Able-1 Operations Center

The BMD/STL Operations Center was established in Los Angeles to control and coordinate all data handling and decision processes that were to

occur during the flight. The specific purposes of the Operations Center were the processing of tracking data received from the ground tracking stations, the determination of the actual trajectory from the tracking data, the derivation and transmission of revised steering data for ground station antennas, interpretation of quick-look telemetry data received from the ground stations during the flight, and the making of decisions as to the time of command transmission for dropping the vernier cluster and firing the retrorocket. Nominal trajectory data were derived before the flight and transmitted to the Able-1 ground stations as well as to certain other cooperating stations. These data were used to plan nominal steering periods and to control antenna steering until more accurate data based on actual tracking were received The Operations Center was in close teletype and telephone communication with AFMTC, Millstone Hill, Manchester, Hawaii, Singapore, and other groups such as the NRL Control Center. Upon the completion of the launch, powered flight, and the vernier firing task, the best estimate of burnout conditions available at AFMTC was transmitted by telephone and teletype to the Operations Center by the vernier firing task group. This estimate of burnout data was used to derive a preliminary correction to the nominal trajectory. As data were received from ground stations, it was transmitted to the Operations Center by teletype and used in a continuing operation in which increasingly accurate estimates of the actual trajectory were calculated on the IBM 704 computer of the Computer and Data Reduction Center of STL. After more accurate trajectories were calculated, revised steering data for the various ground stations was transmitted to them by teletype. This recalculation of steering data continued throughout the flight time.

The basic computer operation involved a least-squares use of deviations of tracking data from nominal values and was based upon a linear expansion of vehicle coordinates around the nominal trajectory. Such a program is quite satisfactory when the vehicle is close to the nominal trajectory. The planned operation called for calculating a new nominal trajectory when early tracking data indicated that the trajectory deviated too far from the nominal for a linear expansion to be adequate.

The planned operation for the determination of the appropriate retrorocket firing time called for a trajectory to be run to the vicinity of the moon every time that a significant improvement in trajectory determination from tracking data was accomplished. Conditions near the moon were examined and a first approximation to the desired time of retrorocket firing was determined from two-body calculations of the vehicle energy with respect to the moon after retrorocket firing. Several trajectories were planned to be run with retrorocket firing times near this approximate time. The resulting lunar satellite trajectories were to be examined and the actual firing time decided on the basis of the nature of the lunar orbits. As approximate and, later, exact times for retrorocket firing were calculated, these were to be transmitted by teletype to the main station at Hawaii, from which commands were to be transmitted to initiate retrorocket firing. Although the retrorocket could have been fired from Hawaii based on times transmitted earlier in the event the Operations Center lost communication with Hawaii, the planned operation called for direct teletype and telephone contact with Hawaii at the time of retrorocket firing to insure that the retrorocket command was transmitted as near the optimum time as possible.

4.6 Trajectory Determination for Specific Flights

4.6.1 August Flight - Missile 127

The Operations Center was manned at approximately T minus 6 hours. Earlier informal checks of station readiness were confirmed by teletype. Discussions between Los Angeles and Cape Canaveral indicated the desirability of an early formal statement of ground station readiness by the Operations Center. Plans for later flights were changed to incorporate the T minus 6 hour readiness report. The planned computer checkout was performed. At the time of lift-off, the Operations Center was in contact with Manchester, Millstone, and AFMTC, and the Operations Center with all participating ground stations in a state of readiness.

The Operations Center received the exact lift-off time, 12:18 GMT, 17 August, from AFMTC by teletype. A clock time versus minutes after lift-off table was calculated. Almost simultaneously, a teletype statement

was received from Millstone that they had not acquired the powered flight and a telephone report was received from AFMTC that the first stage had exploded, and that the first stage powered flight had terminated prematurely. After a short interval, messages were sent to all ground stations that the flight had terminated, and the ground stations and Operations Center were secured.

4.6.2 October Flight - Missile 130

Preliminary readiness checks were made with all STL ground stations during the day of 10 October 1958. A preliminary readiness report was made to AFMTC stating that all ground stations were ready. The Operations Center was fully manned at T minus 4 hours. A formal statement of readiness was given to AFMTC at T minus 60 minutes. At the time of lift-off, all ground stations and the Operations Center were in a state of readiness.

The Operations Center received by teletype the lift-off time 0342/13 EST, 11 October 1958. The vernier firing task reported to the Operations Center that eight vernier rockets had been fired and estimates of the burnout conditions were stated. The burnout altitude reported to the Operations Center was considerably higher than the actual burnout altitude, because of a misinterpretation of the Millstone tracking data, which resulted in a momentary confusion because the burnout energy appeared to be considerably in excess of that required for the lunar flight. The discrepancy was soon realized.

The data furnished the Operations Center by the vernier firing task indicated that the vehicle velocity was low by at least 200 to 300 ft/sec. Momentary confusion again resulted when Manchester reported the vehicle had been acquired at approximately the nominal position. Manchester was informed that the best estimate available at the Operations Center was that the vehicle velocity and position were appreciably below the nominal. The Manchester station discovered that the vehicle was being tracked on a minor lobe of the antenna which by coincidence was approximately as far from the main lobe as the vehicle elevation was in error (approximately 13°). This mistake was rectified and Manchester tracked satisfactorily from approximately T plus 60 minus on. Trajectory determination based upon Manchester angular tracking data and AFMTC range rate data indicated

that the burnout velocity vector was approximately 5° low in the pitch plane and the burnout azimuth was approximately 5° low. Preliminary estimates of burnout velocity magnitude indicated that the burnout velocity was at least 400 ft/sec low and the maximum altitude would be less than 100,000 nautical miles. Difficulties encountered in using satisfactorily the small amount of doppler data that could feasibly be transmitted by teletype indicated the desirability for later flights of further reduction at AFMTC and transmission of reduced results to Operations Center in addition to the rapid return of the doppler data to the Operations Center.

As soon as it was realized that the vehicle velocity was so low that the general vicinity of the moon would not be reached, the nature of the resulting elliptical orbit was examined analytically, graphically, and on the 704 computer. Estimates were made of the probability that the firing of the retrorocket would result in a permanent earth satellite. The probability appeared to be sufficiently high that a significant portion of the remaining ground station activity was devoted to attempts to fire the retrorocket. In order to prevent the possibility of the fourth stage rocket being fired prematurely by spurious signals, the vernier rocket cluster was to have been dropped by command signal during the first pass over Hawaii. Despite the repeated commands to drop the cluster, no positive indication was observed that the cluster had separated. Because of the effect of the presence of the cluster upon the antenna pattern, a change in signal strength should have been observed had the cluster separated. Continued attempts were made from AFMTC and from Hawaii to drop the vernier cluster and to fire the fourth stage rocket.

As further tracking data were received from the Manchester, Millstone, and Hawaii ground stations, increasingly accurate estimates of the vehicle trajectory were calculated. Revised steering data was sent to ground stations by teletype as soon as calculated.

Questions as to the accuracy of the trajectory determination arose when apparent range rate measurements from Hawaii indicated that the vehicle velocity was approximately 3000 ft/sec higher than indicated by the best trajectory estimate available at the Operations Center. Later, the Hawaii

measurements were realized to be spurious because of a lack of firm lock in the doppler circuitry.

The best estimates available of the trajectory based upon all available data are as follows:

Launch time		0342/13 EST 11 October 1958
Burnout conditions	time	0347/20 EST
	altitude	1,410,000 feet
	latitude	30.70° N
	longitude	71.07° W
	velocity magnitude	34,524.5 ft/sec
	velocity azimuth	70.43°
	velocity angle from vertical	64.74°
Maximum altitude (from surface)		70,717 statute miles (61,452 nautical miles)
Re-entry time after lift-off		43 hours 17.5 minutes
	latitude	21.0° S
	longitude	88.1° W

Figures 4-12 through 4-17 compare the actual tracking data with the theoretical tracking data calculated on the basis of the final trajectory parameters summarized above. Figure 4-18 shows the projection of the vehicle path in the plane of the moon's orbit.

4.6.3 November Flight - Missile 129

Preliminary readiness checks were made during the day of 6 November 1958. All ground stations were ready with no serious trouble except for the amplifier in the transmitter at the Hawaii station, and since this trouble was in the process of being corrected by T minus 6 hours, a preliminary readiness report was made to AFMTC, stating that all ground stations would be ready. The Operations Center was fully manned at T minus 4 hours. When the decision to delay the launching one day was made, all ground stations were informed that pending further clarification, a full countdown including ground station readiness checks would begin the following morning. During 7 November, the regular preliminary readiness checks were made and a report was made to
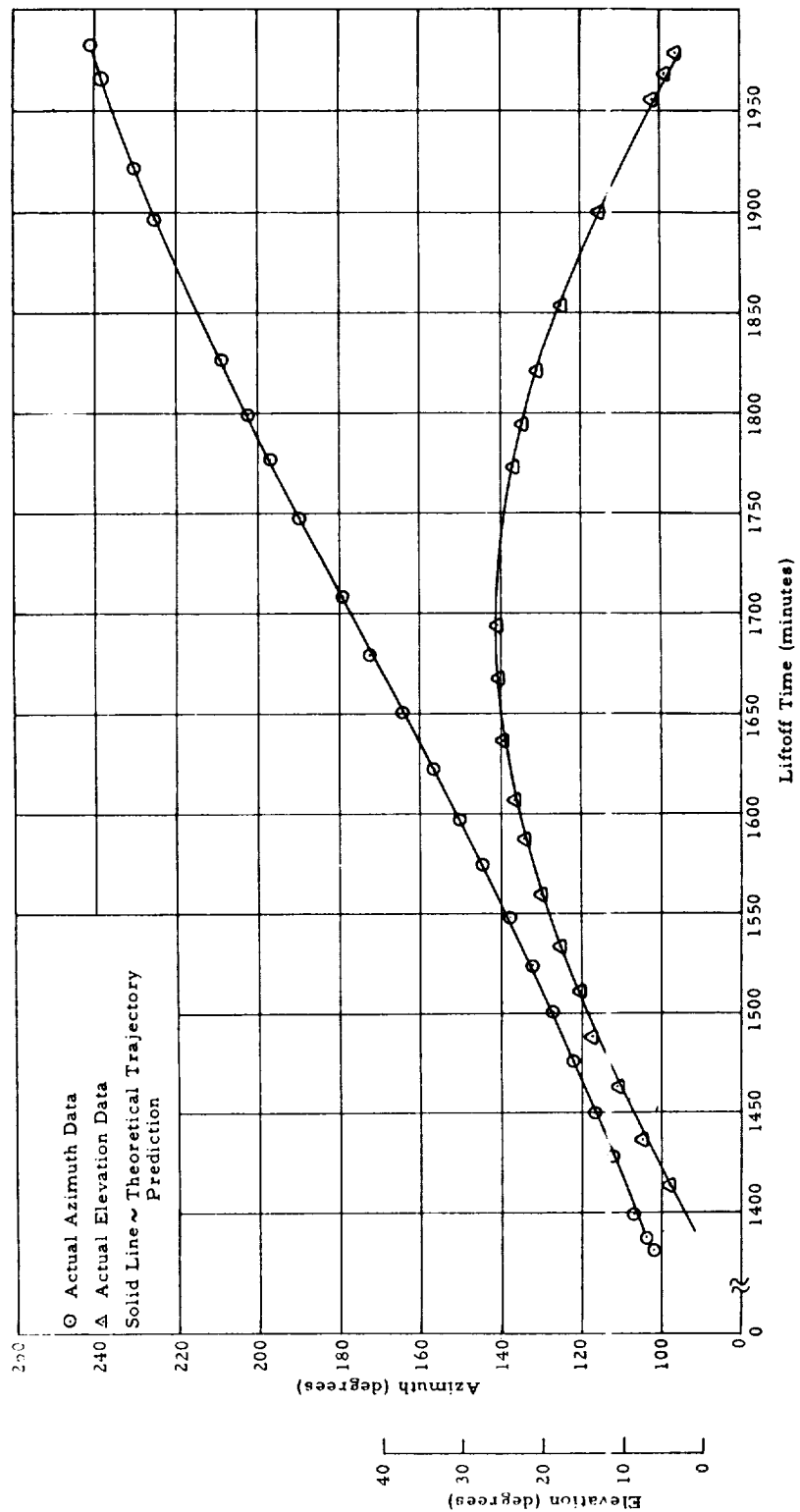
Figure 4-12. Flight II, Actual Tracking Data Versus Theoretical Trajectory Prediction, Manchester (second pass).
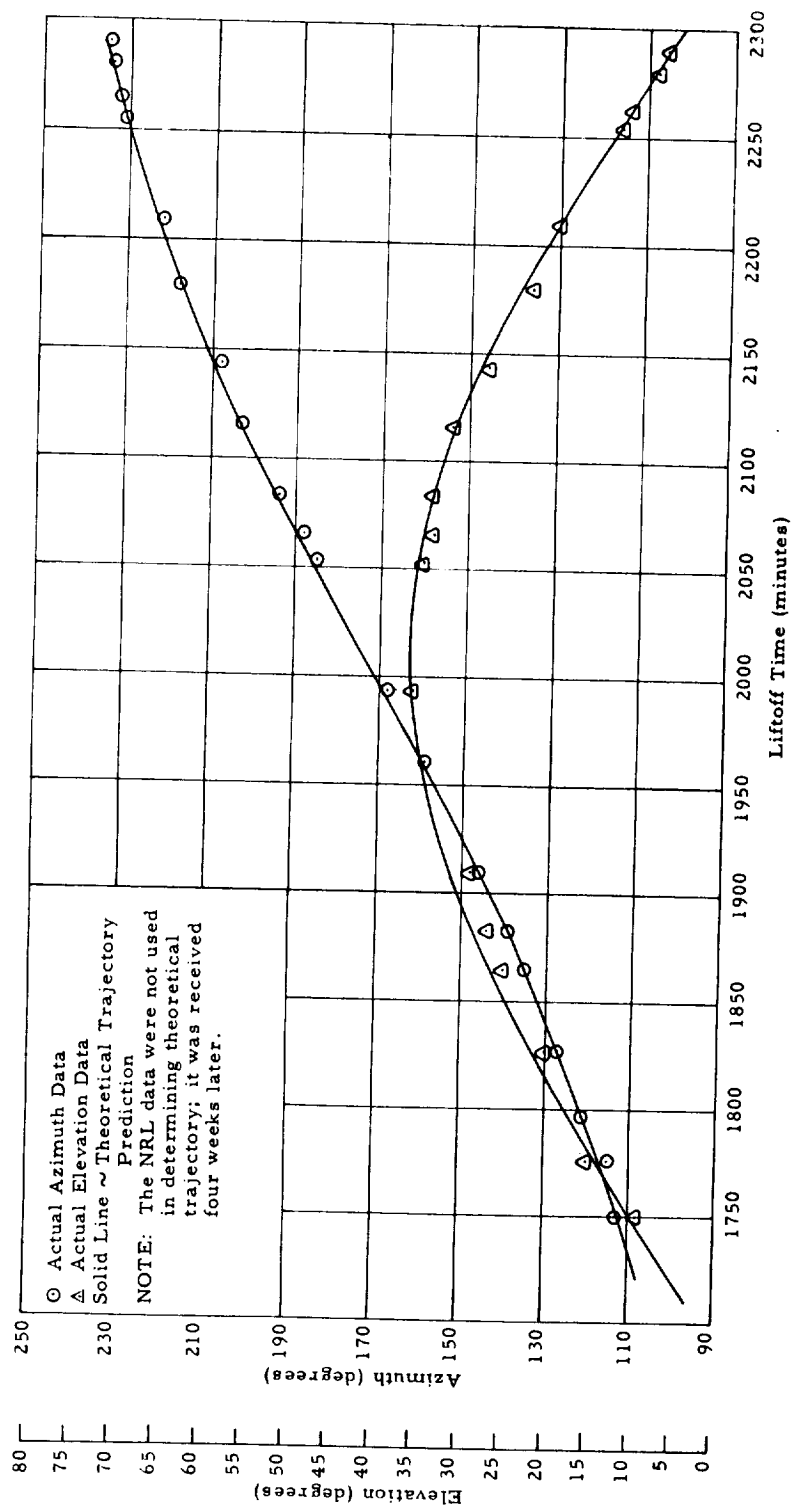
Figure 4-13. Flight II, Actual Tracking Data Versus Theoretical
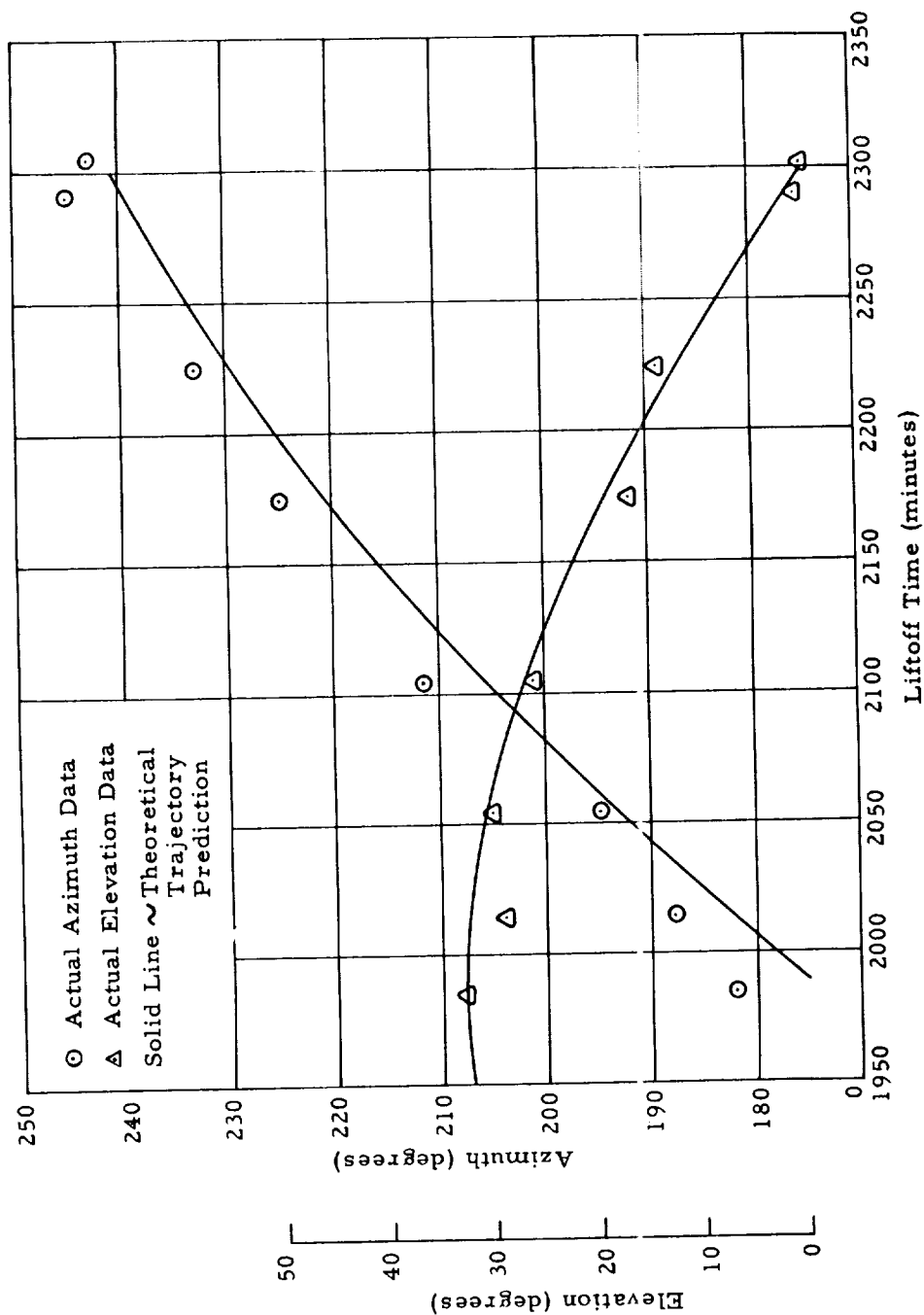Trajectory Prediction, Millstone (first pass).

Figure 4-14. Flight II, Actual Tracking Data versus Theoretical Trajectory Prediction, Millstone (second pass).

Figure 4-15. Flight II, Actual Tracking Data versus Theoretical Trajectory Prediction, Hawaii (second pass).
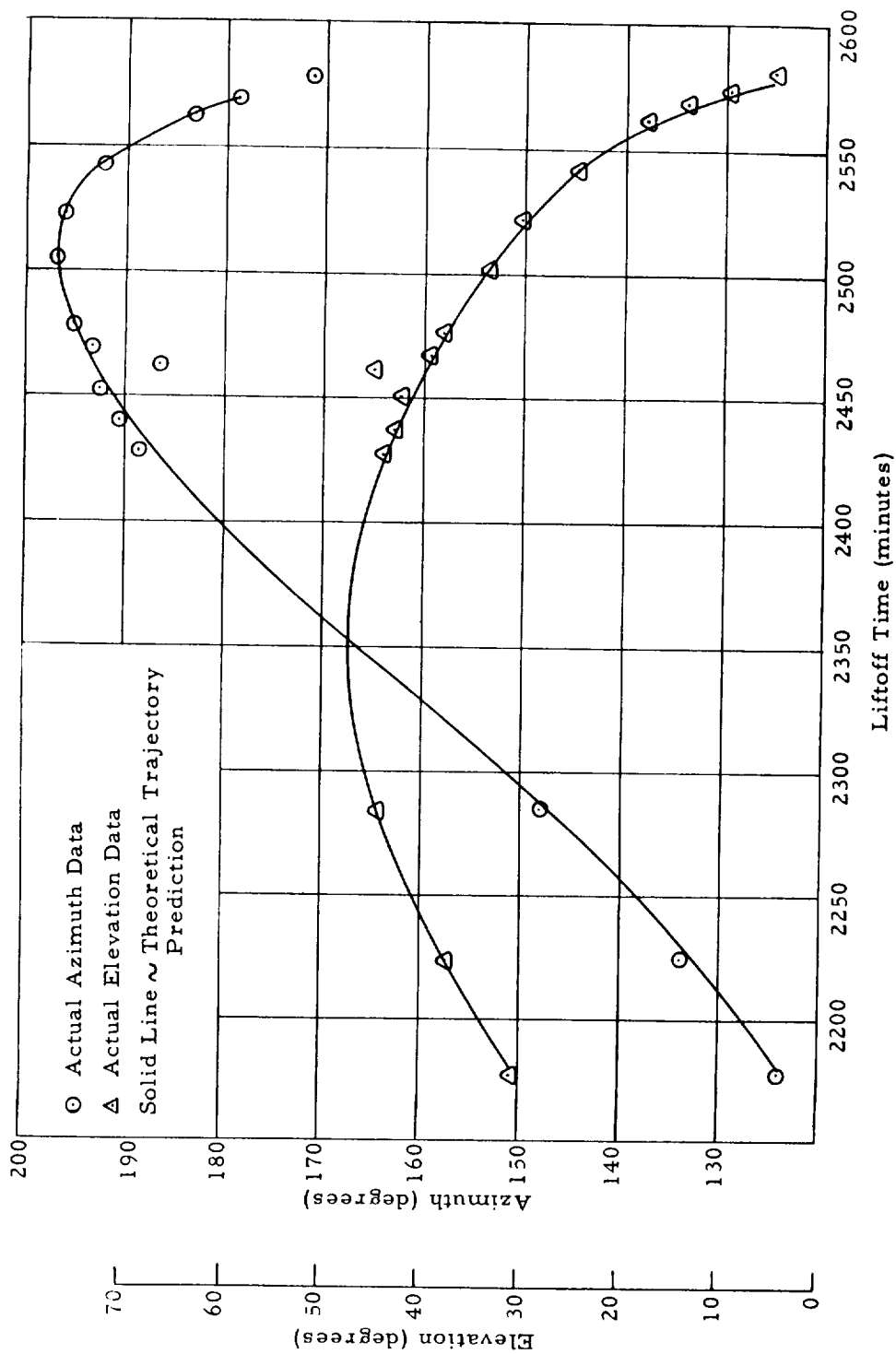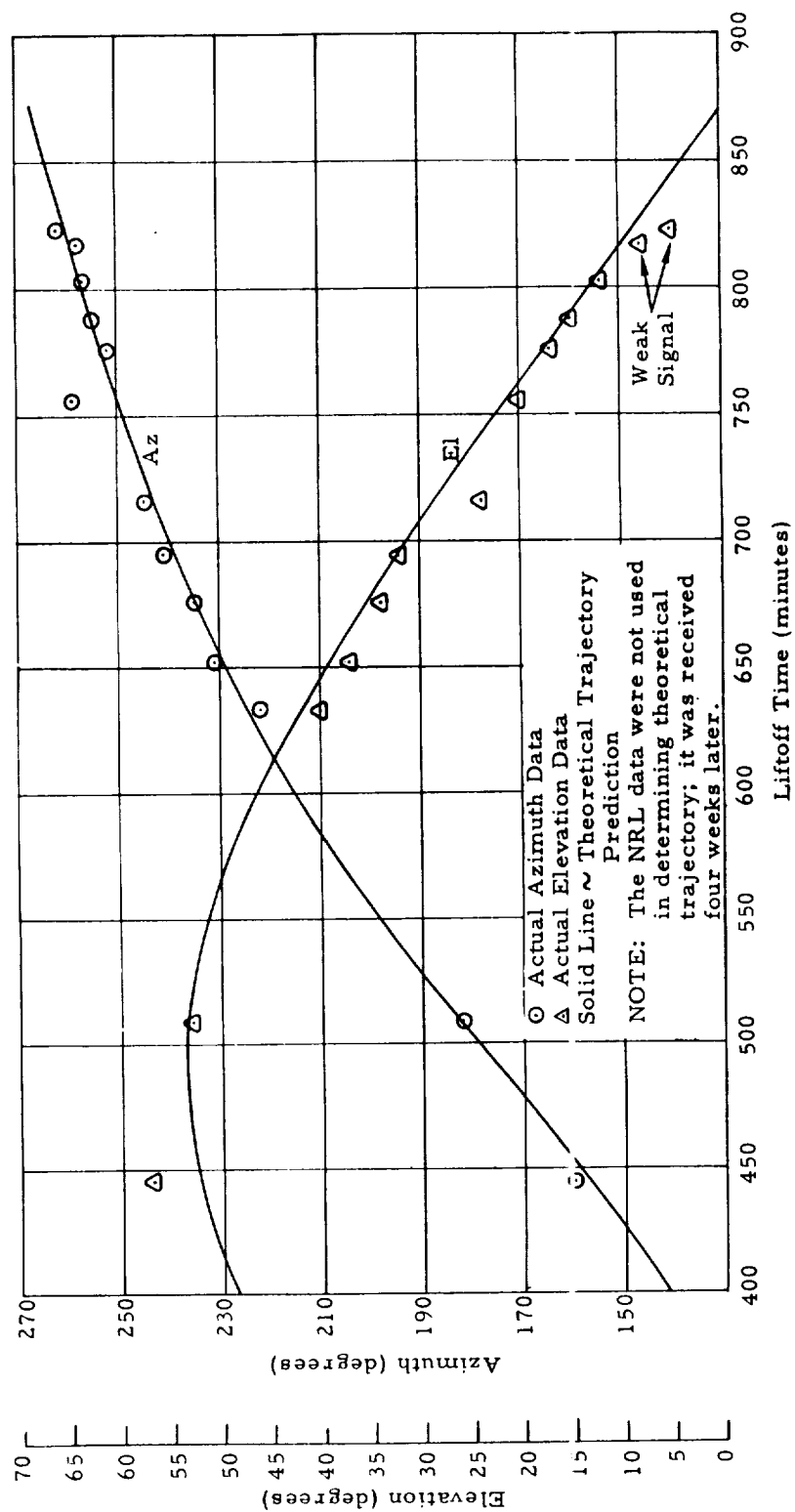
108

Figure 4-16. Flight II, Actual Tracking Data Versus Theoretical
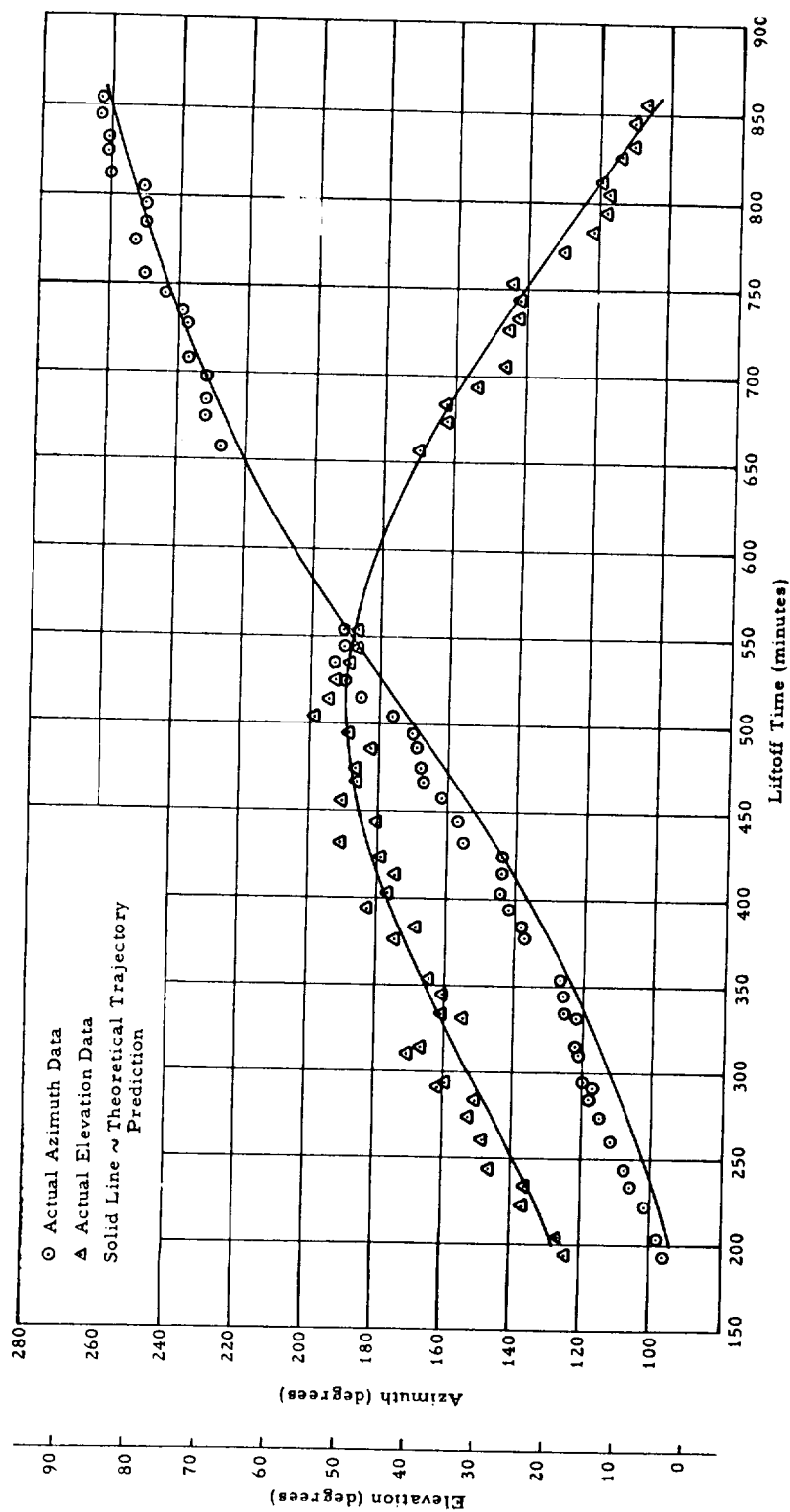Trajectory Prediction, NRL 60-Foot Disk (first pass).

Figure 4-17. Flight II, Actual Tracking Data Versus Theoretical Trajectory Prediction, NRL 60-Foot Disk (second pass).
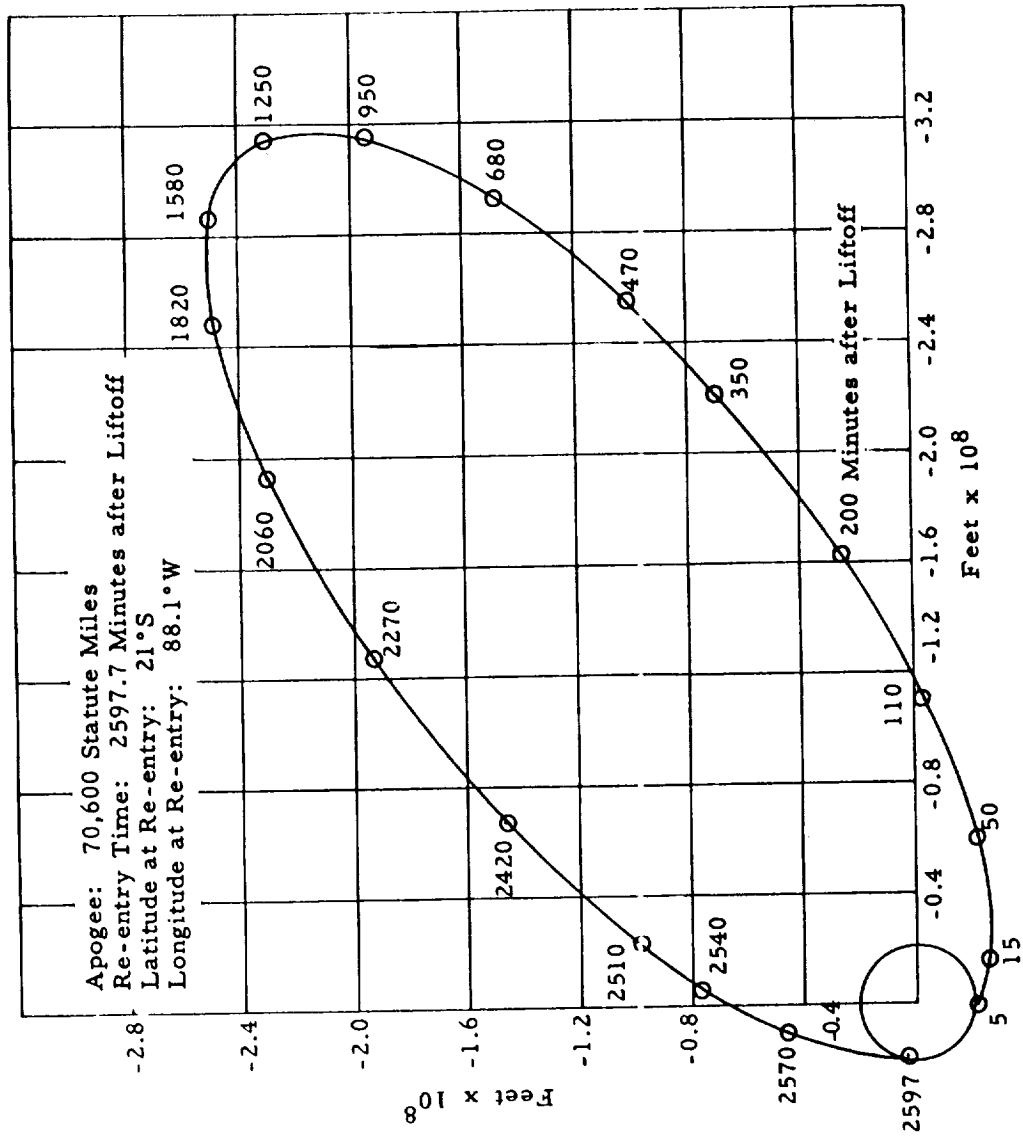
110

Figure 4-18. Flight II, Projection of the Vehicle in the Plane of the Moon's Orbit.

AFMTC at approximately T minus 6 hours that all ground stations were ready. The Operations Center was again fully manned at T minus 4 hours. At the time of lift-off all ground stations and the Operations Center were in a state of readiness. The Operations Center received the lift-off time, 0230/21 EST, 8 November 1958, by teletype from AFMTC. A table of clock-time versus minutes after lift-off was calculated. When AFMTC reported to the Operations Center that the third stage apparently had not ignited, a trajectory based upon nominal Stage 2 burnout condition was started on the 704 computer. While this trajectory was being run, graphical estimates were made of the approximate steering data to be used by Manchester in an attempt to have the Manchester antenna acquire. Elevation tracking data were obtained by Manchester. However, as stated in the Manchester message to the Operations Center, "These data are from the British tracking crew as derived from what appears to be an interference pattern between direct and ground reflected waves." The Manchester station relayed to the Operations Center azimuth tracking data obtained by the interferometer tracking station at Slough. Azimuth tracking data from Fort Monmouth were received. After the end of the flight, skin tracking data from the Millstone radar, the doppler data from AFMTC, and passive tracking data from Malabar were received. During the operation, data were received from the Minitrack stations at Grand Turk and Antigua, but these appeared to be unreliable because of the low elevation angles. Careful analyses of these data later by Vanguard personnel have resulted in what are felt by them to be reliable measurements. These data indicate a maximum altitude of 890 nautical miles and other trajectory parameters that do not differ appreciably from the estimates quoted here.

The general conclusion has been reached that the most accurate estimate of burnout conditions is that obtained from the data derived from powered flight tracking at Cape Canaveral aided by Millstone skin-tracking data. The limited amount of free flight tracking data obtained compares favorably enough with the trajectory obtained from the powered flight estimate to serve as a general confirmation but do not seem to be sufficiently consistent to permit the derivation of a more accurate burnout estimate. The parameters associated with the best estimate of the trajectory are:

Launch time	0230/21 EST 8 November 1958
Burnout conditions time	0234/51
altitude	1,003,000 feet
latitude	29.63°N
longitude	73.7°W
velocity magnitude	23,616 ft/sec
velocity azimuth	77.0°
velocity angle from vertical	71.5°
Maximum altitude (from surface)	963 statute miles (836 nautical miles)
Re-entry time after lift-off	42.4 minutes
latitude	28.7°N
longitude	1.85°E

Figures 4-19, 4-20, and 4-21 compare the actual tracking data with the best estimate of the trajectory. The azimuth data shown on Figure 4-22 are the azimuth measurements from Slough and are included with the Manchester elevation plots for convenience. Figure 4-23 shows altitude as a function of time. Figure 4-24 is a projection of the flight on the surface of the Earth.
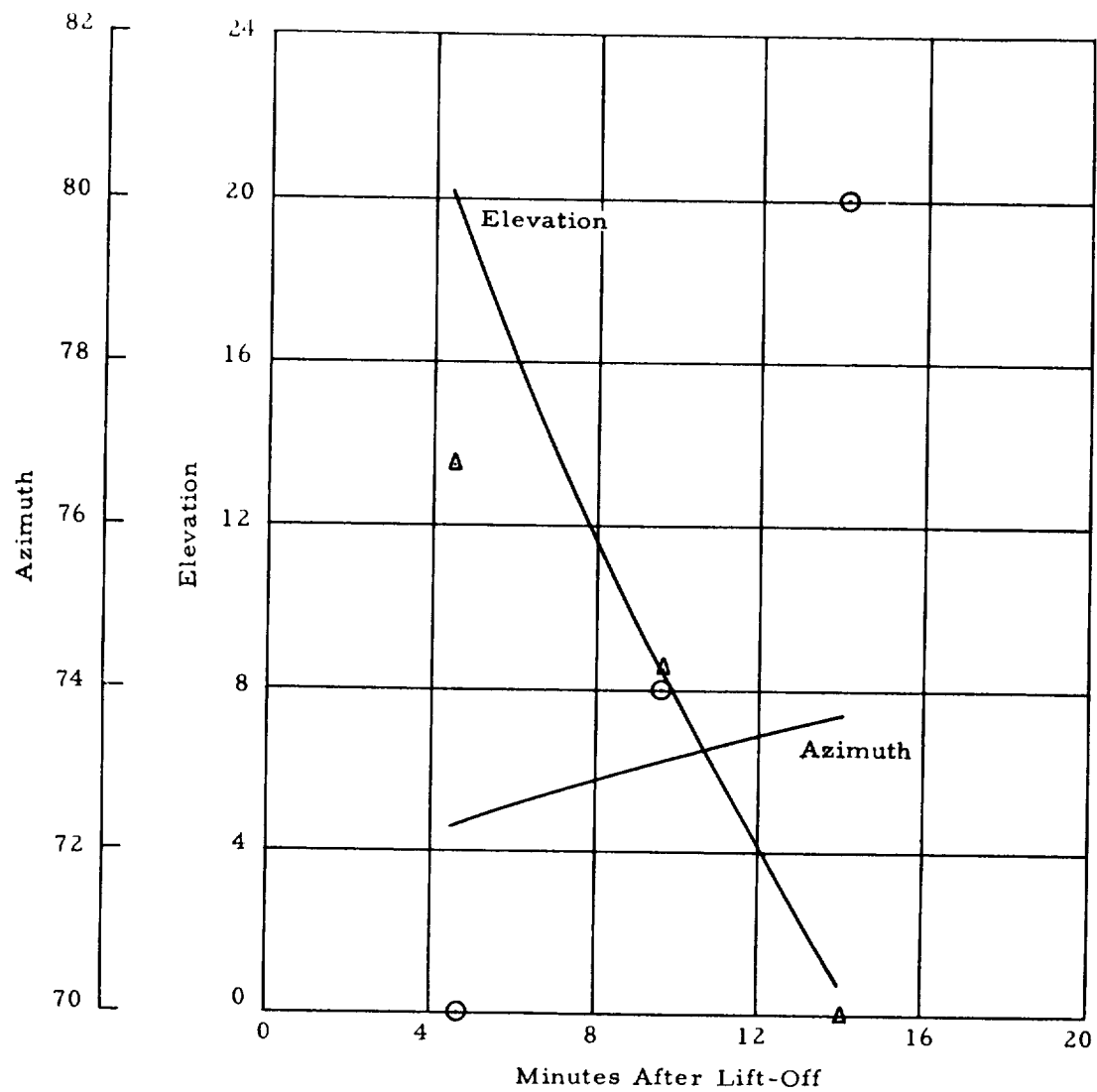
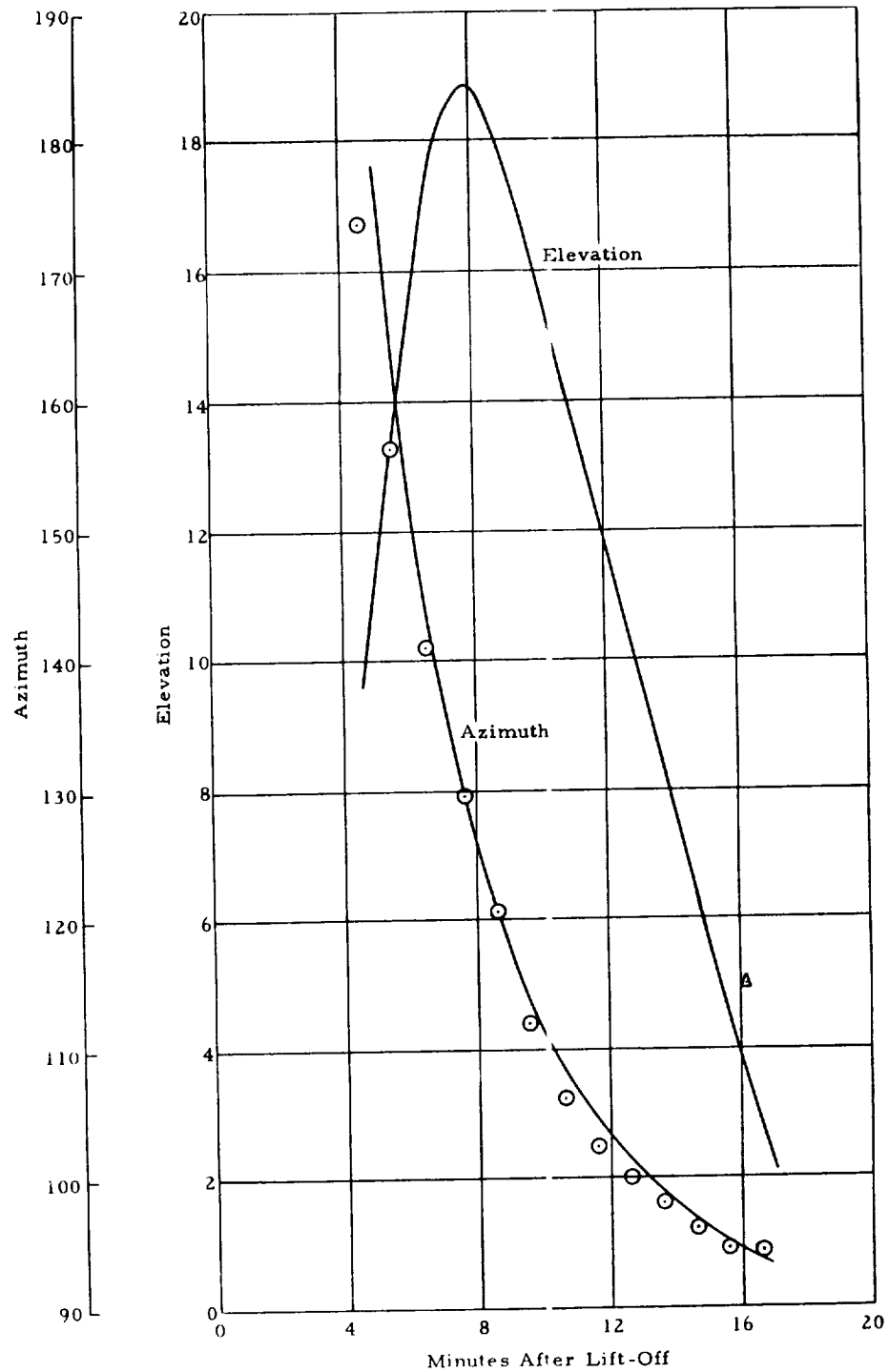Figure 4-19. Tracking Data for Flight III from Malabar

114

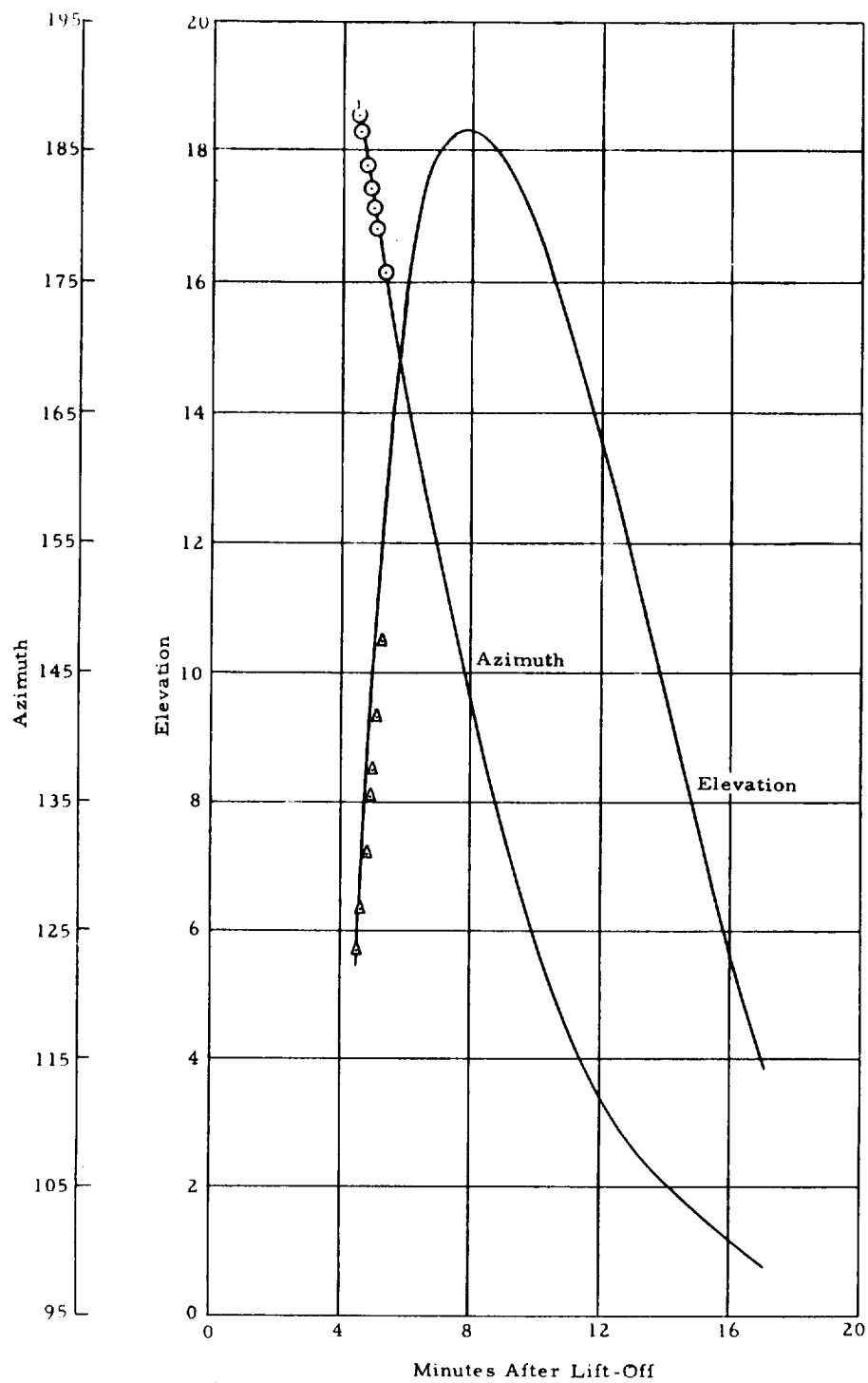Figure 4-20. Tracking Data for Flight III from Fort Manmouth.

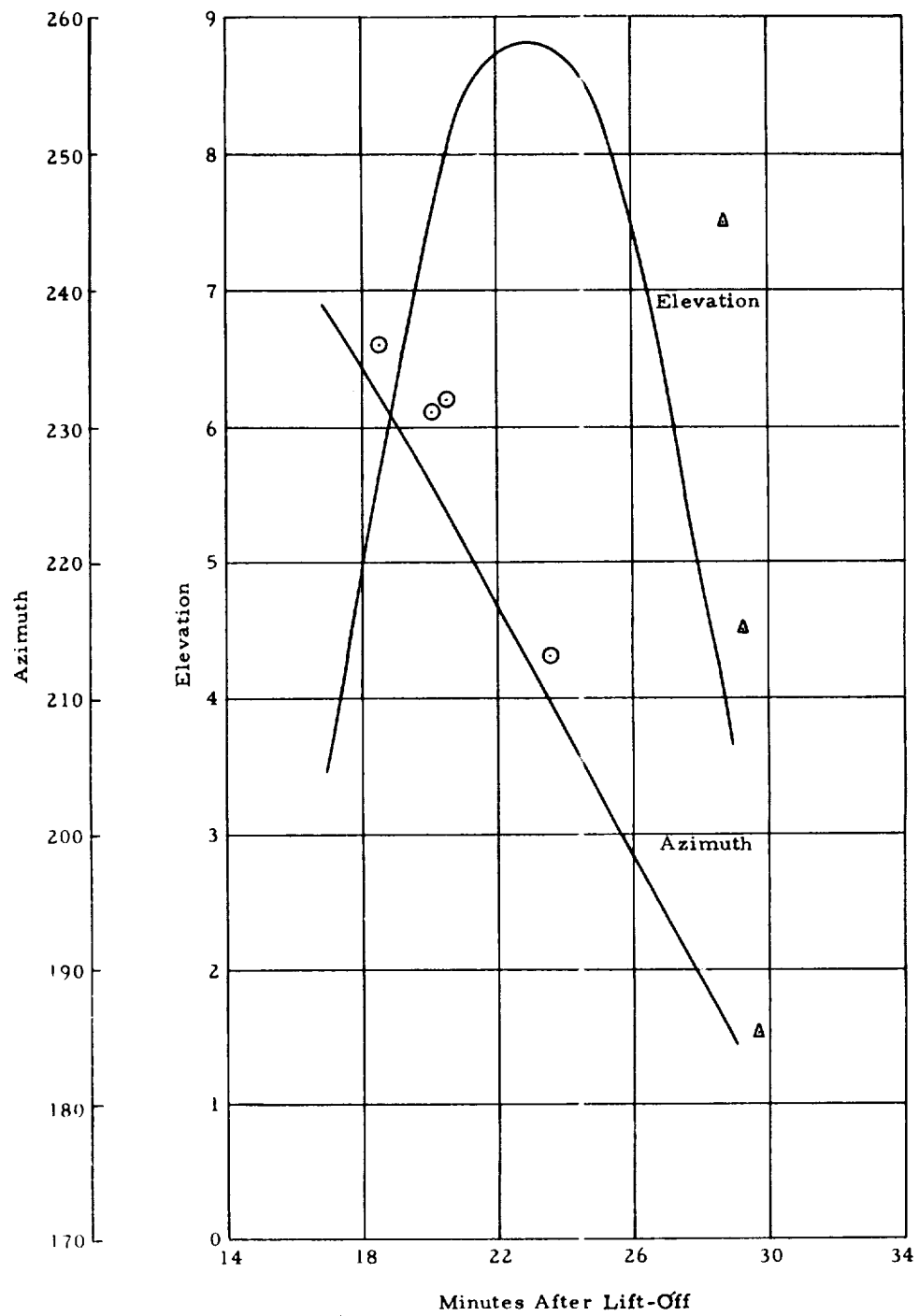Figure 4-21. Tracking Data for Flight III from Millstone.

116

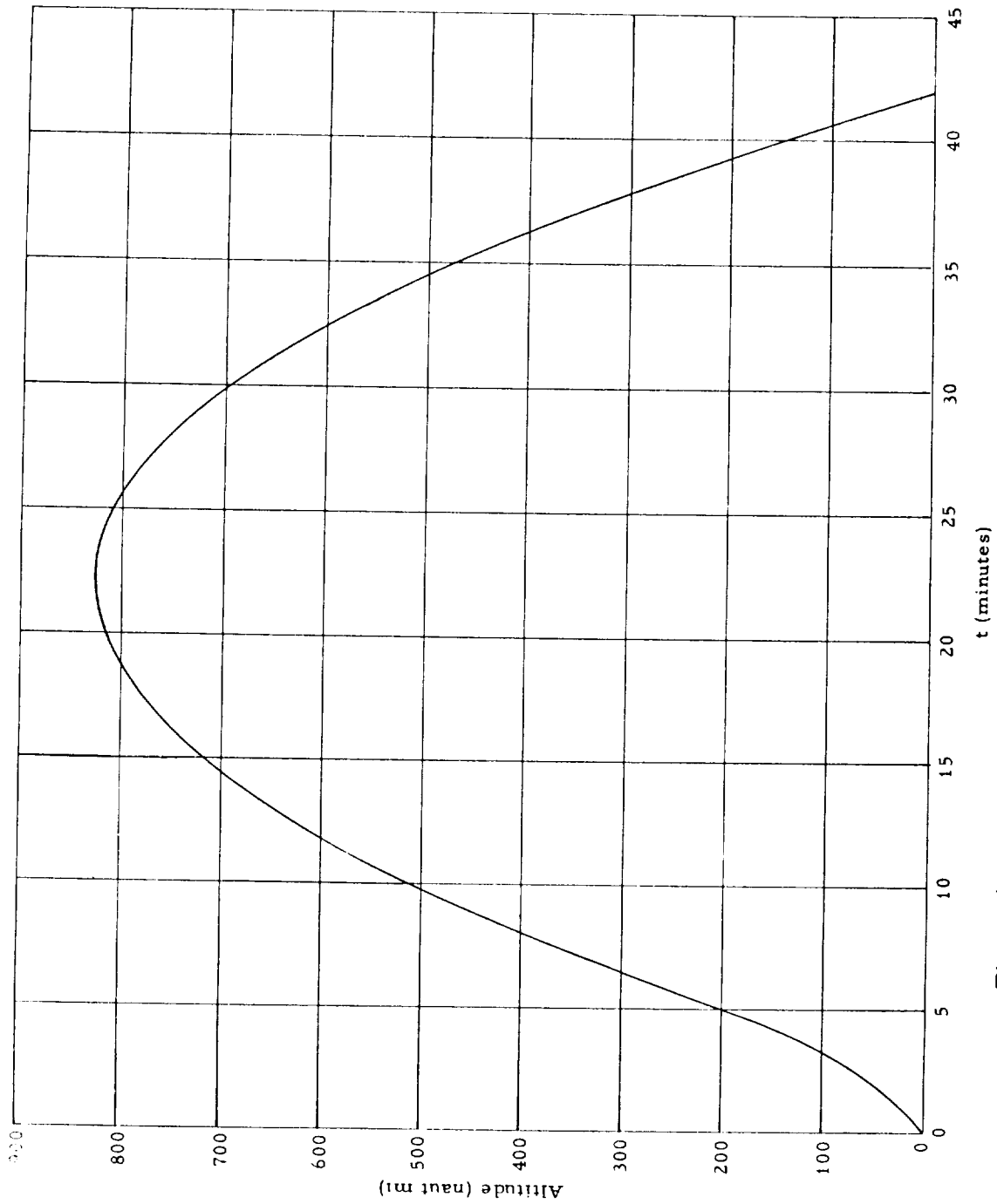Figure 4-22. Tracking Data for Flight III from Manchester
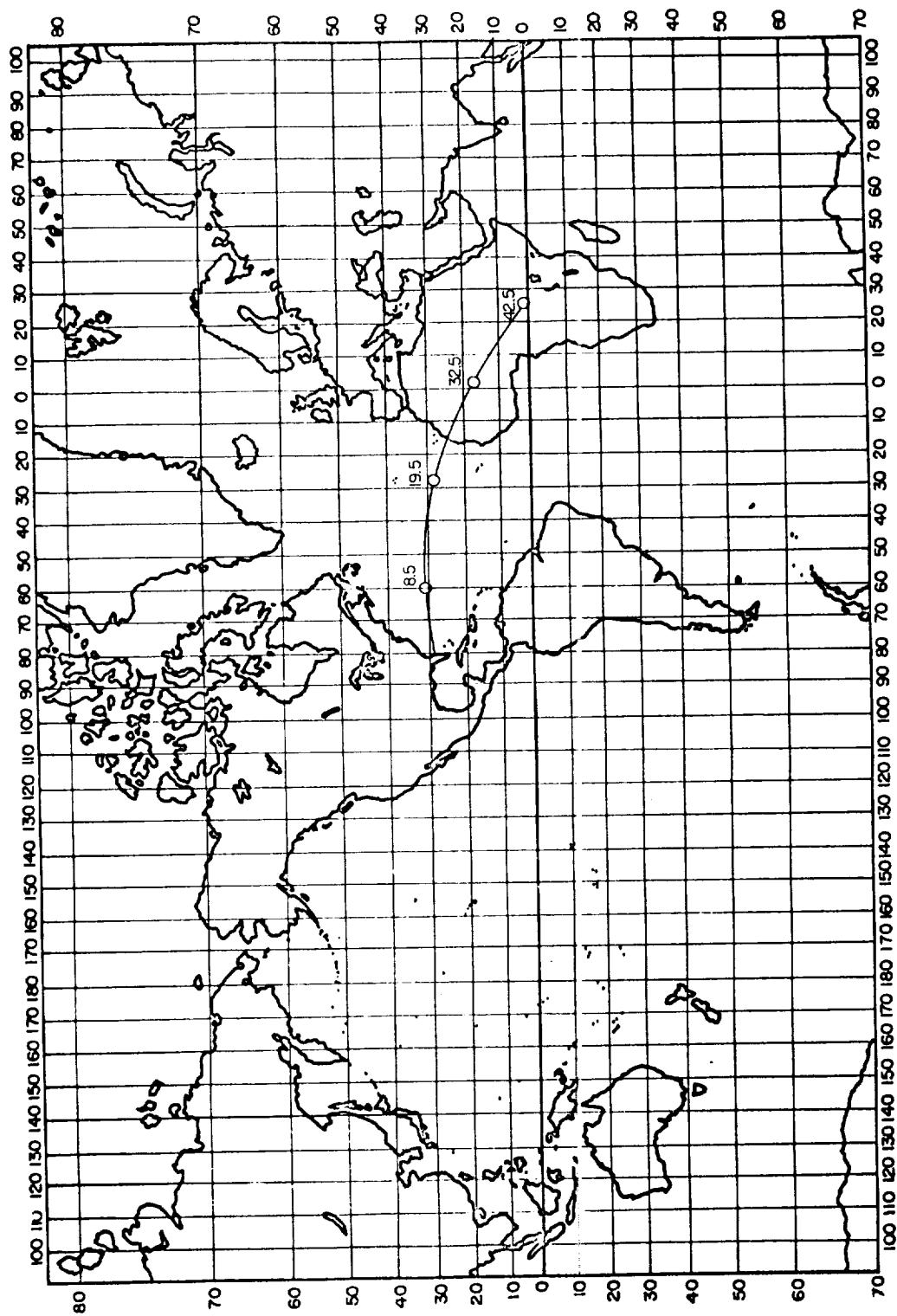
Figure 4-23. Flight III, Altitude Versus Time.

118

Figure 4-24. Flight III, Projection of the Path of the Vehicle on the Earth's Surface.

5.0 FLIGHT HISTORY AND EVALUATION

5.1 Countdown History

All three of the Able-1 vehicles were launched within the time periods allowed. Only one launch attempt was terminated because of equipment malfunction. The following brief summary describes each launch attempt.

5.1.1 Missile No. 1 (Thor Booster No. 127)

The second stage propellant tasks were accomplished in the early afternoon of 16 August 1958. No major difficulty was encountered in these tasks and they were completed approximately in the allotted time.

The DAC engine checks and preparations for electrical systems checks were begun at approximately 1930 hours, 16 August. There were no difficulties encountered with the second stage and the tasks were completed ahead of their allotted time. Communications check was held during the final one-hour period at T minus 35 minutes. All stations reported operating-ready. The radio communication link to Singapore was somewhat noisy but usable.

A major difficulty in the countdown occurred almost precisely at T minus 35 minutes when telemetry modulation of the low-frequency transmitter ceased, although the ground transmitter was not turned on. The signal received from the payload transmitter had the characteristics of a payload doppler receiver locked on an extremely low-level signal with considerable phase jitter. (The threshold level of this receiver was in the order of -140 dbm.) The frequency of the received signal was lower than the normally transmitted frequency. It was decided to turn on the ground transmitter immediately (ahead of schedule) to see if the receiver would lock on the ground transmitter. It did; but when the transmitted signal was removed, the receiver again returned to the weaker signal. A quick survey was made through the Superintendent of Range Operations (SRO) to see if any other receivers or transmitters were on, but none in this frequency range could be located. At T minus 15 minutes a short hold was called in order to turn off the blockhouse telemetry receivers. No effect was noted, so the premise that the interfering signal was local oscillator interference was discarded. It was concluded from the above evidence that the difficulty resulted from an extremely low-level interfering signal which would be expected

to drop below threshold level when the payload had completed the vernier phase of operation. Accordingly, the ground transmitter was turned on at this time and the count was resumed. This decision meant, of course, that the last time the telemetry had been checked was at T minus 35 minutes prior to noticing the interference.

There were no further difficulties during the countdown and the vehicle was launched at 0718, 17 August 1958, approximately 4 minutes after the scheduled time. The flight terminated at 73.6 seconds due to a malfunction in the first stage propulsion system.

5.1.2 Missile No. 2 (Thor Booster No. 130)

The second stage propellant loading task was begun as precountdown task at 0400 EST on 10 October 1958, to allow the work to be done before sunrise. (See Section 3.9.2a). This task was accomplished in less than the scheduled time, with no delays. The range count was picked up at T minus 490 minutes at 1632 EST, 10 October. There was one outstanding problem during the electrical systems test. A short developed in the cabling to the command receiver causing intermittent operation of the "signal present" relay. Since it proved impossible to isolate the short while on the launcher, it was decided to install the spare receiver. The payload checks subsequently proved correct and the missile was readied for flight. This malfunction, of course, delayed the installation of the nose fairing and the ordnance items attached to it. All but approximately 10 minutes of the scheduled 2-hour hold was used up in fixing these difficulties. The remainder of the count proved uneventful and went as scheduled. The missile was launched at 0342:13 EST, 11 October 1958, 13 seconds after the scheduled time. The verrier firing task proceeded as scheduled. Due to an error in data handling, the Azusa data were supplied to the digital computer incorrectly and the results of the calculations based on it were unusable. Provision had been built into the countdown for this occurrence and the correct decision to fire eight vernier rockets was reached. Further details of the trajectory and tracking of this launch will be found in Section 4.

5.1.3 Missile No. 3 (Thor Booster No. 129)

Second stage propulsion tasks were again begun in the early morning at 0400 EST, 6 November 1958. The loading was completed in 3 hours and

45 minutes. Range countdown was initiated at 1411 and proceeded smoothly, being ahead of schedule for most tasks. The weather was very poor; heavy rains and thundershowers passed through the area during the countdown. Base Weather predicted a 50 per cent probability that a front would pass through the area at the scheduled launch time. It was decided to proceed anyway, at least to T minus 35 minutes, to see if the weather would clear. This decision proved to be correct, as the skies were clear at the scheduled launch time.

At T minus 35 minutes prior to the schedule of a 1-hour hold, a chattering valve in the first stage propulsion system led to a cancellation of the firing. It was decided that the difficulty in the first stage system could be repaired and that other systems could be made ready in time to launch on the following day. The payload was removed and returned to the laboratory for convenience in reinstalling batteries, since the launch stand was quite wet from the heavy rains which had occurred during the countdown. In the laboratory the ion chamber was found to be faulty and was replaced. The required leak check on the Able propulsion system was made, and the missile was put in a T minus 490 minute condition. The propellants were not removed. Nonremoval of propellants and performing a leak check are normal procedure for a recycling. The countdown was resumed at T minus 490 minutes at 1519 EST on 7 November. The only difficulty encountered was a broken wire on the preamplifier for the magnetometer experiment. The wire was repaired on the stand. Again, the count was ahead of schedule and the terminal count was begun at 0154, 8 November. All communication systems were operative. The Azusa was periodically reported "out" by the SRO. Apparently, it was operative at launch time. A 90-second hold was called by the Range Safety at T minus 2 minutes for an aircraft which was passing directly over the launch area. Lift-off occurred at 0230:21.0. The fact that the third stage did not fire was indicated immediately to personnel in the vernier firing task by means of telemetry.

5.2 Summary of Flights

5.2.1 Introduction

Prior to the flight of the first Able-1 lunar probe, the Project Able flight test program had demonstrated satisfactory operation of the second stage control, propulsion, and electrical systems. However, this test program indicated that the first stage (Thor) flew higher than specified by the nominal

trajectories, and the result was that the velocity vector at first-stage burnout could deviate from the nominal as much as 5 degrees. Since open loop guidance was planned for the lunar probes, considerable effort was expended in discerning the causes of this first stage error. A primary contributor was found in the programmer calibration procedure at AFMTC. The first stage programmers, which were calibrated on laboratory power, could cause the missile to fly about 2.5 degrees high because of differences in laboratory and missile voltages and waveforms. Therefore, all programmers to be used in the lunar probes were calibrated in the laboratory, and missile voltage was adjusted to yield the proper pitch program. This error is not significant for regular Thor flights because the guidance system modifies the programmed angle prior to main engine cutoff. In addition, it should be observed that these dispersions are well within present Thor specifications. The remainder of the velocity vector error can be attributed to attitude gyro drift, thrust misalignment, and autopilot alignment errors.

5.2.2 First Lunar Probe

The first lunar probe was installed on Thor Missile No. 127. The missile was launched at 0718 EST on 17 August 1958, which was only 4 minutes later than the scheduled launch time of 0714 EST. The flight was normal until 73.6 seconds after lift-off when a turbopump bearing failed and the lox pump stopped. This malfunction was followed by a violent missile motion and a rupture of the main lox tank and/or the main lox duct, and the missile was destroyed by the ensuing explosion.

Analysis of the flight test telemetry indicated proper control system operation and showed that the missile was about 0.2 degree high at the time of the explosion. This value was much less than on some of the Project Able flights for a corresponding flight time, thereby indicating that the inclusion of a programmer had indeed contributed significantly to the velocity vector dispersions noted on the previous missiles.

5.2.3 Second Lunar Probe

For the second probe, the booster was Thor No. 130. The missile was launched at 0342 EST on 10 October 1958, only 13 seconds later than the scheduled time. Excellent performance was obtained from both the first and

second stages. At first stage engine shutdown the velocity was 15,000 ft/sec, which is about 800 ft/sec greater than nominal, and the velocity vector was about 2.5 degrees high.

A smooth transition to second stage operation was accomplished, and a second stage burning time of 104 seconds was obtained. Engine shutdown was commanded by the integrating accelerometer, and the velocity at this time was between 23,125 and 23,150 ft/sec or about 190 ft/sec less than the desired velocity. This difference was primarily due to the fact that the integrating accelerometer was fixed to the missile and hence computed along the lofted trajectory. At shutdown, the velocity vector was lofted by 3 degrees.

At third stage burnout, the inertial velocity was approximately 500 ft/sec less than the desired value of 35,206 ft/sec. Subsequently, all vernier rockets were fired in an attempt to make up the velocity deficit, but their impulse was not sufficient, and escape velocity was not achieved. The fourth stage reached an altitude of 71,700 statute miles, and good payload telemetry data were obtained during the flight.

An attempt was made to convert the payload into a high altitude satellite by firing the fourth stage, but, because of low internal temperatures, the missile batteries were incapable of supplying the ignition current.

Millstone radar data indicated that the velocity vector was about 5 degrees off in azimuth at third stage burnout which implies that the third stage must have been disoriented approximately 16.2 degrees in the yaw axis and pitched up 14.8 degrees. Considerable effort was expended in the analysis of possible causes contributing to such a disturbance. Several causes which were considered and discarded were: (1) failure of one or more of the eight spin rockets, (2) gyro drift during second stage, (3) third stage thrust misalignment, (4) second stage thrust tail-off, and (5) buckling or failure of structure coupling the second and third stages. Consideration of the momentum properties of the missile indicated that an impulse of only 11 lb-ft/sec could change the momentum vector of the third stage by 15 degrees. Since the third stage is ignited while it is still in contact with the second stage, and since the third stage nozzle rests on a beam that is not symmetrically located with respect to the nozzle, such a disturbance could have been caused by asymmetrical gas flow during the separation.

Accordingly, provisions were made to prevent such action in the third missile. Retrorockets were installed on the second stage, and the third stage fire signal was delayed one second after retrorocket firing.

5.2.4 Third Lunar Probe

The booster for the third lunar probe was Thor No. 129. Launch was at 0230 EST, 8 November, 31 seconds after the scheduled launch time for that day. The first stage control system performed satisfactorily, and the cutoff velocity was 200 ft/sec greater than, 1.5 degrees lower than, and 2.3 degrees to the left of nominal.

Second stage operation was completely normal, and the velocity at shutdown was within 40 ft/sec of the desired value. Engine shutdown was commanded by a signal from the ground to a doppler command system which had been installed in the missile payload to reduce the velocity error incurred on the second flight. The spin rockets were ignited and the proper spin velocity of 2.1 rps was achieved. The third stage was separated, but it failed to ignite and the vehicle failed to escape. There is no clear-cut explanation for the failure of the third stage. It may be attributed to several causes, such as (1) a break in the wire to the igniter, (2) failure of the igniter, (3) a poor connection to the igniter, or (4) a failure in the firing signal transmitter.

All tracking stations operated satisfactorily. The payload was tracked for approximately 15 minutes by the tracking facility at Cape Canaveral, but, because of the failure of the third stage, the signals were not obtained at the Manchester station.

5.3   Flight Test Results and Evaluation

5.3.1 Propulsion

    a.   First Stage

        The performance of the first stage propulsion system was high but within the nominal limits for all flights with the exception of Missile 127. The propulsion system in Missile 127 malfunctioned and was the cause of a missile blow up at 73.6 seconds after lift-off. Detailed discussions of the performance of these systems, including the malfunction in Missile 127, are discussed in STL report GM 58-0165-09961.

    b.   Second Stage

        The sequence of operations and the performance results are given in Tables 5-1 and 5-2 . Sufficient impulse was available to provide the required velocity at second stage burnout. Satisfactory electrical and electronic mechanical functioning is demonstrated by the sequence of events data.

Table 5-1   Sequence of Events for Second Stage.

Event	Nominal (sec)	Flight Test Data	
		Missile 130	Missile 129
Command fire	0.0	0	0
TPS switch	0.40	0.3	0.35
Heat Generator Assembly	10.0	9.7	---
Rise time to peak P_C	0.65	0.6	0.5
Command shutdown	---	104.0	108.4
Start of shutdown	---	104.1	108.5
Zero P_C	---	104.4	109.0
Decay time	0.25	0.3	0.5

NOTE: All times are referenced to the time of command to fire.

Table 5-2. Performance Characteristics for Second Stage

Event	Nominal (sec)	Flight Test Data	
		Missile 130	Missile 129
Average P_c	206 psia	207 psia	208 psia
Burning time		104.4 sec	109.0 sec
Average burning time	112 sec		
Total impulse	877,000 lb-sec	765,000 lb-sec	807,000 lb-sec
I_{sp}	271 sec	*	*

*No data available to indicate accurate values.

c.   Third Stage

An analog simulation was carried out to ascertain the dynamics of the spinning, precessing third stage of Missile 130. The simulation included the time varying moments of inertia as well as the jet damping effect. The results of this simulation are summarized in Figures 5-1 and 5-2. The velocity loss in per cent along the original direction is $\delta v/v_o$, and α_{final} is the magnitude of the final angle between the thrust axis and the original axis.

Comparing those with the results of the digital simulation of the entire vehicle (see Section 5.3.8) the following can be demonstrated: The digital simulation implied in attitude change of third stage equivalent to 14.8 degrees pitch up and 16.2 degrees yaw left, or a total offset angle of 21.9 degrees or 0.383 radians for α_{final}. From Figure 5-1 this implies an initial angular rate ω_o of 0.478 rad/sec. This, in turn, from Figure 5-2, indicates a total velocity loss of 8.5 per cent along the original direction. The loss along the original direction from angular effect alone is $\left[1 - \cos (\alpha_{final}) \right] = 7.2°$. Thus the apparent loss in impulse would be 1.3 per cent. This is in very good agreement with the 1.6 per cent degradation in impulse required in the digital simulation.

The conclusions from this are that the hypothesis of a large angular disturbance at the initiation of Stage 3 is consistent with both the measured
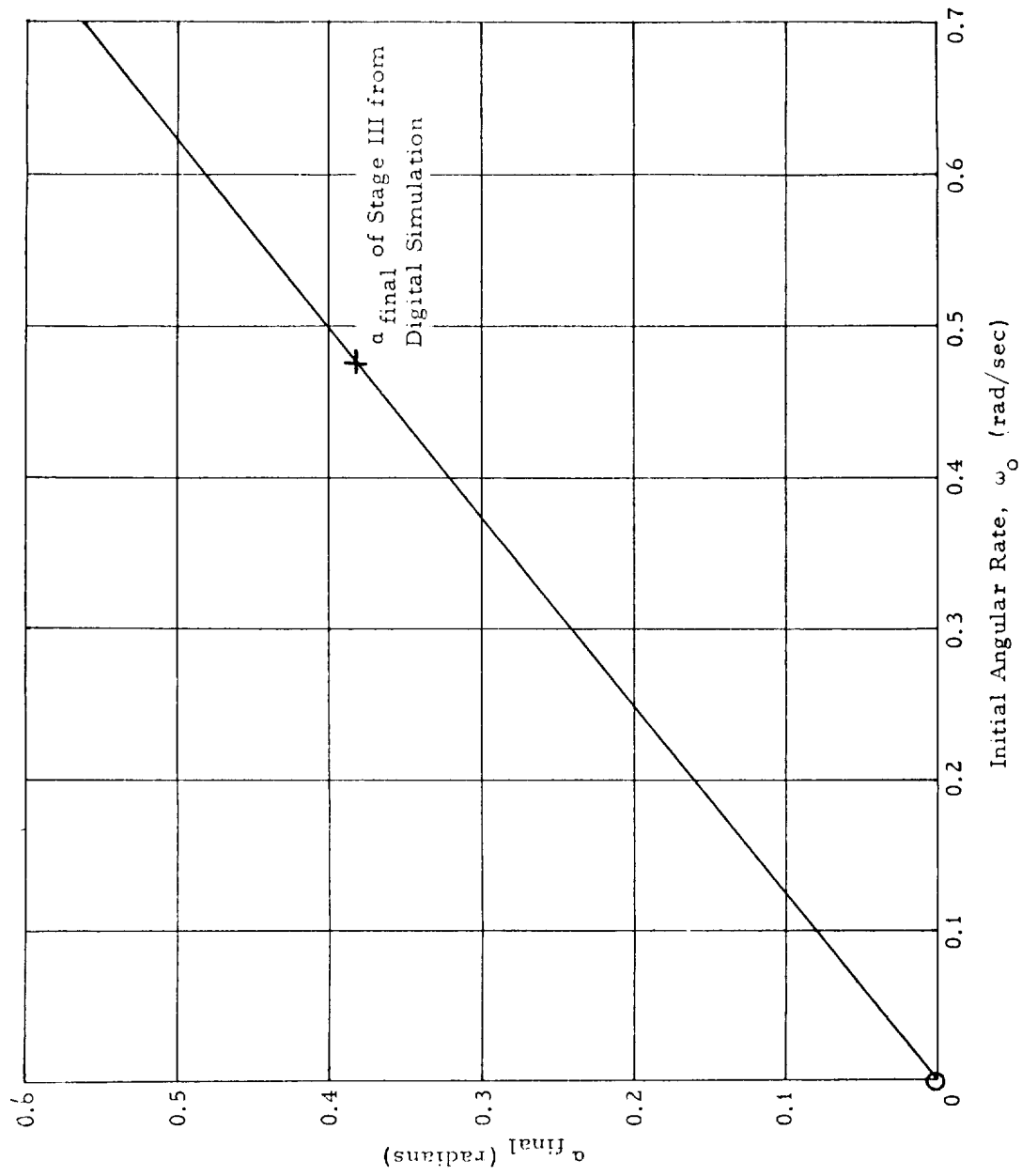
Figure 5-1. Final Third Stage Attitude Deviation Due to Initial Angular Impulse.
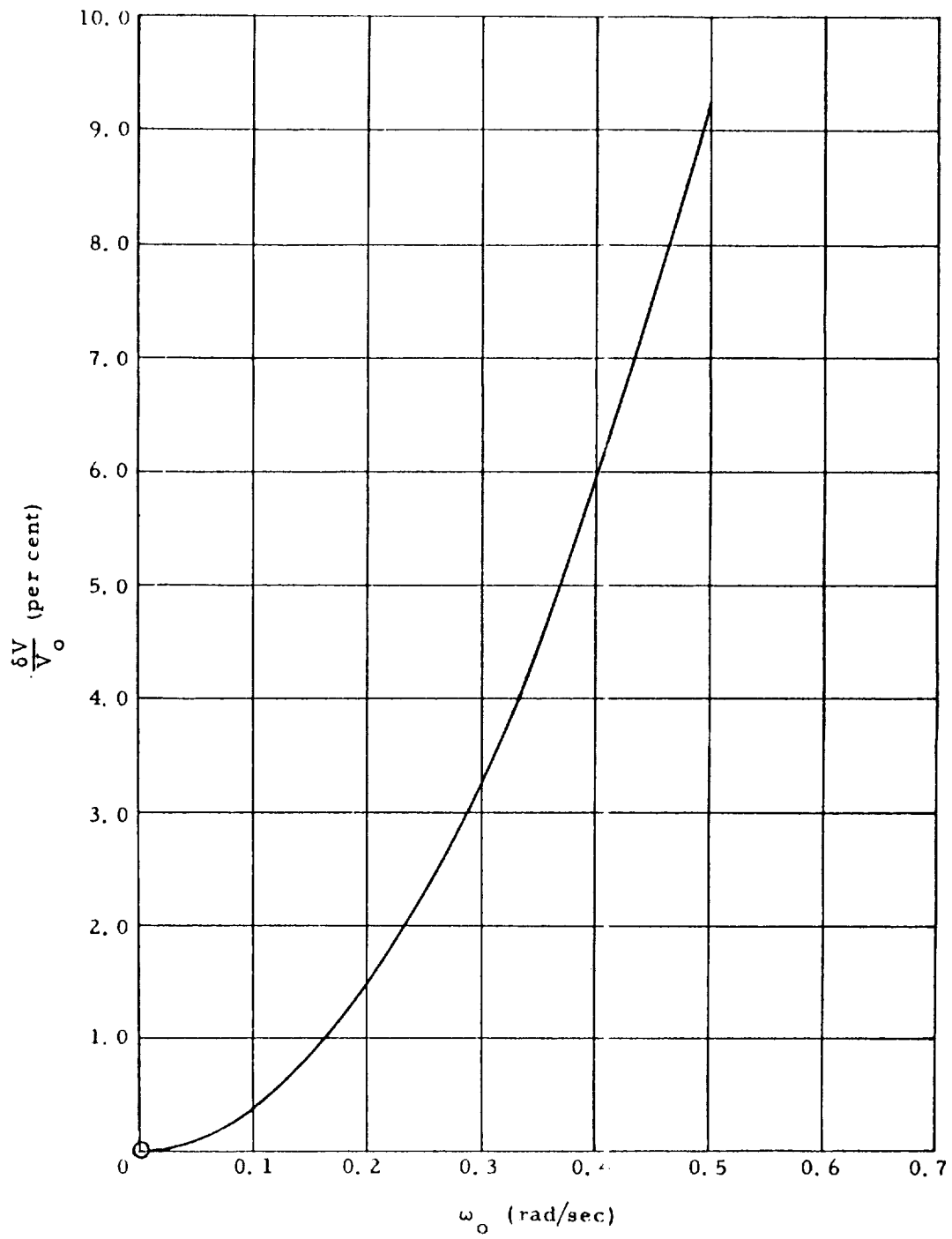
Figure 5-2. Velocity Loss Due to Altitude Deviation as a Result of an Initial Angular Impulse.

range rate and free flight data and a theoretical description of the dynamics of a rocket given such an initial disturbance. It is also indicated that the performance of the ABL 248 rocket was within 1/2 per cent of the predicted value.

It is believed that the third stage of Missile 129 did not receive the firing command from the second stage. This has been attributed to the breaking of a wire during second/third stage separation. Further discussion of this failure is presented in the discussion of staging structure (Section 5.4.2).

d. Vernier and Spin Rockets

The 1XS-50 rockets were used for spin up and for vernier adjustment of velocity. Analysis of the spin rate data from the second and third flights and the vernier velocity gain from Missile 130 (second flight), show the average total impulse per rocket to be approximately 53 lb-sec, thus indicating satisfactory performance.

e. Fourth Stage

A command to fire the fourth stage engine was attempted several times during the flight of Missile 130; no command was attempted during the flight of Missile 129. The fourth stage of Missile 130 failed to ignite on all attempts. This was attributed to a low temperature condition inside the payload which reduced the effectiveness of the igniter battery. As a result, no data is available to evaluate the fourth stage propulsion system.

f. Evaluation of Design

The operational reliability of each stage of the Thor-Able combination is believed to be satisfactory. The turbopump malfunction in the first stage of Missile 127 was corrected and the subsequent firings of Missiles 130 and 129 demonstrated satisfactory system operation. The performance of the first stage of Missile 130 was excellent and that of Missile 129 was well within normal limits.

The operation of the second stage was entirely satisfactory for both Missiles 130 and 129.

Vernier and spin rocket performance was as expected. No data are available on the fourth stage performance. However, it is believed that the failure of this stage to ignite during the flight of Missile 130 was caused by a loss of battery power which resulted from the depressed temperature level on the altered trajectory.

5.3.2 Structure

An examination of the flight data was made for indications of the performance of the structure. Inasmuch as no specific structural measurements were taken, it is impossible to reconstruct an accurate picture of the flight environment and loads. However, there is no indication that any portion of the structure failed to perform properly.

The data presented in Table 5-3 represent the best estimate of the most critical loading conditions which probably occurred. The engine deflection angles were obtained from telemetry, and the angles of attack are calculated from engine deflections assuming the vehicle is trimmed. No estimate of the magnitude or effects of gusts is possible.

Examination of Table 5-3 indicates that the structural loads encountered by Stages 3 and 4 during first stage operation were well below the design loads and hence would indicate no structural failure or excessive deflections during this portion of the flight.

It is believed that all the structure was capable of carrying at least 1.25 times the maximum load that could be expected. No marginal areas of strength are known. Tests were performed on all critical items. Separation of first and second stages results from the initiation of four explosive bolts. While it is believed that separation would be satisfactory, even if one bolt failed to destruct, this has not been proven by tests. Assurance tests and design modification, if need be, would improve reliability.

The second and third stage structure and separation method appear to be structurally adequate. The requirement of a preload in the struts is perhaps less than optimum from the field installation standpoint. Separation will be satisfactory only if both bolts holding the third stage nozzle are destructed. The failure of either bolt to destruct will undoubtedly abort the mission. A design eliminating the preload and requiring the firing of only one of two bolts to obtain separation would improve the reliability of this separation procedure. Such a design has been prepared and will be tested shortly.

The separation of Stages 3 and 4 is accomplished by the firing of a single bolt on the center line and the action of a spring to give a small relative velocity.

Table 5-3. Estimated Environment of the Third and Fourth Stages
from Flight Test Data and Comparison with Design Values

Critical Loading Condition	Item	Flight Test Data			Design Values
		127	130	129	
Maximum Disturbance	Time, sec	68	64	82	64
	Dynamic pressure, q, PSF	810	840	600	850
	Angle of attack, α deg	2.4	1.8	4.75	7.0
	Engine deflection, δ deg	0.96*	0.75*	1.9*	0**
	Axial acceleration, g's	2.24	2.0*	2.7	2.2
	Lateral acceleration on third and fourth stages, g's	0.14	0.10	0.23	1.0
First Stage Burnout	Time, sec	Missile destructed at ≅ 74 sec	156.7	159.2	156.7
	Engine deflection, δ deg		0.55*	0.50*	3.0
	Axial acceleration, g's		12.0*	12.8	13.4
	Lateral acceleration on third and fourth stages, g's		0.14	0.12	0.75

Notes:

1.* These items were obtained from telemetry records.

2. Dynamic pressures and other axial accelerations are nominal.

3. The angles of attack are calculated from the engine deflection assuming the vehicle is trimmed.

4. The lateral accelerations, which are computed using rigid body assumptions, are believed to have a tolerance of ±0.07 g's

5.** Zero engine deflection for design purposes results in a critical lateral acceleration for the third and fourth stages.

This method appears to be quite reliable, simple and free from possible troubles. Some improvement in reliability might be gained by an arrangement in which either one of two bolts could initiate separation.

5.3.3 Separation Failure Discussion, Missile 129

As mentioned earlier in Section 5.3.2, post flight analysis of the data from Missile 130 indicated a trajectory deviation on the order of 5 degrees during third stage firing. Reference GM 65.51-104 indicated that the most likely cause of this deviation was a thrust misalignment during the separation phase, rather than a structural failure. The misalignment was attributed to a nozzle-blocking condition at ignition, caused by the structural asymmetry of the compartment below the third stage nozzle.

To eliminate this condition in the flight of Missile 129, it was decided that the two stages should be separated by approximately one foot before firing the third stage. Missile 129 was modified to accommodate two retrorockets on the second stage, a trailing wire to the third stage igniter, and a pay-out basket (see Figure 5-3) for the excess wire. Four additional spin rockets were added to increase the spin rate to 2.1 cps. During the separation of the third stage from the second, it was observed that the second stage spin rate decreased and that an angular rate normal to the spin axis was introduced. A preliminary analysis of these phenomena indicated the probability of mechanical interference between the two stages during the separation phase. Other possible causes would include the failure of the inter-stage structure or the failure of one of the two explosive separation bolts, either of which could result in an increase in moment of inertia about the spin axis thereby reducing the spin rate and inducing angular momentum about the normal axis.

Analysis of the telemetering and signal strength records for the third lunar probe indicates a disabling mechanical interaction between Stages 2 and 3, immediately following the separation signal for these stages. A good understanding of the magnitude and gross nature of this interaction was derived from studies of the subsequent motions of the respective stages. The interaction probably consisted of two separate collisions between the third stage rocket nozzle and the obstructions on the second stage before the separation necessary to clear these obstructions was achieved (see Figure 5-4 and 5-5). Since the third stage did not fire, it is probable
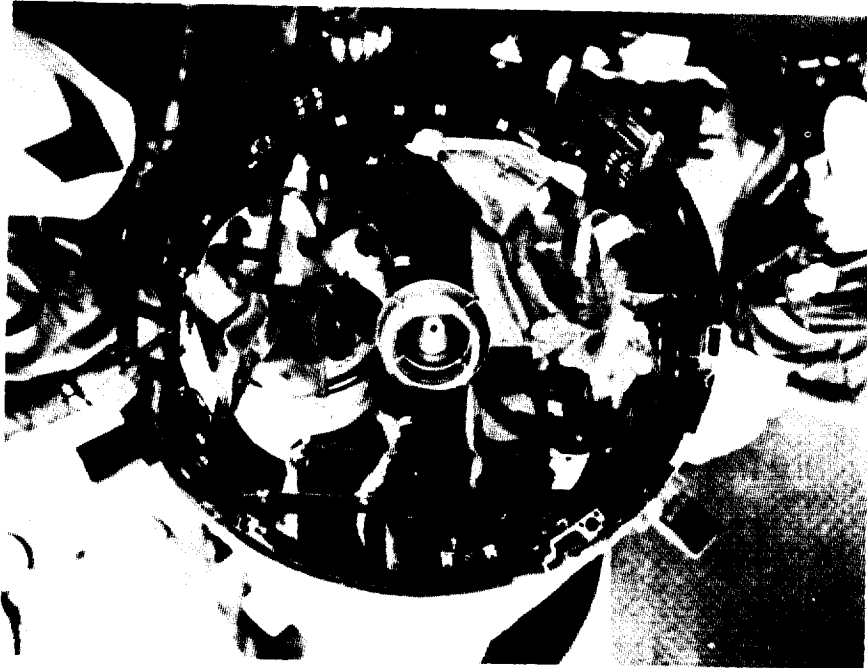
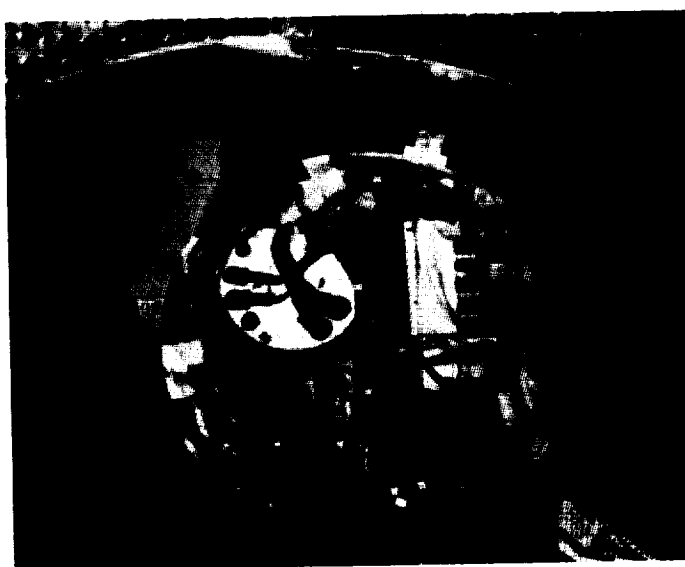Figure 5-3. Second Stage Payout Basket for Excess Wire.

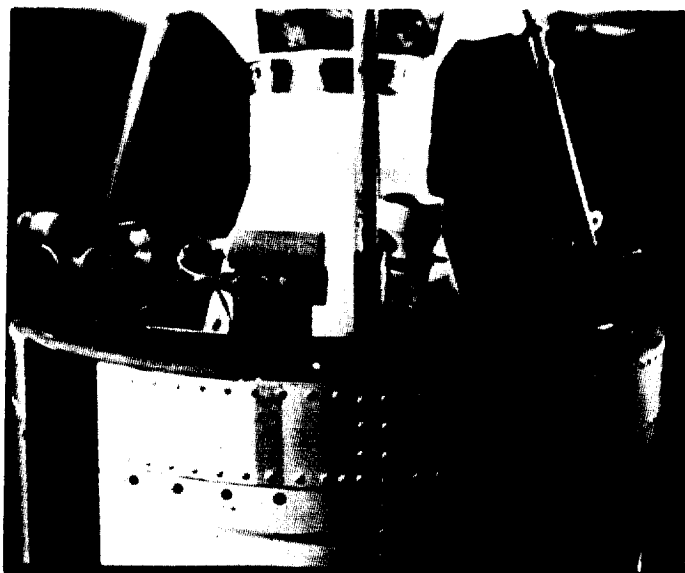Figure 5-4. Second Stage Showing Probable Obstructions.

Figure 5-5.   View of Second and Third Stage.

that the igniter trailing wire was broken in the process and that some of the interaction forces arose from this source.

This failure could not have occurred, however, unless, either some small undetermined triggering separation impulse was present or, as an alternate explanation of much lower probability, that the separation retrorockets mounted on Stage 2 did not fire.

This triggering impulse is masked by the subsequent interaction but it was probably small enough so that if not followed by the disabling interaction, a satisfactory flight could have been achieved. Investigation of this triggering impulse is continuing but no definitive conclusions have yet been reached. It is more fully discussed in a later section.

a. Stage 2 Motion

During the 2-1/2 seconds following the separation signal, at least two torque impulses were applied to the second stage due to interaction with Stage 3. These impulses were sufficient to reduce the second stage roll rate from approximately 2.1 cps to 1.34 cps and to induce a steady state nutation[*] frequency of 0.118 cps. Taking computed values of inertia, this corresponds to a reduction of the roll angular momentum from 580 to 370, or -210 lb-ft/sec; and the introduction of 820 lb-ft/sec of angular momentum about an axis normal to the roll axis. This gives a nutation cone half angle of 66° with a presumed shift of the direction of the angular momentum vector of approximately the same magnitude. Of the initial spin energy for this stage of 3800 lb-ft corresponding to 2.1 cps roll rate, 1900 lb-ft remained as rotational energy of the separated stage about its center of gravity. The remaining 1900 lb-ft of energy being available to increase the third state energy, appear as translational separation energy of the stages and make up impact losses.

Figures 5-6, 5-7, and 5-8 show the primary reduced data which substantiate the foregoing statements. The spin speed of Figures 5-6 and 5-7 was obtained from the integrating acceleration, given a roll position indication as

---

[*]Nutation is defined here to mean the force-free conical motion of the roll axis about the total angular momentum vector when a component of angular momentum about a lateral axis is present in addition to a roll component.
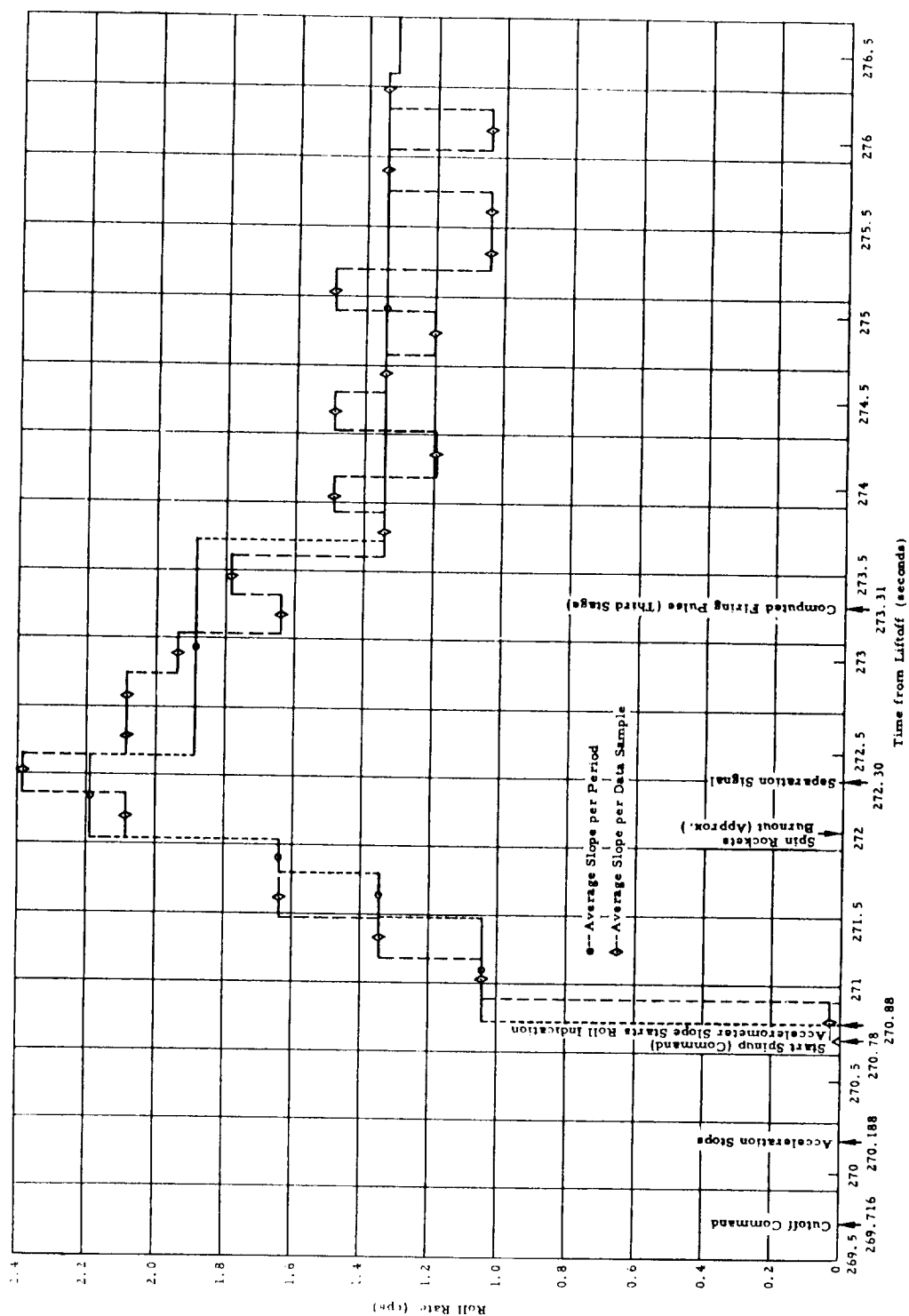
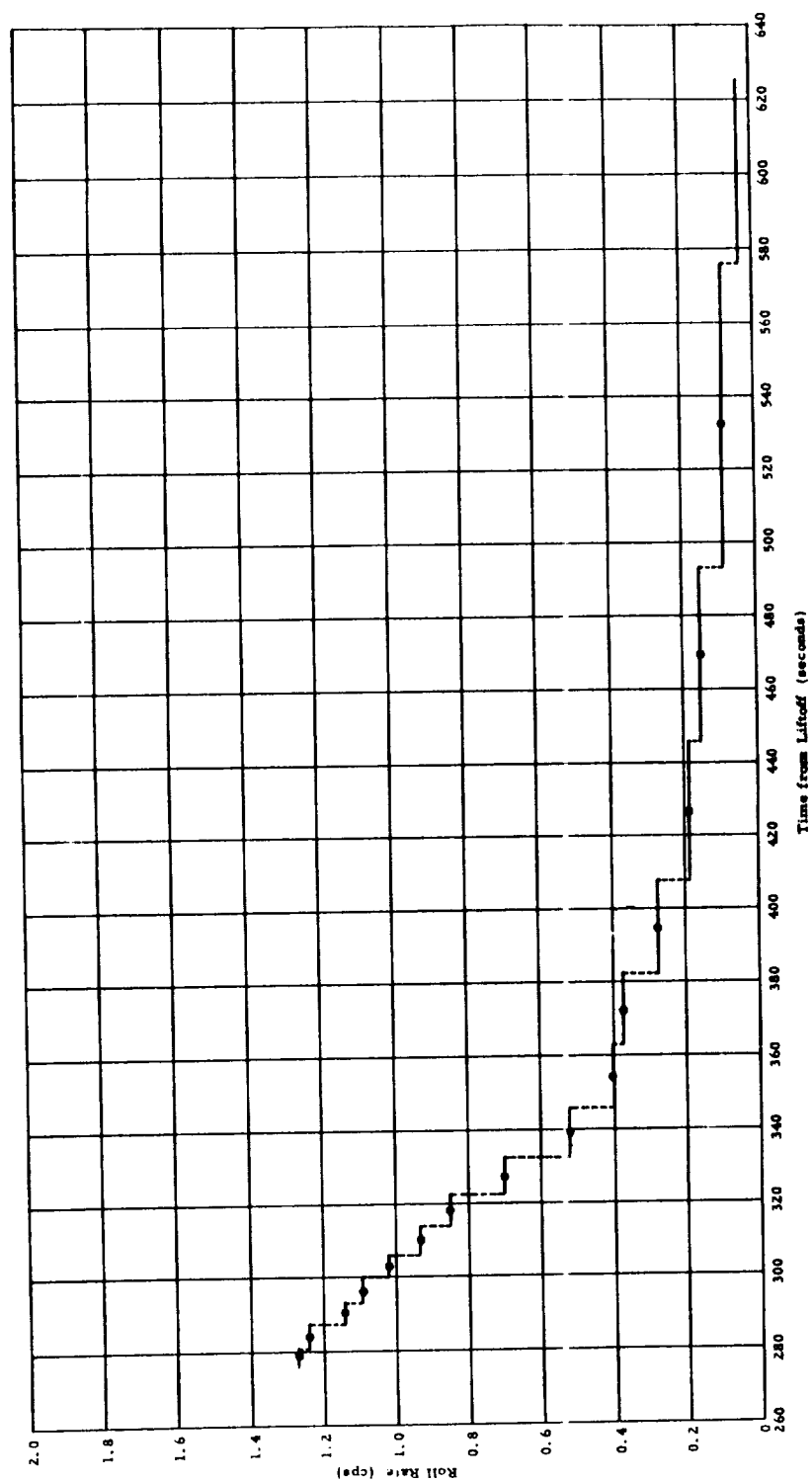Figure 5-6. Able-1 Missile 129 Second Stage Roll Rate, Initial

138

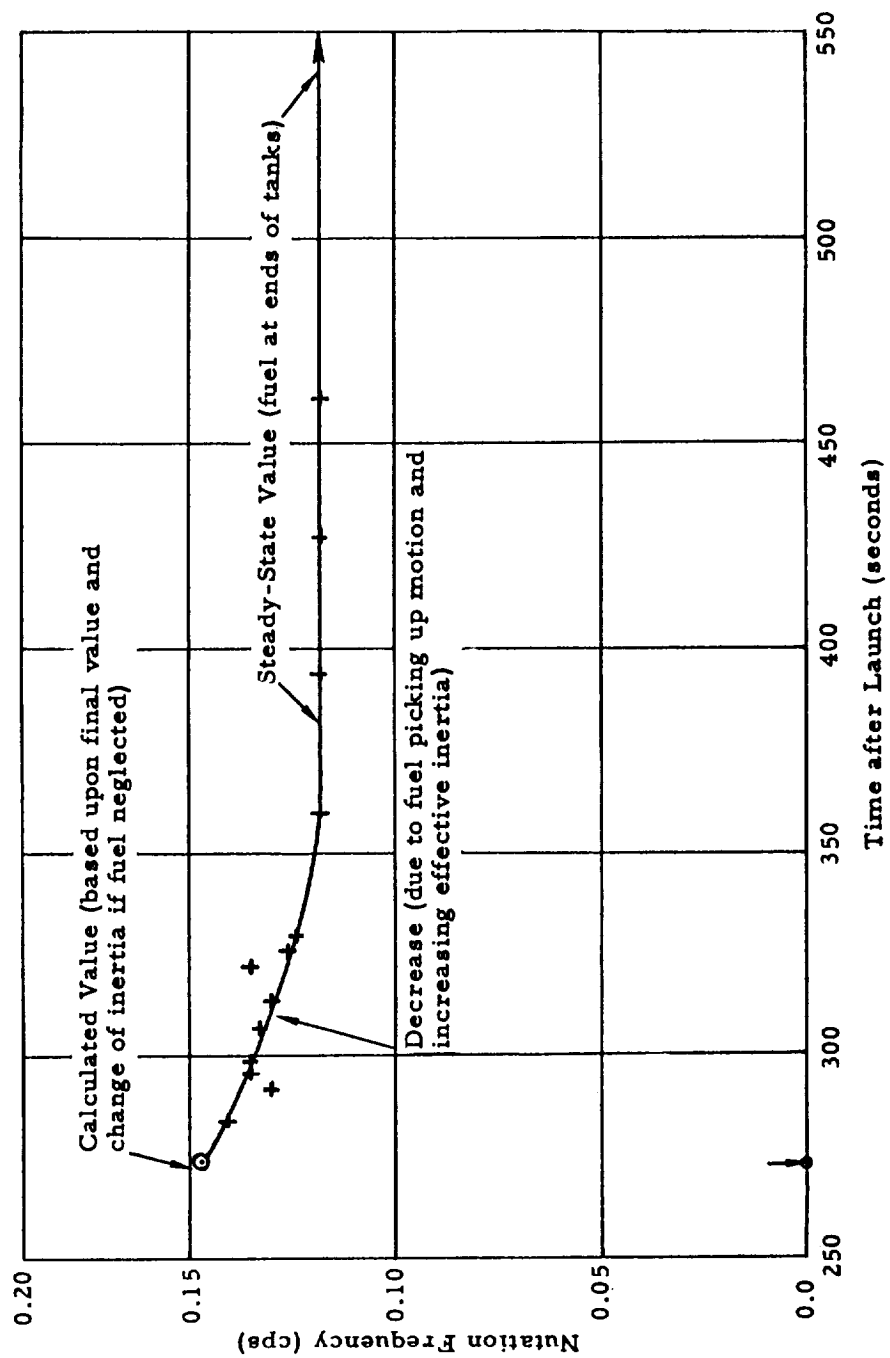Figure 5-7. Able-1 Missile 129 Second Stage Roll Rate

Figure 5-8. Nutation Frequency as a Function of Time.

described in Section 3.5.2(c). This information was verified by the oscillation frequency seen by the pitch and yaw autopilot gyros and by the dominant signal strength frequency, after suitable computations involving the nutation angle were made. The gradual change in spin speed shown in Figure 5-7 is due to fuel sloshing. Such sloshing removes energy from the system, causing the angular momentum to shift from the roll axis (axis of least inertia) to an axis normal to the roll axis (axis of greatest inertia) so that the total vector angular momentum can be conserved while the kinetic energy of rotation decreases. The nutation frequency from the signal strength records where it showed up as a periodic change in the character of the signal. The nutation frequency is equal to the total angular momentum divided by the pitch-yaw inertia, for a roll symmetric body, and hence, for force-free motion, can vary only if the pitch-yaw inertia varies. The change in the nutation frequency shown in Figure 5-8 corresponds to the change in inertia as the residual fuel gradually picks up the body motion and finally settles at the extreme ends of the tanks. The nutation angle was verified, to the extent that it is of the order of 60° from amplitude of the pitch and yaw autopilot gyros. The accuracy of this verification was limited by the fact that a large part of the telemetered signal was saturated.

b. Third Stage Motion After Separation from Stage 2

The motion of Stages 3 and 4 as a unit following separation from Stage 2 was deduced from the following data:

2.36 cps = dominant frequency from magnetometer except at least two other frequencies apparent in the magnetometer experiment

4.72 cps = dominant frequency from signal strength

0.5 cps = nutation frequency from signal strength

The 4.72 cps signal strength was interpreted as the first harmonic (due to a bilateral antenna pattern) of the 2.36 cps magnetometer experiment. An investigation was made of the frequencies which should be apparent for the magnetometer experiment in a nutating body. Three frequencies were found but only one appeared suitable for association with the 2.36 cps signal.

Based upon this interpretation, a nutation angle of 54 degrees and a spin speed of 2.15 cps was deduced. Since the initial spin speed of 2.1 cps is not

known to better than two significant figures, this corresponds to an insignificant impulse about the roll axis, as would be expected from the circular shape of the Stage 2 rocket nozzle and the central location of the igniter trailing wire. An angular momentum of 100 lb-ft/sec was introduced, however, about an axis normal to the roll axis.

c. Over-All Energy and Mementum Conservation

Approximately 50 ft-lb of energy was added to the rotational energy of Stages 3 and 4 leaving 1850 lb-ft of energy left over from Stage 2 for the kinetic energy of separation of the stages and for collision losses. The size of this residual invites the assumption that a large part of this energy was used to increase the linear separation velocity.

Over-all angular momentum conservation considerations are extremely difficult to apply to this separation process due to the large angular mementum associated with the linear separation of the stages. It was felt sufficient to determine that at least two collisions are required to explain the distribution of the angular momentum between roll and normal axes for Stage 2 (due to a greater roll component in relation to roll moment arm than normal component in relation to normal moment arm) and that two appeared enough to explain the differences between the angular impulses between the stages.

d. Fourth Stage Separation

Stage 4 motions, after separation from Stage 3, were investigated to see if this separation occurred satisfactorily in spite of the large shock loads received at the previous separation and the presence of the large nutation.

The observed dominant frequency for the signal strength was 2.21 cps with a second recognizable frequency of 0.276 cps superposed upon it and 1.95 cps was the observed dominant frequency of the magnetometer signal. These three pieces of information were inconsistent until it was recognized that an erroneous value of the inertia ratio was being used. After that, these data were used to give a nutation angle of 13.6 degrees, a spin speed of 1.95 cps and an inertia ratio of 1.14 compared to a recomputed inertial ratio of 1.13.

If the Stage 3/Stage 4 separation had been clean, the nutation angle should have been 9.3 degrees and the spin speed 2.15 cps. Thus there was an interaction, which was somewhat larger than the specifications for this separation, but in view of the previous history it is considered satisfactory.

142

e. Conclusion

It is clear that the gross part of this separation failure could have been avoided if separation of Stages 2 and 3 had been faster, as was the case in Able 1 Flight 2. The separation was slowed, however, to allow the rocket nozzle to clear the asymmetric bulkhead before firing and thereby eliminates the disruption of flow which is believed to have caused the dispersion of Flight 2.

Thus, the corrective measure applied to Flight 3 indirectly caused the gross part of the failure of that flight. Every possible effort is being made to see that subsequent corrective measures are free of this defect.

The final consideration is the determination of the triggering impulse, which might in itself be large enough to cause a significant dispersion. Residual nutation before separation has been eliminated as being one to two orders of magnitude too small. Strain energy of the interstage coupling members is a possibility, but the entire design of the interstage structure has been modified for subsequent shots.

Consequently, it is felt that actual laboratory separation tests offer the only way of insuring that such small separation impulses are absent. However, at this time it is not clear that such tests are feasible.

5.3.4 Ordnance

The operation of the explosive bolts in the first/second stage separation has been correct in that satisfactory separation was attained in the flight of both 130 and 129. The separation bolts between the second and third stages of Missile 130 appear to have operated correctly in that the predictable maximum time lag between the two bolts could not have contributed sufficient impulse to cause the observed trajectory deviation. In the flight of Missile 129, it appears from an examination of the nutation frequency of the separated stages that staging occurred, thus indicating that the second/third stage separation bolts operated correctly. Doppler data from Missile 130 and nutational frequencies from Missile 129 tabulated data both show that the third and fourth stages separated, thereby demonstrating proper bolt operation. The bolts and actuators which separate the nose shroud performed as expected during the flight of Missile 130. Preliminary analysis of the flight test data from Missile 129 indicated that the nose shroud separation mechanism operated correctly.

5.3.5 Integrating Accelerometer

a. Able-1 Missile, Flight Number 1, Thor Missile 127, 17 August 1958

Integrating accelerometer, Serial Number 13, was calibrated to provide a second stage engine cutoff signal at 26,870 ft/sec and a pitch program signal to the autopilot between an interval of 24,980 ft/sec and 26,270 ft/sec. The unit uncaged at lift-off and completed 3.12 cycles of the output signal for an indicated velocity of 4368 ft/sec before termination of the flight at approximately 73 seconds. During the flight period the accelerometer appeared to function normally even though the telemetry signal indicated the improper magnitude. Failure of the telemetry signal to reach its maximum value until the end of 2-1/2 cycles is attributed to moisture in the telemetry unit. This failure prevented detailed velocity analysis except at the cross over points of the telemetry potentiometer.

The second stage inverter frequency during flight exhibited a characteristic trend which has appeared on the previous three missiles of the Able series. The accelerometer calibrations are normally corrected due to the frequency variation in flight; however no attempt was made to correct the indicated velocity due to the short time period of flight and the erratic telemetering signal.

b. Able-1, Missile Flight Number 2, Thor Missile 130, 11 October 1958

Integrating accelerometer, Serial Number 14, was calibrated for a second-stage engine cutoff signal at 26,912 ft/sec and for a pitch program signal between the interval of 25,047 ft/sec and 26,325 ft/sec, i.e., an interval of 1279 ft/sec. The inflight performance was satisfactory and no failures or indications of malfunctioning were detected. The accelerometer uncaged properly at lift-off and had completed 8.95 cycles at the time of arming of the second stage which occurred at approximately 6.39 g's. At first stage burnout the indicated velocity was 18,785 ft/sec. The velocity increased to 18,841 ft/sec at separation of first and second stages. Pitch program signal duration was approximately 11.4 seconds at an average acceleration of 114.9 ft/sec^2 (indicated velocity 1310 ft/sec). Second-stage cutoff command was initiated by the integrating accelerometer at a velocity of 26,916 ft/sec after completing 19.14 cycles of the output signal. Approximately 1 second after second stage cutoff command, the

accelerometer indicated the spin-up of the second and third stages. Spin rate was approximately 1.17 rps. The spin rate gradually decreased to 1.08 rps at approximately 12-1/2 seconds after second stage cutoff command.

The second stage inverter frequency again showed the characteristic trend which had appeared on all previous Able missiles. The frequency changes in an approximate sinusoidal manner to a maximum of 3/4 of a cycle above, and 1/4 of a cycle below the prelaunch value, having a period of approximately 60 seconds.

The frequency gradually decreases in this manner to a value slightly below that at launch by the end of second stage engine burning. This trend indicates that the average frequency over the flight period is approximately 1/2 cycle/second higher than the preflight frequency calibration.

c. Able-1, Flight Number 3, Thor Missile 129, 8 November 1958

Integrating accelerometer, Serial Number 15, was modified to eliminate the cutoff command function and was connected as an arming circuit for doppler command cutoff. The pitch program signal was calibrated for an interval of 25,015 ft/sec to 26,298 ft/sec or an interval of 1283 ft/sec.

The accelerometer uncaged normally at lift-off and completed 8.85 cycles at the time of arming of the second stage. 13.11 cycles had been completed at burnout of the first stage and 13.13 cycles had been completed at the separation of first and second stages. The approximate velocity at separation of first and second stages was 18,494 ft/sec. The second stage program started at an approximate velocity of 25,013 ft/sec and stopped at 26,280 ft/sec for a duration of 1267 ft/sec (11.07 seconds at an average acceleration of 114.5 ft/sec^2). The doppler arm function was calibrated to be initiated at 26,640 ft/sec. Doppler cutoff command was received at a velocity of 27,089 ft/sec after the accelerometer had completed 19.24 cycles of the output signal. After second stage cutoff command, a velocity of approximately 30 ft/sec was gained by the second stage. Second stage spin-up occurred approximately one second after cutoff and a maximum spin rate of approximately 2.19 rps was reached approximately 1.2 seconds later. The spin rate immediately started decreasing, showing several sharp changes in the rate of spin, the major one occurring at approximately one

second after the maximum spin rate had occurred, which corresponds approximately to the time third stage fire signal should have been received. The accelerometer performance was normal in all respects and no indications of failures could be detected.

5.3.6 Second Stage Telemetry Flight Test Results

The telemetry operation for all three flights was normal. All measurements were received, no dropouts have been noted. For Flight Number 1, data was received in the STL telemetry van for 244 seconds after lift-off. For Flight Number 2 data was received for approximately 17 minutes. On Flight Number 3 data was received for approximately 15 minutes. The receiving antenna used was a 7-1/2 turn helix mounted approximately 30 feet high. In all cases the signal was lost due to lack of line-of-sight. For normal flights, data is of interest only until the separation of Stages 2 and 3, approximately plus 270 seconds.

5.3.7 Results of the Vernier Firing Task

In the three live operations that comprised the Able-1 program the vernier operation was completed satisfactorily. In each case the command was sent to fire all eight rockets.

The first launch (August) was of insufficient duration to obtain any information as to the burnout conditions.

The second launch (October) successfully fired all three stages and provided the best test of the procedures set up for vernier operation. The data clearly indicated that free-flight velocity was too low and that the trajectory was lofted at the end of first stage. The doppler data in free-flight indicated that the velocity was several hundred feet per second below nominal. Consequently, all eight verniers were fired and firing was subsequently verified by observation of doppler data.

The third launch (November) progressed sufficiently far that a great deal of information was available. All data indicated that the trajectory was so near to nominal up to Stage 2 burnout that the final decision as to the number of verniers to fire would rest on the performance of third stage. Doppler data from free-flight agrees on this point, namely that the trajectory was nearly nominal. The failure of the third stage to ignite resulted in the decision to fire all eight verniers.

5.3.8 Post-Flight Trajectory Analysis of Lunar Probe (Missile 130)

The following is a summary of the results of an attempt to fit a dispersed trajectory to data gathered from Missile 130. The data used, its expected accuracy, and causes for the discrepancies between the data and the final computed trajectory (referred to as simulation 20) will be described.

The following is a summary of the results of an attempt to fit a dispersed trajectory to data gathered from the subject missiles. In evaluating the performance of a missile flight, the technique of trajectory reconstruction using simulation methods can be helpful. In this approach the actual trajectory is established as accurately as possible and then perturbations are made in various quantities which are used to compute a simulated trajectory. The measured flight data are then compared with the corresponding quantities from the simulated trajectory.

It should be realized that such a technique does not provide the only possible true reconstruction of the flight. However, if the position and velocity components are accurately matched over the entire trajectory and the information from all other data sources on the flight are incorporated into the reconstruction of the trajectory, the results can be accepted as an accurate description of the actual trajectory.

A succession of simulation runs were made using various combinations of autopilot drifts and increased or decreased thrust and weight flow from the propulsion system. In addition, all information concerning burning times and pitching rates and times which was available from telemetry was used. By inserting these quantities into the computer as small perturbations in the preflight nominal performance, a more and more faithful match to the data gathered from the actual flights was achieved. The sections below describe the simulated trajectories which most closely resembled the actual trajectories, and state the perturbations required to generate them.

The digital computer program which was used to calculate all trajectories for this work was a three-dimensional trajectory study program. It obtains true inertial coordinates and employs an oblate earth gravitational potential. This is the same program used to calculate the nominal trajectories for the Able vehicles. By the insertion of program constants, all autopilot and propulsion variations

which continue throughout any stage could be incorporated into the program as well as any peculiarities of sequence (e.g., lengthened first stage vernier period). The best estimates from telemetered quantities of thrust and flow rate programs were used.

a.   Able-1, Missile 2, Thor 130

Several sequences of data were available to be used for calibration of the trial trajectories of Missile 130. First was the STL doppler range rate measurement which was operative and in lock for 740 seconds after lift-off except for a loss of lock for approximately 30 seconds around first stage burnout. Second was the Azusa tracking radar which tracked first stage through burnout and gave velocity as a function of time for this period. Third was the telemetered integrating accelerometer reading which operated through second stage burnout and gave integrated thrust acceleration as a function of time. In addition to those prime sources of data, the Millstone radar operated by Lincoln Laboratories of MIT achieved skin track lock-on to the second stage in free-flight and provided angular data for a period of about 90 seconds after second stage burnout.

Several additional pieces of information were made available from the telemetry records and were incorporated into the simulation where they were applicable. Included in the information obtained from telemetry were burnout times and autopilot variations, and also the engine performance data for Stage 2.

(1)   The following analysis of the powered flight of the second Able-1 missile and Thor 130 embodies the results of a digital simulation (simulation 20) which best matched all available data.

Starting with the first stage, the most significant perturbations were in propulsion. It is known that first stage burned to total fuel exhaustion. However, the burnout time was almost 2 seconds less than nominal. This clearly indicated a higher flow rate than nominal. In addition, the burnout velocity was about 800 ft/sec greater than nominal which implied greater than nominal thrust.

In addition to the propulsion perturbations, angular measurement made by Azusa at first stage burnout indicated some autopilot errors. Telemetered pitch rate showed that the pitch program operated correctly except for an unexplained additional 2.5 seconds on the last step. This resulted in about 1 degree of attitude error in the pitch-down direction. Since the net attitude error

was 2-1/2 degrees in the pitch-up direction, the equivalent pitch gyro drift was approximately minus 60 degrees per hour. The remaining attitude error was a result of the high thrust. In addition to the pitch errors, the azimuth of the burnout inertial velocity vector was almost 1 degree too far north. This would result either from a roll gyro drift or from a yaw gyro drift or both. For simulation purposes a roll gyro drift of minus 5C degrees per hour was arbitrarily chosen.

During the first stage vernier a control system transient resulted in attitude changes of a one-half degree yaw to the right and a one-half degree pitch down. Those were simulated by transient gyro drifts of high value. In addition, it was noted that the vernier period lasted for a total of 2.44 seconds and this was incorporated into the program.

Second stage propulsion perturbations consisted of modifying thrust and flow rate in order to recapitulate the accelerometer and doppler records. The dispersions required to do this were a 3.89 per cent reduction in thrust and a 1.06 per cent increase in flow rate. This means that I_{sp} was about 4.95 per cent below nominal or about 259 seconds. Autopilot dispersions were almost completely masked since a small attitude error is not visible in either range rate or accelerometer readings and the Millstone data was not sensitive enough to give accurate readings of inertial or azimuth. Had the third stage performed correctly, the angular dispersions could have been reconstructed from free-flight.

An attempt was also made to fit a trajectory to the heavily perturbed third stage. The assumption made was that all unexplained angular dispersions as reconstructed from free-flight data resulted from an attitude error in third stage. It was also assumed that this attitude error was due to a transient very near the beginning of third stage burning. To simulate this condition, an extremely large attitude drift (14.3 degrees pitch up and 16.2 degrees yaw left) was introduced during the 2 seconds of free fall between second stage burnout and third stage ignition. In addition, it was necessary to degrade the performance to take into account the impulse lost due to the precessional cone angle. The necessary degradation of only 1.6 per cent implies that precession did not continue throughout burning). (See Section 5.3.1 c.)

Since the only data available during third stage was doppler range rate, no direct evidence of the angular dispersions were available. However, sufficient data were gathered from free-flight to allow an accurate estimate to be made of burnout parameters.

(2) **Discrepancies Between Measured Quantities and Simulation 20, Powered Flight**

Figures 5-9 and 5-10 are a measure of the success of simulation 20 in Stages 1 and 2, respectively. There is a striking improvement in Stage 2 which is probably simply due to the use of the telemetered chamber pressure in the construction of a propulsion profile.

It is known, for example, that the thrust-to-weight ratio at the beginning of Stage 1 was less than simulation 20 shows. However, in order to match end conditions in all measured quantities it was necessary to increase the nominal thrust quantities by 3 per cent, at a uniform rate. This is the reason that the integrating accelerometer output disagrees so violently with the simulated thrust velocity near lift-off. However, this disparity near lift-off between the nominal and simulated profiles is not the only one. The negative trend in all three measured quantities from 90 to about 130 seconds is certainly a result of another profile error. The general upswing of all quantities from 130 to 150 seconds comes from the fact that the residual impulse after burnout is not simulated. Thus, the velocity gain from residual impulse must be included in the main engine burning time which tends to elevate the error near cutoff. A similar trend can be seen in Figure 5-9, especially in V_ξ.

It can be seen from Figure 5-11 that the match to doppler data in the third stage simulation is inexact. However, the error in the doppler data resulting from free electrons in the vicinity of the payload may contribute to this. In addition, the thrust program used is very likely to be in error since it was made from vacuum wind tunnel measurements on a small sample of this type of engine.

The general agreement with projected third stage burnout conditions (see Table 5-4) is encouraging. It is to be noted that an exchange was made between velocity and altitude such that the total energy at burnout agrees with the projected conditions. (The exchange between potential and kinetic energy at this altitude is about 1240 feet per foot per second.)
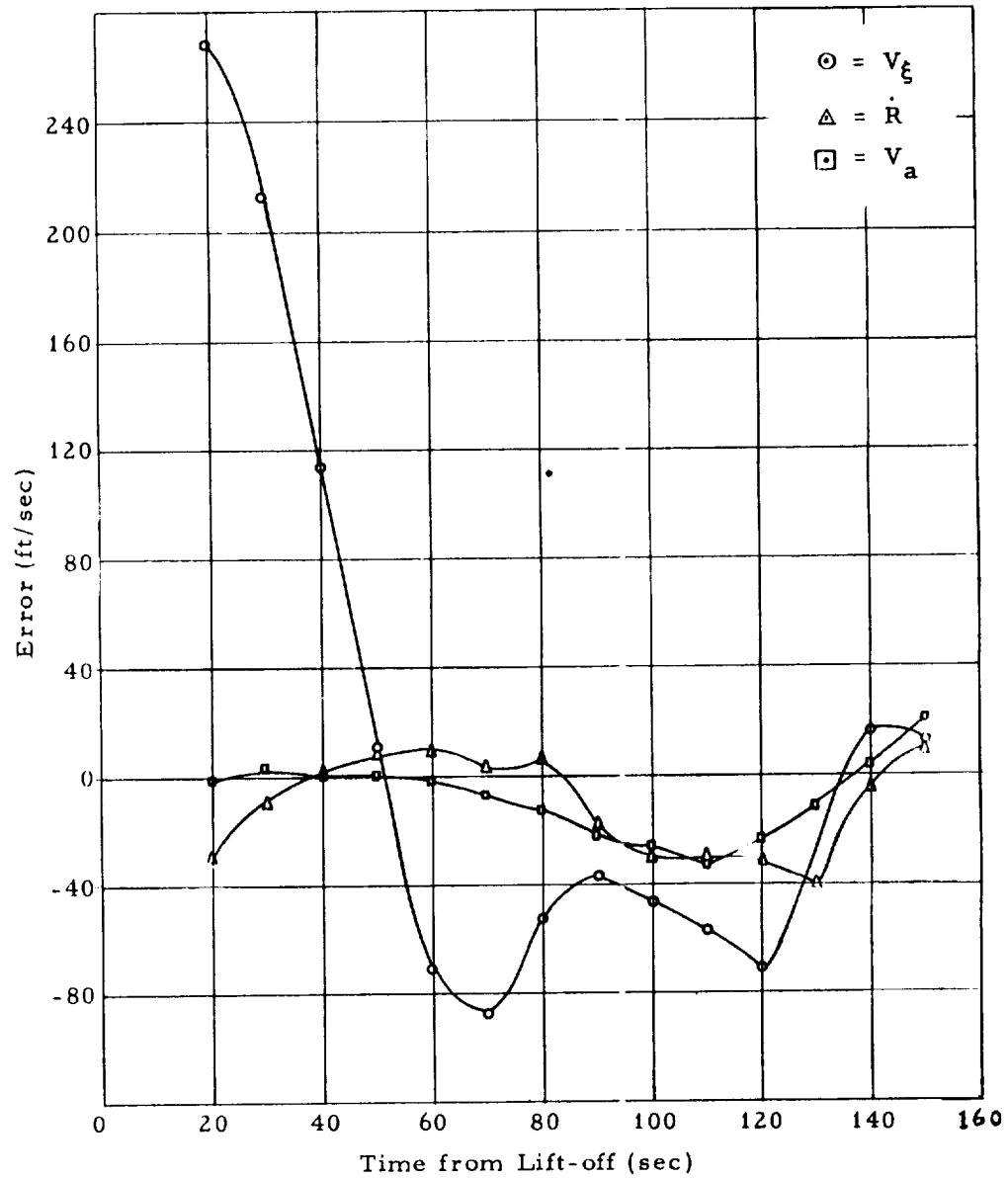
Figure 5-9.   Stage 1 Plot of Simulated Quantities Minus Measured
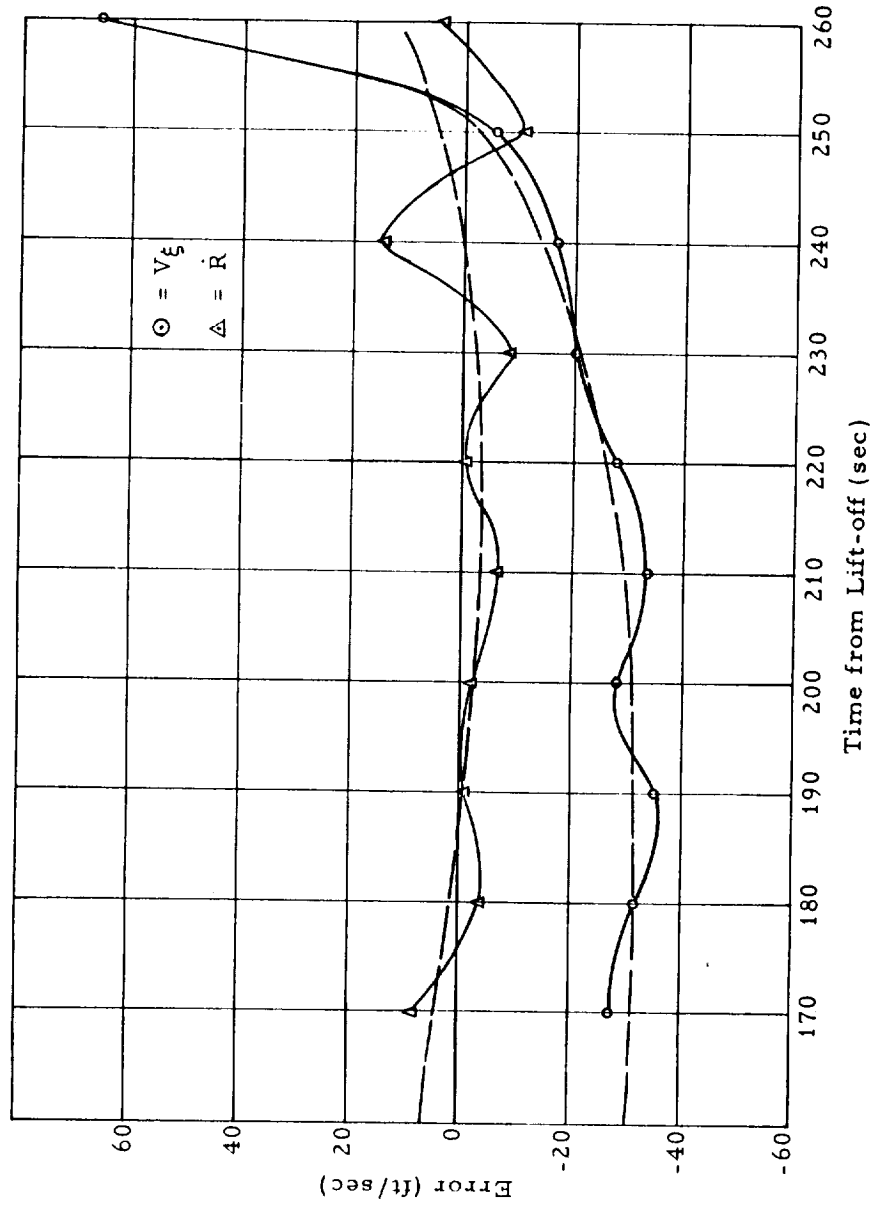Quantities Versus Time from Lift-off.

Figure 5-10. Stage 2 Plot of Simulated Quantities Minus Measured
Quantities Versus Time from Lift-off.
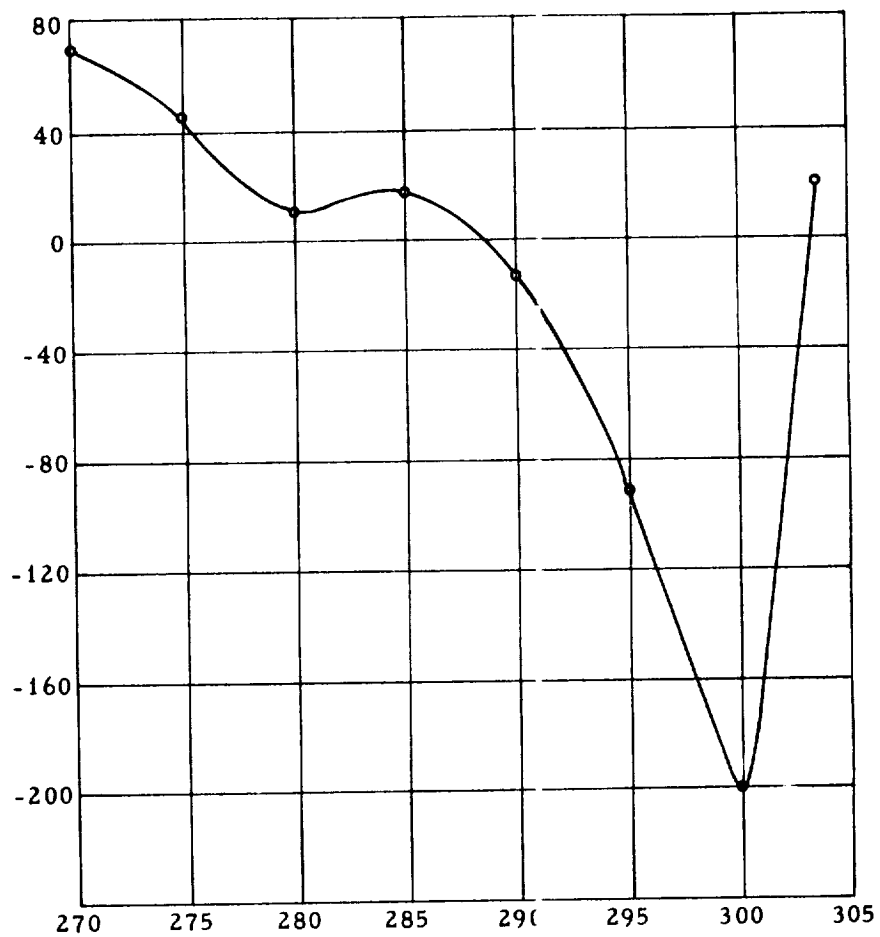
Figure 5-11. Stage 3 Plot of Simulated Range Rate Minus
Measured Range Rate Versus Time from Lift-off.

Table 5-4. Measured Burnout Conditions of Stage 3

Simulated Burnout
Conditions of Stage 3

V_I	34,353 ft/sec	34,296
D	22,372,000 ft	22,448,000 ft
β_I	64.6°	64.6°
Az_I	70.6°	70.6°
a_o	80.5°	80.9°
δ_o	30.7°	30.8°

Table 5-5. Comparison Between Simulated and Nominal
Burnout Conditions

Stage							
2	23331	1002261	70.6	76.4	21939	269.1	Nominal
	23104	1116591	67.5	76.5	21747	263.1	Simulation 20
3	35206	1335377	71.1	77.5	33650	308.1	Nominal
	34293	1540369	64.6	70.6	32918	303.6	Simulation 20

Table 5-5 shows a comparison of the nominal burnout conditions of Stages 2 and 3 with the results of simulation 20.

(3) Discussion and Conclusions

Table 5-6 is a list of all perturbations used in simulation 20 showing the nature of the variations in Thor 13C and Able-1 Number 2.

There are discrepancies between simulation 20 and the measured quantities. This is especially true in the first stage. Here there are errors of as much as 2 per cent in V_ξ and as much as one-half per cent in $\dot{R}$ and V_a. In all likelihood these could be significantly reduced by the use of more realistic thrust and flow rate profiles, but these were not available.

The main dispersions of Stage 1 are shown and the conditions at burnout are very closely matched. Thus, Stage 2, which shows errors much less than Stage 1, is probably fairly precise.

Examining the burnout conditions of Stage 2 allows the following conclusions: Had the third stage not been perturbed in angle the burnout energy would have been low by about 110 ft/sec and the burnout velocity vector would have been lofted by about 3 degrees. Thus, if a burnout velocity of 110 ft/sec out of the 140 ft/sec available from the vernier rockets had been used, the payload would have traveled to within 20,000 miles of the moon. The error of 20,000 miles is therefore, the result of the dispersed angle. Moreover, once the payload had approached to within 20,000 miles of the moon, it was no means impossible that a lunar orbit would have been achieved although the stability of this orbit is undetermined.

The Stage 3 presented in simulation 20 is probably fairly inexact. However, the important conclusions to be drawn are (1) that a very sizeable attitude kick at the beginning is required to explain the angular errors noted at burnout, and (2) that the precession which was present at the initiation of burning was not of sufficient duration to grossly reduce the total impulse.

b. Able-1, Missile 3, Thor 129

(1) Data used:

The data available for analysis of the third lunar vehicle flight of 8 November are: (1) fixed camera position and smoothed velocity data up to

Table 5-6 . Dispersions Used (Simulation 20).

STAGE 1

Propulsion

3.3 per cent high thrust

2.4 per cent high weight flow

Autopilot

-60° per hour pitch gyro drift

-50° per hour roll gyro drift

last pitch program step (0.30455 deg/sec)

operated to 142.5 seconds (extra 2.5 seconds)

STAGE 1 VERNIER

Propulsion

burning time 2.44 seconds (extra 0.44 second)

Autopilot

0.5° yaw to right

0.5° pitch down

STAGE 2

Propulsion

special thrust and flow table

(about -3.8 per cent thrust and +1.1 per cent weight flow)

accelerometer cutoff at 26,965 ft/sec

Autopilot

none (see text)

STAGE 3

Propulsion

-6.4 per cent thrust

-4.8 per cent flow rate

Attitude Error

14.8° pitch up

16.2° yaw left

Autopilot

no autopilot on Stage 3

12.503 seconds of the flight, and Azusa position and velocity data for 29 to 180 seconds of flight from lift-off; (2) doppler command receiver data from lift-off to 848 seconds of flight; (3) integrating accelerometer data from lift-off to 270.01 seconds of flight; (4) telemetry data; (5) weight data; and (6) radar tracking data from various stations.

(2) Detailed Analysis:

Propulsion perturbations in the Thor Stage consisted of raising both thrust and flow rate (without changing I_{sp}) and modifying the thrust profile.

The autopilot perturbations used were a roll gyro drift of $+40°/hr$ and a yaw gyro drift of $50°/hr$. In addition, the pitch program was adjusted according to telemetered rate information and an attitude transient was introduced during first stage vernier period.

Second stage perturbations consisted of propulsion modifications only. The thrust was lowered by 3.5 per cent and weight flow increased raised by 0.1 per cent resulting in an I_{sp} of 261.3 seconds. Telemetry data indicated that third stage separation did occur but doppler range rate data indicated that no third stage firing occurred.

(3) Comparison of Measured Data with Reconstructed Trajectory:

Figure 5-12 shows the differences between the digital simulation and the data taken from various sources. The point for point agreement is sufficiently good and the agreement with projected burnout conditions is quite good (see Table 5-7) so that it is probable that the above mentioned perturbations during powered flight are close to correct.

Table 5-7 also shows the nominal second stage burnout conditions.

(4) Discussion and Conclusions

The use of telemetered quantities to generate a realistic thrust curve for the first stage allowed a very close approximation to be made in simulation to the actual missile. This approximation was further increased by the relatively nominal performance of both stages.

The burnout conditions of the second stage imply that, had third stage performed nominally, the payload would have come within 4000 miles of the lunar surface and a stable orbit could probably have been achieved.
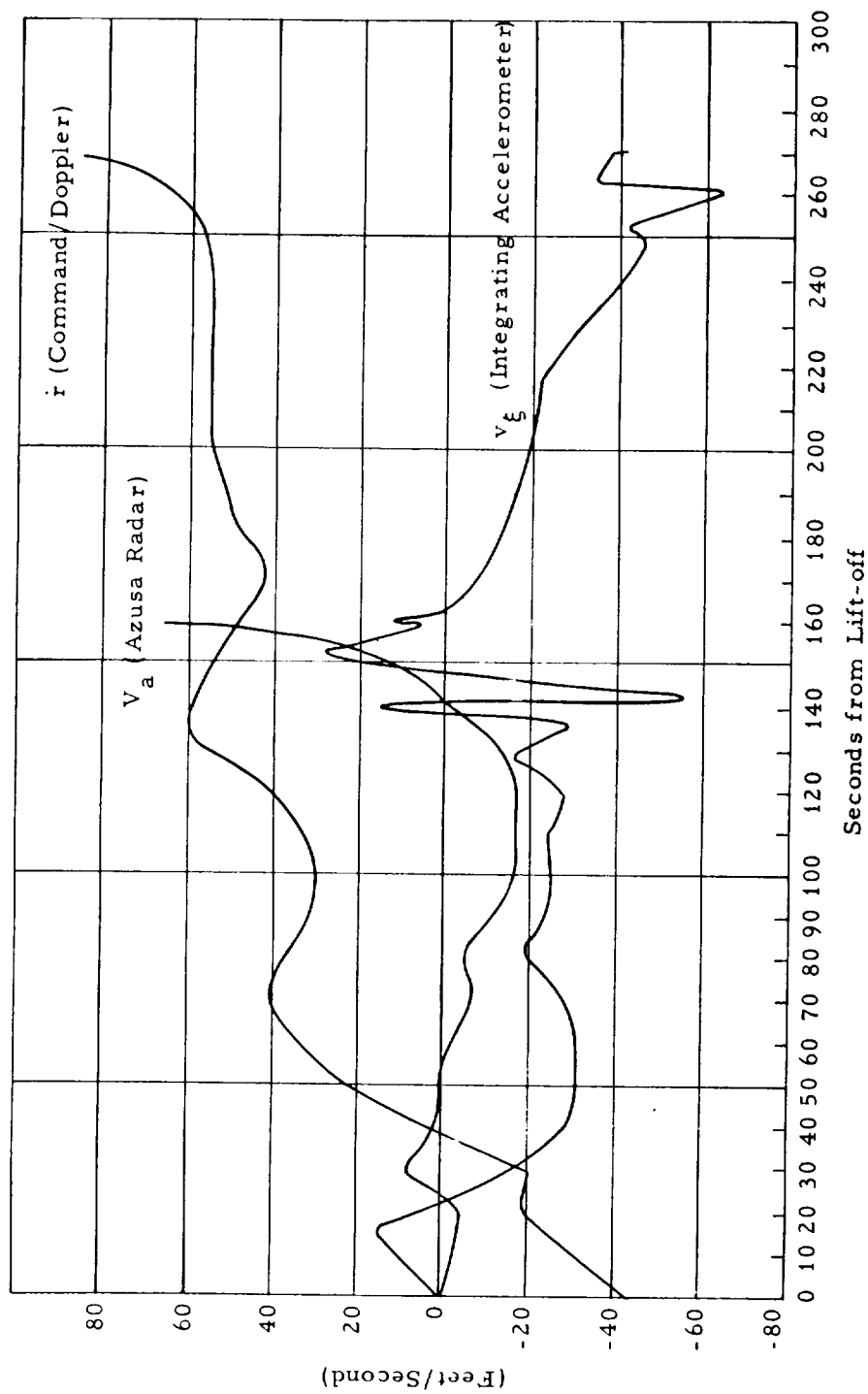
Figure 5-12.   Difference of Simulation from Various Data Sources.

Table 5-7. Comparison of Burnout Parameters

	Projected Burnout Parameters as Derived from Free Flight Data	Burnout Parameters of Digital Simulation	Nominal Burnout Parameters
Inertial Velocity	23,646 ft/sec	23,561 ft/sec	23,521 ft/sec
Angle Between Velocity Vector and Vertical	71.88°	71.93°	70.50°
Angle Between Velocity Vector and North	77.88°	77.48°	79.99°
Distance from Center of the Earth	21,937,600 ft	21,880,802 ft	21,933,011 ft

APPENDIX A
ANALYTICAL AND NUMERICAL STUDIES OF THREE-DIMENSIONAL TRAJECTORIES TO THE MOON[*]

INTRODUCTION

The purpose of this paper is to present theoretical calculations of lunar trajectories from the point of view of the guidance problem. Although there has been much work in the past few years on the general problem of lunar vehicle orbits, little work has been presented that would be directly valuable in designing the guidance for a launch vehicle. The attempt here is to give results which will be immediately useful for present lunar flights. Since the vehicles assumed in this study are ballistic, the guidance problem is simply one of reducing the error at the end of powered flight, that is, at burnout. Errors at burnout are a function of the particular design of a given vehicle, and consequently the analysis of the errors presented here is generalized to make it as useful as possible to all designs. Although a conventional two-dimensional approach is presented, the three-dimensional problems arising from a nonoptimum location of launch sites are also analyzed. To substantiate the conclusions of this paper, a large number of machine calculations were made and are compared directly with the approximate solutions

Section 1 contains the conventional two-dimensional analysis with the usual decomposition of the actual N-body problem, the earth, moon, vehicle, sun, etc., into the more tractable succession of two-body problems. The analytic statement of the required accuracy to impact on the moon's surface is then determined and compared with the actual accuracy needed. However, since the accuracy requirements given assume that the launching may be made directly into the plane of the moon, this solution is not satisfactory for real launch sites which require that the vehicle be launched out of the plane or that the vehicle be turned into the plane of the moon, an extremely expensive alternative for propulsion. Therefore, Section 2 examines the effect on the necessary guidance accuracy of launching out of the plane of the moon. This three-dimensional analysis indicates that the velocity accuracy requirements increase sharply as the plane of the trajectory is inclined with respect to the

---

plane of the moon, and also that the accuracy requirements vary greatly for different launch times, both for given times of the day and given days of the month. For example, from middle latitudes the accuracy requirements coupled with propulsion requirements increase so greatly during several weeks of the lunar month that it is impractical to attempt to come close to the moon. Methods for analytically determining appropriate launch times and azimuths are also given.

Section 3 is a brief application of the ideas presented above to some of the special problems posed by attempting to establish a lunar satellite.

SECTION I

In the initial analytic approximation, the earth-moon-vehicle system will be treated as a succession of two-body problems. That is, the vehicle will be controlled solely by the earth's field in the initial phase, and then pass into a terminal region where only the moon controls its motion. To further simplify the problem, it is assumed that the moon moves in a circular orbit about an inertial earth; the influence of both the sun's and moon's mass on the earth's motion is ignored. In this section it is also assumed that the vehicle at burn-out is moving in the moon's orbit plane. It can be placed there either by a fortuitous location of the launch site, or by expenditure of sufficient fuel to orient the vehicle's velocity vector into the lunar plane. This maneuver is neither necessary nor efficient, but the analytic results are useful as a beginning when approaching guidance problems in the nonplanar case.

The notation used in this section is shown in Figure 1-1. Considering first only the effects of the earth's field, assuming it to be central, the vehicle's equation of motion may be written in an inertial frame of reference centered at the earth as follows:

$$\ddot{r} - r\dot{\theta}^2 = \frac{-\mu_E}{r^2} , \tag{1.1}$$

and

$$r\ddot{\theta} + 2\dot{r}\dot{\theta} = 0 , \tag{1.2}$$

where $\mu_E = GM_E = 1.4076 \times 10^{16}$ ft^3/sec^2. Eliminating $\dot{\theta}$ from Equation (1.1) via the usual angular momentum integral obtained from Equation (1.2), there results

$$\dot{r} = \sqrt{2E + \frac{2\mu_E}{r} - \frac{J^2}{r^2}} , \tag{1.3}$$

where E is the vehicle's total energy (per unit mass) and J is the vehicle's angular momentum (per unit mass).

Because we ignore the moon's mass in the initial phase, the interesting class of orbits, which are true minimum energy trajectories because the mass of the moon is used to pull the vehicle to the moon, are also ignored. These
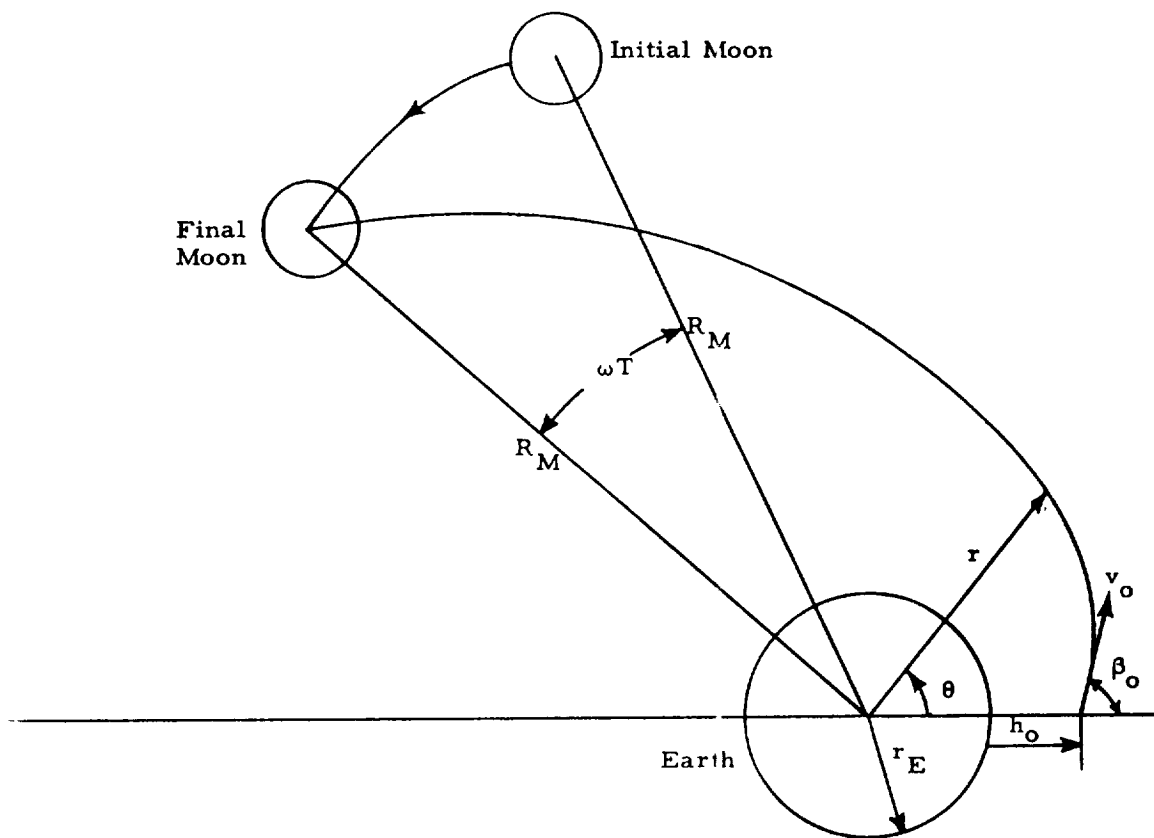
Initial Moon

Final
Moon

R_M

ωT

R_M

r

v_o

β_o

θ

Earth

r_E

h_o

Figure 3A1-1. Planar Geometry.

ω — Angular Velocity of Moon

T — Total Time of Flight

r, θ — Nonrotating Polar Coordinates of Vehicle

v_o — Burnout Velocity

β_o — Burnout Flight Path Angle

r_E — Radius of Earth

h_o — Burnout Altitude

ωT — Angle Moon Rotates During Time of Flight

R_M — Distance from the Center of the Earth
to the Center of the Moon

orbits consist of multiple revolutions of the earth before arrival in the moon's vicinity. Minimum energy, as used here, means the minimum energy to reach the moon's vicinity while moving in an ellipse and without considering the moon's field. The difference between the two definitions implies a change of burnout velocity of approximately 200 ft/sec. The class of orbits ignored pose guidance problems too difficult for the primitive vehicle considered here so that this definition of minimum energy is justified in this context.

We are interested in the time required to go from a radius, r_o, to a radius, r_1. This is obtained immediately from Equation (1.3) as follows:

$$t = \int_{r_o}^{r_1} \frac{dr}{\dot{r}} = \int_{r_o}^{r_1} \frac{dr}{\sqrt{2E + \dfrac{2\mu_E}{r} - \dfrac{J^2}{r^2}}} \qquad (1.4)$$

Since $J = r^2 \dot{\theta}$, we can obtain the total in-plane angular change, θ, from

$$\theta = \int_{r_o}^{r} \frac{J}{r^2 \dot{r}} dr = \int_{r_o}^{r_1} \frac{J \, dr}{r \sqrt{2E r^2 + 2\mu_E r - J^2}} \qquad (1.5)$$

Equations (1.4) and (1.5) may be integrated in closed form (see Section 4) or integrated numerically. Using an earth radius of approximately 2.09×10^7 ft, a mean circular lunar orbit of radius 1.261×10^9 ft, the flight time and in-plane angle can be obtained as functions of burnout angle, and burnout velocity as in Figures 3A1-2, 3A1-3, 3A1-4, and 3A1-5. Unless specifically varied, the burnout altitude, h_o, and burnout angle, β_o, are assumed to be 200 miles, and 70 deg, respectively. These values are reasonable for a multistage, continuous burning vehicle of the type assumed here. Of course, for detailed design work the interaction of β_o and h_o with the powered stage and subsequent ballistic flight must also be considered. Also, we limit the range of burnout velocities under consideration between minimum energy and approximately 36,000 ft/sec since we assume that excess burnout speed will be converted into useful payload unless compelling guidance restrictions dictate otherwise.
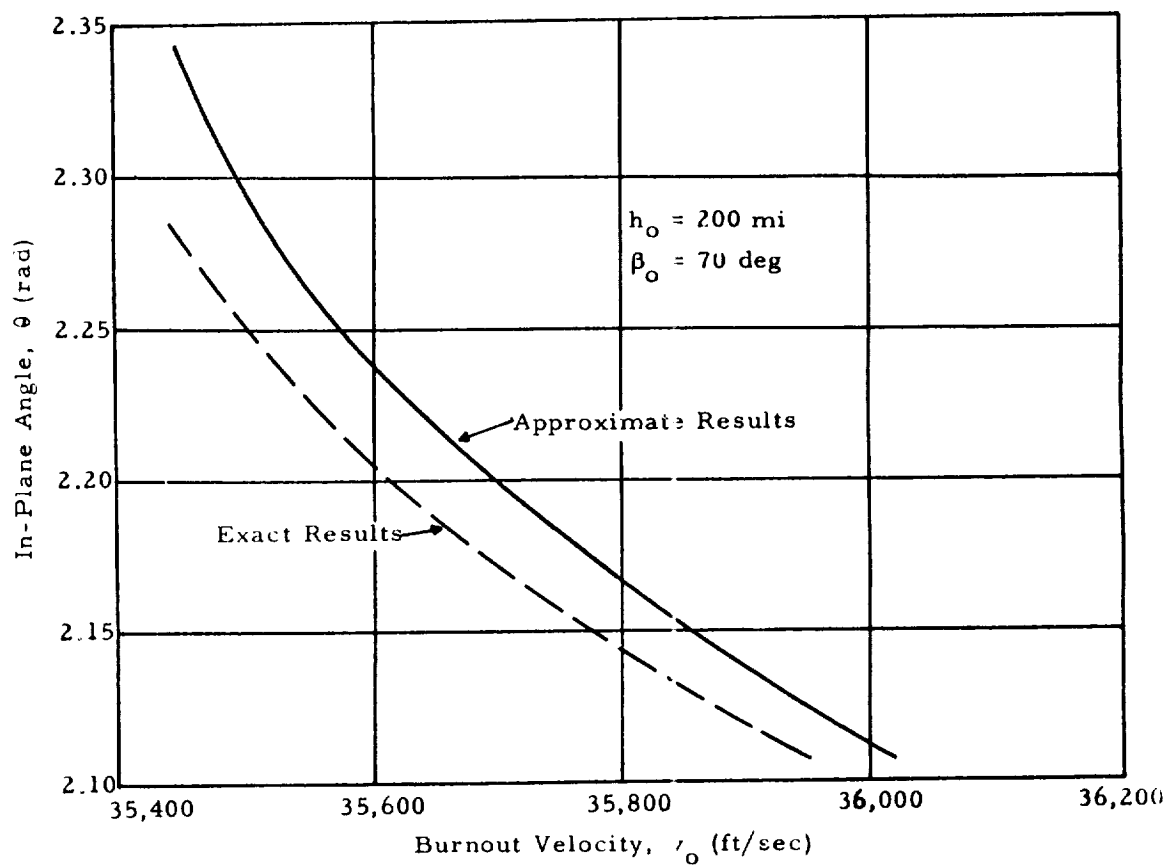
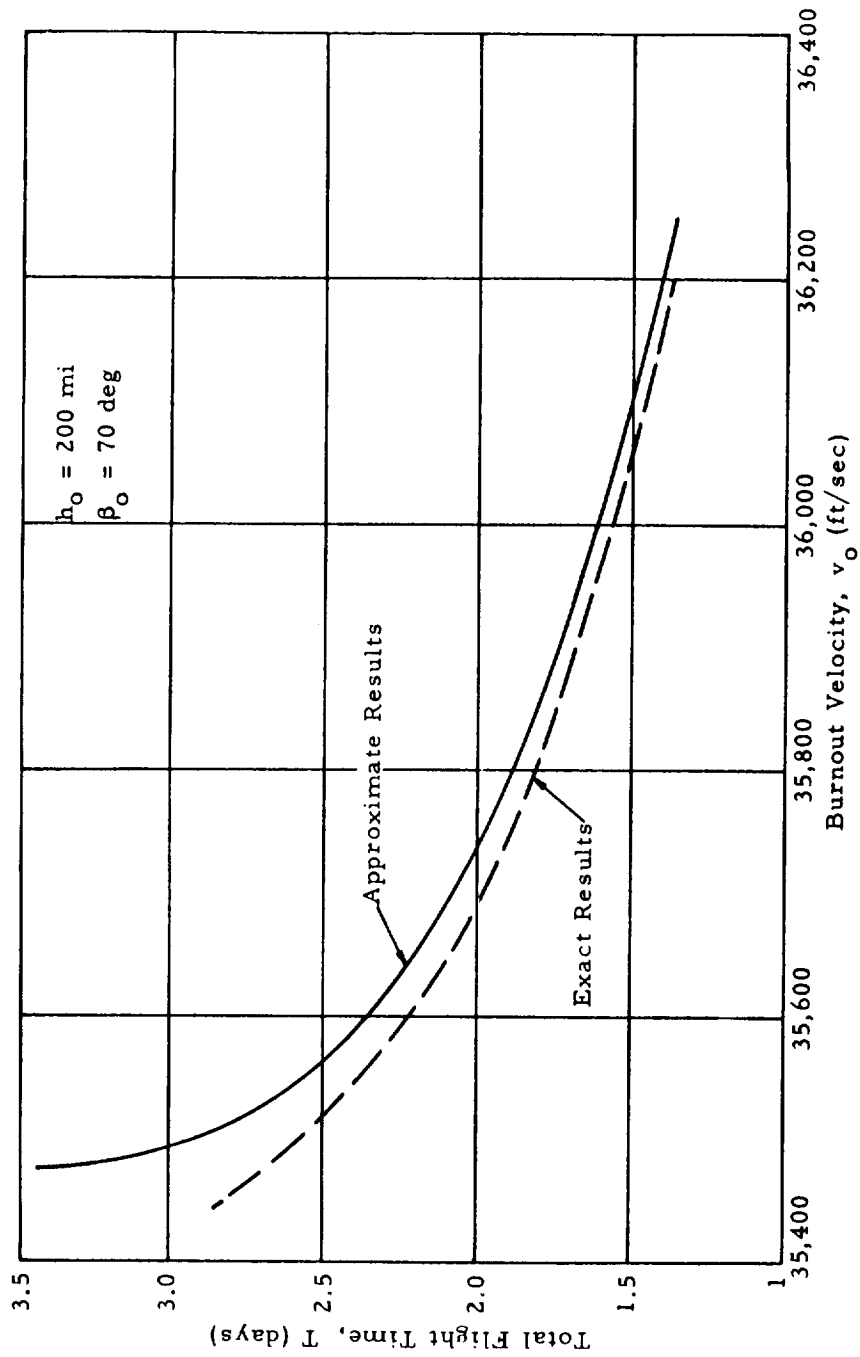Figure 3A1-2. In-plane Angle as a Function of Burnout Velocity.

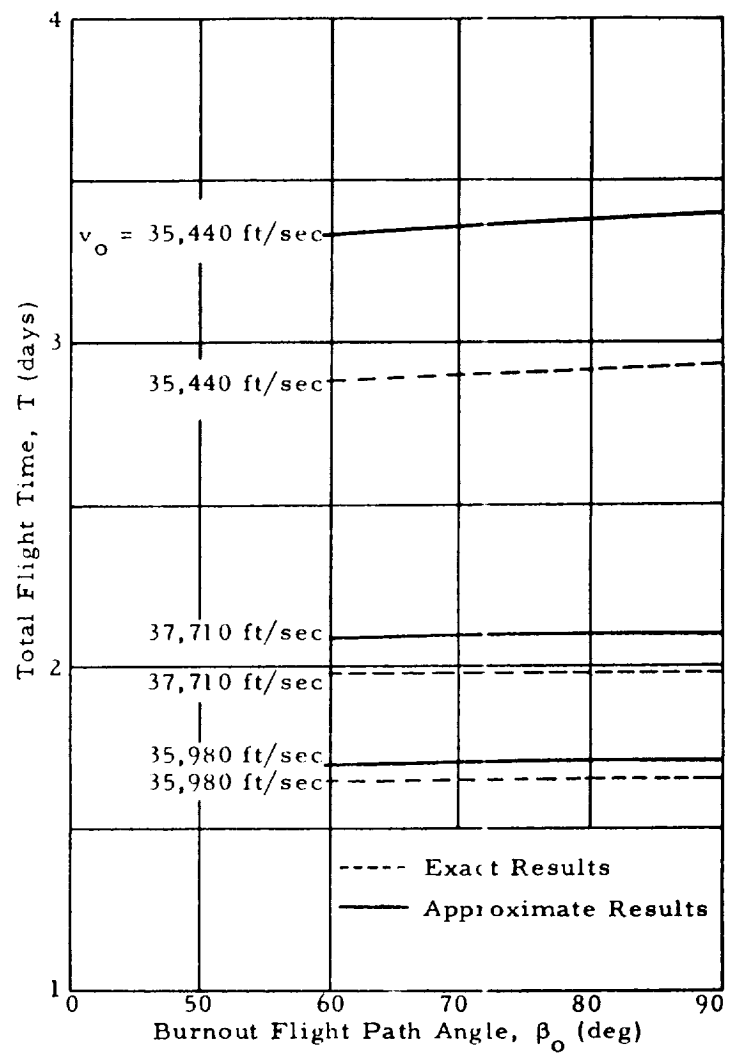Figure 3AI-3. Flight Time as a Function of Burnout Velocity.

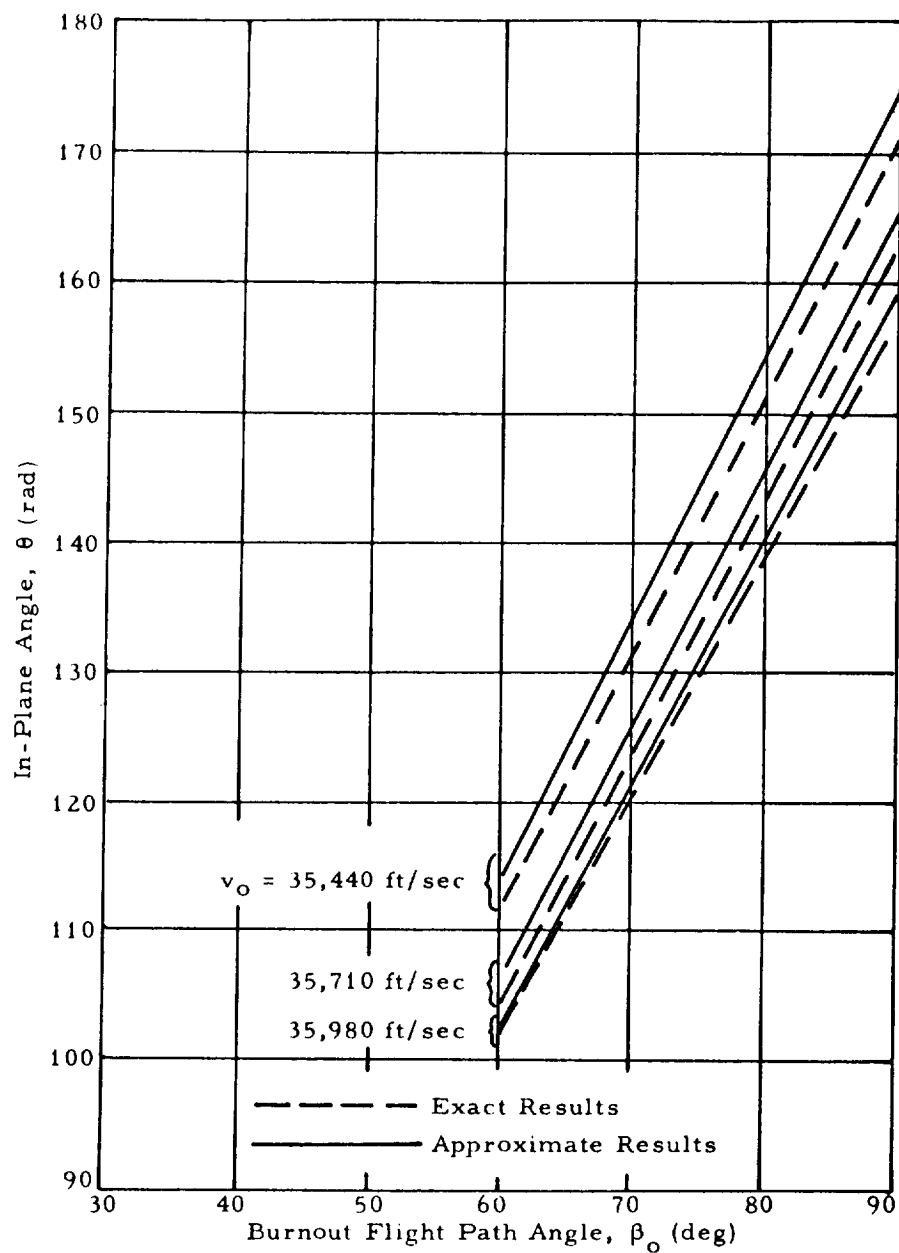Figure 3A1-4. Flight Time as a Function of Burnout Flight Path Angle.

Figure 3A1-5. In-Plane Angle as a Function of Burnout Flight Path Angle.

Because the effect of the moon has been ignored, the flight times and
in-plane angles calculated from Equations (1.4) and (1.5) should be only approxi-
mately valid. The approximation should become increasingly poor as minimum
energy is approached and the vehicle spends more time in the combined field of
earth and moon before arrival. This is borne out by the curves labeled "exact
results" which represent exact numerical integration of the complete
three-body problem.

From Figure 3A1-2, we see that the error in the analytic prediction of
in-plane angle, θ, decreases from approximately 4 deg at minimum energy to
about 1 deg at 36,000 ft/sec. From Figure 3A1-3, we see that the prediction in
time of flight improves even more rapidly as the velocity increases from an
error of approximately 5×10^{5} sec at minimum energy to approximately 8×10^{3} sec
at 36,000 ft/sec. This analytic model, of course, breaks down completely in the
limited range of velocities above exact minimum energy where the orbits may
make numerous rotations about the earth before impacting on the moon. On the
other hand, as the burnout velocity approaches infinity, the vehicle is effectively
being aimed at a point moving in the moon's orbit and the present approximation
becomes exact.

It is evident that the analytic results are inadequate for detailed orbit
calculations unless burnout velocities are several hundred feet per second
above minimum. However, the model may be made sufficiently accurate for
guidance error analyses and design purposes by turning off the earth's field
when close to the moon and calculating the correction due to the moon's
influence alone.

We now proceed to introduce the effects of the moon. To simplify the
calculation in the vicinity of the moon, we will now ignore the curvature of
the moon's orbit geometrically as well as dynamically, and consider the
problem in a moon-fixed coordinate system (see Figure 3A1-6). The velocity
components in this coordinate system are

$$\dot{x} = v_{M} - r\dot{\theta}$$

$$\dot{y} = \dot{r}$$

(1.6)
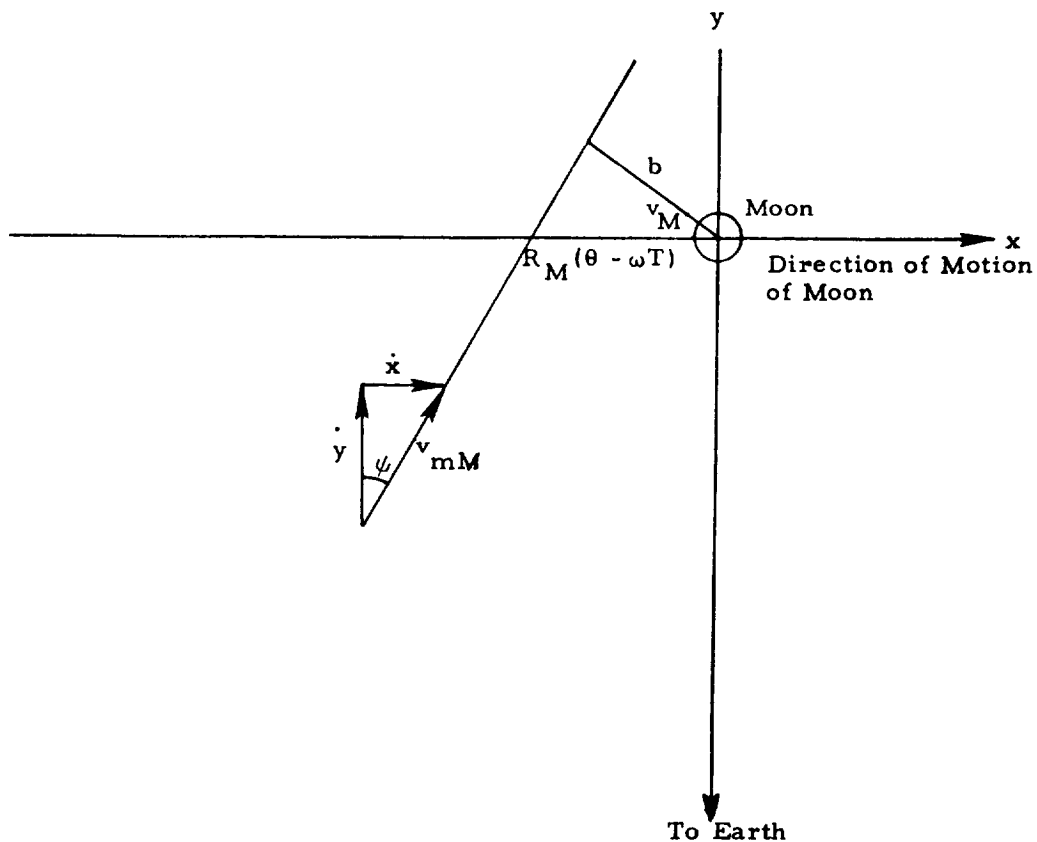
Figure 3A1-6. Geometry in the Vicinity of the Moon.

b	-	Impact Parameter (perpendicular distance between the moon's center and asymptote of the incoming hyperbola.
V_M	-	Velocity of the Moon
V_{mM}	-	Vehicle Velocity Relative to the Moon
$R_M(\theta - \omega T)$	-	Distance from Vehicle to Moon at time Vehicle Crosses Moon's Orbit
ψ	-	Angle Between the V_{mM} and the y-axis
x, y	-	Rectangular Coordinates Centered at Moon (x in moon's orbit, y along radius to earth)

where v_M is the moon's orbital velocity ~ 3370 ft/sec. Using energy and angular momentum relations to compute the inertial injection velocity components,

$$\dot{r} = \sqrt{2E + \frac{2\mu_E}{r} - \frac{J^2}{r^2}} \quad ,$$

$$r\dot{\theta} = \frac{J}{r} \quad . \tag{1.7}$$

The magnitude and angle of vehicle velocity with respect to the moon are then easily calculated from

$$v_{mM} = \sqrt{\dot{x}^2 + \dot{y}^2} = \sqrt{(v_M - r\dot{\theta})^2 + \dot{r}^2} \quad ,$$

$$\Psi' = \tan^{-1}\left(\frac{\dot{x}}{\dot{y}}\right) = \tan^{-1}\left(\frac{v_M - r\dot{\theta}}{\dot{r}}\right) \quad . \tag{1.8}$$

Now the distance the vehicle crosses the moon's orbit ahead of the moon in the absence of the moon's gravity field is given by $R_M(\theta - \omega T)$. This distance is directly related to the "impact parameter"[*], b, (see Figure 3Al*6) by the relation

$$b = (\cos \Psi') R_M (\theta - \omega T) \quad . \tag{1.9}$$

Thus, this model takes the conditions at the moon's orbit calculated without considering the moon's field as the injection conditions for the hyperbolic orbit about the moon.

The impact parameter, b, (from the Rutherford scattering theory) is convenient since it determines the distance of closest approach by recourse to the usual assumptions of conservation of energy and angular momentum in the moon's frame of reference. The small rotation of the coordinate system in the time interval under consideration is ignored. If we assume the vehicle

---

[*] The impact parameter is the perpendicular distance between the moon's center and the asymptote of the incoming hyperbola.

enters the moon's gravity field at a distance, d, and if the vehicle's velocity relative to the moon, v_{mM}, has an angle, ϵ, with respect to the center of the moon (see Figure 3A1-7), then

$$b = d \sin \epsilon .$$ (1.10)

Combining Equation (1.10) with the energy and momentum relations, the maximum impact parameter allowable for collision to result is

$$b_{max} = a_M \sqrt{1 + \frac{2\mu_m}{a_M v_{mM}^2} - \frac{2\mu_M}{d v_{mM}^2}} .$$ (1.11)

where a_M = the moon's radius, and $\mu_M = GM_M = 1/81.375 \, \mu_E$. Since $d \gg a_M$ for any reasonable choice of d, we can approximate b_{max} by

$$b_{max} \cong a_M \sqrt{1 + \frac{2\mu_M}{a_M v_{mM}^2}}$$ (1.12)

The maximum allowable impace parameter, b_{max}, is plotted in Figure 3A1-8 as a function of v_{mM}.

We are now in a position to relate deviations in burnout quantities to changes in $(\theta - \omega T)$, thence to changes in b, and finally to distance of closest approach. The integrals of T and θ, Equations (1.4) and (1.5), can be differentiated and then integrated in a closed form to obtain the first derivatives of $(\theta - \omega T)$ with respect to burnout velocity and flight path angle (see Section 4). This procedure is inadequate where $\partial/\partial v \left[(\theta - \omega T) \right]$ goes through zero (see Figure 3A1-9) since higher derivatives play the dominant role there. In this region the results were computed from tabular values of $(\theta - \omega T)$ as a function of velocity. The maximum allowable $\delta(\theta - \omega T)$ is computed from Equations (1.9) and (1.11) and then converted to maximum allowable errors in burnout quantities through the procedure described above. It should be pointed out that there is an element of arbitrariness in the definition of a standard orbit with respect to which the allowable dispersions of v_o and β_o are calculated. The standard orbit used here is such that the velocity relative
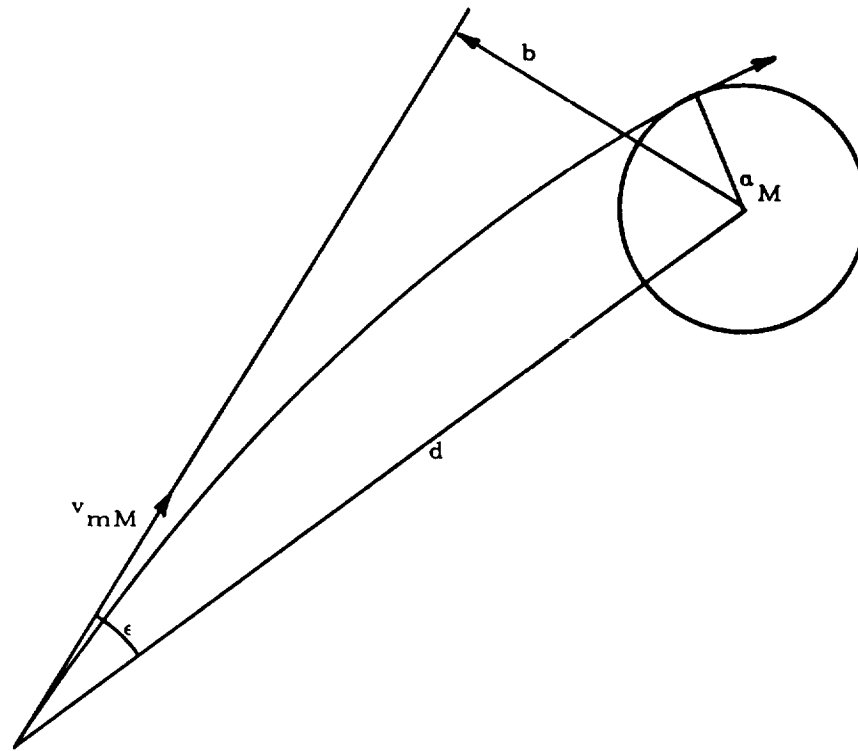
Figure 3A1-7. Effect of the Moon's Gravity on Impact Conditions.

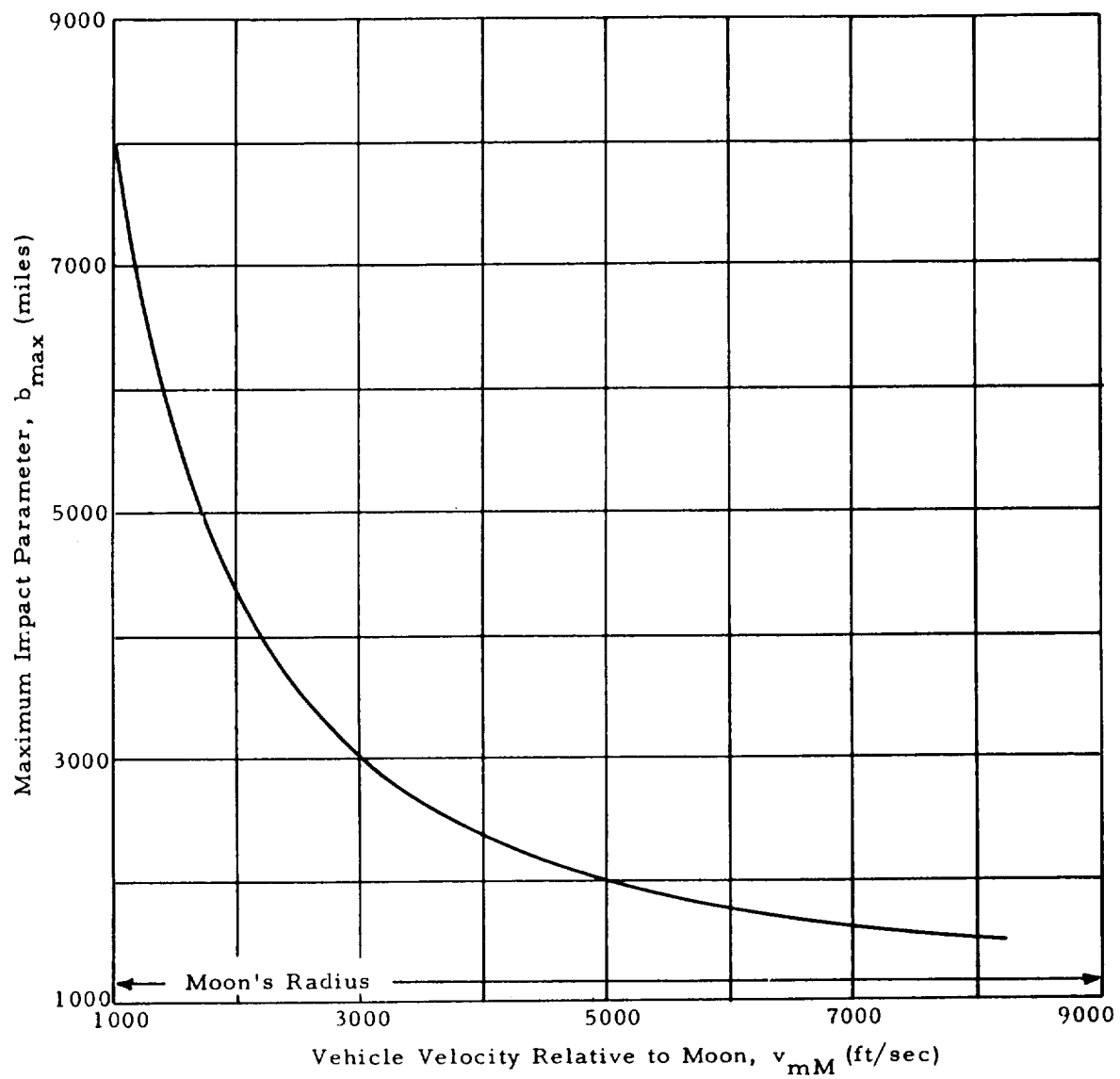|		
v_{mM}	–	Vehicle Velocity Relative to Moon
b	–	Impact Parameter
a_M	–	Radius of Moon
d	–	Vehicle Distance from Moon Upon Entry into Moon's Field

Figure 3A1-8. Maximum Impact Parameter as Function of Vehicle Velocity Relative to the Moon.

to the moon, v_{mM}, is directed at the center of the moon at impact. Because $(\theta - \omega T)$ is not a linear function of v_o for changes of v_o as large as considered here, the allowable spread of velocities is asymmetric about the standard. This asymmetry can be utilized to increase the total velocity tolerance, if the standard v_o is centered in the total allowable velocity spread and v_{mM} on the standard orbit is not aimed at the center of the moon. This choice of a standard, of course, would place more stringent requirements on the control of other burnout variables. For instance, the total allowable variation in β_o would necessarily decrease since impact locations of trajectories with perturbed values of β_o do not exhibit the same asymmetry as the velocity perturbed trajectories do.

The results plotted in Figures 3A1-10 and 3A1-11 show the strong dependence of allowable errors on the initial velocity v_o. A comparison has been made with an exact computer study of this two-dimensional problem and the results of this study are presented also in Figures 3A1-10 and 3A1-11. We note that the discrepancy decreases with increasing velocity; in fact, the discrepancy in calculation of total allowable (δv_o) decreases from 10 ft/sec at minimum energy to ~ 0 ft/sec at $v_o = 36,000$ ft/sec, while the discrepancy in total allowable $(\delta\beta_o)$ decreases from 0.7 deg to ~ 0 deg over the same velocity range.

The effect of β_o on the allowable velocity error is weak for very low or very high values of v_o and is strongest for values in the region where the effects of change in v_o on θ and ωT approximately cancel. The allowable velocity error that is maximum for each value of β_o is found to be a decreasing function of β_o. For example the maximum allowable error of approximately 240 ft/sec for the 70 deg value β_o decreases to 210 ft/sec for β_o equals 80 deg and to 175 ft/sec for β_o equals 90 deg. The increase in allowable velocity errors obtained with smaller values of β_o is not obtained without paying a price, since the velocity v_o at which these maximum values occur increases rapidly as β_o is decreased.

The variations with respect to the burnout altitude have been ignored so far. Variations in h_o are roughly equivalent to variations in v_o, the equivalence being established through requirement of energy conservation of burnout.[*]

---

[*] For example: since $\partial v/\partial h_E = -(\mu_E/v_o r_o^2)$, for $v_o = 36,000$ ft/sec and $r_o = 2.2 \times 10^7$ ft, then $\partial v/\partial h_E = -8$ ft/sec 10^4 ft.

h_o = 200 miles
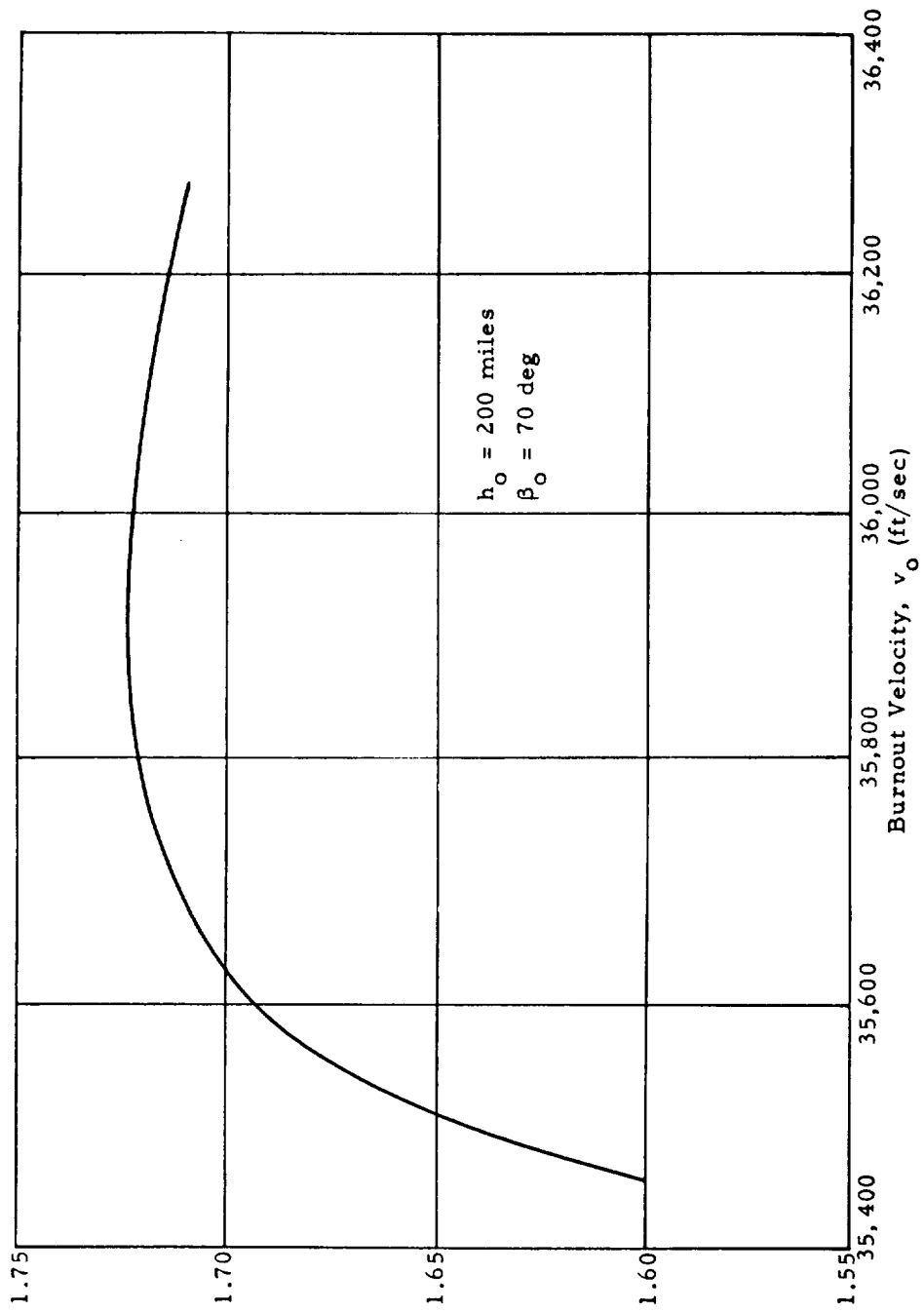β_o = 70 deg

Burnout Velocity, v_o (ft/sec)

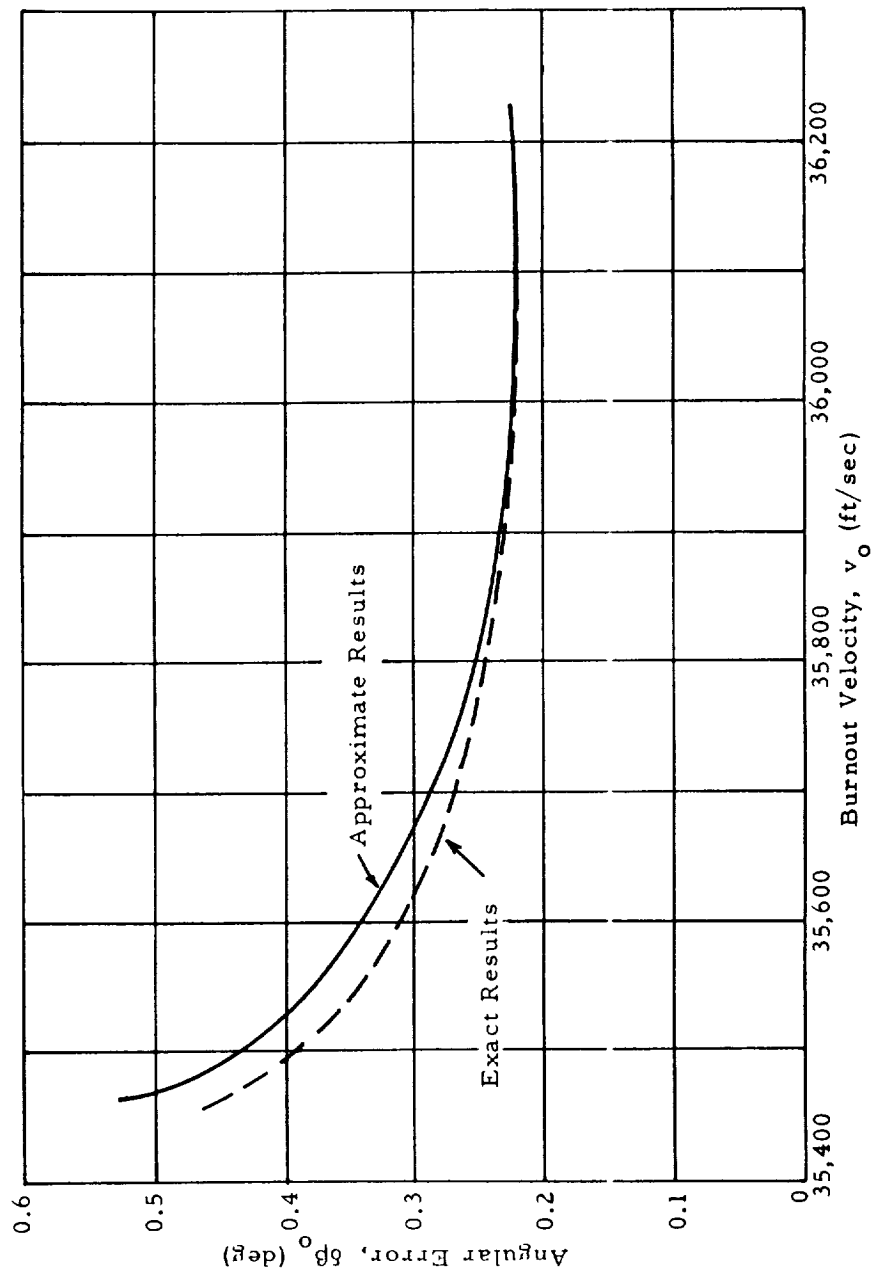Figure 3A1-9. Angular Difference as a Function of Burnout Velocity.

Figure 3A1-10. Allowable Angular Error for Impact, 200-Mile Altitude (β_o = 70 degrees).
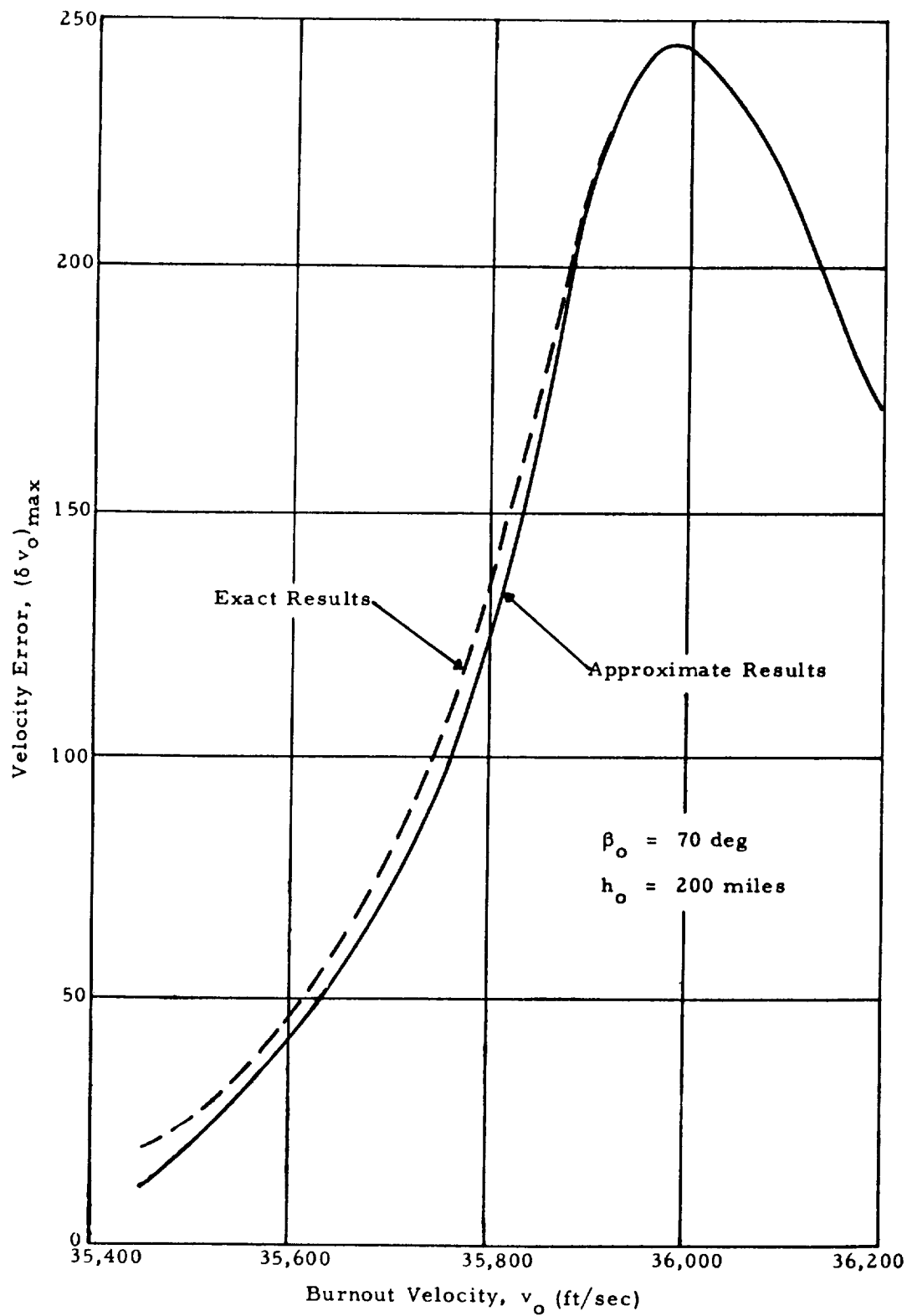
Figure 3A1-11. Allowable Velocity Error for Impact on the Moon.

SECTION II

When the vehicle flies in the moon plane, a two-dimensional flight, the same geometrical relationship between the burnout point and the moon's position recurs once a day. On the other hand, when the burnout point lies out of the moon's plane, the same geometrical relationship occurs only once every lunar month, and then only if we ignore, as we shall, such effects as the variation of inclination of the moon's plane with respect to the equatorial plane. This fact has two consequences: one is that a different set of burnout conditions must be chosen each day to hit the moon; the second is that the sensitivity of the guidance system to error changes each day. Thus, for a three-dimensional flight, one problem is to determine the optimum day of the month for firing, the second is to find the correct combination of burnout azimuth, velocity, and flight path angle.

The notation used in this section is shown in Figure 3A2-1, which is a schematic representation of the surfaces and angles centered at the earth. Before analyzing guidance sensitivity we must set up a procedure to determine a standard trajectory. The general procedure that we will use is to pick a set of burnout variables, v_o, β_o, h_o, that are consistent with booster capabilities, and, from these determine the in-plane angle, θ. The in-plane angle uniquely determines the required azimuth and time of day of firing for each day of the month. At the same time, the in-plane angle and a particular day of the month determine the angle between the moon's plane and the vehicle's plane, u, which is the single quantity necessary to determine the degradation of two-dimensional guidance tolerance to three-dimensional guidance tolerance. Therefore, we can calculate the variation in guidance sensitivity from day to day throughout the lunar month to aid in finding the optimum day for firing.

Referring again to Figure 3A2-1, the following relationships can be deduced for the required burnout azimuth, a_o and θ, as functions of λ_b, the burnout equatorial longitude referred to the lunar descending node, and λ_M, the moon's position in the moon's plane referred also to the lunar descending node:

North
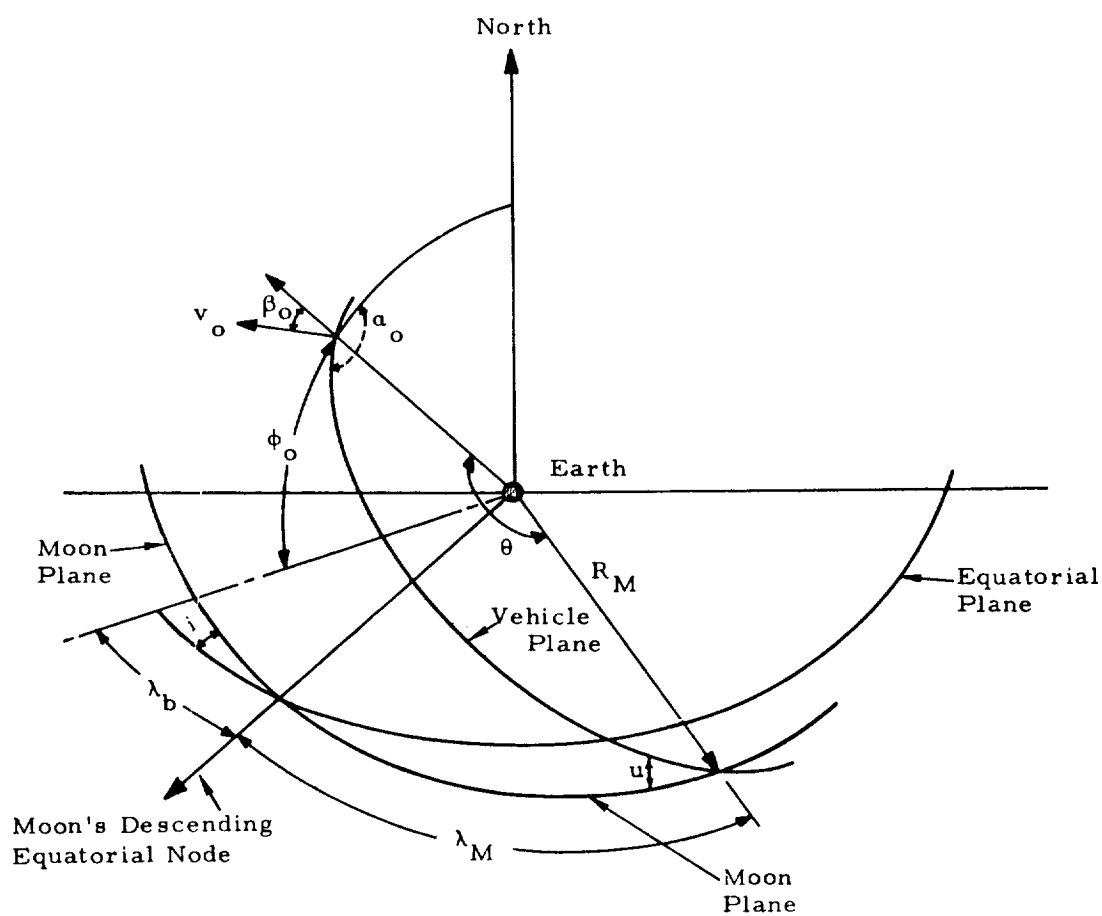
Figure 3A2-1. Geometry of Earth to Moon Trajectory.

α_o	Burnout Azimuth
v_o	Burnout Velocity
β_o	Burnout Flight Path Angle
ϕ_o	Latitude of Burnout Point
θ	In-plane Angle
R_M	Radius of Moon
i	Inclination of Moon Plane to Equatorial Plane
λ_M	Longitude of Moon from its Descending Equatorial Node
u	Angle Between Moon Plane and Vehicle Plane
λ_b	Longitude of Burnout Point from Moon's Descending Equatorial Node

$$\theta = \cos^{-1}\left\{\cos\left(\lambda_M - \gamma\right)\cos\left[\phi_o + \sin^{-1}\left(\sin\gamma\sin i\right)\right]\right.$$
$$\left. - \sin\left(\lambda_M - \gamma\right)\sin\left[\phi_o + \sin^{-1}\left(\sin\gamma\sin i\right)\right]\sqrt{1 - \frac{\sin^2\lambda_b}{\sin^2\lambda}}\right\}, \qquad (2.1)$$

$$a_o = \sin^{-1}\left[\frac{\sin\lambda_b\sin\left(\lambda_M - \gamma\right)}{\sin\theta}\right], \qquad (2.2)$$

where

$$\gamma = \tan^{-1}\left(\tan\lambda_b/\cos i\right) .$$

In Figure 3A2-2, we see θ plotted as a function of λ_b and λ_M for Latitude 30°N. The in-plane angle is essentially a linear function of λ_b and λ_M over the range of angles shown there. These angles were chosen since, as it will turn out, they cover the regions of practical design interest.

Combining Equations (2.1) and (2.2), we see that for a particular burnout latitude, ϕ_o, and for a particular inclination of the moon's plane, i, the burnout azimuth, a_o, is fixed once we fix λ_b and λ_M. Of course, λ_b varies through 360 deg every 24 hours and essentially determines the time of day of firing. On the other hand, λ_M varies only 12 deg to 13 deg per day and within an uncertainty of about 6 or 7 deg determines the day of the month. λ_b and λ_M are already physically related but the rapid variation of λ_b compared to λ_M makes it possible to ignore this relationship for the first approximation and treat the two as independent. Referring to Figure 3A2-3, we see a_o plotted for latitude $\phi_o = 30°N$ as a function of λ_b and λ_M over a range of angles that turn out to be of practical interest to a designer. Also plotted on Figure 3A2-3 are curves of a_o for a fixed θ, that is, for a given set of burnout conditions. These latter curves are obtained from Equation (2.2).

The first general goal of this section is thus achieved, namely the proper firing azimuth and time of day of firing for a given set of burnout quantities and on given days of the month. To make these results more concrete, we

Burnout Latitude, $\phi_o = 30°$N;   Burnout Longitude with Respect to Moon's
Descending Equatorial Node, λ_b (deg - equivalent to hours of the day)
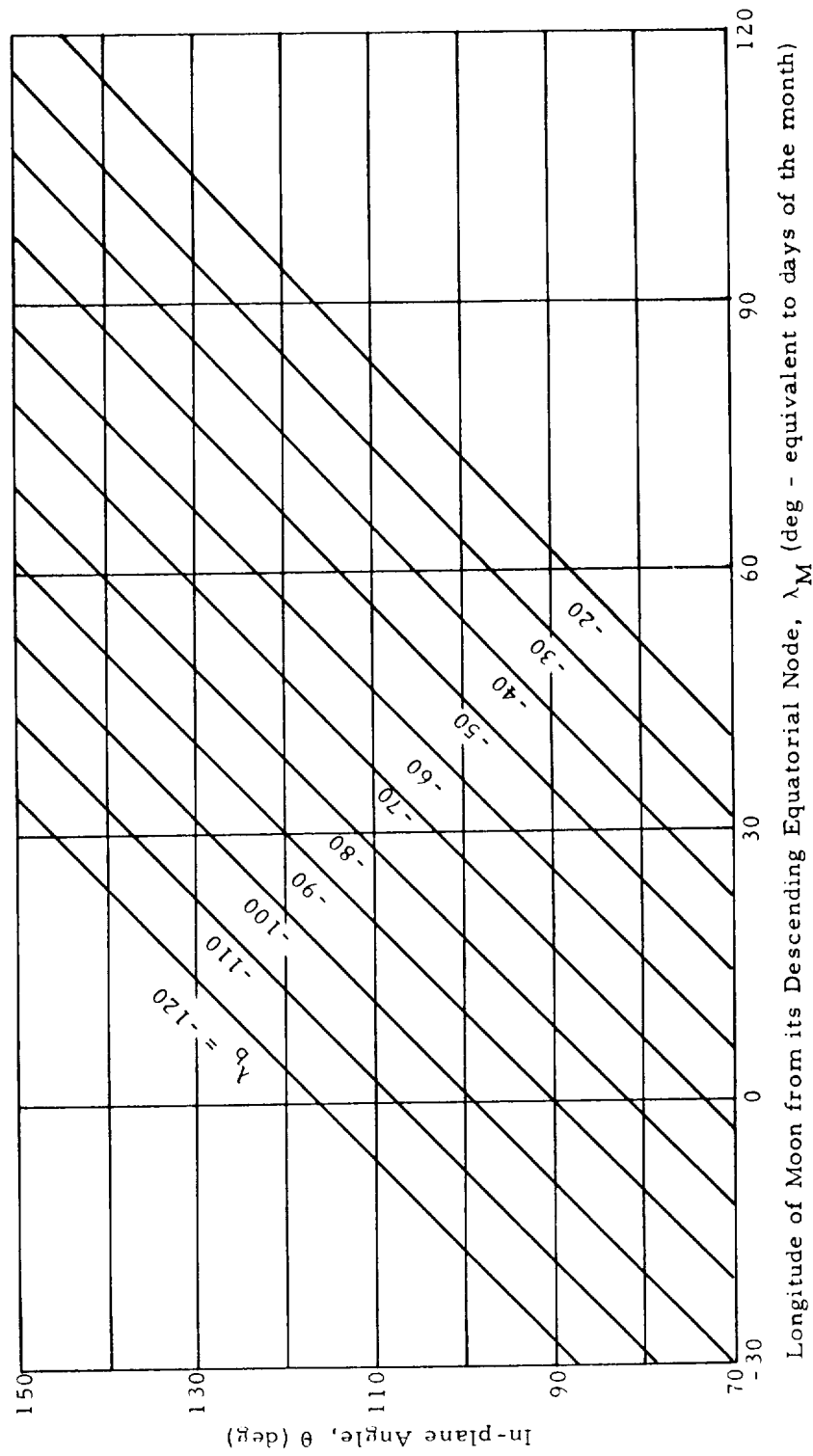

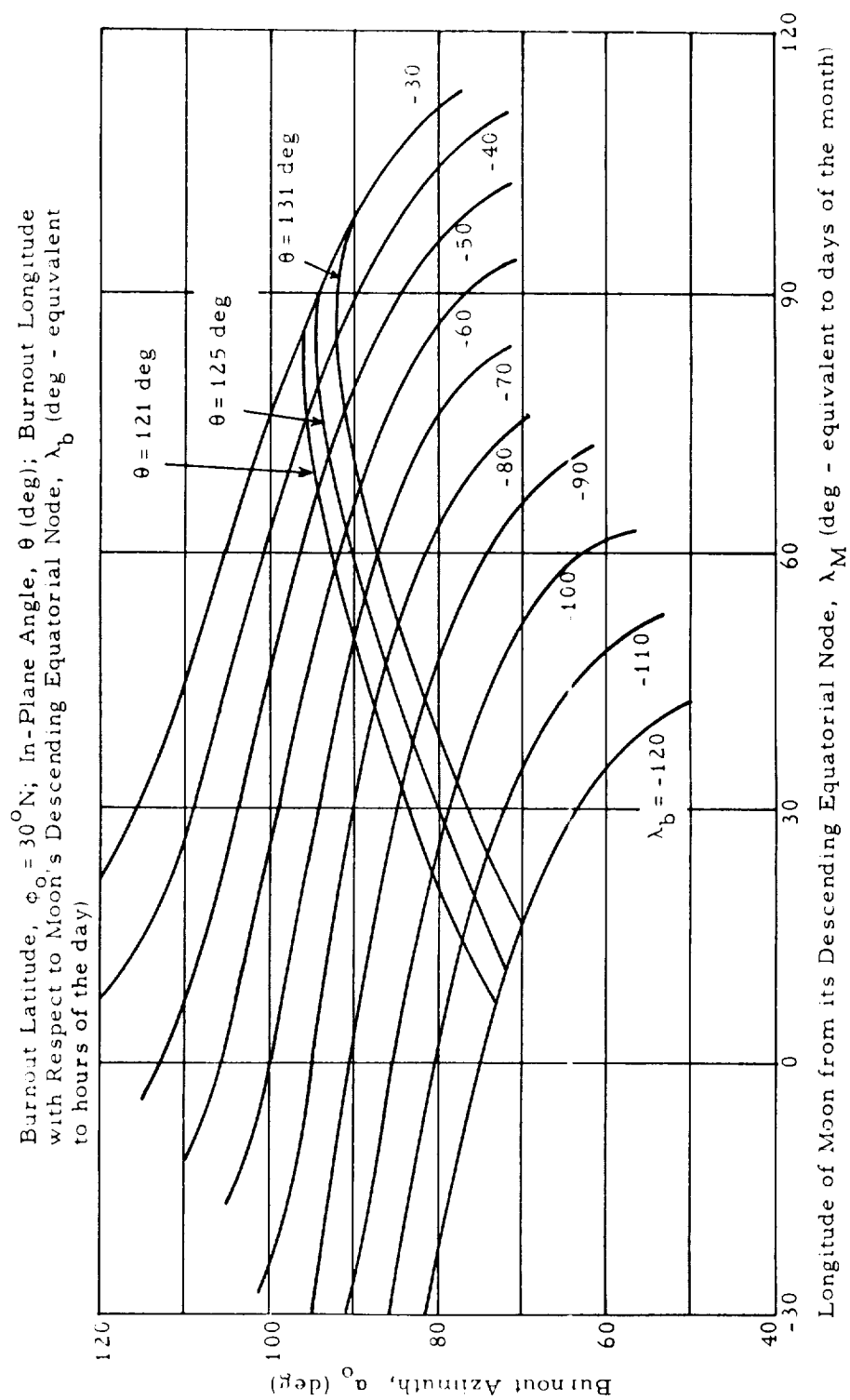Figure 3A2-2. Vehicle's Orbital In-plane Angle as a Function of Time of Day and
Day of the Month.

182

Figure 3A2-3. Burnout Azimuth as a Function of Time of Day and Day of Month.

have converted the in-plane angle, θ, into velocity, choosing β_o = 70 deg and h_o = 200 miles. The results of this substitution are in Figure 2-4 which shows the variation of burnout azimuth throughout the month for various velocities.

Several interesting results can be seen in Figure 3A-2-4. If the burnout velocity is less than v_o = 36,200 ft/sec, the vehicle cannot be fired into the vicinity of the moon during a certain period of the month. This time period is symmetrically located about λ_M = 270 deg, when firing from the Northern Hemisphere, that is, the position of the moon furthest north (see Figure 2-1). We notice that this restricted region becomes larger as the burnout velocity is reduced (β_o and ϕ_o remaining fixed) because the in-plane angle increases and it becomes more difficult to fit in the angular sector defined by θ. Of course, if the burnout angle, β_o, can be varied,[*] the angular sector can be changed and other launch times become available. But for any given β_o, the general symmetry holds. At burnout velocities just above minimum energy, about 2 weeks of the lunar month are excluded as possible firing days.

For any velocity, the orbit with the maximum allowable azimuth occurs when the moon at impact is furthest south, that is, when λ_M = 90 deg. Since orbits with burnout azimuths near 90 deg take maximum advantage of the earth's rotation, the class of orbits with burnout velocities less than $\sim$36,100 ft/sec which impact when the moon is halfway between descending and ascending nodes makes most efficient use of the booster capabilities.

On the other hand, there are several reasons why this may not be the optimum orbit. First, the location of various downrange equipment may dictate that the vehicle flies in a certain band of azimuths. Figure 3A2-4 shows that for velocities less than 36,100 ft/sec, orbits with southerly azimuths are impossible, while for velocities above 36,200 ft/sec, northerly azimuths are impossible. In addition, as we shall show later, the orbit making optimum use of booster capabilities is not necessarily the orbit making best use of guidance capabilities.

---

[*] Since a β_o of 70 deg is about optimum, any change will result in a payload penalty.

184
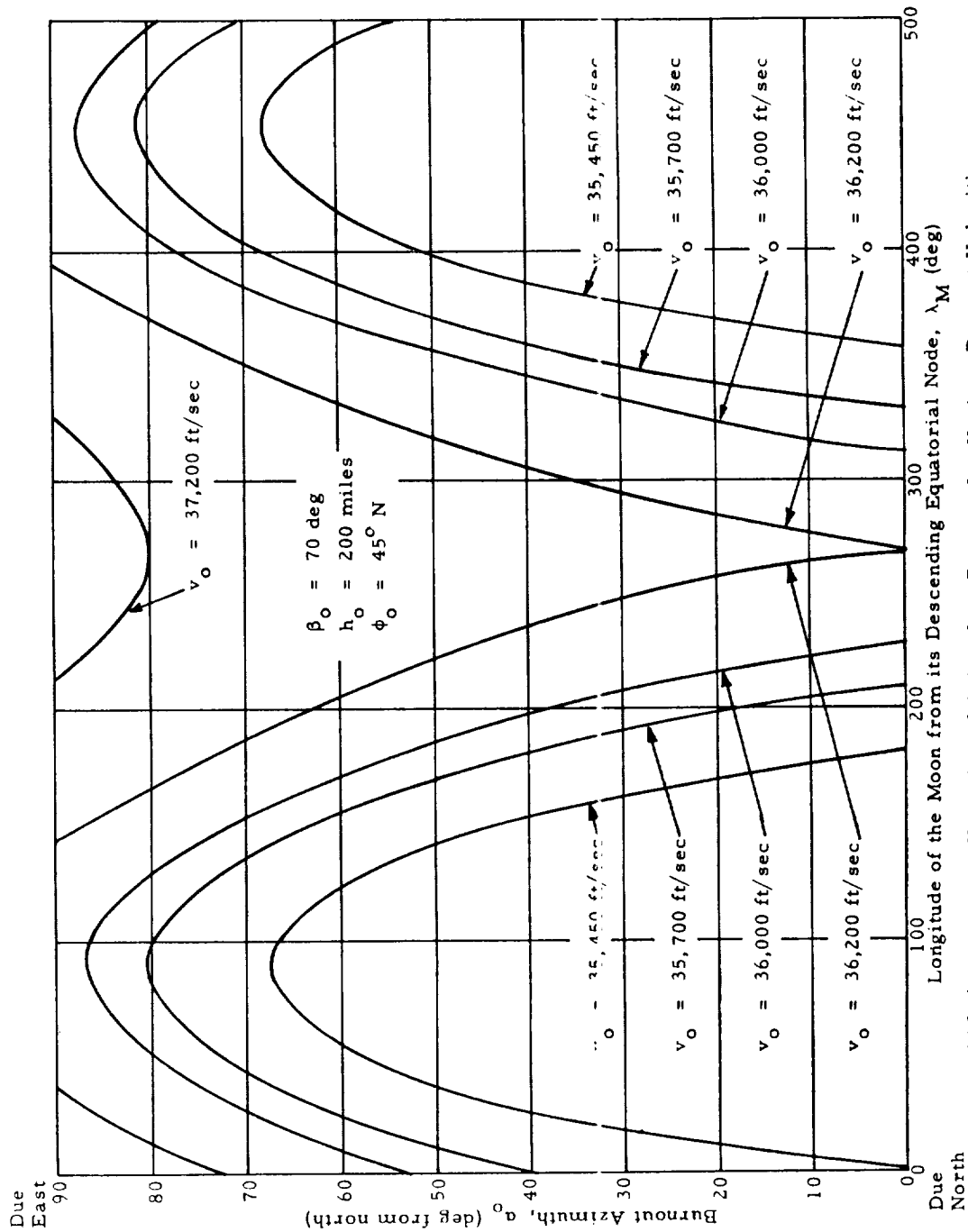

Figure 3A2-4. Necessary Variation of Azimuth at Burnout for Various Burnout Velocities and Time of Month (less than 0° azimuth, no launch possible).
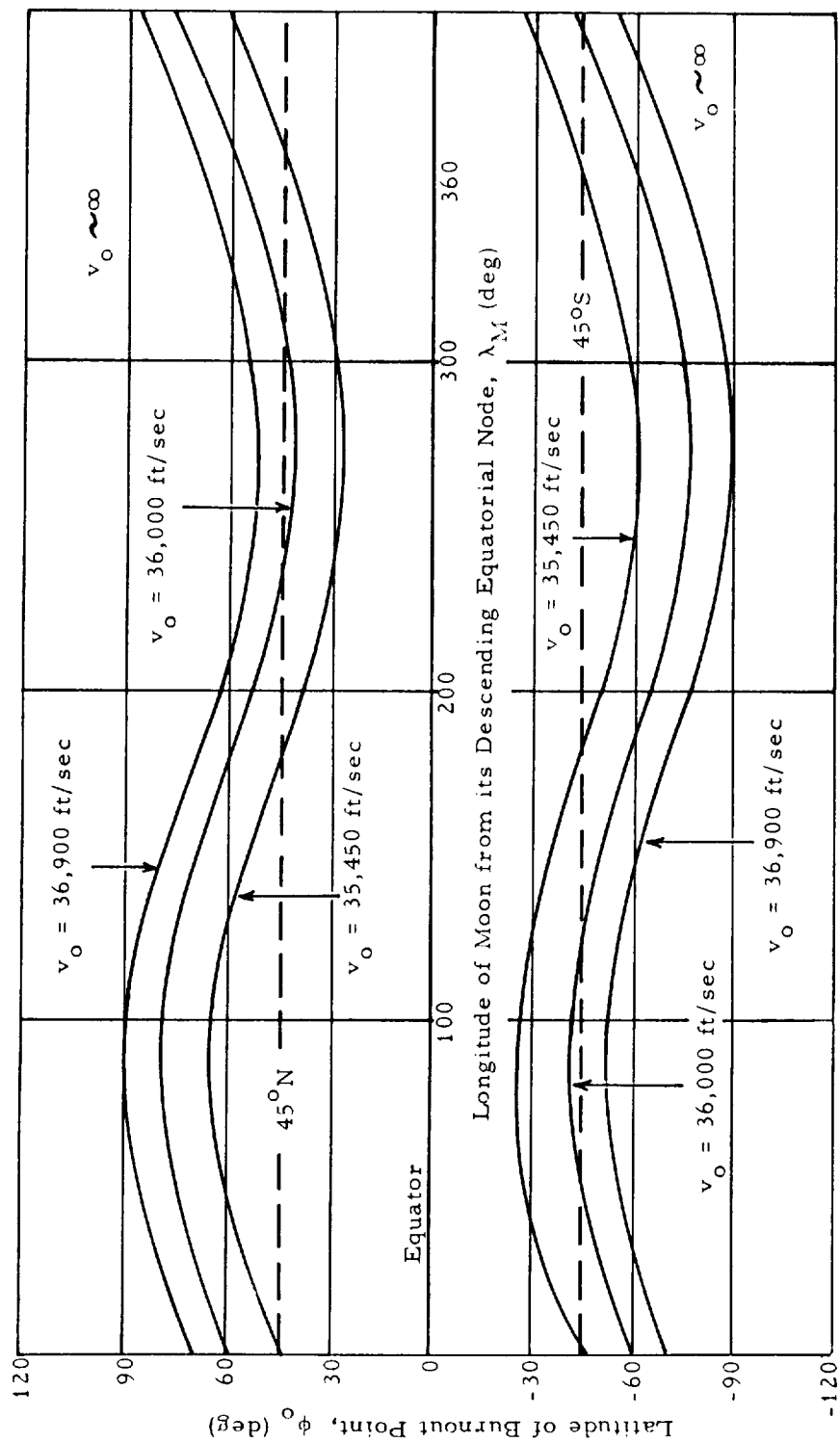
Figure 3A2-5. Maximum Allowable Latitudes of Burnout for Various Times of the Lunar Month.

Athough Figure 3A1-4 refers to 45°N the results for 45°S can be attained by translating the curves 180 deg along the λ_M axis and reading the azimuths as angles from south. To illustrate this north-south symmetry further and show the variation of excluded regions as burnout latitude is varied, we note the following result: on a given day of the month, and for a given set of two-dimensional burnout conditions, the furthest north (south) a burnout point may be situated is for that orbit oriented due north (south). This result may be shown by finding implicitly, in Equation (2.2), the maximum ϕ_o for a fixed θ and λ_M and variable λ_b.

Using the condition that $a_o = 0$, Equation (2.2) gives for this maximum latitude

$$\phi_{o_{max}} = \pi - \theta + \sin^{-1} (\sin \lambda_M \sin i) . \tag{2.3}$$

Values of $\phi_{o_{max}}$ from Equation (2.3) are shown in Figure 3A2-5. There we see that the restriction in days of the month vanishes for any velocity if burnout occurs at a latitude within about 30°N and 30°S On the other hand, if burnout is at the North Pole, the minimum allowable velocity is 36,900 ft/sec and firing can occur only on one day of the month.

Two additional facts must be considered before practical use may be made of Figures 3A2-4 and 3A2-5. First, it is more useful to correlate the appropriate burnout azimuth and the maximum allowable burnout latitude with the launch day, not impact day. To do this, the moon's angular rotation during the time of flight is subtracted from λ_M and one obtains an angular position of the moon that can be immediately converted to a particular launch day. The other fact that must be considered is the latitude change of the vehicle during powered flight, which itself may extend 10 to 20 deg. Curves of burnout azimuth for fixed burnout latitudes thus refer to launch points with variable latitudes. Since the latitude adjustment for powered flight is largest for azimuths closest to due north, those orbits with velocities below 36,200 ft/sec will have large adjustments in the neighborhood of the excluded regions. Since, parabus ceterus, the correction for powered flight reduces the required azimuth, the excluded period will enlarge.

Another general criterion useful for optimizing an orbit is to reduce its sensitivity to burnout perturbations. With this criterion in mind we turn to a consideration of the angle between the vehicle plane and moon plane, u.

The strong maximum in two-dimensional velocity tolerance (see Figure 3A1-11) occurs because as the burnout velocity increases above minimum energy, the sensitivity of in-plane angle, θ, to velocity increments decreases until near 36,000 ft/sec and equals the sensitivity of time of flight to velocity increments. Since the two angular position errors, that of the vehicle and the moon, are in opposite directions, the orbit becomes insensitive to velocity perturbations. However, if the orbit is inclined to the lunar plane, the two angular deviations no longer lie in the same plane and no first order cancellation can occur. Thus, the larger the inclination between the two planes, the more the velocity tolerance is reduced. On the other hand, the time of flight is insensitive to errors in β_0 (see Figure 3A1-3), so that only the vehicle's angular position error, $\Delta\theta$, is important in this case, and the miss as a result of errors in β_0 should be roughly independent of the angle between the planes.

Referring to the geometrical relations in Figure 3A2-1, we can write at once a relation between u, λ_M, and λ_b as follows:

$$\sin u = \frac{\sin \lambda_b \sin \left[\phi_0 + \sin^{-1}(\sin \gamma \sin i)\right]}{\sin \gamma \sin \theta (\lambda_b, \lambda_M)} , \qquad (2.4)$$

in which θ may be treated as a function λ_b and λ_M through Equation (2.1). The results of Equation (2.4) have been plotted in Figure 3A2-6 for burnout latitude 30°N. If θ is given a fixed value, then a relationship exists between λ_b and λ_M and we arrive at the curves of u for constant θ, also shown in Figure 3A2-6.

The curves in Figure 3A2-6 for fixed θ demonstrate a useful result that for any given set of two-dimensional burnout conditions, the minimum in u occurs on a day of the month such that the burnout longitude from the northern hemisphere is -90 deg with respect to the lunar equatorial descending node. For the southern hemisphere the minimum u of course, occurs when $\lambda_b = +90$ deg. These results may also be obtained from Equation (2.4) by
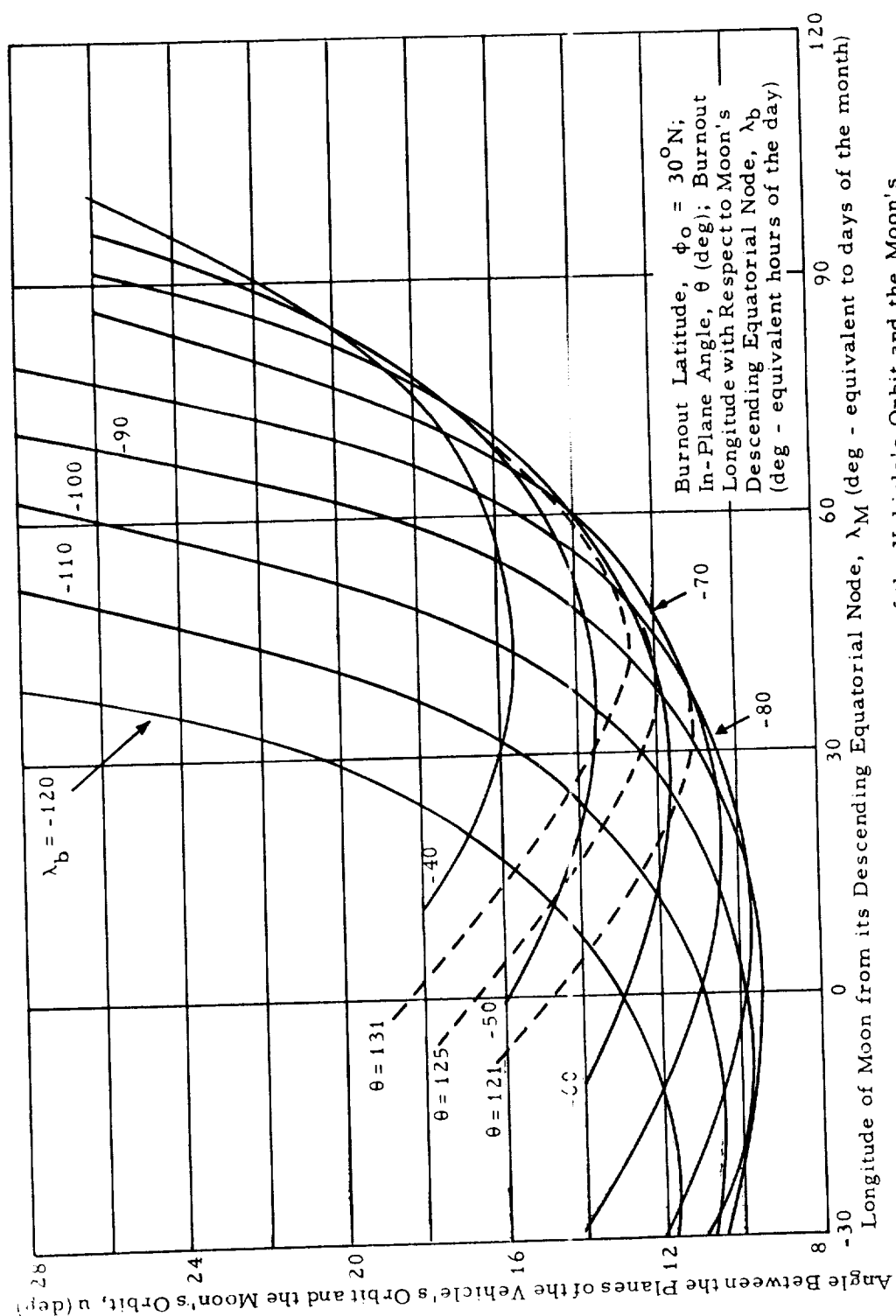
188

Figure 3A2-6. Inclination Between the Planes of the Vehicle's Orbit and the Moon's Orbit as a Function of Time of Day and Day of the Month.

varying u with respect to λ_M and λ_b and holding θ fixed. The required relationship between the variation of λ_M and λ_b when θ is fixed can be obtained through Equation (2.1). Substituting λ_b = -90 deg in Equation (2.4), we obtain minimum u for various θ,

$$\sin u_{min} = \frac{\sin (\phi_0 - i)}{\sin \theta} \quad \text{Northern Hemisphere}$$

$$\sin u_{min} = \frac{-\sin (\phi_0 + i)}{\sin \theta} \quad \text{Southern Hemisphere}$$

(2.5)

The results of Equation (2.5) are plotted in Figure 3A2-7. As in Figure 3A2-5, we see the appearance of maximum allowable burnout latitudes when velocities are sufficiently low. In fact, from Figure 3A2-1 it follows that when the minimum inclination between the planes is $\pi/2$ for a given in-plane angle, then the orbital azimuth is due north in the Northern Hemisphere or due south in the Southern Hemisphere. Therefore, when the minimum inclination is $\pi/2$, the orbit is starting from the maximum allowable latitude for that velocity. Figure 3A2-7 indicates that the minimum u is zero for $|\phi_0| \leq \pm i$ since once a month the burnout point lies in the lunar plane, so that Figure 3A2-7 is complete as indicated.

The angle between the planes, u, is important for determining the change in guidance sensitivity. Guidance sensitivities in the more general case considered here may be found in a manner analogous to that used in Section 1. That is, we calculate the orbit to the moon in two parts: the first controlled only by the earth's field, and the second controlled only by the moon's field. The results of the first calculation at $r = R_M$ are taken as the asymptotic conditions for the selenocentric hyperbola.

First, then, we determine the position of the vehicle relative to the moon at the time its distance from the earth is equal to the moon's orbital distance. Suppose deviations in burnout variables have caused in-plane angle deviations, $\Delta \theta$, and time of flight deviations, ΔT. Then Figure 3A2-8a gives the exact geometrical relationship for this situation. However, we ignore the small curvature of the moon's orbit over the arc, ωT, and the angular separation
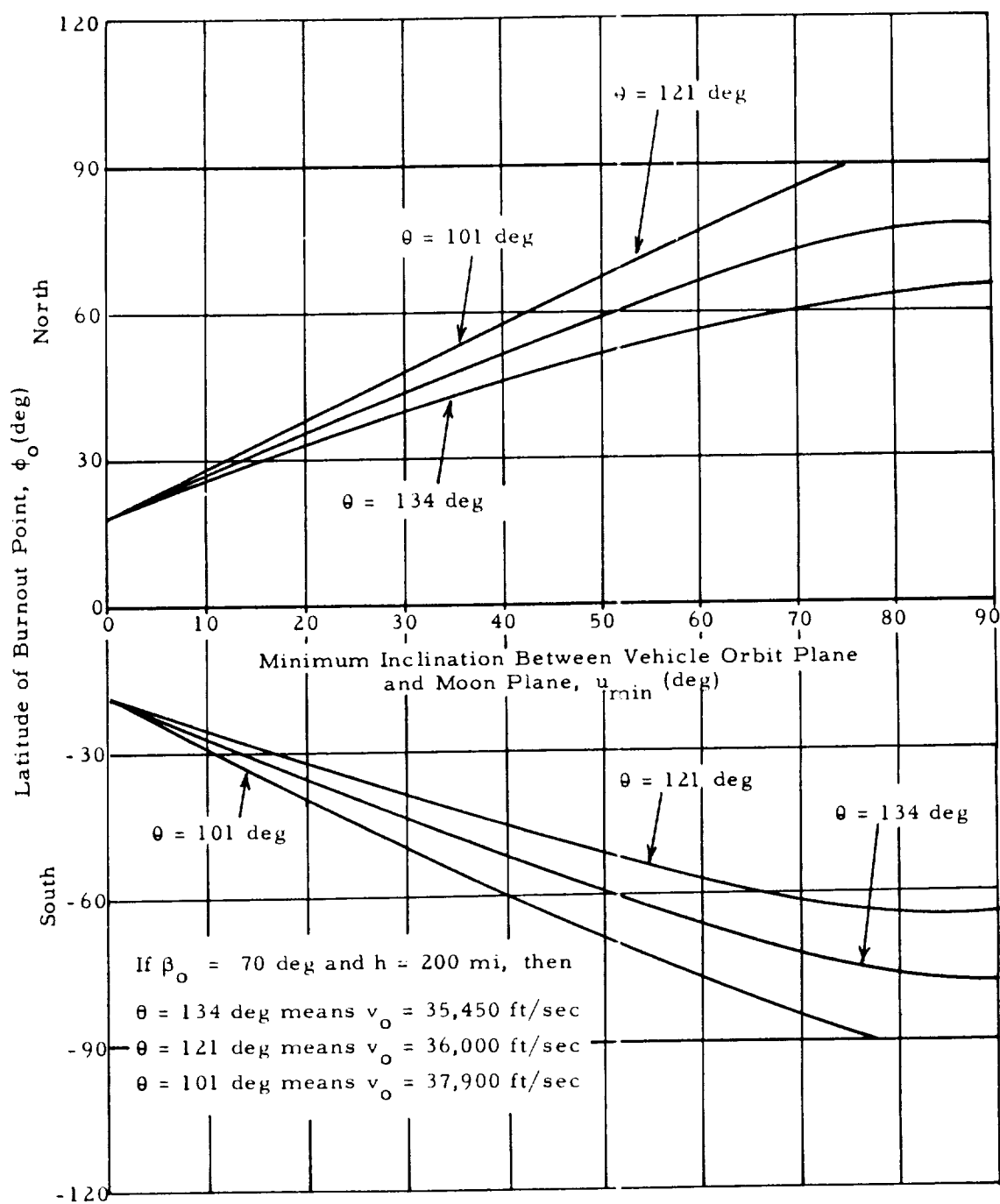
Figure 3A2-7. Minimum Inclination for Various Burnout Latitudes and In-plane Angles.
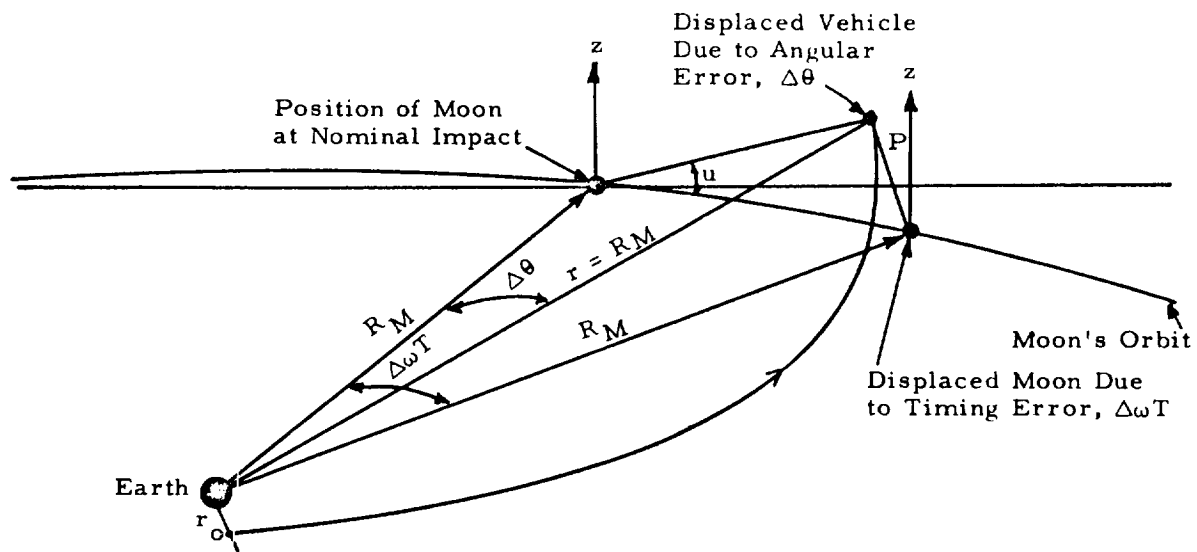
Figure 2-8a.   Geometry of Earth-Moon-Vehicle System for a Nonstandard Orbit.
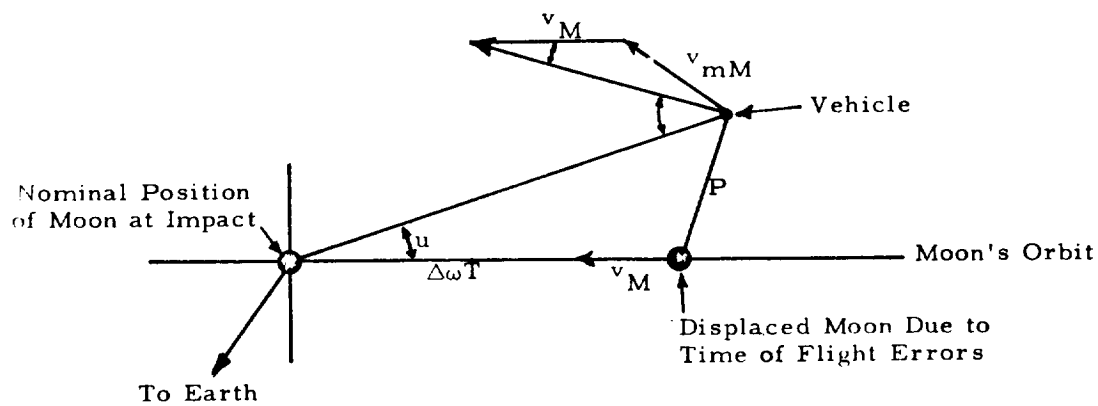

Figure 3A2-8b.   Details of Geometry in the Vicinity of the Moon.

of the vehicle from the z-axis when $r = R_M$. Referring to Figure 3A2-6b which shows our approximation in detail, we see that P, the distance from the vehicle to the moon at the time $r = R_M$, is given by

$$P = R_M \left[(\Delta\theta - \Delta\omega T)^2 + 4\Delta\theta \, \Delta\omega T \, \sin^2 \frac{u}{2} \right]^{1/2} \tag{2.6}$$

The first term in Equation (2.6), $R_M (\Delta\theta - \Delta\omega T)$, is the two-dimensional orbital miss, that is, the distance measured along the moon's orbit between the vehicle at crossing and the moon. As in the two-dimensional case, the next step is to determine an impact parameter, b, and then from it, calculate a distance of closest approach assuming conservation of energy and momentum in the moon's frame of reference. Letting v_{mM} be the vehicle's velocity relative to the moon, we can reduce the problem to that of determining the angle, η, (see sketch) since the impact parameter

$$b = P \sin \eta.$$
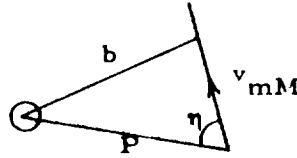
By considering the geometric relations in Figure 3A2-6b we arrive at the following expression for η

$$\cos \eta = \left[1 - \left(\frac{R_m \, \Delta\theta \, \sin u}{P} \right)^2 \right]^{1/2} \left[1 - \left(\frac{v_I}{v_{mM}} \sin \xi \right)^2 \right]^{1/2}$$

$$+ \frac{R_m \, \Delta\theta}{P} \frac{v_I}{v_{mM}} \sin^2 u \cos \sigma , \tag{2.7}$$

where ξ is the angle between the vehicle's inertial velocity, v_I, and the moon's velocity, v_M, and σ is the angle between P and v_I. For most velocities of practical interest, it turns out that η is close to 90 deg and that P itself may be used as the impact parameter.

For example, if the vehicle burns out at 30°N Latitude and -90 deg Longitude from the moon's descending equatorial node and with v_o = 36,000 ft/sec, β_o = 70 deg and h_o = 200 miles, we find the following results as the vehicle enters the moon's field of influence. The vehicle is moving almost radially from the earth and ξ = 85 deg. Its inertial velocity is almost perpendicular to the moon's velocity and σ = 84.5 deg. Taking into account the other factors in Equation (2.7), we find that η = 86 deg. In other words, the vehicle's velocity relative to the moon is almost perpendicular to the distance between the vehicle and the displaced moon, and, therefore, this distance can be used directly as the impact parameter. For lower burnout velocities the vehicle's orbit is less inclined to the moon's orbit and η decreases and P becomes larger than the impact parameter. The guidance tolerance for impact calculated using P as impact parameter is therefore a lower bound on the more exact calculation which takes η into account and computes a smaller impact parameter. This is not critical since, as we shall see, with decreasing velocity the lower bound approaches the upper bound, that is, the two-dimensional velocity tolerance shown in Figure 3A1-11.

In order to compare the two-dimensional and three-dimensional velocity guidance tolerances, we select a burnout latitude of 30 deg and a time of day and month such that for each velocity considered, the orbit has the minimum inclination with the lunar plane, u_{min}. Then for each velocity we use the machinery set up in Section 1 for the two-dimensional case to compute the maximum allowable impact parameter, and the angular sensitivities, $\Delta\theta = (\partial\theta/\partial v)\,\Delta v$, $\Delta\omega T = \omega(\partial T/\partial v)\Delta v$. This is sufficient, together with the value of u_{min}, to compute the maximum allowable velocity error, which is shown in Figure 3A2-9. Near the guidance minimum point, the term $(\Delta\theta - \Delta\omega T)$ vanishes so that

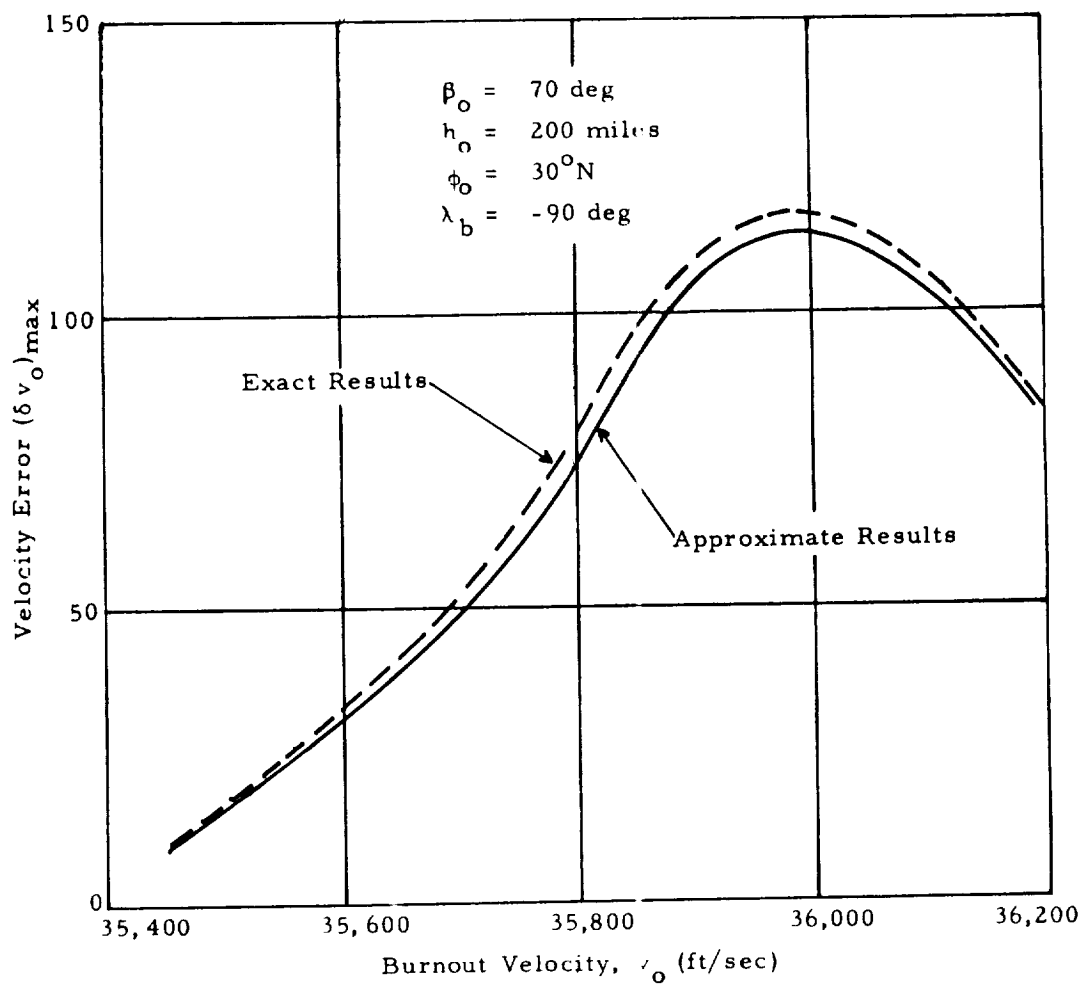$$P \cong 2\,R_M\,\Delta\theta\,\sin\frac{\eta}{2} \qquad\qquad (2.8)$$

Figure 3A2-9. Maximum Allowable Velocity Error for Impact on the Moon (burnout time chosen to minimize angle between vehicle plane and moon plane).

and, therefore, the peak of the velocity tolerance curve is most sensitive to inclinations of the orbit plane. As the velocity is lowered, the first term in Equation (2.6) becomes more significant and thus the three-dimensional tolerance approaches the two-dimensional.

Also, in Figure 3A2-9 the results of exact computer calculations for the same burnout conditions are shown. It is evident from the 10 per cent discrepancy between the two curves that the analytic model is quite adequate for design purposes.

Since in Section 1 it was shown that the time of flight is insensitive to β_0 (see Figure 3A1-4), the three-dimensional impact parameter calculated from Equation (2.6) should reduce, in this case, to the two-dimensional. Figure 3A2-10 shows a comparison of exact machine calculations at 30°N Latitude and minimum inclination, and indeed the exact curve is within 10 per cent of the two-dimensional exact curve. The discrepancy with the analytic curve of Figure 3A2-10 at low velocities reflects both the inability of the crude underlying model to account for all the curvature in the orbit due to the moon's field and the nonzero sensitivity of time of flight to changes in β_0.

Considering the velocity sensitivity, again it is apparent from Equation (2.4) that, for a given θ, increasing the latitude of the burnout point increases u and so reduces the total velocity tolerance for impact to result. Furthermore, the inclination of the two planes is also increased if the burnout point is not halfway between the ascending and descending lunar nodes. Both of these effects are demonstrated in Figure 3A2-11 which gives the variation of velocity tolerance throughout the month for several burnout velocities.

It can be noted from Figure 3A2-11 that the velocity tolerance for the orbit with burnout velocity closest to guidance optimum, 36,000 ft/sec, has the largest percentage decrease throughout the month while the lowest velocity is least affected. We also note that the three-dimensional velocity tolerance for lunar impact does not possess the symmetries with regard to λ_M already noted for burnout azimuth. The cause of this is that u, itself, takes one lunar month to complete a cycle. On the other hand, similar curves will apply to 45°S if the λ_M-axis is translated 180 deg.
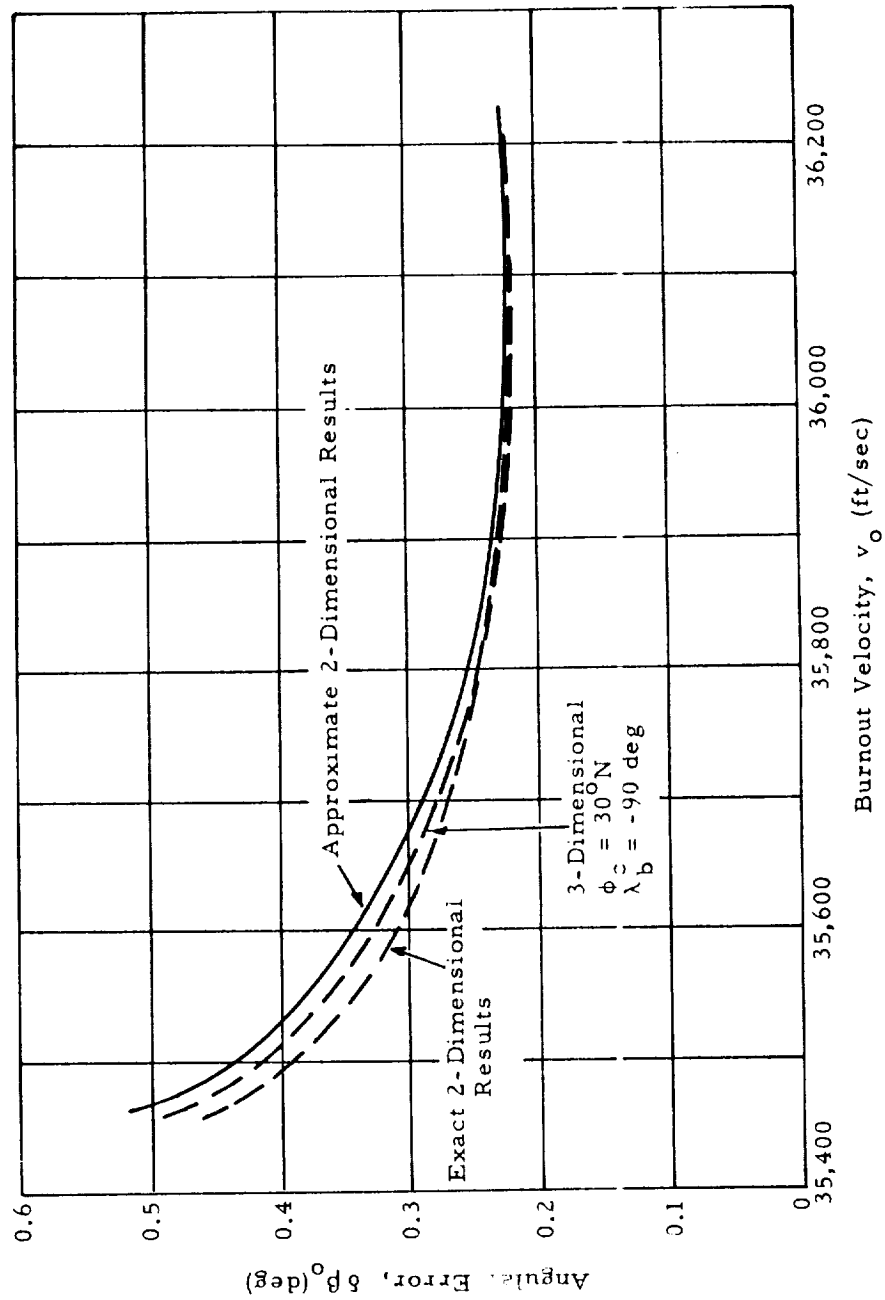
Figure 3A2-10. Maximum Allowable Angular Error for Impact on the Moon (burnout time chosen to minimize angle between vehicle plane and moon plane).
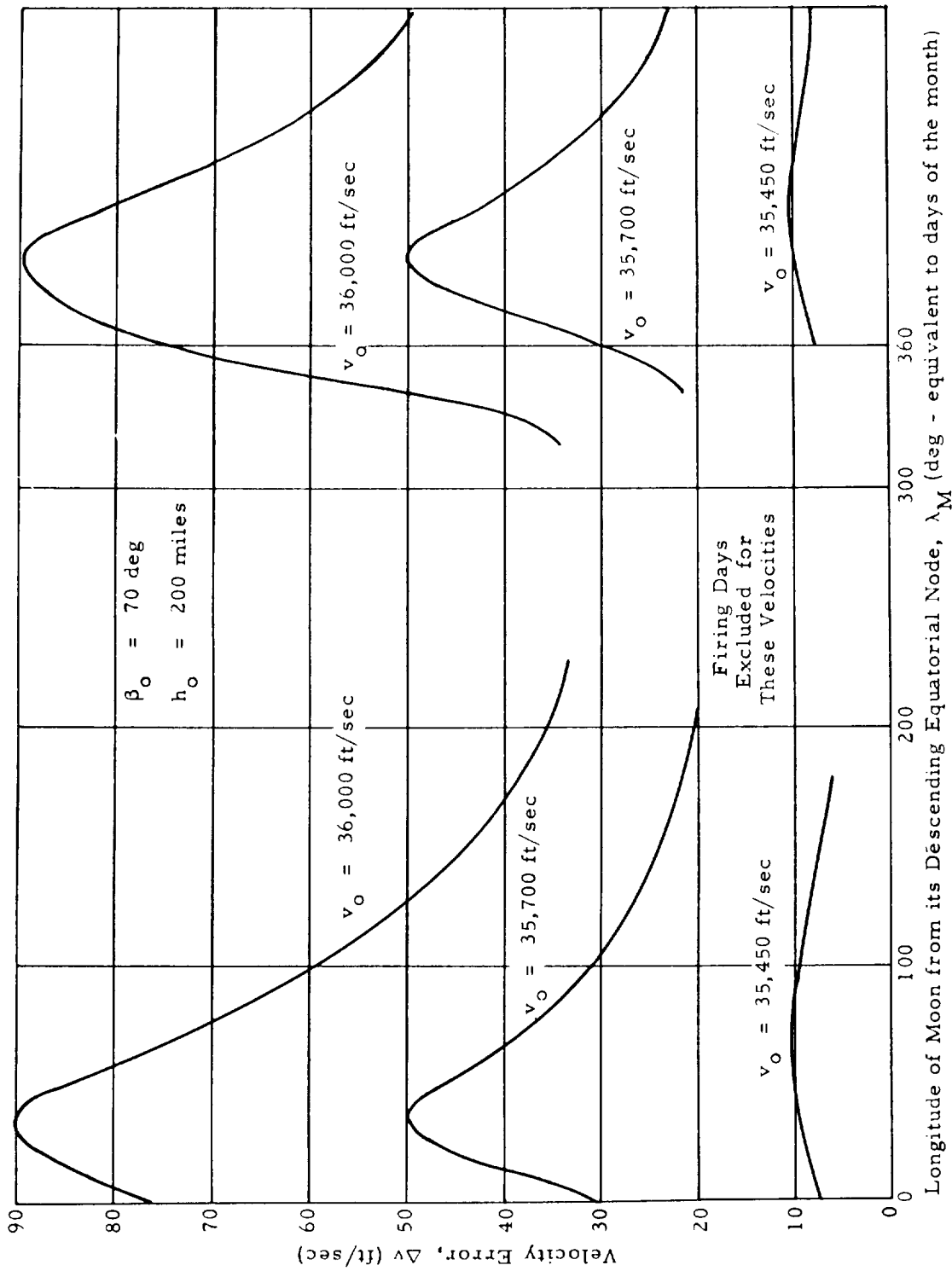
Figure 3A2-11. Total Allowable Velocity Error for Impact on the Moon (burnout latitude, 45° N).

We are now in a position to estimate what values a designer would be most likely to choose for burnout variables. If sufficient propulsion capability exists and velocity control is a problem, the total probability of a successful impact may be maximized by choosing a burnout velocity of 36,000 ft/sec (see Figure 3A2-11), the day of impact with λ_M = 34 deg and time of day with λ_b = -90 deg. From Figure 3A2-4 we see that burnout azimuth for this velocity and time of launch is about 74 deg. Of course, if β_0 other than 70 deg or h_0 = 200 miles were chosen, the numbers would change somewhat but the reasoning would be the same.

If, however, the designer wished to maximize the payload for a given booster configuration or if the guidance system had more difficulty controlling burnout flight path angle, β_0, than v_0, then he would choose a burnout velocity of $\sim$35,450 ft/sec with impact day when λ_M = 90 deg, burnout when λ_b > -90 deg, and a burnout azimuth of $\sim$68 deg. The velocity tolerance would be only slightly less than maximum for this velocity but be a factor of 10 below the tolerance for v_0 = 36,000 ft/sec.

SECTION III

The previous sections demonstrated that a relatively simple analytic model is capable of accurate prediction of guidance sensitivities for orbits designed to impact on the moon. In this section we show that the same ideas can be applied to guidance problems arising when the orbit is designed to satellite the moon instead. The allowable velocity and burnout angle tolerances for a successful satellite are not the same as those for impact on the moon and are functions of additional design factors as well.

Before discussing the guidance sensitivities, we note some of the well-known results concerning the restricted three-body problem that are useful as a background for this discussion. The earth-moon-vehicle system of differential equations has a first integral of motion, the Jacobi integral. In a system of rectangular coordinates rotating with the earth and moon with origin at the barycenter of the system, z-axis along the axis of rotation, and x-axis towards the moon, the Jacobi integral can be written as

$$J = v^2 - \omega^2 (x^2 + y^2) - 2(U_E + U_M) \quad , \tag{3.1}$$

where v is the vehicle's velocity in the rotating frame of reference, ω is the angular rate of rotation of the moon, and U_E, U_M are the earth's and moon's gravitational potentials at the vehicle's position. For a given value of J the vehicle is restricted to a region of space defined by Equation (3.1) and the condition that $|v| \geq 0$. The particular Jacobi surface of interest to us is the largest one which is still closed about the moon since this provides a sufficient condition for a stable satellite around the moon. Setting $J = J_o$ for this surface, then if the vehicle is inside the surface with $J = J_o$, it will remain inside the surface indefinitely. We are ignoring, of course, the small effect of the sun on the vehicle's motion.

In Figure 3A3-1 we see the projection of this surface on the x, y-planes. The projection on the x, z-plane is almost identical. This surface was computed for mean moon parameters, $R_M = 1.26 \times 10^9$ ft, $\omega = 2.66 \times 10^{-6}$ rad/sec, and $M_M/M_E = 1/81.345$. Superimposed on this surface are
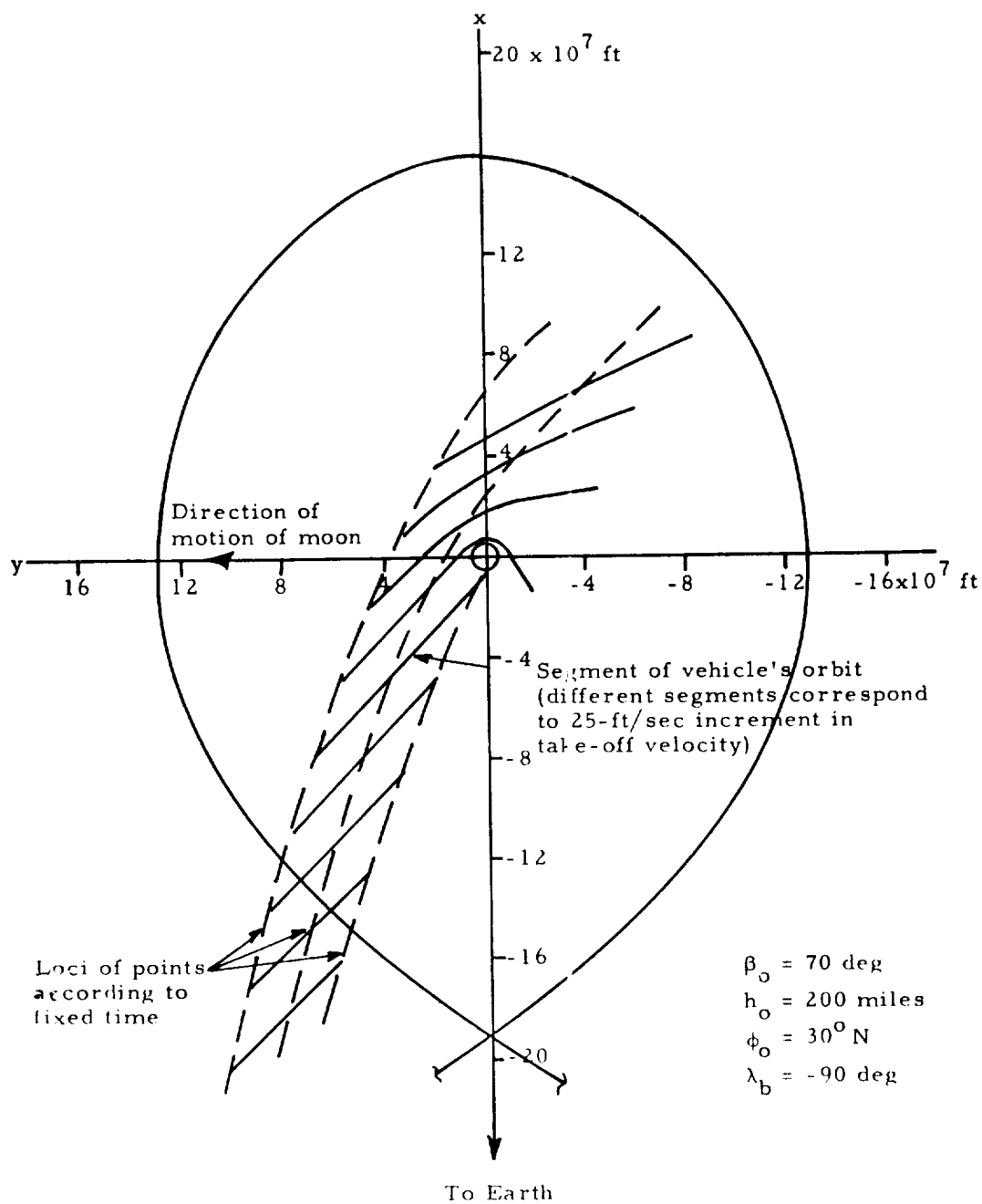
Figure 3A3-1. Variation of Orbits Inside the Critical Jacobi Region
as a Result of Burnout Velocity Increments.

projections of terminal portions of orbits with burnout conditions similar to those of Section 2, namely β_o = 70 deg, h = 200 miles, and various burnout velocities. These orbits burn out at 30^oN latitude and at a time of month such that λ_o = -90 deg (i. e., conditions for minimum angle between orbit plane and vehicle plane).

The point of interest about these orbits is that the locus of points corresponding to a given time on an orbit lie roughly along a straight line, and are almost linearly distributed along this locus according to the variation in burnout velocity. From Figure 3-1 we see that the locus is inclined to the earth-moon line by about 30 deg in the moon plane and turns out to be inclined by about 12 deg in the plane perpendicular to the moon plane. The linear displacement along the locus is about 1.2×10^6 ft$/$ft$/$sec in burnout velocity change.

If we desire only that the vehicle ultimately be in a stable orbit about the moon, then locating the position of the standard orbit is relatively simple. As has been pointed out elsewhere, we must provide an additional velocity increment after entering the surface defined by J_o to convert the vehicle's selenocentric hyperbola into an elliptical orbit. Ignoring for the moment the moon's influence on the locus described above, the standard trajectory should be such that the maximum segment of the locus is included in the Jacobi surface at the time of adding the velocity increment. This assumes the velocity increment is added in the simplest possible way, that is, according to a predetermined time.

With this criteria for the standard orbit the velocity and angular tolerances at burnout are easily calculated. For the conditions presented in Figure 3-1, the maximum line segment is about 3×10^8 ft and therefore the velocity tolerance is ± 125 ft/sec. The standard burnout azimuth and flight path angle are easily calculated using the methods of Sections 1 and 2. The allowable tolerances on these quantities are obtained by observing that the locus can be shifted approximately 5×10^7 ft laterally and 5×10^7 vertically before there is a significant reduction in length contained in the surface, J_o. Converting the lineal displacements into an angular displacement, $\Delta \theta$, we use the methods of Sections 1 and 2 to relate $\partial \theta / \partial \beta$ to the maximum allowable $\Delta \theta$.

The $\partial\theta/\partial\beta$ to be used here is that obtained without considering the moon's influence. The result for the set of burnout conditions in Figure 3A3-1 is $\delta\beta_0 = \pm1.2$ deg.

The consequence of requiring that the vehicle satellite, instead of impacting, is twofold: first, the burnout velocity tolerance for a successful flight at burnout velocities just above minimum energy is increased until it is comparable to the maximum tolerance for impact (see Figure 3A2-9), which occurs at 36,000 ft/sec; second, the burnout angular tolerance is held comparable to the tolerance for impacting the moon at minimum energy (see Figure 3A2-10). As a consequence, the two optimum guidance sensit vities for impact have been achieved at a single velocity which is itself, nearly the least possible to reach the vicinity of the moon.

The angle between the planes, u, will play a role here as well as for impact orbits since tilting the vehicle plane relative to the lunar plane has the effect of also tilting the locus with respect to the x-axis. Therefore, there will be a day-to-day variation in velocity guidance tolerance of the type found for impact orbits (see Figure 3A2-11).

This is, of course, a grossly simplified picture of the guidance problems. The orbit locus is significantly distorted in the neighborhood of the moon (see Figure 3A3-1) so that the velocities corresponding to orbits passing near the moon require special treatment. Another problem arises since some of the orbits, after the addition of the necessary velocity increment, will intersect the moon's surface instead of satelliting. On the other hand, if criteria of indefinite capture is relaxed, the tolerances can be enlarged. Figures 3A3-2a and 3A3-2b and Figures 3A3-3a and 3A3-3b give examples of orbits with $J > J_0$ which make many circuits of the moon before eventually drifting back toward the earth. The analytic treatment of the behavior of such orbits is difficult and perhaps best conducted on a digital computer.
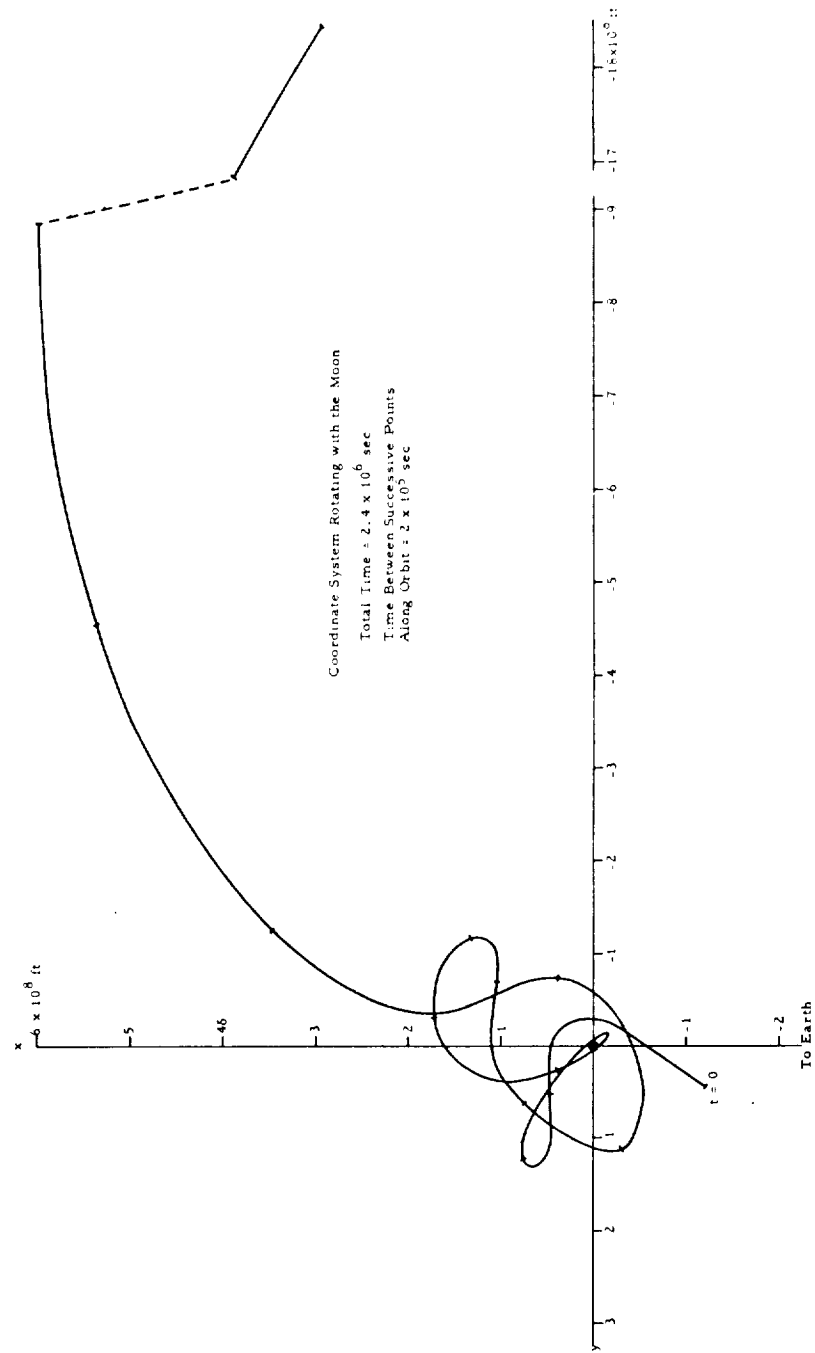
Figure 3A-2a. Plot of an Unstable Orbit About the Moon.

204
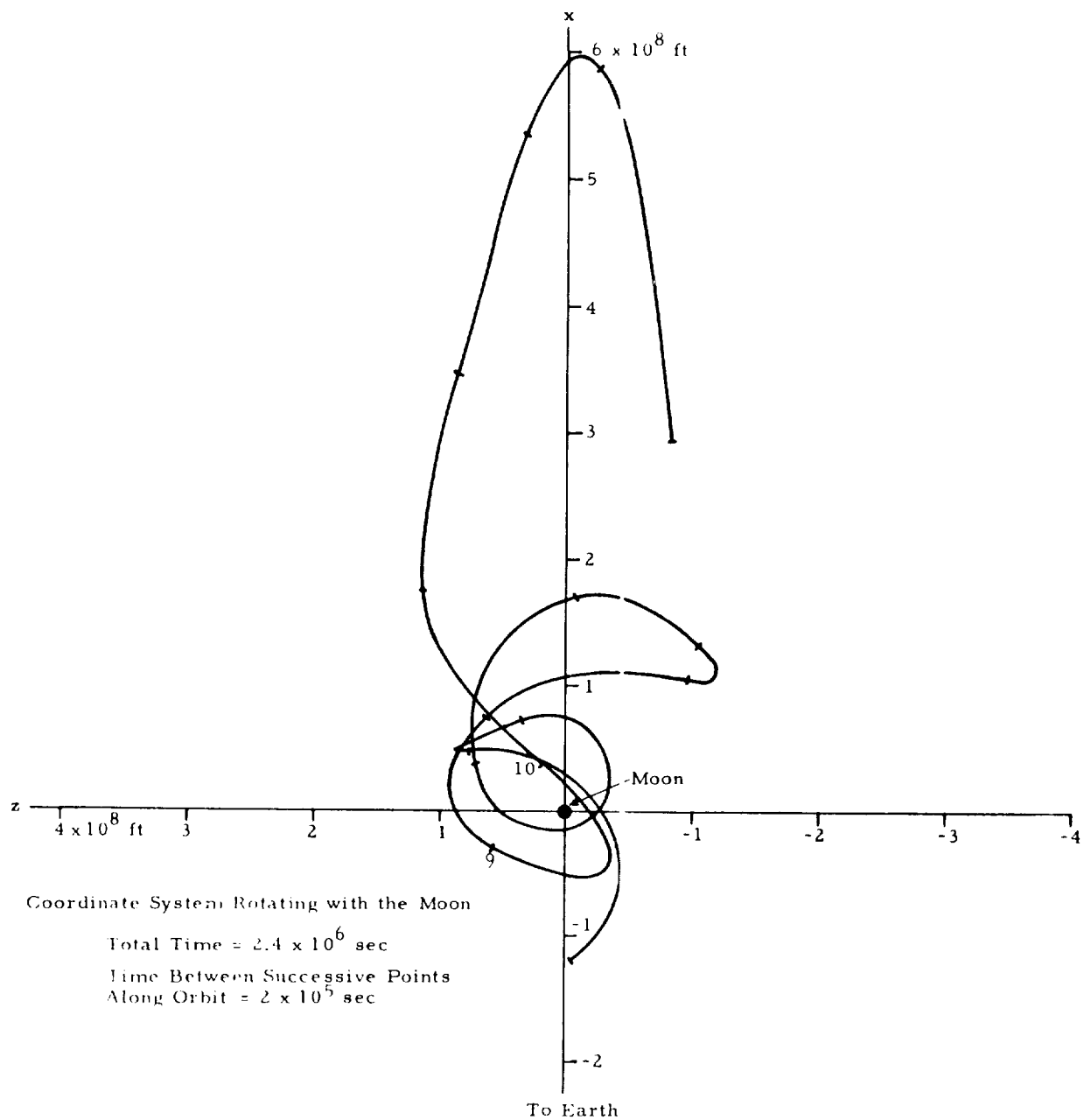
Figure 3A-2b. Plot of an Unstable Orbit Projected Perpendicular to the Moon Plane (z-axis along moon's axis of rotation). (Same orbit as Figure 3A-2a.)

x

−16 x 10⁸ ft

−12

−8

−4

Moon

16   12   8   4   t = 0   −4   −8   −12   −16x10⁸ ft

−4

−8

Moon's
Rotational
Axis   −12
Earth

−16

Rotating Coordinate System

Total Time Elapsed 3.0 x 10⁶ sec

Δt = 2 x 10⁵ sec Between Points

−20

−24

−28

−32
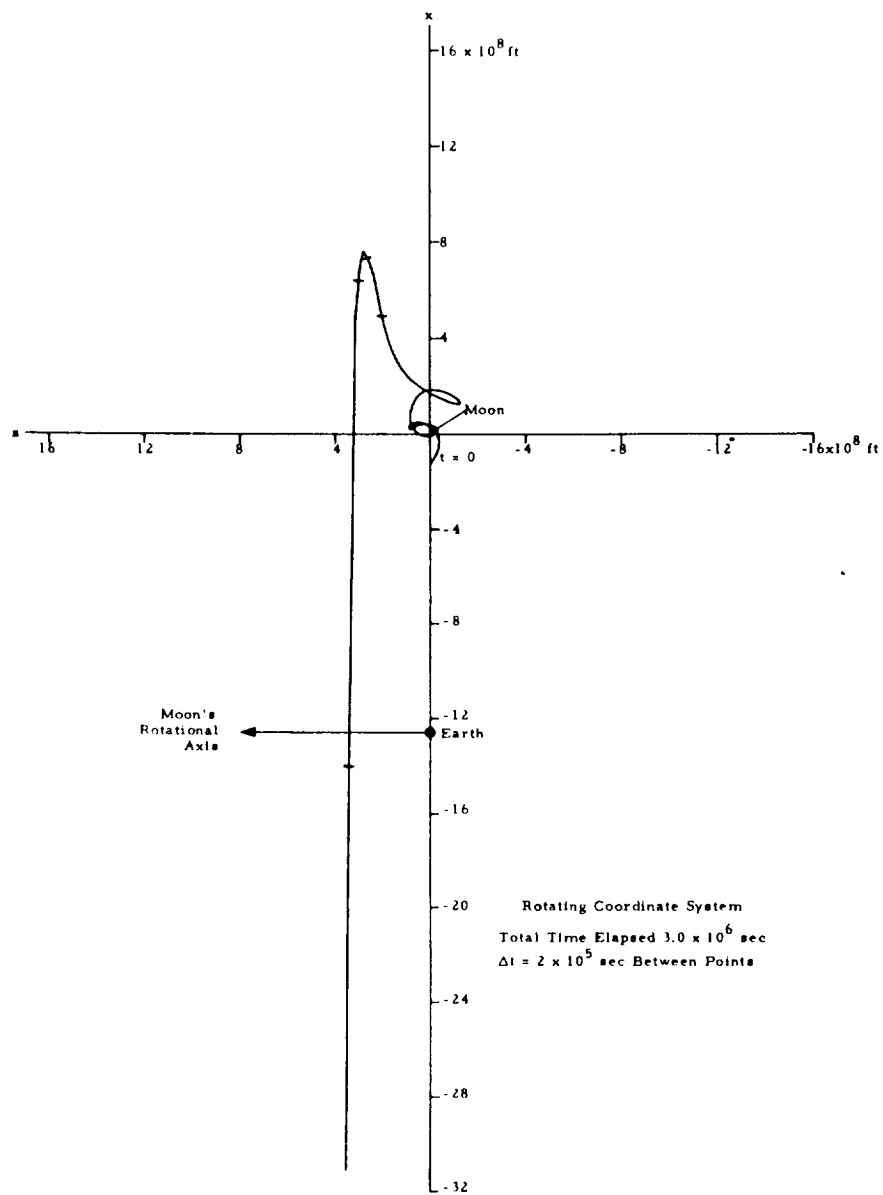
Figure 3A-3a.   Plot of an Unstable Lunar Orbit (projection of
vehicle orbit in plane perpendicular to moon's
orbit).
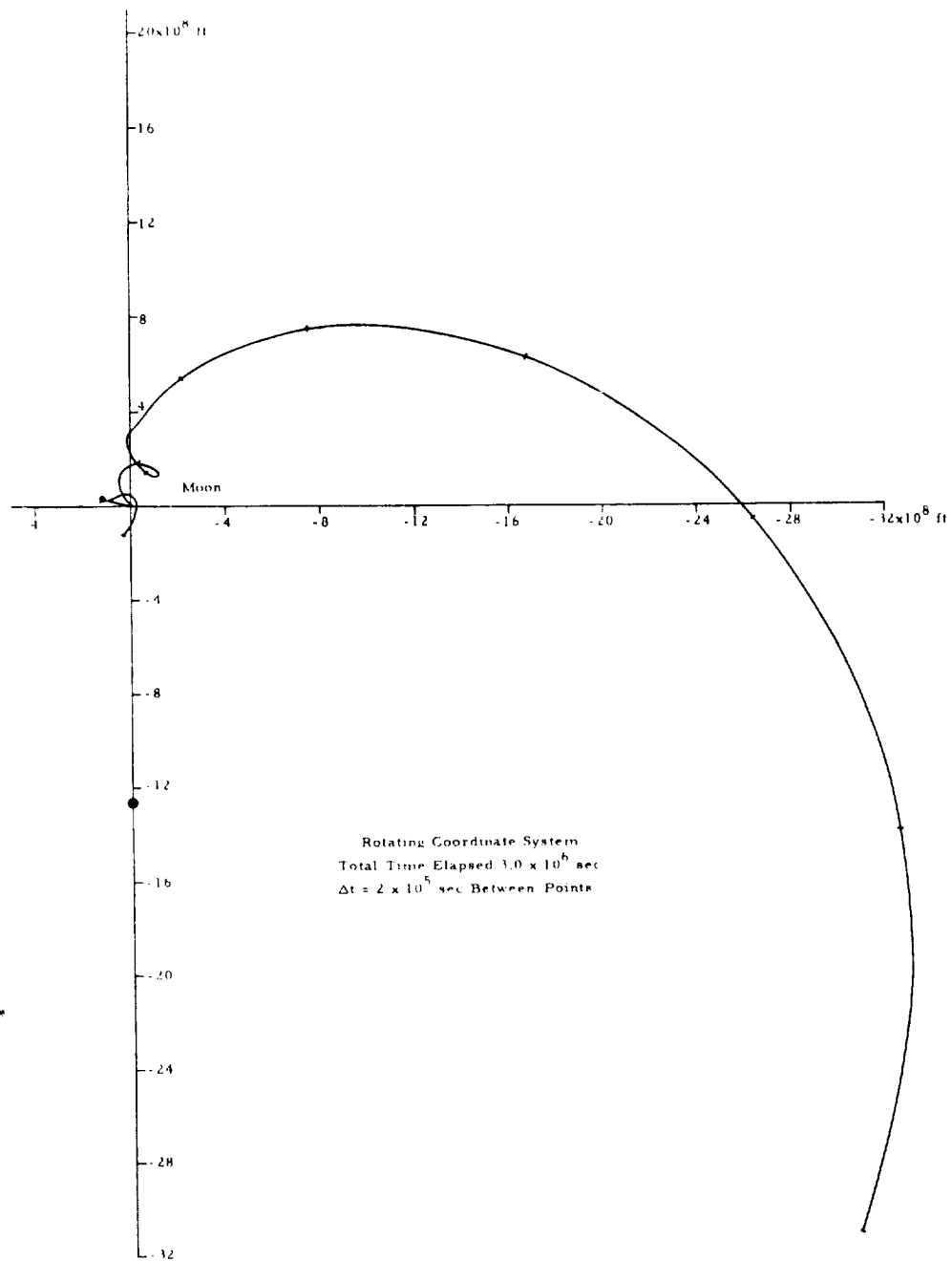
Figure 3A-3b.   Projection of an Unstable Lunar Orbit into
                Moon's Orbital Plare.   (Same orbit as
                Figure 3A-3a.)

SECTION IV

EVALUATION OF TIME AND ANGLE INTEGRALS

The time to go from a radius, r_o, to a radius, r_1, can be obtained explicitly by integration of Equation (1-4) as

$$t = F(r_1) - F(r_o)$$

where the analytical form of F depends upon the sign of the energy, E. If E is negative (vehicle velocity less than escape velocity),

$$F(r) = \frac{1}{2E} \left[\sqrt{2Er^2 + 2\mu_E r - J^2} + \frac{\mu_E}{\sqrt{-2E}} \sin^{-1}\left(\frac{\mu_E + 2Er}{\sqrt{\mu_E^2 + 2EJ^2}} \right) \right].$$

If E is zero (vehicle velocity equal to escape velocity),

$$F(r) = \frac{J^2 + \mu_E r}{3\mu_E^2} \sqrt{-J^2 + 2\mu_E r}$$

If E is positive (vehicle velocity greater than escape velocity),

$$F(r) = \frac{1}{2E} \left[\sqrt{2Er^2 + 2\mu_E r - J^2} \right.$$

$$\left. - \frac{\mu_E}{\sqrt{2E}} \ln\left(\mu_E + 2Er + \sqrt{2E}\sqrt{2Er^2 + 2\mu_E r - J^2} \right) \right]$$

The angular change is obtained by integration of Equation (1-5) as

$$\theta = G(r_1) - G(r_0) \quad ,$$

where

$$G(r) = \sin^{-1}\left(-\frac{\mu_E r - J^2}{r\sqrt{\mu_E^2 + 2EJ^2}}\right)$$

APPENDIX B

OPTICAL MEASUREMENT OF THE LUNAR PROBE (SECTION 42)

A.   Criteria for the Feasibility of Obtaining a Telescope Photograph

Four criteria must be met to assure the feasibility of photographing a space vehicle with a large astronomical telescope. These are summarized in the following paragraphs.

1.   The object must be bright enough to be above the threshold photographic visibility of the telescope. Under ideal conditions, the 48-inch Schmidt telescope has a limiting photographic magnitude of 21.0, which corres- ponds to the apparent brightness of a star one million times fainter than the faintest star visible to the unaided eye. The exposure time required to reach this limit on a fast blue-sensitive emulsion is about ten minutes. The sky must be quite dark (no twilight or moonlight) to allow the full 10-minute exposure. The 200-inch telescope can photograph objects nearly ten times fainter, but only with about three times the exposure time required for the 48-inch telescope. Accurate position data and tracking are far more critical.

2.   The object must have a slow enough angular rate of motion to permit its tracking with the telescope. Inasmuch as the object will probably be two faint to see visually with a guiding telescope, it is also required that fairly accurate angular velocities for the object be known, so that it can be tracked by the telescope automatically. The Palomar telescopes (48 inch and 200 inch) can be driven at rates slightly different from that of the diurnal motion of the sky so that these telescopes can follow planets, asteroids, or the moon. The maximum automatic rate (with respect to the sky) is only a few minutes of arc per hour except in the easterly direction where an hourly rate of a little over a half degree is possible in order to track the moon. The 200-inch telescope can be set at an automatic nonsidereal rate in either right ascension (east-west) or declination (north south), but the 48 inch telescope is equipped only with a right-ascension nonsidereal rate. However, the 48-inch telescope is so equip- ped that it is possible to guide the telescope to sufficient accuracy manually at

any rate up to about 10 minutes of arc per hour. It is seen, therefore, that the design of these astronomical telescopes is such that it is not possible to track objects unless they are very far from the earth, and consequently have slow angular motions relative to the stars. Artificial satellites, in particular, with maximum altitudes of only a few thousand miles, do not meet this criterion. These remarks, of course, refer to the tracking of an object so that over a time exposure its image is stationary on the photographic emulsion. It might be possible to record the track of an object who se image streaks across the emulsion (e. g., a meteor), but it must be brighter than the limiting magnitude of the telescope by an amount roughly equal to the ratio of the limiting exposure time to the time the image remains on an emulsion grain. As shall be shown in the next Section, the brightness of a space-probe vehicle is usually so low that accurate tracking is necessary.

3. Most astronomical telescopes have relatively small fields of view. Even astrographic and Schmidt telescopes designed for survey work generally have small fields compared to ballistic cameras, meteor cameras, and satellite-tracking cameras. Fairly accurate positions are therefore required if the object is to be photographed with an astronomical telescope. To be within the usable fields of the 60- or 100-inch telescopes (on Mount Wilson) or 200-inch telescope (on Palomar Mountain) a position would have to be accurate to 22, 13, or 8 minutes of arc, respectively. However, if the only positions available are from radio data, they probably can not be relied upon to be accurate to move than 1 degree, and possibly only to within 2 or 3 degrees. Thus, of the large telescopes in the Southern California area, only the 48-inch Schmidt, with a 6. 6- by 6. 6-degree field would be of use.

4. A final, and most vital, criterion that must be met is that the object must be at least 2 or 3 degrees (in some compass directions, even higher) above the horizon long enough to record its image photographically, unless the object has a brightness substantially above the photographic density of about 0. 7, for normal development. Furthermore, the exposure must be made in a dark sky, in the absence of twilight and moonlight. At elevation angles of 20 degrees or less, atmospheric extinction begins to seriously limit the effectiveness of the exposure; at 5-degree elevation the extinction may

reduce the limiting magnitude of the telescope by two magnitudes or more (a magnitude is a factor of 2.5 in light intensity), and the brighter sky near the horizon will necessitate a shorter exposure time, further reducing the photographic limit.

In summary, unless the object is at least four or five magnitudes brighter than the telescope limit, it is doubtful if it will be recorded unless it is at least 10 degrees above the horizon and the sun is at least 18 degrees below the horizon (the criterion for astronomical twilight) for a long enough period to obtain a limiting photographic exposure.

B.   The Criteria Applied to Able-1

1.   Criterion 1

The apparent brightness of an object illuminated by sunlight depends upon its distance, size, albedo, shape, angular distance from the sun in the sky, and orientation. The expected magnitudes of the third stage of Able-1, diffusely reflecting sunlight, at those times when it would have been at least 25 degrees away from the sun in the sky, usually ranged from 17 to 18 for a distance of 100,000 miles (two-thirds day after launch) and from 15 to 16 for a distance of 40,000 miles (one-fourth day after launch). The range in expected magnitude results from (1) the range of possible angular distances from the sun, (2) the range of possible orientations (these factors varied from one launch date to the next as well as with the flight time), and (3) an uncertainty in the albedo. The corresponding expected magnitudes for the fourth-stage payload usually ranged from 20 to 24 for 100,000 miles and from 18 to 22 for 40,000 miles. The range in expected magnitude for the payload is greater than for the third stage since the peculiar shape and coloring of the object makes its brightness very sensitive to its orientation. If the surface of the missile is smooth enough to produce appreciable specular reflection it could appear somewhat brighter than indicated above in favorable orientations. A more detailed discussion of the brightness of space vehicles will be given in a separate report that is now in preparation.

2.   Criterion 2

The angular velocity of the vehicle as seen from the earth would have depended, of course, upon its distance. It would also have varied, for a given distance, from one launch date to the next. At a range of 100,000 miles, the nominal angular rate was about a degree per hour, but in the same general direction as the lunar motion. Thus, at 100,000 miles it could have been tracked nearly automatically with the 48-inch telescope, and slight, periodic, manual adjustments of the telescope could be made with enough accuracy to track the object to within a few seconds of arc. The scale of the 48-inch Schmidt is 67 inches per millimeter, small enough so that tracking of this accuracy should be sufficient to record an object as bright as the third stage fairly easily, provided it is not too near the horizon. At a distance of 40,000 miles, the hourly motion would have been about 2 degrees--to fast to track automatically. However, rough manual tracking could be done, and at that closer range the third stage might have been bright enough to record even with poor tracking. It is doubtful that the fourth stage could be recorded with the 48-inch telescope in either case. It is necessary that accurate angular rates of the vehicle be made available. Fortunately, although the positions from an ephemeris obtained from radio data are not good, the errors in the angular rates are of higher order, and for exposure times as short as those required by the 48 inch telescope, are not serious.

3.   Criterion 3

Nominal trajectories were available for the Able-1 probe for each of the possible launch dates several weeks in advance. The actual trajectories could not be expected to follow the nominal ones accurately. However, as the flight commenced, data were to be gathered at the Inglewood headquarters from the various radio tracking stations. Within a few hours after lift-off, it was expected that the new trajectory ephemeris would give positions good to within 2 or 3 degrees, accurate enough to put the object in the field of the 48-inch telescope. During the initial few hours after lift-off even the nominal ephemeris should have been good enough if the missile was even approximately on course. It should be noted that the positions given

in both the nominal and improved ephemerides are for the fourth-stage payload while it was the third stage that was expected to be bright enough to photograph with the 48-inch telescope. The separation velocity of the third and fourth stages however, was to be small (less than 100 ft/sec) and the greatest component of this velocity would be in the radial direction from the earth; therefore, at least for the first three quarters of a day, the third and fourth stages should have been within a few minutes of arc of each other. It is conceivable that the fourth stage might have been recorded on a photograph taken with the 48-inch Schmidt. If not, a Schmidt photograph of the third stage would have fixed the position of the fourth stage accurately enough that it could possibly have been photographed with a larger telescope.

4. Criterion 4

Whether or not the third and/or fourth stages would be above the Palomar horizon at night could be determined at once from the nominal trajectories. The nominal trajectories indicated that if the missile were fired on either of the first two of the possible dates in either August or September, lift-off would occur in the early morning hours, Pacific Standard Time, and that the third and fourth stages would be well above the western horizon after the end of twilight on the following evenings, about two-thirds of a day after launch, and at a distance of approximately 100,000 miles. Lift-off was scheduled in the late evening, Pacific Time, for the first two November dates. The object then would have been well above the eastern horizon before morning twilight the following morning, at a distance of approximately 40,000 miles. During most of the possible flights, there would have been time to obtain two or three photographs at the first opportunity, and one or two additional photographs about 24 hours later. Only if the missile were launched on the first three of the possible days in October would it be too near the sun to appear above the horizon while the sky was completely dark. It is unfortunate, from this point of view, that the launching occurred on the first possible date in October.

In summary, it is seen that both the third and fourth stages would be too faint to photograph with any existing ballistic camera or satellite camera. However, for most of the possible launch dates, it should have been

possible, weather permitting, to obtain photographs of the third stage, and remotely possibly the fourth stage, with the 48-inch Schmidt telescope on Palomar Mountain. This is the only telescope on the west coast, and one of the few in the world, that would have been suitable. However, if successful photographs could have been obtained with the Schmidt, thereby obtaining a better position, it might have been possible to obtain additional plates, possibly even of the fourth stage, with any of two or three other telescopes. Incidentally, Able-1 was the first space vehicle (and only, to date of writing) that met the criteria for feasibility of photography with a large astronomical telescope.

C. The Program for Obtaining Photographs

Permission to use the 48-inch Schmidt telescope for photographing Able-1 was granted by Dr. I.S. Bowen, Director of the Mount Wilson and Palomar Observatories. Photographs were to be obtained by Dr. George O. Abell, a guest investigator at the observatories, or Dr. Guido Munch, a staff member of the observatories and a consultant to STL. (Dr. Munch has been on leave of absence to Europe since August 1958, but made the original arrangments for the photography of the August shoot.)

The August and September shoots were to have been launched in early morning, Pacific Time. Had either been successful, it was planned to pick up the best trajectory data available by 3:30 p.m. the same afternoon, and to proceed at once to Palomar, arriving by evening when the third stage should be bright enough to photograph in the western sky. In the case of the November shoot, the third stage would have been west of the sun, above the eastern horizon before sunrise. Therefore, it was planned, in November, to leave for Palomar immediately following a successful launch with the hope that the trajectory of the object would be close enough to the nominal trajectory to find it in the field of the Schmidt telescope. In each case, as many plates would have been taken as possible, and whenever feasible, additional plates 24 hours later.

In October, unless the shoot were delayed to the last possible day, it was not expected that photographs would be possible from Palomar, because of the proximity of the missile (in direction) to the sun. As it happened, the writer was the scheduled observer at the 48-inch telescope during the October

launch dates. Periodic communication was maintained with STL in case the missile deviated from the nominal trajectory in such a way that a photograph would be possible. Unfortunately, despite its large deviation from its planned trajectory, the missile was never in the Palomar sky during the night.

The emulsion to have been used was the Eastman 103a-0, a fast, blue-sensitive emulsion of low reciprocity failure. Although a yellow- or red-sensitive emulsion would provide slightly better contrast of the missile against the sky in case there had been any moonlight or twilight, the gain would have been more than offset by the longer exposure time and more critical tracking required. It was intended to track on the object by setting the telescope motion from the best trajectory data available. The stars, therefore, would have been trailed. A full exposure of 10 minutes would have been made if the sky were dark enough.

Any photographs obtained were to have been turned over to STL on an indefinite loan. Any release of photographs or information to the public was to be made only by the Ballistic Missile Division of the Air Force.

216

APPENDIX C

GROUND STATION DATA ACQUISITION PLAN (Section 4.2)

I.   GENERAL INFORMATION

  A.   Introduction

      The following sets forth the station procedure   adopted in the third
flight.

  B.   General

      1.   The WWV, WWVH, or British timing should stand out loud and
clear at the beginning of each tape. It is better to use station time as per,
"on the mark it will be...," than an unreadable WWV time standard.

      2.   Whenever calibration runs are made onto a tape, e.g., local
telemeter VCO frequency versus input voltage, the tone should be held for at
least one minute (at 7.5 in/sec) since at eight times playback speed this time
is only + 7 seconds.

      3.   Calibrations for AGC and signal strength are urgently required for
postflight analysis. These calibrations must be complete so that VCO frequency
on the tape is known in terms of signal strength. Since manual gain control is
employed at all stations, it is essential to have the family of curves relating
VCO (signal-strength) frequency versus signal strength for various gain settings,
and also the gain-setting VCO frequency versus gain setting. Otherwise, the
signal-strength data is useless.

      4.   Voice annotation should be loud and clear. Otherwise, numerous
tape reruns are required to understand the talk.

      5.   In the last flight, some tapes had no 12.5-kc wow and flutter and
some had undecipherable time (track 2). Emphasis should be placed upon
this information; otherwise, the accuracy of the data is severly compromised.

      6.   Where omitted, include "write in GMT" on all Sanborn recordings
about once per hour; place write-in across record.

      7.   Ship Sanborn record each day with tapes. These records are very
useful.

C.   Calibrations to be Performed with Each Station Operating Cycle

1.   AGC Calibration - Set AGC meter to 0.05 ma.   Record on Sanborn paper, channel 7, in pencil, that the mark made by the pen corresponds to 0.05 ma.   Speak onto voice track of Ampex tape that the tone being recorded on track 1 and subcarrier oscillator channel 3 corresponds to 0.05 ma on the AGC meter.   Measure the SCO frequency on the HP counter and record this reading on the data sheet and on voice.   Allow the condition to exist for one minute.

Repeat each of the above steps for the values of 0.10, 0.20, 0.30, 0.50, 0.60, 0.70, 0.80, 0.90, and 1.00 ma allowing one minute of record for each setting.   The AGC meter readings can be obtained in the case of station having manual gain control by manually setting gain-control voltage until the AGC meter reads the appropriate value.   For other stations the output of a signal generator shall be put into the receiver and the loop locked.   Meter reading can then be adjusted by signal level into the receiver.

2.   Signal-strength Calibration - Set signal-strength meter to read 10 μamp.   Record on Sanborn paper, channel 4, in pencil, that the mark made by the pen corresponds to 10 μamp.   Speak on the voice track of the Ampex that the tone being recorded on track 1 and SCO channel 1 corresponds to 10 μamp on the signal-strength meter.   Measure the SCO frequency on the HP counter and record the reading on the data sheet and on voice.   Allow this condition to exist for one minute.

Repeat above steps for signal-strength meter readings of 20, 30, 40, 50, 60, 70, 80, 90, and 100 μamp allowing one minute of record for each. Signal-strength meter readings can be obtained by placing a signal generator output into the receiver, locking the loop, and adjusting the input level until the signal-strength meter reads the proper value.

3.   Input DBM Calibration - Apply -90-dbm signal to the input of the preamplifier.   Lock the loop and adjust manual tuning so that the phase error meter reads zero.   (If manual gain control is used, adjust gain control so that signal-strength meter reads full scale.)   Record on the data sheet both the AGC and signal-strength meter readings.   Repeat for input signal levels of -100, -110, -120, -130, -140, and -150 dbm.

D. Remote Telemetry Channel Assignments

The new assignments of channels for remote telemetry are as follows:

Channel 1 -- (400 cps) ion chamber 2-3 minutes of analog signal followed by 20 seconds of in-flight calibration marker with one-second rise and fall.

Channel 2 - (560 cps) magnetometer-- steady 2-cps tone with possibly variable amplitude.

Channel 3 --(730 cps) STL television-- exponentially-stepped signal at basic 2-cps rate, should operate for a period during ascent phase from earth and when past moon.

Channel 4 - (960 cps) micrometeorite and compartment temperature occasionally exponentially stepped 10-per cent shift to new steady value riding upon slowly varying analog.

Channel 5 - (1300 cps) cosmic rays-- binary coded exponential transitions with period perhaps 10 seconds to one minute. Transitions 10 per cent of band.

Channel 6 - (1700 cps) cosmic rays and magnetometer AGC--binary-coded exponential transitions with period perhaps 1-5 minutes riding on slowly varying analog. Transitions 10 per cent of band.

E. Miscellaneous Instructions

1. All tape recording is to be done at 7.5 in/sec.

2. All Sanborn chart recording is to be done at 1 mm/sec unless at station discretion speed needs to be increased as below.

3. For ranging experiments, Sanborn chart speed is to be 100 mm/sec.

F. Transmitter Assignments

Two transmitters are being carried in the vehicle.

1. High power

    a. frequency - 108.06 mc,

    b. power output - 350 mw,

    c. lifetime - 10-15 days, and

    d. doppler interrogated and disables telemetry.

2. Low power

    a. frequency - 108.09 mc,

    b. power output - 150 mw,

    c. lifetime - approximately two days, and

    d. multiplexed onto telemetry, noninterrogable.

II. GROUND STATION FORMAT

A. Hawaii

1. Introduction

Since two transmitters are being carried in the vehicle and two receivers and recorders are available, the following procedure is recommended:

Receiver A - permanently tuned to 108.06 mc, and

Receiver B - tuned to 108.09 mc for the first two days until backup transmitter ceases to function. Subsequent to that time receiver B should be retuned to 108.06 mc for standby.

When doppler interrogation is taking place, the 108.06-mc transmitter will be utilized by the doppler link, thus, the magnetic tape recorder will quite suddenly be recording doppler information and not telemetry. At the point where doppler command takes over the high-power transmitter, receiver B should begin to record telemetry on the standby tape recorder. It would be more convenient from the format standpoint to keep the telemetry on one tape recorder and put doppler on the other, but this is impractical. After two days, or when the low-power transmitter fails, simple A-B operation of the tape recorders can be established functioning from receiver A with receiver B in standby condition only.

2. Magnetic Tape Recording Format

The format for both tape recorders is made identical for simplicity.

Track 1 - local telemetry as follows:

Channel 1 - AM detector (in-phase component) d-c level--receiver 1

Channel 2 - PM detector (quadrature component) d-c level--receiver 1

Channel 3 - Gain-control bias--receiver 1

Channel 4 - Unassigned

Channel 5 - Time ticks--1 and 0 seconds from HP counter

Channel 6 - Latitude phase 1 or latitude sum --difference

Channel 7 - Latitude phase 2 or longitude sum--difference

Channel 8 - Longitude phase 1 or latitude sum--reference

Channel 9 - Longitude phase 2 or longitude sum--reference

Channel 10 - Gain-control bias--receiver 2, 12.5 kc wow and flutter compensation

Track 2 - WWV or equivalent at beg nning of tape to establish an absolute time base for the whole tape. This reco-ding should be monitored by earphone while being made and a loud, clear signal obtained unambiguously giving Zebra time. If it appears from the monito: that the recording is not clear local station time to ± 5 seconds will suffice. The local station time, "on the mark it will be...," should be stated in Zebra time. When timing reference has been achieved at the beginning of the tape, the remainder of the tape is to be utilized for voice intercom* and annotation.

Track 3 - receiver AM detector output (in-phase component of subcarrier composite spectrum).

Track 4 - pseudodoppler (100 mc--receiver VCO beat frequency).

Track 5 - ranging modulation transmitted signal.

---

* The intercom assignment previously on Track 3 and the 8.5-kc speed-lock signal requirement is deleted.

Track 6 - ranging modulation recording signal.

Track 7 - receiver PM detector output (quadrature component of subcarrier composite spectrum; this channel constitutes the remote telemetry real-time output).

Ranging modulation will be placed on a 6.75-kc FM carrier prior to recording so as to provide the needed low-frequency response.

3.   Strip-chart Format

3.1 Sanborn 8 Channel

Channel 1 - remote telemetry subcarrier number 1

Channel 2 - remote telemetry subcarrier number 2

Channel 3 - remote telemetry subcarrier number 3

Channel 4 - remote telemetry subcarrier number 4

Channel 5 - remote telemetry subcarrier number 5

Channel 6 - remote telemetry subcarrier number 6

Channel 7 - AM detector (in-phase component) d-c level

Channel 8 - gain-control bias

Marker   - 1- and 10- second timing marks

(Write-in GMT to be done across chart.)

3.2 Sanborn 6 Channel

Channel 1 - latitude phase 1 or latitude sum - difference

Channel 2 - latitude phase 2 or longitude sum - difference

Channel 3 - longitude phase 1 or latitude sum - reference

Channel 4 - longitude phase 2 or longitude sum - reference

Channel 5 - AM detector (in-phase component) d-c level

Channel 6 - gain-control bias

Marker   - 1- and 10-second timing marks

(Write-in GMT to be done across chart.)

During ranging experiments, the telemetry is disabled in the vehicle. While the experiment is in progress, channels 5 and 6 of Sanborn number 2 will be patched for ranging modulation transmitted and received respectively.

B. Manchester

1. Introduction

The Manchester receiver will be tuned to 108.09 mc prior to launch so as to be tuned to the low-power telemetry transmitter, thus signal coverage for telemetry should be available without interruption by doppler interrogation. It is highly essential that every attempt be made to obtain the best telemetry record possible from the moment of first acquisition and for the first 10 to 15 hours thereafter. Upon decision, jointly, between the Manchester station and the Los Angeles Command Center, some time subsequent to the launch, crystal changeover to 108.06 mc should be made in order to utilize the high-power transmitter after initial doppler interrogation has ceased; however, this changeover should not compromise station operation and will depend on tracking requirements and telemetry requirements in existence during first hour of flight.

2. Magnetic Tape Format

Track 1 - local telemetry as follows:

Channel 6 - AM detector (in-phase component) d-c level

Channel 7 - PM detector (quadrature component) d-c level

Channel 8 - gain-control bias

Channel 9 - unassigned

Channel 10 - time ticks--1 and 10 seconds from HP counter;

12.5-kc wow and flutter compensation (because of the analog nature of some of the information, it is important that wow and flutter compensation be included on all tapes).

Track 2 - WWV or equivalent at beginning of tape to establish an absolute time base for the whole tape. This recording should be monitored by earphone while being made and a loud, clear signal obtained unambiguously giving Zebra time. If it appears from the monitor that the recording is not clear, local station time to ± 5 seconds will suffice. The local station time, "on the mark it will be,..," should be stated in Zebra time. When timing reference has been achieved at the beginning of the tape, the remainder of the tape is to be utilized for voice intercom* and annotation.

---

* The intercom assignment previously on Track 3 and the 8.5-kc speed-lock signal requirement is deleted.

Track 3 - receiver AM detector output (in-phase component of subcarrier composite spectrum).

Track 4 - pseudodoppler (100 mc--receiver VCO beat frequency).

Track 5 - unassigned

Track 6 - unassigned

Track 7 - receiver PM detector output (quadrature component of subcarrier composite spectrum; this channel constitutes the remote telemetry real-time output).

3. Strip-chart Format

Channel 1 - remote telemetry subcarrier number 1

Channel 2 - remote telemetry subcarrier number 2

Channel 3 - remote telemetry subcarrier number 3

Channel 4 - remote telemetry subcarrier number 4

Channel 5 - remote telemetry subcarrier number 5

Channel 6 - remote telemetry subcarrier number 6

Channel 8 - gain-control bias

Marker - 1- and 10-second timing marks.

C. Singapore

1. Introduction

Since only one receiver is available it should be tuned to 108.06 mc to enable reception from the high-power transmitter. In the advent of notice from the Communication Center at Los Angeles that long-term doppler will begin, the 108.09 mc channel should be utilized for the first two days only. Subsequent to that time, the low-power transmitter will lose battery power.

2. Magnetic Tape Format

Track 1 - local telemetry as follows:

Channel 1 - AM detector (in-phase component) d-c level

Channel 2 - PM detector (quadrature component) d-c level

Channel 3 - gain-control bias

Channel 4 - unassigned

Channel 5 - time ticks--1 and 10 seconds from HP counter 12.5-kc wow and flutter compensation.

Track 2 - WWV or equivalent at beginning of tape to establish an absolute time base for the whole tape. This recording should be monitored by earphone while being made and a loud, clear s gnal obtained unambiguously giving Zebra time. If it appears from the monitor that the recording is not clear, local station time to ± 5 seconds will suffice. The local station time, "on the mark it will be...," should be stated in Zebra time. When timing reference has been achieved at the beginning of the tape, the remainder of the tape is to be utilized for voice intercom* and annotation.

Track 3 - receiver AM detector output (in-phase component of subcarrier composite spectrum).

Track 4 - pseudodoppler (100 mc--receiver VCO beat frequency).

Track 5 - unassigned

Track 6 - unassigned

Track 7 - receiver PM detector output (quadrature component of subcarrier composite spectrum; this channel constitutes the remote telemetry real-time output).

Ranging modulation will be placed on a 6.75-kc FM carrier prior to recording so as to provide the needed low-frequency response.

3. Strip-chart Format

Channel 1 - remote telemetry--subcarrier number 1

Channel 2 - remote telemetry--subcarrier number 2

Channel 3 - remote telemetry--subcarrier number 3

Channel 4 - remote telemetry--subcarrier number 4

Channel 5 - remote telemetry--subcarrier number 5

---

*The intercom assignment previously on Track 3 and the 8.5-kc speed-lock signal requirement is deleted.

Channel 6 - remote telemetry--subcarrier number 6

Channel 7 - AM detector (in-phase component) d-c level

Channel 8 - gain-control bias

Marker   - 1-and 10-second timing marks.

D. AFMTC

1. Introduction

Because of doppler commitments, this station will be unable to obtain telemetry during the first 17 minutes. Subsequent to that time, every attempt should be made to obtain telemetry on the 108.06-mc channel.

2. Magnetic Tape Format

Track 1 - local telemetry as follows:

Channel 1 - AM detector (in-phase component) d-c level

Channel 2 - PM detector (quadrature component) d-c level

Channel 3 - gain-control bias

Channel 4 - unassigned

Channel 5 - time ticks--1 and 10 seconds from HP counter

12.5-kc wow and flutter compensation.

Track 2 - WWV or equivalent at beginning of tape to establish an absolute time base for the whole tape. This recording should be monitored by earphone while being made and a loud, clear signal obtained unambiguously giving Zebra time. If it appears from the monitor that the recording is not clear, local station time to ± 5 seconds will suffice. The local station time, "on the mark it will be...," should be stated in Zebra time. When timing reference has been achieved at the beginning of the tape, the remainder of the tape is to be utilized for voice intercom* and annotation.

Track 3 - receiver AM detector output (in-phase component of subcarrier composite spectrum).

---

* The intercom assignment previously on Track 3 and the 8.5-kc speed-lock signal requirement is deleted.

Track 4 - pseudodoppler (100-mc--receiver VCO beat frequency).

Track 5 - unassigned

Track 6 - unassigned

Track 7 - receiver PM detector output (quadrature component of subcarrier composite spectrum; this channel constitutes the remote telemetry real-time output).

Ranging modulation will be placed on a 6.75-kc FM carrier prior to recording so as to provide the needed low-frequency response.

3. Strip-chart Format

Channel 1 - remote telemetry--subcarrier number 1

Channel 2 - remote telemetry--subcarrier number 2

Channel 3 - remote telemetry--subcarrier number 4

Channel 4 - remote telemetry--subcarrier number 5

Channel 5 - remote telemetry--subcarrier number 6

Channel 6 - AM detector (in-phase component) d-c level

Channel 7 - ranging sinusoid transmitted

Channel 8 - ranging sinusoid received plus write-in GMT

Marker   - range time or 1 and 10 second timing ticks from HP counter.

The paper speed recommended is 1 mm/sec ordinarily, and 100 mm/sec for recording ranging sinusoid signals. However, the 1-mm/sec speed is subject to modification as the appearance of the data dictates. Up to T plus 17 minutes, the remote telemetry is not available to this station and subsequent to T plus 17 the ranging signal is not present. If range time cannot be placed on marker channel, it should be substituted on to Sanborn channel 2 in lieu of remote telemeter.

III. QUICK-LOOK DATA REQUIREMENTS

At approximately one-hour intervals, the data from remote telemeter channels 1, 2, 4, 5, and 6 will be read and a message prepared for transmission to TLM at the BMD/STL Communications Center, Los Angeles. The time when data is read and recorded will not, necessarily, immediately precede

the transmission of the message to TLM. For the first 20 hours, a schedule for messages to TLM has been devised to minimize interference with other message transmissions. This schedule is shown in the table below.

A. Channel 1 - (400 cps) Ion Chamber

1. Select a short (few-second) sample of strip chart data and read the d-c value in terms of VCO frequency. The accuracy of the reading should be two per cent, or one small division on the strip chart paper assuming that the ± 7.5-per cent deviation channel edges correspond to the chart graph edges.

2. Repeat above for the calibrate level nearest the place where the data level was determined.

3. Note the Zebra time that the reading was taken to the nearest minute. One such pair of readings each hour is required except as follows:

During first hour, certain stations will be asked by TWX for informal reports on this channel. This is to be done without compromising higher priority station duties. The stations to be interrogated for this information will be individually TWX'd.

B. Channel 2 - (560 cps) Magnetometer

1. Select a 15- or 20-second sample of Sanborn record and read the peak-to-peak value of the 2-cps sine wave in terms of a percentage of full channel bandwidth (band edge-to-edge excursion). The reading accuracy should be two per cent, or one small division on the Sanborn paper assuming the ± 7.5 per cent deviation channel edges correspond to the chart graph edges.

2. Note the Zebra time that the reading was taken to the nearest minute.

One such reading each hour is required.

C. Channel 3 - (730 cps) STL Television

No quick-look data requirements except as follows:

Occasionally, information may be requested from a particular station concerning this data. This will be a low-priority item.

D. **Channel 4 - (960 cps) Micrometeorite and Compartment Temparature**

1. Starting at the place on the Sanborn record where the previous reading ended, count the total number of excursions (counts). Do not count those excursions which are due to a switching from telemeter to doppler or vice versa.

2. Determine, to the nearest minute, the total time interval over which the counts were made. Do not include, in this interval, any intervals during which the doppler signal was transmitted.

3. Select a short (few-second) sample of strip-chart temperature data and read the d-c value in terms of VCO frequency. The accuracy of the reading should be two per cent, or one small division of the strip-chart paper assuming that the ±7.5 per cent deviation channel edges correspond to the chart graph edges.

It is additionally important to know whether the VCO is in its lower or upper state with respect to micrometeorites.

4. Note the Zebra time when the reading of counts was ended, to the nearest minute.

E. **Channel 5 - (1300 cps) Cosmic Rays**

1. Starting at the place on the Sanborn record where the previous reading ended, count the total number of excursions (counts). Do not count those excursions which are due to a switching from telemeter to doppler or vice versa.

2. Determine, to the nearest minute, the total time interval over which the counts were made. Do not include, in this interval, any intervals during which the doppler signal was transmitted.

3. Note the Zebra time when the reading of counts was ended, to the nearest minute.

One such reading each hour is required except as follows: during first hour, selected stations may be interrogated by TWX for additional information concerning this channel.

F. **Channel 6 - (1700 cps) Cosmic Rays and Magnetometer AGC**

1. Starting at the place on the Sanborn record where the previous reading ended, count the total number of excursions (counts). Do not count

those excursions which are due to a switching from telemeter to doppler or vice versa.

2. Determine, to the nearest minute, the total time interval over which the counts were made. Do not include, in this interval, any intervals during which the doppler signal was transmitted.

3. Select a short (few-second) sample of strip-chart magnetometer AGC data and read the d-c value in terms of VCO frequency. The accuracy of the reading should be two per cent, or one small division of the strip-chart paper assuming that the ± 7.5-per cent deviation channel edges correspond to the chart graph edges.

4. Note the Zebra time when the reading of counts was ended, to the nearest minute.

One such reading each hour is required except as noted for channels 1 and 5.

The special requirements during first hour will be sent as individual interrogations. It is expected that data rates on these channels may vary appreciably during this time. If the demand for this data is too great, the decision may be made during flight to examine it at the stations concerned at some later time for delayed transmission subsequently to obtaining the data.

IV. DISCRIMINATOR LOOP FILTER BANDWIDTH

Hallamore discriminator channel selector switch settings should always be as narrow as possible and yet hold lock

The phase-locked loop filter cutoff frequency in cycles per second for the Hallamore discriminators are as follows:

	Std.	Med.	Nar.
Channel 1	54	9	0.9
Channel 2	76	13	1.3
Channel 3	100	17	1.7
Channel 4	130	22	2.2
Channel 5	176	32	3.2
Channel 6	230	43	4.3